MOLECULAR MECHANISMS OF HEPATOCELLULAR CARCINOMA DEVELOPMENT INDUCED BY DEFICIENT TRANSCRIPTIONAL COREGULATORS

By

Yueqi Zhang

A DISSERTATION

Submitted to
Michigan State University
in partial fulfillment of the requirements
for the degree of

Cell and Molecular Biology – Doctor of Philosophy

2024

ABSTRACT

Liver cancer is the 7th most common and 3rd most lethal malignancy in humans worldwide, and it is one of the few types of cancers that still have a rising incidence rate and death rate in the United States. Hepatocellular carcinoma (HCC) accounts for about 90% of liver cancer cases. The incidence rate and death rate of HCC are increasing faster in females than in males, and nonalcoholic fatty liver disease/nonalcoholic steatohepatitis (NAFLD/NASH) is the rising etiology for HCC in both sexes. The molecular mechanisms of HCC development are poorly understood, and the current theories have contributed very little to the medical practices for HCC. Nuclear receptor coactivator 5 (NCOA5) and 30-kDa Tat-interacting protein (TIP30, also known as HTATIP2) are two transcriptional coregulators involved in HCC development.

My dissertation research uses novel genetically engineered mice with manipulated NCOA5 and TIP30 expression to model spontaneous HCC development and fill in the knowledge gaps in the molecular mechanisms of NAFLD/NASH-related HCC development in both sexes. The first part of my research identified $p21^{Cip1/Waf1}$ (also known as cyclin-dependent kinase inhibitor 1A, CDKN1A) as the critical factor upregulated in hepatocytes by *Ncoa5* deficiency in male mice and promotes a pro-tumorigenic inflammatory microenvironment that results in spontaneous HCC. The second part of my research discovered that NCOA5 haploinsufficiency in myeloid-lineage cells sufficiently causes NASH and HCC in male mice. I identified platelet factor 4 (PF4) overexpression in the intrahepatic macrophages of male mice with myeloid-lineage-specific *Ncoa5* deletion as a potent mediator to trigger lipid accumulation in hepatocytes by inducing lipogenesis-promoting gene expression. The third part of my

research discovered that heterozygous *Tip30* deletion promotes HCC development in *Ncoa5*$^{+/-}$ mice in a female-biased manner. The mechanisms of HCC development in female mice appear different from those in males. I identified hyperpolarization-activated cyclic nucleotide-gated cation channel 3 (HCN3) as a novel oncogenic factor for female HCC that is upregulated by *Ncoa5* and *Tip30* deletion specifically in female mice.

In summary, my dissertation study established p21 and PF4 as novel factors that promote a pro-tumorigenic microenvironment in the development of NASH-related HCC and identified HCN3 as a novel female-biased HCC driver. My work highlights the crucial role of the pro-tumorigenic microenvironment in HCC development and exposes that mechanisms of HCC development can differ significantly in males and females.

ACKNOWLEDGEMENTS

It would not have been possible for me to complete the work presented in this dissertation without the support of people I met in my life. I hope these simple words express my deep appreciation for each of them.

First of all, I must thank my parents for allowing me to pursue my childhood dream of being a scientist. I never knew what my parents wanted me to be, but they taught me what is right and how to be a good person, and they let me pursue what I believe is right. I would not have made it this far in my education and research without my parents' understanding and support. As the only child in the family, I am sorry that my selfish choice kept your only son seven thousand miles away for seven years. Thank you to my girlfriend, Lanxi, who has been my motivation and support since we were together ten years ago. Without you, I would not have made it to live and study here these years.

Especially, I want to thank my mentor, Dr. Hua Xiao. Thank you for allowing me to study in your lab and for your tremendous effort in my training. You helped me navigate the difficult path of academia and living in a foreign country. You educated me both in science and life. I want to thank the members of the Xiao lab for their efforts that made this dissertation study possible. A special thanks to Xinhui, who warmly accommodated me in the Xiao lab, trained me meticulously, and brought my value to light. Thank you to Yue Luo for your company and contribution to this work. I also want to thank Jake Reske, who introduced me to bioinformatic analysis. I appreciate Kairui Sun and Jack Yang for their hard work in performing some experiments for me.

I must thank my committee, Dr. Eran Andrechek, Dr. Kathleen Gallo, Dr. Dohun

Pyeon, Dr. Hongbing Wang, and my former committee members, Dr. Susan Conrad and Dr. Rupali Das, for their valuable guidance and feedback. Your suggestions and insights were instrumental to this work. A special thank you to Dr. Hongbing Wang and Dr. Qing-Sheng Mi for the support and collaboration that made this study possible.

I have been privileged to work with the amazing departments and facilities of Michigan State. Thank you to Amy Porter and Jessielee Neuman of the Investigative HistoPathology Laboratory for your swift and consistent work that boosted our discovery. Thanks to the Campus Animal Resources staff for maintaining an optimal place for mouse studies. I want to thank the Cell and Molecular Biology program for funding and advisory assistance that helped me earn the degree. I want to thank Lauren Aitch and the Aitch Foundation for funding and their selfless commitment to fighting cancer.

Finally, thank you to Michigan State University, the most welcoming and peaceful place for my life in the United States.

TABLE OF CONTENTS

LIST OF ABBREVIATIONS

HCC – hepatocellular carcinoma

NAFLD – nonalcoholic fatty liver disease

NASH – nonalcoholic steatohepatitis

NCOA5 – nuclear receptor coactivator 5

TIP30 – 30-kDa Tat-interacting protein, also known as HTATIP2

PF4 – platelet factor 4

HCN3 – hyperpolarization-activated cyclic nucleotide-gated cation channel 3

HBV – hepatitis B virus

HCV – hepatitis C virus

PDL1 – programmed death-ligand 1

T2DM – type 2 diabetes mellitus

ROS – reactive oxygen species

ER (organelle) – endoplasmic reticulum

ERK1/2 – extracellular signal-regulated kinases 1/2

AKT – Ak strain transforming

GHR – growth hormone receptor

IGF1 – insulin-like growth factor 1

KEAP1 – Kelch-like ECH-associated protein 1

NRF2 – nuclear factor erythroid 2-related factor 2

NHEJ – non-homologous end-joining

NF-κB – nuclear factor kappa-light-chain-enhancer of activated B cells

JNK – c-Jun N-terminal kinase

DEN – diethylnitrosamine

MDSC – myeloid-derived suppressor cell

Treg – regulatory T cell

NET – neutrophil extracellular trap

HSC – hepatic stellate cell

DPP4 – dipeptidyl peptidase 4

CXCL10 – C-X-C motif chemokine ligand 10

PD-1 – programmed cell death protein 1

IL-10 – interleukin 10

ECM – extracellular matrix

PDAC – pancreatic ductal adenocarcinoma

ER (molecule) – estrogen receptor

PTPRO – protein tyrosine phosphatase receptor type O

STAT3 – signal transducer and activator of transcription 3

SHP – small heterodimer partner

AMPK – AMP-activated protein kinase

AMP – adenosine monophosphate

SREBF1 – sterol regulatory element-binding factor 1, as known as SREBP1

HGP – hepatic glucose production

MAPK – mitogen-activated protein kinase

PPARγ – peroxisome proliferator-activated receptor γ

NAD^+ – nicotinamide adenine dinucleotide

AR – androgen receptor

PRL – Prolactin

TNF – tumor necrosis factor

LPS – lipopolysaccharide

c-myc – cellular myelocytomatosis, also known as MYC

TSPY – testis-specific protein Y encoded

SRY – sex-determining region on Y chromosome

OCT4 – octamer-binding transcription factor 4, also known as POU5F1

PDGFRα – platelet-derived growth factor receptor alpha

PI3K – phosphoinositide 3-kinase

RBMY – RNA-binding motif gene on Y chromosome

GSK3β – glycogen synthase kinase 3β

HBx – HBV X protein

c-src – cellular sarcoma

HNF4α – hepatocyte nuclear factor 4α

ATP – adenosine triphosphate

SWI/SNF – SWItch/Sucrose Non-Fermentable

CBP – CREB-binding protein

TAF – TATA-box binding protein-associated factor

PGC1α – peroxisome proliferator-activated receptor-gamma coactivator 1α

TRβ – thyroid hormone receptor β

GR – glucocorticoid receptor

MEF2C – myocyte-specific enhancer factor 2C

NRF1 – nuclear respiratory factor 1

ERRα – estrogen receptor-related receptor α

SRC1 – steroid receptor coactivator 1, also known as nuclear receptor coactivator 1 (NCOA1)

E2F1 – E2F transcription factor 1

AP1 – activator protein 1

MMTV – mouse mammary tumor virus

BCL2 – B-cell lymphoma 2

EGF – epidermal growth factor

PIP3 – phosphatidylinositol (3,4,5)-trisphosphate

PTEN – PIP3 phosphatase and tensin homolog

NR1D1 – nuclear receptor subfamily 1 group D members 1

CIA – coactivator independent of AF2

AF2 – activation function 2

LXR – liver X receptor

RORA – retinoic acid-related orphan receptor-alpha

GWAS – genome-wide association study

SNP – single nucleotide polymorphism

TLR3 – toll-like receptor 3

ABCA1 – ATP binding cassette subfamily A member 1

SNCOA5 – shortened NCOA5

ERE – estrogen response element

SNV – single nucleotide variation

mTOR – mammalian target of rapamycin

HIV1 – human immunodeficiency virus 1

SCLC – small-cell lung cancer

OPN – osteopontin

CCND1 – cyclin D1

NADPH – nicotinamide adenine dinucleotide phosphate

SDR – short-chain dehydrogenases/reductases

HuR – Hu antigen R

SNAIL – snail family transcriptional repressor 1

EMT – epithelial-mesenchymal transition

MPG – N-methylpurine DNA glycosylase

CDKN1A – cyclin-dependent kinase inhibitor 1A, also known as p21

IHC – immunohistochemistry

RT-qPCR – quantitative real-time reverse transcription polymerase chain reaction

qChIP – quantitative chromatin immunoprecipitation

CPT – camptothecin

BSA – bovine serum albumin

DMSO – dimethyl sulfoxide

ATCC – American Type Culture Collection

STR – short tandem repeat

NPC – nonparenchymal cell

PC – parenchymal cell

DEG – differently expressed gene

AMLN – Amylin liver NASH

CM – conditioned medium

GeRP – glucan-encapsulated siRNA particle

NC – negative/non-targeting control

GAGE – Generally Applicable Gene-set Enrichment

KEGG – Kyoto Encyclopedia of Genes and Genomes

PF4V1 – PF4 variant 1

ssGSEA – single-sample Gene Set Enrichment Analysis

OB – obese

ALT – alanine aminotransferase

DHA – docosahexaenoic acid

BMI – body mass index

HbA1C – hemoglobin A1C

AST – aspartate transferase

AA – arachidonic acid

HC – healthy control

ES – embryonic stem

GTT – glucose tolerance test

ITT – insulin tolerance test

HPF – high-power field

EP – Endo-Porter

AFP – α-fetoprotein

GO – Gene Ontology

ELISA – enzyme-linked immunosorbent assay

EV – empty vector

PP5 – PLC/PRF/5

Pg – progesterone

PR – progesterone receptor

PRE – progesterone response element

TG – thapsigargin

VC – vector control

OS – overall survival

DFI – disease-free survival/interval

DSS – disease-specific survival

PFI – progression-free survival/interval

NTE – new tumor event

CHAPTER 1: Introduction

1.1 Preface

Part of this chapter is a modified version of a previously published review article in *International Journal of Molecular Sciences*, Volume 22, **Zhang, Y.**, Wang, H. and Xiao, H., Metformin actions on the liver: protection mechanisms emerging in hepatocytes and immune cells against NASH-related HCC, pp.5016. I wrote the original manuscript and edited and revised the article.

1.2 Basics of hepatocellular carcinoma and its emerging etiologies

Liver cancer is the 7th most common and 3rd most lethal malignancy in humans globally[1,2], and it is one of the few types of cancers that still have a rising incidence rate and death rate in the most developed country, the United States[3]. Hepatocellular carcinoma (HCC) accounts for about 70-90% of liver cancer cases, and more than 90% of HCCs develop in livers with chronic diseases[4]. Most HCCs develop in an identifiable population associated with well-established and well-researched risk factors, the majority of which are infection by hepatitis B virus (HBV) and hepatitis C virus (HCV), excessive alcohol consumption, and metabolic syndromes including diabetes and nonalcoholic fatty liver disease (NAFLD). All these risk factors can induce prolonged hepatitis, and indeed, HCC is a prototypical inflammation-associated cancer.

Although the disease etiologies and risk factors are clearly defined and the molecular classification of HCC has been described[5-7], molecular mechanisms of HCC development are still understudied. The current molecular classification of HCC has contributed very little to medical practices or even the design of clinical trials[3]. The first-line systemic therapies approved for advanced HCC are small molecule inhibitors and antibodies targeting receptor tyrosine kinases and their ligands, as well as the immune checkpoint molecule programmed death-ligand 1 (PDL1). They have limited efficacies and response rates. At the same time, molecular classification has yet to play a role in treatment decisions.

The global epidemic of obesity and type 2 diabetes mellitus (T2DM) lowers individuals' quality of life and lifespan and increases risks for dangerous comorbidities, including various types of cancers. People with obesity or T2DM often have excessive

lipid storage in the liver, a marking characteristic of NAFLD. Insulin resistance, the key to T2DM pathogenesis, also spontaneously results in NAFL. Thus, patients with T2DM would inevitably develop liver steatosis to some degree. When NAFLD progresses and causes hepatic inflammation and hepatocyte damage, it is known as nonalcoholic steatohepatitis (NASH). While simple steatosis is not considered a major risk factor for adverse outcomes in patients[8], NASH increases the risk for liver failure and HCC[9]. With cell death and chronic inflammation in NASH, fibrosis usually develops and can progress to cirrhosis, a well-established risk factor for HCC[10]. It should be noted that NASH-related HCC can develop in the absence of cirrhosis or fibrosis[11]. While HCV infection is still a significant etiology for HCC in the US, metabolic syndrome is recognized as the emerging driving force for HCC incidence growth[12]. Indeed, along with the escalating prevalence of obesity, HCC has become the fastest-growing cancer in the US[13]. Moreover, metabolic disorder-related HCC was observed to have a higher mortality risk compared to other nonalcoholic etiologies, including HBV and HCV[14]. The increasing prevalence of NAFLD, also known as the hepatic manifestation of metabolic syndrome, may directly account for the growth of HCC incidence and mortality[13]. Elucidating the molecular mechanisms underlying NAFLD-related HCC development is the key to preventing and treating HCC associated with this growing etiology.

Another general risk factor for HCC is the male sex, where the disease is 2-4 times more frequent in males[15], and a similar male predominance of HCC development is observed in rodent models of HCC[16]. Surprisingly, despite this male predisposition, both incidence and death rates of HCC are rising faster in females than in males[3]. Over the past few decades, efforts have been made to understand the mechanisms

underlying the sex difference in HCC development. This has led to the discovery of the protective role of estrogen, a female hormone, in HCC development[17]. However, subsequent studies have not supported hormonal treatments as a part of the therapies against HCC. Moreover, the molecular mechanism underlying female HCC remains poorly understood as previous studies were carried out mainly in men and male animal models due to the sex disparity of HCC incidence. Therefore, it is urgently needed to understand better the mechanisms causing and protecting against HCC in females to develop novel diagnostic and therapeutic strategies for females with HCC.

In the following sections of this chapter, I will describe the current knowledge on molecular mechanisms underlying HCC development associated with NAFLD[18] and sexes. Then, I will introduce the two transcriptional coregulators, nuclear receptor coactivator 5 (NCOA5) and 30-kDa Tat-interacting protein (TIP30, also known as HTATIP2), that play roles in hepatocarcinogenesis. As presented in the remaining chapters of my dissertation, I generated genetically engineered mouse models of HCC with manipulated NCOA5 and TIP30 expression and conducted mechanistic research to shed light on the knowledge gaps in the molecular mechanisms of HCC development related to NAFLD and the female sex.

1.3 Mechanisms of HCC development using NAFLD-related HCC as an example

1.3.1 Overview

Chronic liver disease is a critical precondition for HCC development in adulthood. The malignant transformation of the mature hepatocyte or progenitor cell is widely recognized as the result of accumulated genetic and epigenetic alterations from the long-term vicious cycle of hepatocyte damage, inflammation, and compensatory

proliferation of cells. Thus, both the risk factors that induce NASH and the pathological abnormalities of established NASH that promote the vicious cycle and alterations could contribute to the initiation of HCC over time.

1.3.2 Risk factors and preconditions of NASH promote HCC development

The current model for the pathogenesis of NAFLD/NASH is the "multiple-hit" theory[19], where multiple insults disrupt the normal metabolic activity of the liver, resulting in a highly heterogeneous disease in terms of both driving mechanisms and manifestations. The various hits that induce NASH, including many interlinked factors such as obesity, T2DM, insulin resistance, dyslipidemia, and altered microbiome, may also promote HCC.

Indeed, these hits are common in individuals with NAFLD/NASH. A meta-analysis of global NAFLD epidemiology revealed that 81.83% of NASH patients had obesity, and 43.63% of NASH patients had T2DM[9]. Moreover, in a cohort of patients with hypertransaminasemia and T2DM, all patients had biopsy-confirmed NASH[20]. Up to 70% of individuals with obesity have dyslipidemia[21]. Further, as diacylglycerol and ceramide inhibit insulin signaling[22,23], it is suggested that dyslipidemia may directly contribute to insulin resistance in NAFLD. Elevated serum insulin and glucose levels are usually seen in individuals with impaired insulin sensitivity. While the cause-effect relationship among all these conditions and NASH is tangled, these conditions overwhelm the hepatocyte with carbohydrates and fatty acids. The excessive metabolic substrates promote metabolic abnormality and the production of toxic metabolites in hepatocytes that stress and damage the cell, which further demolishes hepatocytes' ability to handle substrates[24]. This cycle results in hepatocyte injury and subsequent

hepatic inflammation, which separates NASH from simple NAFL and promotes the development of HCC.

Many of these hits inducing NAFLD/NASH cause oxidative stress in the hepatocyte, which may induce oxidative DNA damage over time. Specifically, fatty acid overload in hepatocytes leads to the overproduction of reactive oxygen species (ROS) in NASH. Insulin resistance in adipose tissue induces increased lipolysis and fatty acid flux into the liver. High glucose availability in T2DM, hyperinsulinemia in insulin resistance, and high dietary sugar intake also promote the *de novo* fatty acid synthesis in hepatocytes[25]. In response to fatty acid overload, there is an increase in fatty acid β-oxidation at the expense of ROS production in the hepatocyte. The fatty acid is also disposed of by conversion into triglyceride, which is then either transported out as very low-density lipoprotein or stored in lipid droplets, a neutral form of lipid usually recognized as non-toxic. Excessive fatty acid can also lead to the overproduction of diacylglycerols and ceramides, which can induce lipotoxicity by promoting ROS overproduction and triggering hepatocyte apoptosis[26]. NAFLD patients usually have elevated bile acid levels throughout the body, which links closely to the leaky gut condition and dysbiosis in NAFLD patients[27]. Increased bile acid is hepatotoxic as it generates ROS and damages the mitochondria[28]. The leaky gut condition, which is related to the ability of bile acid to increase intestinal permeability, enables endotoxins from the microbiome to activate the host immune system and, in turn, causes hepatocyte stress and damage. Oxidative stress, lipotoxicity, and hepatotoxic bile acid also induce endoplasmic reticulum (ER) stress, which is the hub of hepatocarcinogenesis. Moreover, chronic low-grade ER stress, similar to that observed

in mice fed with a high-fat diet, leads to increased hepatic gluconeogenesis and, in turn, results in hyperglycemia, forming another vicious cycle[29]. In summary, several risk factors and preconditions for NAFLD/NASH could induce both oxidative stress and ER stress, which are well known to promote hepatocarcinogenesis.

Other factors involved in NAFLD/NASH development may also link to HCC development. An emerging view of the causative role of macrophages in the pathogenesis of NAFLD/NASH is that intrahepatic macrophages can function in this process independent of their proinflammatory status. Specifically, macrophages can promote disease establishment by producing non-inflammatory factors such as IGFBP7 and miR-144, which regulate antioxidative response and metabolic activities of hepatocytes[30,31]. Whether dysregulated intrahepatic macrophages can promote hepatocarcinogenesis with non-inflammatory factors is still an open question, but such a possibility should not be neglected. Also, hyperinsulinemia, usually seen in preconditions of NAFLD/NASH, may promote HCC development through several mechanisms. On the one hand, insulin can promote the proliferation of malignant cells by activating the insulin receptor IR-A isoform, which is less common and mainly expressed in fetal and cancer cells. The activation of the IR-A isoform stimulates the activation of extracellular signal-regulated kinases 1/2 (ERK1/2) and Ak strain transforming (AKT) and, in turn, leads to anti-apoptotic and pro-proliferative effects[32,33]. On the other hand, a high serum level of insulin increases the hepatic expression and surface translocation of growth hormone receptor (GHR)[34]. This leads to elevated activation of GHR, thereby stimulating the production and secretion of mitogenic insulin-like growth factor 1 (IGF1), which has been found to increase in different malignancies,

including HCC. Moreover, high insulin levels also reduce the expression of IGF1 binding proteins, leading to higher IGF1 bioavailability and consequently elevated activity and mitogenic effect[35]. Other functionally relevant mechanisms that link hyperinsulinemia to HCC include an insulin-mediated increase of matrix protein secretion and impairment of β-oxidation of fatty acid[36].

1.3.3 Pathological abnormalities of established NASH promote HCC development

Patients with fully established NASH have a higher risk (annual incidence from 2.4% over seven years to 12.8% over three years, or 5.29 per 1000 person-years) for HCC compared to individuals with obesity or patients with simple NAFLD (0.44 per 1000 person-years) or T2DM[9,37-39]. Particular abnormalities of established NASH, absent in metabolic syndrome and simple steatosis, promote HCC initiation. Such abnormalities include DNA damage, inflammation and dysregulated immune system, and fibrosis/cirrhosis.

1.3.3.1 DNA damage

NASH patients with HCC have more hepatic DNA damage resulting from oxidative stress compared to NASH patients without HCC[40]. Various mechanisms might cause the increased DNA damage. These include elevated oxidative stress, the survival of hepatocytes with excessive DNA damage, changes in the DNA damage repair process, or a combination of these in patients with NASH-related HCC. The first circumstance may result from long-term necroinflammation or stress from chronic dysregulated metabolism in hepatocytes, as discussed earlier. Abnormal consecutive activation of the antioxidative KEAP1-NRF2 (Kelch-like ECH-associated protein 1-nuclear factor erythroid 2-related factor 2) pathway can induce the survival of

hepatocytes with excessive DNA damage, and corresponding mutations were found in human HCC samples[41]. Excessive metabolic substrates inhibit the autophagy pathway, helping the hepatocyte with DNA damage escape from autophagy-dependent cell death[42]. Impaired DNA damage repair has been found in NASH patients. Schults *et al.* discovered that NASH patients with high neutrophilic influx had significantly reduced nucleotide excision repair capacity resulting from impaired damage recognition[43]. Non-homologous end-joining (NHEJ) for DNA double-strand break repair has been found to increase in HCC, and the key enzyme DNA-dependent protein kinase is upregulated and associated with poor survival[44]. NHEJ can be error-prone in certain situations, and increased NHEJ can promote HCC initiation and progression. Although the relationship between changes in NHEJ and NAFLD/NASH is not yet established, some hints are present. For example, the critical enzyme in the *de novo* fatty acid synthesis, FASN, has been found to upregulate NHEJ[45].

1.3.3.2 Hepatic inflammation and dysregulated immunity

Extensive studies have established the pivotal role of chronic hepatic inflammation and dysregulated immunity in NASH-related HCC development. The innate and adaptive cell immune populations, including macrophages, T cells, neutrophils, NK cells, B cells, and others, have dysregulations that promote hepatocarcinogenesis.

Macrophages and myeloid-derived suppressor cells

Intrahepatic macrophages in the NASH condition can be very heterogeneous. According to their origin and activation status, with the help of novel single-cell sequencing technology, intrahepatic macrophages in NASH can be divided into tissue-

resident Kupffer cells, monocyte-derived temporary macrophages, monocyte-derived inflammatory macrophages, and others[46]. In mechanistic studies, macrophages are usually classified into Kupffer cell and infiltrating macrophage/monocyte-derived macrophage or functionally categorized into classically activated M1 or alternatively activated M2 macrophage, albeit an oversimplified model. It was not until recently that the detailed transcriptional difference between Kupffer cell and hepatic infiltrating macrophage was appreciated[47]. Alterations in the intrahepatic macrophage are important in driving the pathogenesis and progression of NASH as well as HCC development in NASH. The intrahepatic macrophage is commonly believed to have gone through M1 polarization in NAFLD and NASH in response to hepatocyte damages and cytokines or immunogens from the leaky gut, which in turn increases proinflammatory cytokine and ROS release and further stresses the hepatocyte and augments the inflammation. Proinflammatory cytokines also induce insulin resistance by activating NF-κB (nuclear factor kappa-light-chain-enhancer of activated B cells) and JNK (c-Jun N-terminal kinase) pathways[48]. Although there is some new insight about whether macrophage goes through M1 activation in early NAFLD or obesity rather than influencing hepatic homeostasis with non-inflammatory factors, there is little doubt that intrahepatic macrophages are more proinflammatory in fully established NASH. In contrast, while chronic hepatic inflammation is the rising environment for HCC, in the initiation and progression of HCC, intrahepatic macrophages are observed to undergo M2 activation that induces immunosuppression and produces mitogens to promote survival and proliferation of tumor-initiating cells or tumor cells. It has been demonstrated in the diethylnitrosamine (DEN) induced mouse model of HCC that the

Western diet can induce NASH and promote macrophage M2 activation and HCC development[49]. Myeloid-derived suppressor cells (MDSCs) are a heterogeneous population of myeloid cells whose number increases in pathological conditions, including NASH and HCC[50-52]. MDSCs have a potent immunosuppressive effect, and their activities against the anti-tumor function of intrahepatic macrophage and cytotoxic CD8 T cells have been observed in HCC[53,54].

T cells

Cytotoxic CD8 T cells are essential in the clearance of malignant cells, and their number in NASH liver increases in response to proinflammatory cytokines. However, an increased number and enhanced activation of CD8 T cells have been suggested to promote NASH establishment and NASH to HCC transition in a mouse model for NASH[55]. Moreover, persistent activation of CD8 T cells, frequently seen in the NASH condition, will induce CD8 T cell exhaustion and the activation of other immunosuppressive types of machinery, eventually leading to the loss of surveillance against malignant cells. In the pathogenesis and progression of NASH, CD4 T cells are biased towards Th1 and Th17 phenotypes and promote steatosis and inflammation[56-58]. In contrast, like the notion that tumor-targeting helper CD4 T cell is usually beneficial in the HCC stage, the loss of specific subtypes of CD4 T cells that presumably recognize neoantigen is important in the progression from NASH to HCC. As shown by Ma *et al.*, significantly decreased CD4 T cell number could be seen in different mouse models for NASH-related HCC in the NAFLD stage, and CD4 T cell depletion caused more hepatic tumor lesions[59]. The reduced CD4 T cell might be due to cell death induced by excessive hepatic fatty acid taken by CD4 T cell and subsequent increased

mitochondrial ROS production[59]. A subset of CD4 T cells, regulatory T cell (Treg), is important in restricting inflammation and resolving the wound healing process. Thus, Treg can be beneficial in controlling NASH progression and in the recession of fibrosis. Decreased Treg cell number was seen in several studies using mouse models of NAFLD, as reviewed by Van Herck *et al.*[56], which is probably the result of elevated ROS[60]. In contrast, in the HCC stage, Treg is increased in patients and preferably located at the tumoral lesion[61,62]. Functional assays indicated that HCC-associated Treg could inhibit CD8 T cell expansion[62]. However, no study has provided in-depth insight explaining if the transition from decreased Treg in the NASH stage towards increased Treg in the HCC site is regulated by tumor cells or is an event that could appear in NASH condition in response to high CD8 T cell activity and fibrosis/cirrhosis.

Neutrophils

In response to damage or infection, neutrophils are quickly recruited as the effector cells of innate immunity in various tissues. They are known to infiltrate fatty livers and contribute to NASH pathogenesis[63]. Neutrophils were recently revealed to promote the progression of NASH to HCC by releasing neutrophil extracellular traps (NETs). Increased NETs in NASH livers recruit macrophages and promote HCC-inducing chronic liver inflammation[64]. NETs also promote NASH-related HCC by inducing the differentiation of CD4 T cells into Tregs through enhancing mitochondrial oxidative phosphorylation[65].

NK cells

NK cells are the innate cytolytic cells with a tumor surveillance role and are particularly abundant in the liver in both humans and mice[66]. Apart from direct tumor

surveillance, NK cells can also induce the apoptosis of hepatic stellate cells (HSCs), thus restricting fibrosis[67]. While NK cells are beneficial against the progression from NASH to HCC in these ways, NK cells can promote hepatic inflammation through cytokine secretion and induction of hepatocyte death. Indeed, NK cells have been demonstrated to play an evil role in promoting chronic inflammation of NASH in mouse models[68,69], and an immunoregulatory role of NK cells on polarizing macrophage towards M1-like phenotypes has been described in a mouse model of NASH[70]. However, a recent study showed that in a human cohort, the number, frequency, phenotype, and functionality of NK cells in both the circulation and tissues, including adipose tissue and liver, was not substantially changed in biopsy-confirmed NAFL or NASH patients compared to healthy controls[71]. While the clinical relevance of the NK cell's role in NASH is still under debate, reduced NK cell number and activity have been reported in human HCC and are associated with poor prognosis[72]. The abnormal NK cells with inhibited activity in the HCC microenvironment could be induced by several factors, including increased Tregs, increased MDSCs, and high expression of immune checkpoint receptor Tim-3 in NK cells[72-74]. An intriguing question would be whether the chronic inflammation in NASH could exhaust NK cells and contribute to the suppressive phenotype of NK cells in HCC[75], although research has shown that NK cells might not be changed in NASH patients[71]. A recent study shed some light on this question. Nishina *et al.* demonstrated that CD26 expressed by HCC cells serves as a peptidase (DPP4, dipeptidyl peptidase 4) to truncate chemokine CXCL10 (C-X-C motif chemokine ligand 10) and restricts NK cell recruitment and activation. Using a mouse model for NASH-related HCC, they showed that continuous administration of DPP4 inhibitor to

mice started around the time of NASH development did not improve the parameter of NASH but reduced liver tumor volume and number and increased the infiltration of activated NK cells to both the tumor and non-tumor liver[76]. Further study is needed to elucidate if the NK cell defects in NASH-related HCC are solely induced by tumor cells and tumor microenvironments.

B cells

B cell actively promotes NAFLD/NASH pathogenesis and progression through antibody-dependent and independent mechanisms[77-80]. However, high B cell infiltration to HCC correlated with prolonged survival after curative resection, which could result from the anti-tumor immunoglobulin production of B cells[81]. Moreover, Zhang *et al.* found that in their HCC patient cohorts whose etiology was not revealed, the density of B cells decreased in the tumor compared to non-tumor liver, and increased B cell infiltration to the tumor was associated with better survival[82]. Similar to other immune cells, not all subtypes of B cells are friendly in HCC. A PD-1^{hi} (programmed cell death protein 1 high) B cell subset has been identified in human HCC, which can suppress anti-tumoral T cell immunity and promote tumor growth through IL-10 (interleukin 10) secretion[83]. B cells with FcγRII$^{low/-}$ activated phenotype have been found in human HCC with a high frequency, which also suppresses cytotoxic T cell activity[84]. The generation of pro-tumor immunosuppressive B cells has been linked to NASH. The accumulation of IgA-producing cells expressing PD-L1 and IL-10 that can suppress cytotoxic CD8 T cells has been demonstrated in humans and mice with NAFLD[85]. The generation of immunosuppressive B cells could correspond to the demand for limiting CD8 T cell-induced tissue damage in NASH conditions and could be induced by factors produced

by intrahepatic macrophage and CD4 T cells. Thus, depending on their phenotypes, B cells play different roles in both the NASH and HCC stages, where immunosuppressive B cells are generated to restrict chronic inflammation of NASH fueled by diverse immune populations, including B cells. However, this type of B cell also compromises CD8 T cell activity, resulting in HCC initiation.

Taken together, the dysregulated immunities in NASH and HCC have many distinctions, which are also reviewed elsewhere[86]. However, the transitions from the dysregulated immunity of NASH to a differently dysregulated immunity in HCC could rationally occur, altering several types of immune cells. For example, the chronic activation of CD8 T cells in NASH induces tissue damage and NASH progression, and at the same time, activates immunosuppressive types of machinery and promotes T cell exhaustion, leading to reduced activity of CD8 T cells, surveillance evasion of tumor-initiating cell and subsequently enhanced immunosuppression driven by cancer cells. As shown in many studies using mouse models, the attenuation of dysregulated immunities either in the NASH stage or the HCC stage could inhibit the initiation and progression of NASH-related HCC.

1.3.3.3 Cirrhosis

While NASH-related HCC can develop in the absence of cirrhosis or fibrosis, cirrhosis is associated with a higher risk of HCC in NASH conditions, as demonstrated in many observational studies, including a recent one. A retrospective cohort study in the US matching 296,707 NAFLD patients with controls found an annual incidence of 10.6/1000 person-years in NAFLD patients with cirrhosis versus 0.08/1000 person-years in those without cirrhosis[87]. Fibrosis, the key feature of cirrhosis, is induced by

chronic necroinflammation in NASH. In this process, HSCs are activated and transdifferentiated into the myofibroblasts that produce extracellular matrix (ECM). ECM is usually made to maintain the liver structure and can be gradually removed after acute or curable liver injury as the reproduction of hepatocytes and wound healing proceeds. However, in a chronic injury like NASH, excessive ECM persists and accumulates, leading to cirrhosis and permanent loss of liver function. Liver cirrhosis is present in 70~90% of HCC patients, but 20 to over 50% of NAFLD-associated HCCs develop from non-cirrhotic liver[88,89]. An important question would be: is cirrhosis that sometimes precedes NASH-related HCC a direct contributor to HCC development or just an indicator of the severity of necroinflammation in NASH and a part of the constant tissue regeneration process? The opposite view of the common notion that cirrhosis is a risk factor for HCC is continuously rising, suggesting that fibrosis may impose physical space restriction on HCC development and promote immunosurveillance, thus impeding HCC development[90]. Considering this view and the fact that most NASH patients do not have cirrhosis, and NASH-related HCC can develop in the absence of cirrhosis[87], prevention and treatment methods for NASH-related HCC should not be limited to those that possess the effect to improve cirrhosis. This is especially reasonable for the treatment of cancer since it has been shown that in pancreatic ductal adenocarcinoma (PDAC) patients, fewer myofibroblasts in tumor correlated with reduced survival, and in mouse models for PDAC, the depletion of myofibroblast and the reduction of tumor-stromal content has detrimental rather than beneficial effect[91,92]. Nevertheless, liver cirrhosis, a possible result of NASH progression and HCC risk factor that can be monitored non-invasively by elastography, might serve as a useful marker in identifying

medication that reduces HCC risk in NASH patients by improving cirrhosis.

In summary, the process of NAFLD-related HCC development is the transformation of susceptible hepatocytes or progenitor cells in a chronically pro-tumor microenvironment. A question remains: how crucial is the pro-tumor microenvironment in the development of HCC? Can altered non-parenchymal cells sufficiently transform the parenchymal cells of the liver? The fact that we are shifting to rely on boosting the immune system instead of directly inhibiting the growth of tumors to treat HCC hints at a more critical role of non-parenchymal cells in hepatocarcinogenesis.

1.4 Sex-related mechanisms of HCC development

1.4.1 Overview

The previous section discussed the mechanisms of NAFLD-related HCC development in detail. The central theme revolves around a cyclic process involving cell stress and damage, immune response, and regeneration. This cycle ultimately results in the accumulation of genetic and epigenetic alterations, contributing to the development of HCC. This process is also a common theme in other etiologies of HCC, including excessive alcohol consumption and viral infection. However, one factor adds to the complexity of hepatocarcinogenesis mechanisms: the sex of organisms. In fact, the incidence rate of HCC and the survival time of patients are significantly different for males and females. Moreover, HCCs from male or female patients have differentially activated oncogenic pathways[93]. HCC has the most significant sex differences in autosomal mutational profiles among cancers of non-reproductive tissues in 18 tumor types examined[94], suggesting different mechanisms underly HCC development between men and women. The factors underlying the sex-related mechanisms of HCC

development include sex hormones, non-sex-hormonal sex-differential factors, and sex disparities in environmental exposure. Significantly, genetic and epigenetic differences between men and women critically affect susceptibility to cancer, while environmental exposures alone may only explain some of the sex disparities in cancer[95].

1.4.2 Sex hormones and HCC development

Sex hormones influence the development of malignancies, including HCC. The male-to-female HCC incidence rate ratio peaks at 50-54 years of age and decreases thereafter[96], supporting the role of sex hormones in the sex discrepancy of HCC development in humans. The current knowledge attributes a vast part of the sex discrepancy of HCC development to the protective effect of estrogen and the harmful effect of the androgen receptor. The activities of sex hormones are not limited to the activation of nuclear receptors and subsequent transcriptional regulation by them. Nevertheless, I will focus on the interactions between HCC development and the activation of estrogen receptors and androgen receptors.

1.4.2.1 Estrogen and estrogen receptors

Estrogen and androgen receptors are the nuclear receptor class of transcription factors. Typically, they bind their steroid ligands in the cytosol and recognize their response elements in the nucleus to regulate gene transcription. They can also bind genomic DNA indirectly by interaction with other transcription factors[97]. The activation of estrogen receptors inhibits multiple HCC-promoting processes, including inflammation, fat accumulation, and fibrosis. It also suppresses pro-tumor pathways and oncogene expression in HCC cells to attenuate HCC progression.

A seminal study reported that male's high production of proinflammatory cytokine

IL-6 is crucial in the male-biased HCC development in the carcinogen DEN-induced mouse model of HCC, where the elevated IL-6 expression can be inhibited by estrogen or estrogen receptor α (ERα) agonist[98]. ERα possibly inhibits IL-6 transcription by disrupting the NF-κB-mediated transcription activation of proinflammatory cytokine genes[99-101]. Activated ERβ can similarly repress the transcription of proinflammatory cytokine genes[102]. Liganded ERα can also bind to the promoter and activate the transcription of protein tyrosine phosphatase receptor type O (PTPRO), an inhibitor of the proinflammatory signal transducer and activator of transcription 3 (STAT3) signaling[103].

Estrogen acts on ERα expressed in hepatocytes to inhibit the triglyceride accumulation in the liver[104,105]. It is reported that the loss of hepatocyte ERα increased the expression of lipid synthesis genes and disrupted the regulation of other genes related to lipid metabolism[106,107]. Mechanistically, ERα indirectly regulates lipid synthesis gene expression by controlling the transcription factor small heterodimer partner (SHP) and microRNA mir-125b[108-111]. Non-canonical membrane-associated ERα, when activated, is also reported to reduce hepatic lipids. The underlying mechanisms are the phosphorylation of AMP-activated protein kinase (AMPK) by ERα and subsequent inhibition to *de novo* lipogenesis by acetyl-CoA carboxylase phosphorylation and repressed expression of cholesterol synthesis genes by the phosphorylation of sterol regulatory element-binding factor 1 (Srebf1)[112]. Estrogen treatment also promotes fatty acid oxidation in mice[113]. In addition, ERα is important in regulating hepatic glucose production (HGP), as ERα knockout promotes HGP and impairs insulin's suppression to HGP[106,114]. Activated ERα stimulates hepatic

cholesterol secretion to bile, which might increase hepatic lipid removal[115].

Liver fibrosis is more common in males than in females. As discussed previously, fibrosis is the result of liver damage; thus, it is perceivable that anti-inflammatory and anti-steatosis estrogen and estrogen receptors can inhibit cirrhosis[116-118]. Apart from interfering with the root cause, estrogen can directly inhibit fibrosis. Estrogen can directly inhibit the proliferation and ECM secretion of HSCs[119], which is initially inferred to be mediated by ERβ rather than ERα[120]. The role of ERβ is supported by later studies showing that ERβ agonist inhibits HSC activation[121], and the antagonist of ERβ, but not ERα, blocks estrogen's inhibition to the oxidative stress-induced HSC activation[122]. The repressive effect of activated ERβ to HSC activation might be through the inhibition of ROS-mitogen-activated protein kinase (MAPK) pathways[122]. Other mechanisms of estrogen's inhibition to fibrosis include increasing the expression of miR-19b that targets fibrosis-promoting growth factor receptor-bound 2 and increasing the expression of anti-fibrotic miR-29, but the related downstream signaling is unknown[123,124].

Estrogen and estrogen receptors can attenuate HCC progression by inhibiting oncogene expression and suppressing oncogenic pathways in HCC cells. As mentioned above, they inhibit STAT3 and MAPK signaling, two important oncogenic pathways. Estrogen attenuates the progression of orthotopic homograft of HCC by mediating cell cycle arrest, apoptosis, and reduced invasion[125]. The researchers suggested that the activation of ERα is crucial in the process where it inhibits NF-κB-mediated oncogenic pathways[125]. ERα is also shown to directly bind the promoter of the oncogenic metastasis associated 1 gene and repress its expression and subsequent oncogenic activites[126]. The expression of potentially oncogenic peroxisome proliferator-activated

receptor γ (PPARγ) in HCC cells is inhibited by activated ERα and ERβ[127]. Activated ERα inhibits the induction of potentially oncogenic miR-21[128]. ER is found to directly bind and activate the promoter of genes encoding enzymes in the *de novo* nicotinamide adenine dinucleotide (NAD^+) synthesis that protects cells from HCC-causing DNA damage. However, the article did not mention the exact isoform of ER involved[129].

1.4.2.2 Androgen and androgen receptor

The role of androgen receptor (AR) in hepatocarcinogenesis and HCC progression is more evident than the role of androgens. AR's promotion to HCC development is established by a seminal study that generated hepatocyte-specific AR knockout mice and demonstrated that knockout mice developed delayed and less DEN-induced HCC[16]. Notably, the study showed comparable testosterone levels in control and hepatocyte-specific AR knockout mice and a similarly reduced HCC burden in female mice with hepatocyte-specific AR knockout compared to control female mice. Moreover, AR overexpression strongly promotes anchorage-dependent and -independent growth of human HCC cells regardless of androgen treatment[16]. These results establish the model where AR, rather than androgens, is crucial in HCC development. Other studies all support this model[130]. However, this model raises the question of whether AR-related mechanisms of HCC development contribute to the sex disparity of the disease at all. As androgens and AR are reported to protect against steatosis and fibrosis[131], similar to estrogen and estrogen receptors, the contribution of AR to HCC development is mainly to the transformation of cells and disease progression. A few mechanisms underlying the direct stimulation of oncogenesis by AR were reported, including enhancing ROS generation and DNA damage, inhibiting p53-

mediated DNA damage repair and apoptosis[16], direct activation of the promoter of gene encoding cell cycle-related kinase and subsequent activation of β-catenin[132], and direct transcriptional activation of the pri-miR-216a whose mature form targets the tumor suppressor cell adhesion molecule 1[133].

1.4.3 Non-sex-hormonal sex-differential factors in HCC development

A small number of genes differentially expressed between males and females are identified to be involved in the process of hepatocarcinogenesis. These genes can be partially regulated by sex hormones in gene expression or encoded by the sex chromosomes, resulting in different levels between sexes and sex-different HCC development.

Prolactin (PRL) is an estrogen-responsive pituitary hormone also expressed in males. DEN induces more frequent and malignant HCCs in *Prl* knockout mice than wild-type mice in both sexes[134]. Mechanistically, PRL functions through its binding to short-form prolactin receptor in hepatocytes and promotes the degradation of the tumor necrosis factor (TNF) receptor-associated factor, resulting in inhibited activation of MAPK, NF-κB, and AKT signaling pathways induced by IL-1β, TNF-α, or lipopolysaccharides (LPS)[134]. As males also express the PRL receptor mediating the protective effect against HCC development, male mice were shown to benefit from pro-PRL treatment[134], and females might be naturally protected by higher PRL expression, especially during pregnancy.

Adiponectin is an important adipokine produced by the adipose tissue. The androgen testosterone was found to activate JNK and concurrently decrease adiponectin production by adipose tissue[135]. Indeed, adiponectin levels are lower in

male mice than female mice and increase to the level of females in castrated males. Adiponectin knockout female mice had increased growth of subcutaneously allografted HCC cells, and males with adiponectin overexpression developed fewer DEN-induced liver tumors. The proposed underlying mechanism is the adiponectin-induced AMPK and p38α activation in allografted cancer cells[135]. The demonstrated effect of adiponectin against HCC in this study is more likely to be related to the progression than the initiation of disease.

The expression of miR-26a and miR-26b was higher in the nontumor liver of female HCC patients compared to male patients, while the tumors had reduced miR-26 expression[136]. Although the mechanism underlying differential miR-26 levels between sexes is unknown, miR-26a was shown to target the transcripts of cyclin D2 and E2 directly, and therapeutic delivery of miR-26a inhibited HCC progression[137]. Since a sex-related regulation of miR-26 expression in the liver has yet to be described 14 years after the initial finding of the sex-discrepant expression, miR-26 expression may be associated more with the degree of HCC malignancy than sex. Similarly, a cytochrome P450 superfamily enzyme, CYP39A1, was found to be expressed higher in the nontumor liver of female HCC patients compared to male patients and had reduced expression in HCC samples[138]. Beyond its P450 enzyme activity, CYP39A1 suppresses c-*myc* (cellular myelocytomatosis, or MYC) transcriptional activity, and its overexpression inhibited the initiation and progression of HCC in mouse models[138]. The sex-related expression regulation of CYP39A1 was also not discussed in this study.

Factors encoded by genes on the Y chromosome can naturally have differential expression between sexes due to different gene dosages. Some of these factors are

involved in HCC development and may contribute to its sex differences. The Y-located testis-specific protein Y encoded (TSPY) is expressed in the HCCs of a subset of male patients and correlated with poor survival of male patients[139,140]. The overexpression of TSPY in an HCC cell line upregulated cell-cycle-related genes and suppressed tumor suppressor genes[140]. The sex-determining region on Y chromosome (SRY) was initially identified as an oncogenic transcription factor that directly activates the promoter of the octamer-binding transcription factor 4 (OCT4 or POU5F1) gene and indirectly promotes MYC activation by regulating the expression of a transcriptional coactivator[141,142]. In HCC cell lines, knocking down SRY suppressed anchorage-independent growth, invasiveness, tumorigenicity, and other cancer stem-like phenotypes[141,142]. Later, frequent SRY overexpression was found in male HCC samples, and male and female mice with liver-specific SRY overexpression were found to have increased susceptibility to DEN-induced HCC development. The proposed mechanism of accelerated oncogenesis of mice with hepatic SRY overexpression is the upregulation of platelet-derived growth factor receptor alpha (PDGFRα), a reported target of SRY, and subsequent activation of PI3K (phosphoinositide 3-kinase)/AKT pathway[143]. In normal conditions, the RNA-binding motif gene on Y chromosome (RBMY) is exclusively expressed in the testis. It was abnormally detected in some HCCs from male patients and proposed as an oncogene due to its ability to transform the mouse fibroblast NIH/3T3 cells[144]. The oncogenic property of RBMY was then validated using a liver-specific transgenic mouse model with and without DEN treatment, where RBMY overexpression induced spontaneous HCC and increased the susceptibility to DEN-induced HCC[144,145]. The underlying mechanism was finally identified as RBMY's

inhibition to the activity of glycogen synthase kinase 3β (GSK3β) and subsequent activation of β-catenin signaling, and high RBMY expression was also found to be associated with poor prognosis of HCC patients[146]. In summary, males' Y chromosome encompasses several proto-oncogenes that are active in male HCCs.

1.4.4 Sex disparities in environmental exposure to HCC risk factors

The sex disparities in environmental exposure to HCC risk factors should be categorized into two types. The first type of sex disparity is history or social-related, for example, the disparity of alcohol exposure. The second type of sex disparity of exposure results from the interaction between HCC risk factors and the genetic and epigenetic differences between the sexes.

Females consumed less alcohol, contributing to the sex disparity of HCC development[147]. However, such difference has been diminishing in recent years[148], and it is important to note that females are more susceptible to liver damage induced by alcohol due to females' smaller gastric ethanol metabolisms[149]. The rising HCC incidence in females in the US thus might partially be attributed to females' increased alcohol consumption.

More females are obese than males, possibly due to higher fat accumulation in females driven by evolution[150]. Moreover, a more significant portion of HCC cases were attributable to excess body weight in females than in males[150]. Females' higher susceptibility to fat-related HCC might contribute to the faster increase of HCC incidence rate in females compared to males in the background of the global epidemic of obesity.

The relative prevalence of HBV and HCV between sexes is region-dependent,

albeit HBV infection is mostly more prevalent in males[151]. In the viral etiology of HCC, the interactions between sex hormones and viral infection are important in the sex disparities of carcinogenesis. In short, the replication of HBV is stimulated by androgen signaling and inhibited by estrogen signaling[152]. Mechanistically, activated AR directly binds the HBV enhancer I region and increases the production of HBV RNAs[153]. Moreover, the HBV X protein (HBx) was found to enhance the transcriptional activity of AR by activating the c-*src* (cellular sarcoma) and inactivating GSK3β[154], forming a vicious cycle that constantly boosts HBV transcription and, subsequently, virus replication. In contrast, ERα represses HBV gene transcription indirectly by interacting with hepatocyte nuclear factor 4α (HNF4α) and disrupting its binding to the HBV enhancer I[155]. Altogether, males are more exposed to HBV-related HCC development.

Overall, tremendous differences exist between mechanisms of hepatocarcinogenesis in males and females, and males' and females' HCC have vastly different mutational profiles and oncogenic pathway activation. Although many sex differences of HCC have been identified, a stunning gap in our current knowledge is that no mechanism that preferably drives HCC development in females has been reported.

1.5 Transcriptional coregulator and cancer development

1.5.1 Overview

Optimal transcription activation of genes by RNA polymerase II requires basal transcription machinery, transcription activators that bind the cis-regulatory region, and transcriptional coregulators. Transcriptional coregulators can be coactivators or corepressors depending on the direction of transcriptional regulation. Still, one transcriptional coregulator can be a coactivator for the transcription of one gene and a

corepressor for another gene. Transcriptional coregulators are recruited onto gene promoters to influence the gene transcription rate by interacting with DNA-binding transcription factors, and they are not basal transcription factors. Given this broad definition, it was estimated that thousands of proteins could be classified as transcriptional coregulators[156]. They usually function in multi-protein complexes and modulate transcription through diverse mechanisms, including chromatin remodeling, post-translational modifications of non-histone proteins, and recruitment of the basal machinery and other coregulators[157]. Therefore, transcriptional coregulators can have vastly different molecular functions, including the activities of acetyltransferase, deacetylase, methyltransferase, demethylase, ubiquitin ligase, deubiquitinating enzyme, adenosine triphosphate (ATP) -dependent chromatin remodeler, kinase, phosphatase, protein recruiter, and others. The same transcriptional coregulator can have interaction domains compatible with different transcription factors, and it can also have different domains that repress or activate transcription via different mechanisms. To regulate biological processes at the transcription level, cellular signaling pathways frequently modulate the activities of transcriptional coregulators by altering their expression level and post-translational modifications.

Many coregulators tend to form complexes that are used universally by various transcription factors to regulate the transcription of all genes controlled by RNA polymerase II. Examples include components of the SWItch/Sucrose Non-Fermentable (SWI/SNF) chromatin remodeling complex, CREB-binding protein (CBP)/p300, TATA-box binding protein-associated factors (TAFs), and mediator protein complexes. However, some transcriptional coregulators can be associated with a specific general

physiological process by regulating the transcription of different genes with different transcription factors and functional domains[157]. For example, peroxisome proliferator-activated receptor-gamma coactivator 1α (PGC1α) regulates the stress-responding energy metabolism with various transcription factors, including PPARα, PPARγ, thyroid hormone receptor β (TRβ), glucocorticoid receptor (GR), myocyte-specific enhancer factor 2C (MEF2C), nuclear respiratory factor 1 (NRF1), HNF4α, and estrogen receptor-related receptor α (ERRα)[158-160]. To interact with different transcription factors, PGC1α uses multiple domains, one of which contains the classic leucine-rich LxxLL motifs[161] (L, leucine; x, any amino acid) and facilitates binding with PPARα, GR, HNF4α, and ERRα. Another proline-rich domain mediates the interaction with PPARγ and NRF1, while a third domain facilitates the interaction with MEF2C. A robust transcriptional activation domain in the N-terminal facilitates the recruitment of RNA polymerase II complex and other transcriptional coregulators, activating the transcription of target genes[162]. The target genes are involved in fatty acid oxidation, tricarboxylic acid cycle, oxidative phosphorylation, mitochondrial biogenesis, and glucose uptake[158].

Similarly, transcriptional coregulators can be the central modulator of carcinogenesis. Steroid receptor coactivator 1 (SRC1, or nuclear receptor coactivator 1, NCOA1) is the first authenticated nuclear receptor coactivator[163]. The SRC family of coactivators has three structurally similar members: SRC1, SRC2, and SRC3 (or NCOA1~3). They are named because of their interaction with nuclear receptors for estrogen, androgen, and progesterone, which is mediated by the nuclear receptor interacting domain containing three LxxLL motifs[164,165]. Other domains of SRC family proteins facilitate interactions with non-nuclear-receptor transcription factors, including

STAT3, p53, NF-κB, E2F transcription factor 1 (E2F1), and activator protein 1 (AP1), and cofactors, including CBP/p300, SNI/SWF chromatin remodeling complex, and others[166]. They also have a C-terminal histone acetyltransferase domain to directly modulate transcription[167]. SRCs are widely reported to promote the development of hormone-responsive cancers, especially breast cancer and prostate cancer. They are referred to as master regulators of cancer progression and metastasis by some researchers[168]. Mice containing the mouse mammary tumor virus (MMTV) -SRC3 transgene develop spontaneous mammary gland tumors, establishing SRC3 as an oncogene[169]. In ER-positive breast cancer, SRC3 activates the transcription of ER-regulated genes, including cyclin D1 and progesterone receptor that promote cell proliferation[170,171]. In mouse models of mammary gland cancer driven by *c-neu* (HER2 or ERBB2) or *ras*, deletion of *Src3* also delayed cancer development[172,173], supporting SRC3's role as an integrator of various oncogenic signaling pathways in breast cancer. Examples of these pathways include NF-κB-mediated B-cell lymphoma 2 (BCL2) expression in response to TNFα, IGF1-IGFR-PI3K-AKT pathway, E2F1-mediated cell-cycle-related gene expression in response to epidermal growth factor (EGF) or IGF1, and metalloproteinase gene expression mediated by polyoma enhancer activator 3/AP1[166].

Some coregulators can simultaneously influence carcinogenesis through transcription regulation and non-transcriptional mechanisms. Phosphatase and tensin homolog (PTEN) is a phosphatase that directly interferes with the PI3K/AKT oncogenic pathways by dephosphorylating phosphatidylinositol (3,4,5)-trisphosphate (PIP3) that activates AKT[174]. The phosphatase and tumor suppressor PTEN can also be found in

the nucleus, and its nuclear localization is crucial to its tumor-suppressing functions in patients[175]. Hepatocyte-specific *Pten* knockout induces spontaneous NASH and HCC in mice. However, the model cannot determine the relative contribution of PTEN's PIP3 phosphatase activity versus nuclear activity to its tumor-suppressing effect[176]. PTEN can function as a transcriptional coregulator in the nucleus and suppresses the malignant transformation of the cell. PTEN was found to directly interact with the transcription factor p73 to activate the transcription of apoptotic genes in cells challenged with genotoxic stress[177]. The proposed mechanism of transcriptional regulation is that PTEN binds p73 at its autoinhibitory sterile α-motif domain and enables the interaction with the cofactor CBP/p300[177]. Using PTEN as an example, a transcriptional coregulator can have substantial extranuclear activities unrelated to its transcriptional regulatory activities, and somehow, both the extranuclear and intranuclear activities influence carcinogenesis.

1.5.2 Nuclear receptor coactivator 5

1.5.2.1 The identification of NCOA5 and its unique structure

Nuclear receptor coactivator 5 (NCOA5), also called CIA, was initially identified as a coactivator for the nuclear receptor subfamily 1 group D members 1 and 2 (NR1D1 and NR1D2). It was named a coactivator independent of AF2 (CIA) since it was purified in an effort to identify novel coregulators that act independent of transcription factors' activation function 2 (AF2) motif that usually mediates ligand-dependent binding of coactivators[178]. Although identified by its interaction with NR1D1 and NR1D2 that lack AF2, NCOA5 also interacts with AF2-containing classic steroid hormone receptors ERα and ERβ and the deorphanized nuclear receptor liver X receptors (LXRs)[178,179]. Thus, it

is commonly referred to as NCOA5, although it is structurally distinct from the p160 family nuclear receptor coregulators NCOA1~3. NCOA5's structure is unique in two aspects. First, the protein has a motif with the amino acid sequence of IQSLINLL that contains overlapping LxxLL motif and ΦxxΦΦ (Φ, hydrophobic amino acid) motif that are used by coactivators and corepressors to interact with nuclear receptors. Second, NCOA5 has both a C-terminal transcription activation domain and an N-terminal transcription repression domain. With the two different binding motifs, NCOA5 interacts with nuclear receptors in both ligand-dependent and -independent manners[178]. NCOA5 can activate or repress transcription with the transcription activation and repressor domains, and the direction of transcription regulation is likely highly dynamic as the appearance of other coregulators can invert the direction of regulation[180]. The molecular mechanisms by which NCOA5 activates or represses transcription are unknown. A possible mechanism of NCOA5's repression to transcription is mediated by the arginine and aspartic acid-rich (R/D) region in the transcription repression domain, where it may bind RNA and repress the activity of RNA polymerase II, as NCOA5 was found to bind the coding region of genes that it repressed and was not released during transcription elongation[180].

1.5.2.2 NCOA5 is linked to carcinogenesis and modulates immune response, glucose and lipid metabolism, and cell growth

Not many genes have been validated as directly regulated by NCOA5, but the first one identified had already linked NCOA5 to carcinogenesis. ERα activates c-*myc* transcription in a ligand-dependent manner in breast cancer[181]. Jiang *et al.* from Dr. Hua Xiao's lab found that NCOA5 is associated with the c-*myc* promoter in ER-positive

breast cancer cells in an estrogen-dependent manner and is not dissociated in transcription elongation. NCOA5 alone does not significantly influence the activation of the c-*myc* promoter by liganded-ERα. But when expressed with another cofactor, TIP30, NCOA5 represses the c-*myc* promoter activated by liganded-ERα[180]. In human neuronal cells, NCOA5 was found to interact with ERα and the distal promoter of the retinoic acid-related orphan receptor-alpha (RORA) gene and enhance the RORA transcription with liganded-ERα[182]. Since the downregulation of RORA was implicated in the development of autism spectrum disorder and the autoimmune disease multiple sclerosis[182,183], NCOA5 is again beneficially regulating the transcription of genes. Interestingly, salmon NCOA5 was found to bind CpG oligonucleotides directly, which can trigger an immune response in salmon leukocytes, possibly via NCOA5's R/D region[184]. Because this DNA binding has low specificity and is not involved in transcription, NCOA5 is still regarded as a transcriptional coregulator, and no other direct binding of NCOA5 to DNA has been reported. Like the case for PTEN, NCOA5 might have functions unrelated to transcription regulation. At that time, a genome-wide association study (GWAS) reported the association of an NCOA5 single nucleotide polymorphism (SNP) with susceptibility to psoriasis, an autoimmune disease[185]. These studies suggest a role of NCOA5 in immune response, albeit one study indicated a mechanism unrelated to transcription regulation, and others did not propose a mechanism. Meanwhile, a study identified a planarian protein homologous to human NCOA5 as essential for the maintenance of the stem cell pool in planarians. NCOA5 was also detected in the pluripotent inner cell mass of mouse blastocysts[186]. Studies thus far offer us a glance at the theme of NCOA5's function, which is regulating immune

response and cell growth.

The seminal study for the physiological function of NCOA5 came out at the same time. Gao *et al.* from Dr. Hua Xiao's lab reported that *Ncoa5* heterozygous deletion in mice induces spontaneous development of NASH-like features and HCC in a male-biased manner[187]. *Ncoa5*$^{+/-}$ male mice displayed increased liver damage and IL-6 expression in intrahepatic macrophages. As mentioned previously, a mechanism by which female is more protected from HCC is that liganded-ERα represses NF-κB-mediated transcription activation of proinflammatory cytokine, including IL-6, while the low estrogen level in males likely renders such repression less effective. Gao *et al.* found that NCOA5 knockdown increased IL-6 expression, and estrogen treatment induced NCOA5's association with IL-6 promoter in macrophage cell lines. These results suggest a new mechanism of NCOA5's transcription regulation function: enhancing liganded-ERα's repression to transcription mediated by NF-κB. Indeed, the study showed that NCOA5 repressed promoter activation induced by LPS and NF-κB in a macrophage cell line. The study also partially attributed the glucose intolerance phenotype of *Ncoa5*$^{+/-}$ male mice to high IL-6 expression, as *Il-6* deletion ameliorated such phenotype. Notably, this study establishes NCOA5 as a haploinsufficient tumor suppressor for HCC, reassuring the role of NCOA5's transcription regulation activities in carcinogenesis. Also, the results of this study suggest a role of NCOA5 in glucose and lipid metabolism, which is potentially related to immune response modulated transcriptionally by NCOA5. The interconnecting roles of NCOA5 in modulating immune response and lipid metabolism were reiterated by an elegant study that identified LXRs as a new type of transcription factor directly interacting with NCOA5. Gillespie *et al.*

found that the crosstalk between the toll-like receptor 3 (TLR3) inflammatory signaling and the lipid efflux process in macrophage is regulated by NCOA5. In macrophages, sterol-activated LXR stimulates the transcription of the gene encoding ATP binding cassette subfamily A member 1 (ABCA1), a membrane lipid transporter**.** In response to inflammatory signals that activate TLR3 signaling and lipids that activate LXR, NCOA5 is recruited to the promoter of *Abca1* and functions as LXR's corepressor, reducing ABCA1 expression and lipid efflux[179]. Reduced lipid efflux can turn macrophages into foam cells, changing the phenotype of macrophages and their immune functions[188].

The possibility that NCOA5 regulates cell growth was also hinted at in Gao *et al.*'s study because young *Ncoa5*$^{+/-}$ male mice already had increased liver damage. Notably, *Ncoa5*$^{-/-}$ mice could not be generated due to the infertility of *Ncoa5*$^{+/-}$ male mice. Xiao's lab later found that IL-6 was also increased in the epididymis of *Ncoa5*$^{+/-}$ male mice, resulting in decreased sperm motility and abnormal sperm morphology, rendering *Ncoa5*$^{+/-}$ male mice infertile[189]. However, *Ncoa5*$^{-/-}$ mice were still not generated even though *Il6* deletion restored most of the *Ncoa5*$^{+/-}$ male mice's fertility[189]. It again suggests that NCOA5 regulates cell growth. Later, NCOA5 overexpression was shown to suppress the proliferation of HCC cell lines and reduce the growth of HCC xenograft in mice[190], and NCOA5 was found to interact with the developmental regulator T-box transcription factor 18 and relieved its repression to the promoter containing T-box binding element[191].

In summary, studies strongly imply that NCOA5 functions in modulating immune response, glucose and lipid metabolism, and cell growth, and naturally, NCOA5 is linked to carcinogenesis.

1.5.2.3 Different functions of NCOA5 in different tissues and cancer types

Studies exploring the association of NCOA5 with different types of cancers bloomed after the identification of NCOA5 as a haploinsufficient tumor suppressor for HCC. However, epidemiological, *in vitro*, and xenograft tumor studies indicate that NCOA5 expression in cancer cells does not always benefit patients. Before diving into various functions of NCOA5 in different types of cancer, it is important to stress that two variants of NCOA5 have been found by the Xiao lab in liver samples from diabetes and HCC patients. At the same time, other studies did not specify the form of NCOA5 in their analysis. These two NCOA5 variants have altered functions compared to wild-type NCOA5[187,190]. The first variant, shortened NCOA5 (SNCOA5), was identified in liver and HCC samples of male HCC patients and normal males[187]. The gene has an extended exon 7, introducing a frameshift and a premature stop codon that eliminates exon 8, which contains the transcription activation domain. SNCOA5 failed to enhance the transcription from an estrogen response element (ERE) promoter activated by liganded-ERα. Although SNCOA5 was shown to be frequently upregulated in HCC samples compared to adjacent non-tumor livers, its specific function is unknown[187]. Another variant, NCOA5T445A, results from a single nucleotide variation (SNV) identified in the adjacent non-tumor livers of patients with concurrent HCC and T2D. The SNV causes a threonine to alanine substitution of wild-type NCOA5 and dampers the proliferation suppression effect of overexpressed NCOA5 to HCC cells *in vitro* and in xenograft mouse model[190]. Thus, it is likely important to determine the form of NCOA5 examined in studies that associate NCOA5 expression with cancer progression.

Several cohort studies reported the association of NCOA5 expression with the

progression of various cancers. NCOA5 low expression was found to be associated with the progression or poor prognosis of esophageal squamous cell carcinoma[192], papillary thyroid carcinoma[193], and cervical squamous cell carcinoma[194]. On the other hand, in patient cohorts of breast cancer[195,196], colorectal cancer[197], and epithelial ovarian cancer[198], high NCOA5 expression was reported to be associated with clinicopathological features, disease progression, or poor prognosis. Although we must caution that different NCOA5 variants in cancer cells might complicate the interpretation of study results, NCOA5 is likely to have different functions in different cell types and tissues.

The detailed mechanisms by which NCOA5 regulates the progression of these cancers are unclear. Some of these studies included mechanistic research that used *in vitro* cell culture or xenograft tumor mouse model to determine the effect of manipulated NCOA5 expression level on the malignancy of cancer cells and the activation of key oncogenic pathways. Pathways observed as influenced by NCOA5 expression in cancer cells include PI3K/AKT[197] and NOTCH3[194]. Interestingly, a similar effect of NCOA5 overexpression on PI3K/AKT/mTOR (mammalian target of rapamycin) activation was reported in bovine mammary epithelial cells. However, this study found that NCOA5 was associated with mTOR promoter[199], suggesting a mechanism unrelated to PI3K/AKT/mTOR signal transduction. The study by He *et al.* reported that NCOA5 knockout in an HCC cell line with high NCOA5 expression inhibited cell proliferation and migration[200], quite the opposite effect compared to the report where overexpression of wild-type NCOA5 in other two HCC cell lines repressed malignancies[190]. The lack of consistency of NCOA5's roles in different types of cancer

might reflect the nature of NCOA5 with dual nuclear receptor binding motifs and both transcription activation and repression domains. The availability of other companion coregulators and the precise expression level of NCOA5 might determine the regulated genes and regulation directions. It can also be caused by neglecting the effect of different NCOA5 variants that may exist in the examined cancer cell lines. In the other spectrum of NCOA5 research, an NCOA5 SNP, once reported as associated with psoriasis[185], was found to be associated with the susceptibility to another two autoimmune diseases, Behçet's disease and multiple sclerosis[201-204]. These reports continuously suggest that NCOA5 has physiological functions that modulate immune responses.

Our understanding of molecular mechanisms by which NCOA5 regulates carcinogenesis has stagnated in recent years, even though many more studies are looking into the association between NCOA5 and cancer. In the model that most faithfully reflects the physiological function of NCOA5, the *Ncoa5*$^{+/-}$ male mouse model of HCC, there are likely other molecular mechanisms by which NCOA5 inhibits HCC development that are worth exploring. Firstly, although heterozygous *Il6* deletion in *Ncoa5*$^{+/-}$ male mice significantly reduced tumor numbers and volumes, mice developed HCC as frequently as those without *Il6* deletion. Even homozygous *Il6* deletion did not completely prevent HCC development in *Ncoa5*$^{+/-}$ male mice. These results indicate mechanisms other than IL-6 upregulation that promote HCC. Secondly, since NCOA5 is a corepressor to the NF-κB-activated *Il6* transcription in intrahepatic macrophages, how is macrophages' NF-κB signaling pathway activated in the first place? Thirdly, does NCOA5 have different functions in hepatocytes and intrahepatic macrophages? Finally,

how does the crosstalk between NCOA5-deficient hepatocytes and macrophages cause the spontaneous transformation of hepatocytes or progenitor cells?

1.5.3 30-kDa Tat-interacting protein (TIP30)

1.5.3.1 The identification of TIP30 as a tumor suppressor and transcriptional coregulator

30-kDa Tat-interacting Protein is also known as the human immunodeficiency virus 1 (HIV1) Tat interactive protein 2 and is usually abbreviated as TIP30 or HTATIP2. It was independently identified and cloned by two groups. Shtivelman identified a gene whose RNA was absent in a subset of highly aggressive small-cell lung cancer (SCLC) cell lines and named it CC3. CC3 was found to induce apoptosis in SCLC cells deprived of growth factors or treated with chemotherapeutic drugs and suppress SCLC cell metastasis *in vivo*[205]. In a separate effort to identify cellular proteins that interact with the activation domain of the Tat transcription factor encoded by the HIV1 genome, Dr. Xiao *et al.* identified and purified a protein with an apparent molecular weight of 30 kDa and named it TIP30. The TIP30 cDNA was cloned and sequenced, and TIP30 was validated to enhance the transactivation by Tat[206]. After the CC3 gene sequence appeared in the public database, it was realized that CC3 and TIP30 are the same protein[207]. In a later effort to determine whether TIP30 is a tumor suppressor, TIP30 deficiency was found to induce spontaneous development of carcinomas in female mice in various organs, including the liver, thymus, ureter, and others. HCC was the most frequent cancer type among tumors developed in female mice with TIP30 deficiency[208]. Thus, TIP30 was initially identified as a transcriptional coregulator and tumor suppressor.

1.5.3.2 TIP30 regulates transcription as a coregulator

The molecular mechanism by which TIP30 regulates the Tat-mediated transcription was delineated later and linked to TIP30's pro-apoptotic function. TIP30 possesses kinase activity in its N-terminal region and mediates the phosphorylation of the C-terminal domain of the largest subunit of RNA polymerase II, stimulating Tat-mediated gene transcription. Cell apoptosis and growth suppression mediated by TIP30 overexpression also rely on the kinase activity of TIP30[209].

The first identified cellular transcription factor interacting with TIP30 is ERα, and the first identified cellular target of TIP30 is c-*myc*. TIP30 can be recruited by liganded-ERα to the promoter of the c-*myc* gene together with NCOA5 and acts as a corepressor. Loss of TIP30 was found to increase ERα-mediated transcription of c-*myc* *in vitro* and increase c-*myc* expression in mouse mammary glands[180].

Several other cellular genes were identified as TIP30 targets, including osteopontin (OPN) and cyclin D1 (CCND1). OPN is an extracellular matrix protein secreted by cancer cells that promotes progression. In human HCC cells, TIP30 was found to repress the transcription of *OPN* by binding to the promoter region associated with the transcription factor ETS1 that activates *OPN* transcription. TIP30 interacts with ETS1 and inhibits the binding of coactivators to repress *OPN* transcription[210]. In lung adenocarcinoma cells treated with EGF, TIP30 can associate with the promoter of *CCND1* and repress its transcription activated by EGF treatment through the recruitment of histone deacetylase 1. The study was not able to identify the transcription factor bound by TIP30 in the *CCND1* promoter and hinted at the direct regulation of transcription by TIP30[211]. However, no study suggests the direct recognition and binding

of DNA by TIP30.

The interaction between HIV1 Tat and TIP30 can also influence cancer metastasis. The introduction of Tat was found to reverse the inhibition of lung cancer metastasis by TIP30 overexpression. Although the study attributed this effect to the non-transcriptional function of TIP30, which we will discuss later, sequestering TIP30 to Tat is likely to relieve the repression of other pro-metastatic gene transcription by TIP30 or might hijack TIP30 to promote the oncogenic gene transcription activated by Tat[212]. In summary, the tumor-suppressing effect of TIP30 is mediated, at least partially, through TIP30's function as a transcriptional coregulator.

1.5.3.3 TIP30 regulates nuclear transport

As presented earlier, certain transcriptional coregulators have non-transcriptional activities, and sometimes, their transcriptional and non-transcriptional functions are both related to carcinogenesis. TIP30 has been found to regulate nuclear transport, membrane fusion, and metabolism via non-transcriptional mechanisms and suppress carcinogenesis or cancer progression.

The kinase activity of TIP30 relies on the N-terminal region nucleotide binding motif for ATP. However, it was also reported that the motif facilitates the binding of nicotinamide adenine dinucleotide phosphate (NADPH), and TIP30 has some structural similarity to the short-chain dehydrogenases/reductases (SDR) family[207,213,214]. Although TIP30 has three of the four necessary parts of the catalytic machinery of SDR reductases, it lacks the required and conserved asparagine residue that stabilizes the structure of the active site[207,215]. It is still unclear whether TIP30 is a reductase or not, and TIP30 can be a reductase and kinase because there are proteins like biliverdin IXα

reductase that catalyze both redox reaction and phosphorylation[216]. Nevertheless, the NADPH binding of TIP30 was proposed as important in TIP30's regulation of nuclear transport[216], although such a hypothesis has not been validated.

King *et al.* found that TIP30 is associated with importin and the nuclear pore complex, and when overexpressed, TIP30 can inhibit nuclear import *in vitro*. The authors suggested that the pro-apoptotic activity was related to the nuclear transport inhibition induced by TIP30 overexpression[217]. Another group further developed this idea. Guo's group found that, in cells under oxidative stress, TIP30 ectopic expression increased the expression of p53, which can induce cell death. They proposed a mechanism where the stabilization of p53 mRNA was elevated by increased cytoplasmic localization of the RNA binding protein Hu antigen R (HuR), which was mediated by TIP30's inhibition of nuclear import under oxidative stress. TIP30 was shown to be oxidized in this setting, but it was not clear whether TIP30 oxidation is necessary for its pro-apoptotic activity[218]. Guo's group followed up this activity of TIP30 in a study where TIP30 was suggested to inhibit the nuclear localization of snail family transcriptional repressor 1 (SNAIL), and increased TIP30 inhibited the epithelial-mesenchymal transition (EMT) of HCC cells by preventing the activity of SNAIL in the nucleus[219]. The same mechanism was proposed in TIP30's inhibition of the EMT of NSCLC cells, but with a twist where HIV1 Tat was shown to repress such activity of TIP30 by inhibiting TIP30's association with importin[220].

In glioblastoma cell lines, TIP30 was shown to inhibit the nuclear localization of the DNA repair enzyme N-methylpurine DNA glycosylase (MPG). Thus, decreased TIP30 expression in glioblastoma cells may confer resistance to DNA-damaging

treatment by increased DNA damage repair by nuclear MPG[221].

In exploring the pathogenesis of remyelination failure in multiple sclerosis, TIP30 overexpression was found to block the differentiation of an oligodendrocyte precursor cell line by preventing the nuclear translocation of Notch1 intracellular domain[222]. Intriguingly, both NCOA5 and TIP30 appear to be related to the pathogenesis of multiple sclerosis, and NCOA5 and TIP30 repress the c-*myc* transcription in cooperation. A chapter of my dissertation will demonstrate that NCOA5 and TIP30 can cooperate to suppress the development of HCC.

1.5.3.4 TIP30 regulates membrane fusion, mRNA translation, and immune cell functions

TIP30's non-transcriptional activities are not limited to changing nuclear import by association with the nuclear pore complex, but it also associates endosomes and influences endocytosis and vesicle membrane fusion[223]. Importantly, TIP30 was found to facilitate the endocytic degradation of activated EGFR. Reduced TIP30 expression resulted in the trapping of activated EGFR in the early endosome, where EGFR can continue to activate downstream signaling pathways, including the oncogenic AKT pathway[224,225]. These findings revealed a new mechanism by which TIP30 can suppress carcinogenesis. Indeed, in the MMTV-Neu mouse model of mammary gland cancer, *Tip30* deletion led to delayed EGFR degradation, sustained EGFR signaling, and dramatically accelerated onset of mammary gland cancer[226]. *TIP30* knockdown in human lung adenocarcinoma cells also delayed EGFR degradation and increased AKT activation[227]. Several metabolic pathways are under the regulation of AKT. In HCC cell lines, TIP30 negatively affected lipid metabolism through AKT/mTOR signaling pathways and SREBF1 expression[228]. TIP30 knockdown in an HCC cell line also

activated the oncogenic β-catenin pathway, which is likely mediated through AKT/ GSK3β/β-catenin signaling.

Another non-transcriptional function of TIP30 is regulating mRNA translation. TIP30 was found to bind the eukaryotic elongation factor and interfere with the binding of other critical factors required for translational elongation. TIP30's inhibition to translation is physiologically important because *Tip30* deficient mice had increased cardiac protein synthesis, cardiomyocyte growth, and susceptibility to cardiac hypertrophy and failure during cardiac overload[229].

In 2023, two articles started to investigate the role of TIP30 in immune cells. Cardinale *et al.* found that the activation of CD4 T cells can be inhibited by *TIP30* knockdown, and the proliferation of CD4 T cells was changed when TIP30 expression was manipulated, albeit the direction of changes seems dependent on the culture conditions. The study also nominated *TIP30* as the causal gene for an SNP linked to the diagnosis age of type 1 diabetes because no other nearby gene is expressed in the immune system[230]. Patel *et al.* found that monocyte/macrophages isolated from patients with chronic limb-threatening ischemia had increased expression of *TIP30*. These monocyte/macrophages had impaired capacity to promote neovascularization, and when TIP30 expression was silenced, the angiogenic ability was restored, and the expression of arteriogenic regulators was upregulated[231]. The molecular mechanisms by which TIP30 regulates the functions of these immune cells are unknown, and it is not clear if TIP30 also regulates the function of other immune cells. The role of TIP30 in various immune cells could be a direction for future study.

1.5.3.5 TIP30 and various cancers

A large portion of TIP30 research includes clinical studies that detected decreased expression of TIP30 in tumor tissues or linked decreased TIP30 expression to the progression or poor prognosis of various cancers. These cancers include prostate cancer[232], gastric cancer[233], HCC[219,234-236], lung cancer[237,238], colorectal cancer[239], pancreatic cancer[240], esophageal cancer[241], head and neck cancer[242,243], glioma[244], gallbladder cancer[245], and bladder urothelial cancer[236]. However, the studies that focus on the physiological role of TIP30 in pre-cancer tissues that suppresses carcinogenesis are still limited to those carried out in the Xiao lab, including the study combining *Tip30* deletion mice with MMTV-Neu mouse model of mammary gland cancer[226] and the study investigating the spontaneous lung cancer in *Tip30* knockout mice[227]. Importantly, *Tip30* deletion was found to induce more frequent spontaneous HCC in female mice than in male mice in the initial study that defined TIP30 as a tumor suppressor[208]. Still, the mechanism has yet to be investigated.

1.6 Rationale for dissertation

In the US, NAFLD/NASH is currently the primary increasing etiology of HCC and will become and remain the major HCC etiology. Understanding the molecular mechanisms of NAFLD-related HCC development, which is one of the goals of my dissertation, is relevant to the prevention and treatment of this type of cancer.

To achieve this goal, I generated novel genetically modified mouse strains related to the *Ncoa5*$^{+/-}$ mice, the *Ncoa5*$^{+/-}$*p21*$^{+/-}$/*Ncoa5*$^{+/-}$*p21*$^{-/-}$ strain and the *Ncoa5*$^{\Delta M/+}$ (myeloid-lineage-cell-specific *Ncoa5* deletion) strain. I continuously investigated the role of NCOA5 in HCC development because deletion of the gene encoding the previously

identified factor that causes HCC development in *Ncoa5*$^{+/-}$ male mice, *Il6*, did not block HCC development and only reduced tumor size. I hypothesized that additional factors are critical in the development of HCC in *Ncoa5*$^{+/-}$ male mice. Also, as it became clear recently that both the hepatocyte and the intrahepatic macrophage are important players in the pathogenesis of NASH and NASH-related HCC, we needed to delineate the contributions of *Ncoa5* haploinsufficiency in hepatocytes and intrahepatic macrophages to NASH-related HCC development, because NCOA5 was shown to function in both types of cells. I hypothesized that *Ncoa5*-deficient intrahepatic macrophages play a central role in the development of NASH and NASH-related HCC. Our conventional *Ncoa5* deletion model could not answer this question, and a cell-type-specific *Ncoa5* deletion mouse strain needed to be generated.

Using genetically engineered mice with manipulated expression of the transcriptional coregulator NCOA5 to model and study the HCC pathogenesis has several advantages. Firstly, HCC spontaneously develops in aged male *Ncoa5*$^{+/-}$ mice, which loyally reflects the higher incidence of HCC in old men. Secondly, *Ncoa5* deletion in male mice induces the early establishment of decreased insulin sensitivity, the following onset of liver steatosis and chronic liver inflammation, and later development of HCC in NASH livers that faithfully model NASH-related HCC in humans. With the timings of each stage of NASH-related HCC known precisely, I can capture molecular changes in each disease stage by systems biology approaches and identify key factors that induce disease initiation and progression. Thirdly, the heterogeneous deletion of transcriptional coregulator is more relevant in modeling the genetic predispositions for carcinogenesis that persist along inheritance in humans compared to the forced

overexpression or knockout of key regulators because the genetic predispositions in humans are often gene heterozygosity and SNP that mildly change the function or expression level of proteins. Two chapters of my dissertation describe the development of novel mouse models and the experimental results of molecular, cellular, and systems biology approaches that establish cyclin-dependent kinase inhibitor 1A (CDKN1A, also known as p21) and platelet factor 4 (PF4) as novel factors that promote a pro-tumorigenic microenvironment in the development of NASH-related HCC and feature the possibility that macrophages play a central role in the pathogenesis of NASH and NASH-related HCC.

Many studies exploring the molecular mechanisms of HCC development, including mine, may have inherent limitations. For instance, the identified mechanisms might apply primarily to the development of HCC in males. This limitation arises from the fact that female mice in these models often do not exhibit frequent occurrences of HCC, and the samples are predominantly derived from male mice. Thus, the second goal of my dissertation is to better understand the molecular mechanisms of HCC development in females. This goal was envisioned because I hypothesized that *Ncoa5*$^{+/-}$ female mice would develop HCC if the *Tip30* gene were also deleted, and the underlying molecular mechanism of hepatocarcinogenesis would be different from that of *Ncoa5*$^{+/-}$ male mice. This hypothesis was formulated because NCOA5 is a transcriptional coregulator for the female hormone receptor ERα; NCOA5 and TIP30 directly interact with each other and regulate transcription cooperatively; *Tip30* deletion induced more frequent spontaneous HCC in female mice than in male mice; and I found female but not male *Ncoa5*$^{+/-}$ mice had early upregulation of *Tip30*. In a chapter of my

dissertation, I described the generation of *Ncoa5*$^{+/-}$*Tip30*$^{+/-}$ mice, the development of HCC in female *Ncoa5*$^{+/-}$*Tip30*$^{+/-}$ mice, and the identification of a novel mechanism of HCC development that applies to females. I identified hyperpolarization-activated cyclic nucleotide-gated cation channel 3 (HCN3) as a novel female-biased HCC driver. I stressed that mechanisms of HCC development can differ significantly in males and females.

This work furthered the current understanding of the molecular mechanisms of HCC development. The following chapters describe the studies' backgrounds, designs, results, and discussion in more detail.

CHAPTER 2: NCOA5 Deficiency Promotes HCC Development in Male Mice through p21 Upregulation and a Subsequent Hepatic Proinflammatory Microenvironment

2.1 Preface

Part of this chapter is a modified version of a previously published article in *Oncogene*, Volume 39, Williams, M., Liu, X., **Zhang, Y.,** Reske, J., Bahal, D., Gohl, T.G., Hollern, D., Ensink, E., Kiupel, M., Luo, R., Das, R. and Xiao, H., NCOA5 deficiency promotes a unique liver pro-tumorigenic microenvironment through p21WAF1/CIP1 overexpression, which is reversed by metformin, pp.3821-3836. Springer Nature (2020). Reproduced with permission from Springer Nature.

The project described in the article was started by a former graduate student, Mark Williams, and a former visiting scholar, Xinhui Liu, in the Xiao lab. I continued their research and contributed a significant portion of the article's methodology, experiment design, investigation, results, writing, editing, and revision. I introduced other coauthors' work published in the article in the Introduction section. In the Results section, I presented my published results in the article and unpublished results related to this topic that will be included in a future research article.

2.2 Abstract

Molecular mechanisms underlying HCC development are inadequately understood, and their further elucidation can lead to the identification of new prevention and therapeutic targets for HCC. We previously demonstrated a unique pro-tumorigenic niche in livers of the *Ncoa5*$^{+/-}$ male mouse model of HCC, which is characterized by altered expression of a subset of genes, including *p21*$^{WAF1/CIP1}$ (*p21*) and proinflammatory cytokine genes, increased putative hepatic progenitors, and expansions of immunosuppressive cells. Here, I found that deletion of the *p21* gene alleviated the key features associated with the pro-tumorigenic niche in the livers of *Ncoa5*$^{+/-}$ male mice and significantly reduced HCC incidence. NCOA5 is associated with the *p21* promoter, and *NCOA5* knockdown increased *p21* mRNA level in response to genotoxic and cytokine stress in an HCC cell line. Together, these results suggest that *p21* overexpression is essential in the development of the pro-tumorigenic microenvironment induced by NCOA5 deficiency, and NCOA5 is likely a corepressor of *p21* transcription.

2.3 Introduction

Liver cancer is the 7th most common and 3rd most lethal malignancy in humans globally[1,2]. HCC is the most common form of primary liver cancer. Although curative treatment options are available for early-stage HCC patients, relapses are frequent, and the disease is often diagnosed in the advanced stage[5,246]. New therapeutic targets and strategies for HCC and biomarkers that predict patient responses are urgently needed because of the limited response rates, efficacies, and choices of currently available systemic treatments for advanced HCC[5,247].

Identifiable risk factors, including HBV, HCB, excessive alcohol consumption, and metabolic syndromes, promote the development of HCC. The underlying HCC development is often described as the result of a pro-tumorigenic hepatic microenvironment characterized by chronic inflammation, hepatocyte damage, and regeneration. The past decades have witnessed the identification of various cellular factors and pathways that drive the initiation and progression of HCC[5,247]. For example, proinflammatory cytokines produced by intrahepatic macrophages and hepatocytes have been shown to promote the hepatocarcinogenesis of various carcinogen/diet-induced and genetically engineered mouse models of HCC by activating the NF-κB and STAT3 signaling pathways[98,248,249]. Despite these findings, the molecular mechanisms underlying the formation of the pro-tumorigenic hepatic microenvironment require further elucidation.

The Xiao lab previously reported that male mice carrying a heterozygous deletion of the *Ncoa5* gene exhibit glucose intolerance, chronic hepatic inflammation, and a high incidence of HCC[187,250]. p21, a potent cyclin-dependent kinase inhibitor when localized at the nucleus, was aberrantly upregulated in the cytoplasm of hepatocytes of *Ncoa5*$^{+/-}$ male mice. The *Ncoa5*$^{+/-}$ male mice have a unique liver microenvironment with altered expression of a subset of genes, including *p21* and proinflammatory cytokine genes, and increased putative HPCs early in life. In aged *Ncoa5*$^{+/-}$ male mice, immunosuppressive cells, including MDSCs and M2 macrophages, expand before the onset of HCC. Such a hepatic microenvironment was suspected to be the pro-tumorigenic niche that promotes the HCC development of *Ncoa5*$^{+/-}$ male mice. Using *p21* deletion mice, I demonstrated that upregulated p21 expression is required to form

the hepatic pro-tumorigenic niche and the subsequent hepatocarcinogenesis in *Ncoa5*$^{+/-}$ male mice. My data also indicate that NCOA5 may act as a corepressor to regulate the transcription of p21 directly.

2.4 Results

2.4.1 Heterozygous deletion of p21 inhibits the formation of the pro-tumorigenic niche in the livers of Ncoa5$^{+/-}$ *male mice*

The spontaneous HCC development in *Ncoa5*$^{+/-}$ male mice is preceded by a unique hepatic microenvironment with the characteristics of altered expression of a subset of genes, including *p21* and proinflammatory cytokine genes, increased putative hepatic progenitors, and elevated immune cell infiltration. To explore the role of p21 overexpression in the formation of the pro-tumorigenic niche, I sought to determine if the downregulation of *p21* alleviates the features of the niche. To avoid the complications of influencing the cell cycle by complete *p21* ablation, I generated a cohort of *Ncoa5*$^{+/-}$ and *Ncoa5*$^{+/-}$*p21*$^{+/-}$ male mice and aged them to 5 months. The mRNA expression of genes previously identified as altered by *Ncoa5* deletion in younger male mice was assessed in the livers of *Ncoa5*$^{+/-}$ and *Ncoa5*$^{+/-}$*p21*$^{+/-}$ male mice. The mRNA levels of 14 early upregulated genes identified in the livers of *Ncoa5*$^{+/-}$ male mice at 20 weeks of age were measured. Reduced mRNA expression of *p21* was accompanied by significant decreases (2 genes) or trending decreases (10 genes) in mRNA levels of measured genes in livers of *Ncoa5*$^{+/-}$*p21*$^{+/-}$ double mutant mice compared to livers of *Ncoa5*$^{+/-}$ mice (Fig. 1.1).

Moreover, immunohistochemistry (IHC) analysis revealed that the numbers of cytoplasmic p21-positive hepatocytes, macrophages, and putative HPCs were all

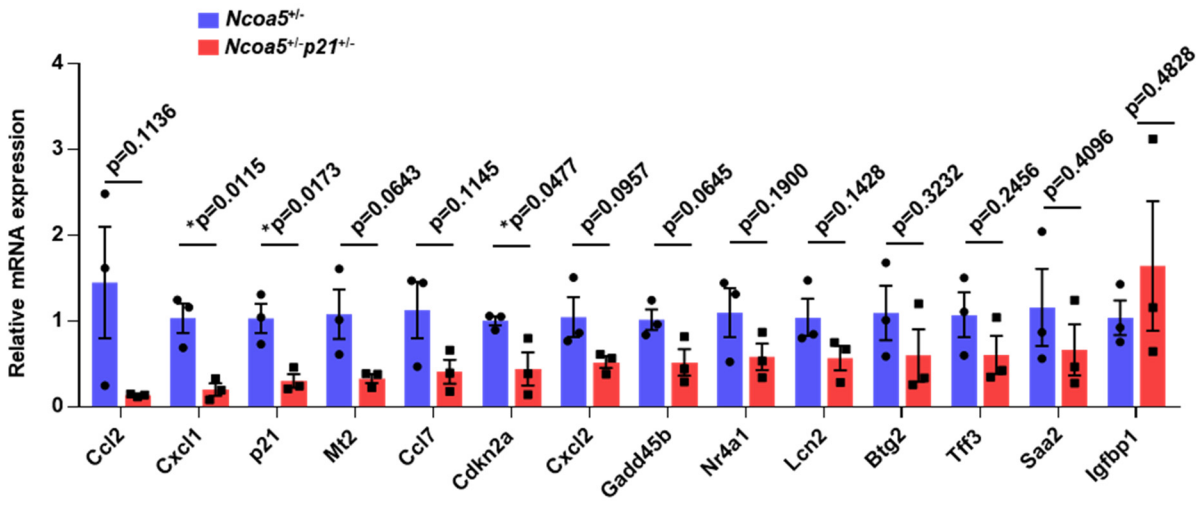

Figure 1.1 Effect of *p21* heterozygous deletion on the mRNA expression of early upregulated genes in livers of *Ncoa5*$^{+/-}$ male mice. Quantitative real-time reverse transcription polymerase chain reaction (RT-qPCR) analysis of 14 genes in livers of *Ncoa5*$^{+/-}$*p21*$^{+/-}$ and *Ncoa5*$^{+/-}$ mice at the age of 5 months using TaqMan Custom Array. These 14 genes were identified as the early upregulated genes in the livers of *Ncoa5*$^{+/-}$ mice. Mouse n=3 in each group. Data represent mean ± SEM. Two-tailed unpaired Student's t test. *p<0.05.

reduced in livers of *Ncoa5*$^{+/-}$*p21*$^{+/-}$ male mice compared to *Ncoa5*$^{+/-}$ male mice (Fig. 1.2). These results support the hypothesis that increased p21 expression plays a critical role in the development of the hepatic pro-tumorigenic niche.

2.4.2 p21 genetic deficiency suppresses the HCC development of Ncoa5$^{+/-}$ *male mice*

To validate the crucial role of p21 upregulation in the hepatocarcinogenesis of *Ncoa5*$^{+/-}$ male mice, I generated a cohort of wild-type, *p21*$^{+/-}$, *p21*$^{-/-}$, *Ncoa5*$^{+/-}$, *Ncoa5*$^{+/-}$*p21*$^{+/-}$, and *Ncoa5*$^{+/-}$*p21*$^{-/-}$ male mice and monitored their liver tumor development for 18 months. 81.25% of C57BL/6 *Ncoa5*$^{+/-}$ male mice in this cohort spontaneously developed liver tumors by 18 months of age, similar to the previously reported incidence of the 129 × C57BL/6 or BALB/c genetic background *Ncoa5*$^{+/-}$ male mice. Strikingly, *p21* heterozygous deletion or complete knockout significantly reduced the liver tumor incidence of *Ncoa5*$^{+/-}$*p21*$^{+/-}$ and *Ncoa5*$^{+/-}$*p21*$^{-/-}$ male mice compared to *Ncoa5*$^{+/-}$ male

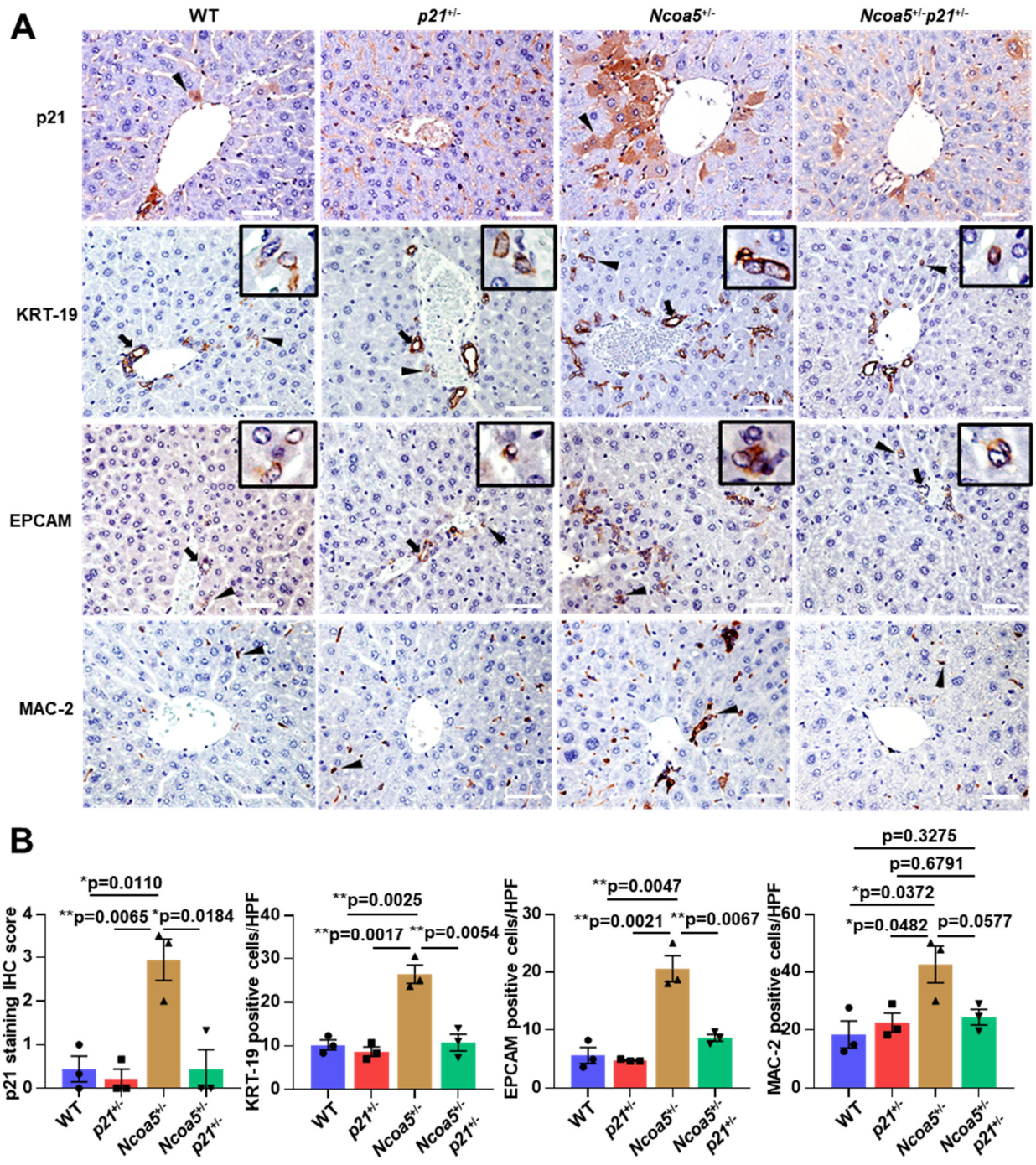

Figure 1.2 Effect of *p21* heterozygous deletion on the cytoplasmic p21 expression in hepatocytes and numbers of HPCs and macrophages in livers of *Ncoa5*$^{+/-}$ male mice. Representative images (A) and quantification of IHC staining (B) of p21, HPC markers KRT-19 and EPCAM, and macrophage marker MAC-2 on liver sections of 5-month-old *Ncoa5*$^{+/-}$*p21*$^{+/-}$ and *Ncoa5*$^{+/-}$ male mice (n = 3). Interlobular bile ducts (arrow) were excluded from the counting, while other KRT-19 or EPCAM-positively stained cells (arrowhead) were counted as putative HPCs. Insets show details of putative KRT-19 or

Figure 1.2 (cont'd)
EPCAM-positive cells. The arrowheads in images of IHC staining of MAC-2 indicate MAC-2 positive cells. Scale bar: 50 μm. Data represent mean ± SEM. Two-tailed unpaired Student's t test. *p < 0.05, **p < 0.01.

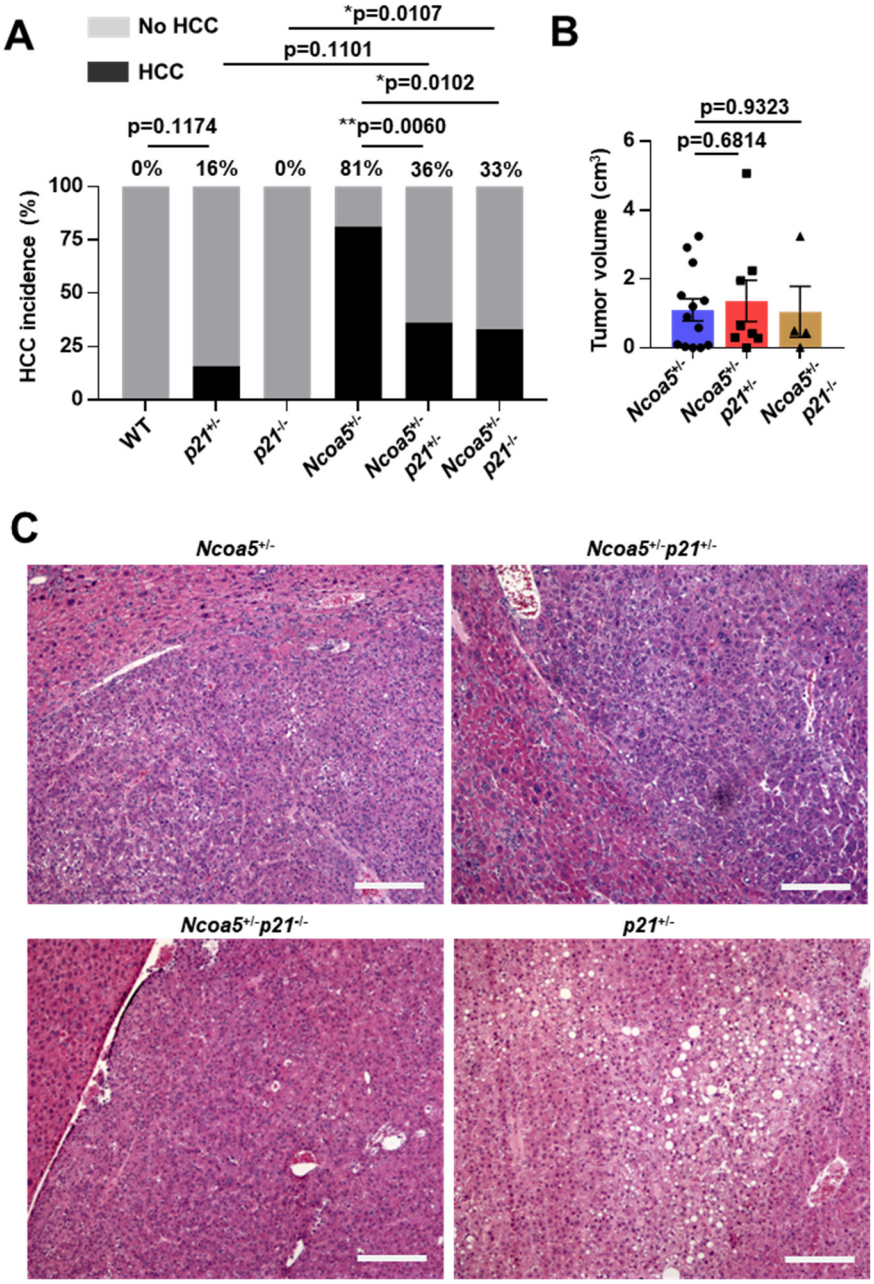

Figure 1.3 Effect of *p21* deficiency on the HCC development of *Ncoa5*$^{+/-}$ male mice. (A) HCC incidence of 18-month-old male mice with indicated genotype. Mouse n=20, 25, 22, 16, 22, and 12. Chi-squared test was used except that Fisher's exact test was used when the 2x2 contingency table has number = 0. **p<0.01, *p<0.05. (B) Liver tumor volume of 18-month-old male mice with indicated genotype. Tumor n=13, 8, and

Figure 1.3 (cont'd)
4. Two-tailed unpaired Student's t test. (C) Representative H & E staining photos of moderately differentiated HCCs from 18-month-old male mice with indicated genotype. Scale bar: 200 μm. Data represent mean ± SEM.

mice (Fig. 1.3A). The volume of liver tumors from *Ncoa5*$^{+/-}$ male mice was not significantly changed by *p21* deficiency (Fig. 1.3B), and liver tumors of *Ncoa5*$^{+/-}$ male mice with or without *p21* deletion or knockout are all well to moderately differentiated HCCs (Fig. 1.3C). Consistent with a previous report, *p21* knockout did not induce spontaneous HCC in male C57BL/6 mice[251]. Interestingly, 16% of male C57BL/6 mice with *p21* heterozygous deletion developed spontaneous HCC by 18-month-old, and the HCCs are well to moderately differentiated with seemingly larger steatosis area compared to HCCs induced by *Ncoa5* deletion (Fig. 1.3C). These results confirmed that upregulated p21 is critical in inducing spontaneous HCC development in *Ncoa5*$^{+/-}$ male mice by promoting a pro-tumorigenic inflammatory microenvironment.

2.4.3 NCOA5 represses p21 transcription

Next, I explored the molecular mechanism underlying the *p21* upregulation in *Ncoa5* deficient male mice. Because NCOA5 co-represses *IL6* transcription activated by NF-κB, and NF-κB also regulates *p21* transcription[252], I hypothesized that NCOA5 represses p21 transcription as a corepressor. The HepG2 human HCC cells consecutively express p21 in normal culture conditions. Quantitative chromatin immunoprecipitation (qChIP) assay results indicated that NCOA5 is associated with the p53 and NF-κB p65 binding sites of the *p21* promoter in HepG2 cells (Fig. 1.4A). I used a previously published shRNA carried by lentivirus[187] to generate HepG2 cells with stable *NCOA5* knockdown. *NCOA5* mRNA expression was significantly decreased in

cells transformed with *NCOA5* shRNA virus compared to cells transformed with scramble control shRNA virus (Fig. 1.4B). Control and *NCOA5* knockdown cells were treated with recombinant IL-6 or camptothecin (CPT) to activate NF-κB or genotoxic stress-induced *p21* transcription, respectively. In HepG2 cells treated with bovine serum albumin (BSA) or dimethyl sulfoxide (DMSO) vehicle controls, *NCOA5* knockdown already significantly increased *p21* mRNA level (Fig. 1.4C, ***p=0.0008 or 0.00097 when tested with two-tailed unpaired Student's t test, respectively). In cells treated with IL-6 or CPT, *NCOA5* knockdown further augmented *p21* expression (Fig. 1.4C). These results indicate that NCOA5 might co-repress *p21* transcription regulated by NF-κB and p53.

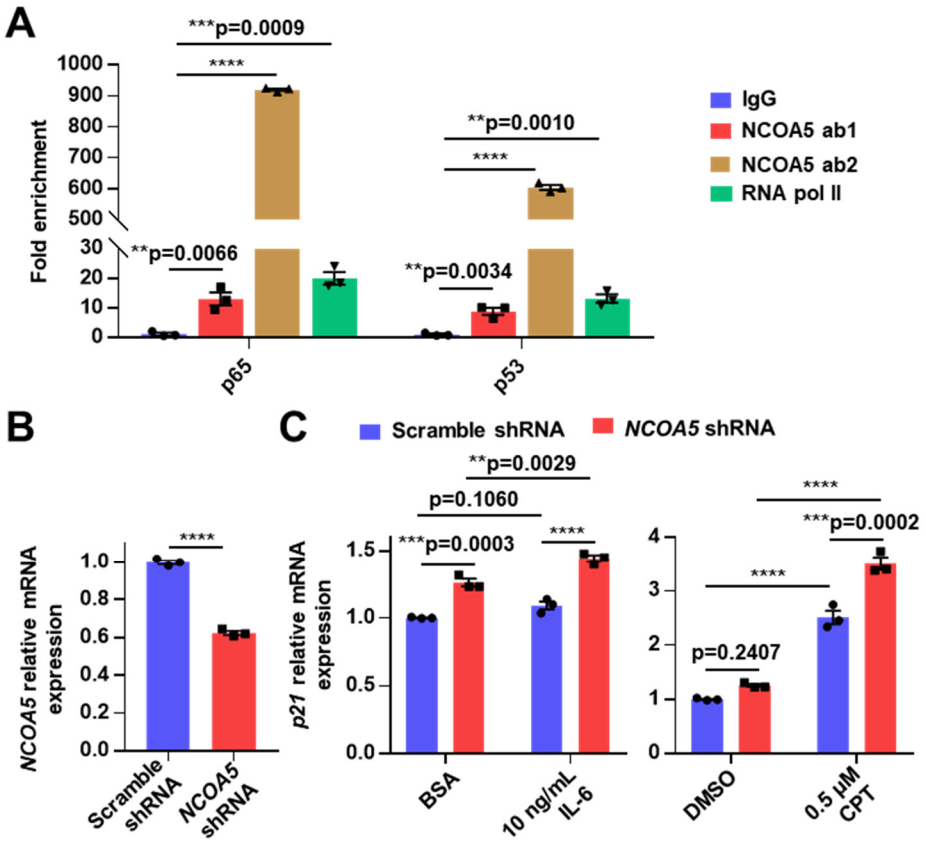

Figure 1.4 The association of NCOA5 with *p21* promoter and the effect of *NCOA5* knockdown on *p21* mRNA expression. (A) qChIP assay results showing the real-time

Figure 1.4 (cont'd)
qPCR amplification of sequences surrounding the p65 and p53 binding sites of the *p21* promoter in chromatin DNA precipitated by antibodies as indicated from HepG2 cells. Fold enrichments were calculated against signals from IgG samples. Two-tailed unpaired Student's t test. (B) RT-qPCR validation of shRNA-mediated *NCOA5* knockdown in HepG2 cells. Two-tailed unpaired Student's t test. (C) RT-qPCR analysis showing the mRNA level of *p21* in BSA or 10 ng/mL IL-6 (left) or DMSO or 0.5 μM CPT (right) treated HepG2 cells with and without NCOA5 knockdown. Representative data of two repeats. p calculated with two-way ANOVA Tukey's multiple comparisons test was labeled in the figure. Two-tailed unpaired Student's t test ****p=0.0008 or 0.00097 within BSA or DMSO treatment groups, respectively. ****p<0.0001, ***p<0.001, **p<0.01. Data represent mean ± SEM.

2.5 Discussion

In this study, I uncovered a new mechanism that promotes HCC development in male mice with *Ncoa5* deficiency. The upregulation of p21 in the livers of *Ncoa5*$^{+/-}$ male mice is essential in the formation of a pro-tumorigenic hepatic microenvironment characterized by chronic inflammation and increased HPCs. *p21* heterozygous deletion is able to reverse the expression of early-upregulated genes and decrease the numbers of HPCs and macrophages in the livers of *Ncoa5*$^{+/-}$ male mice. The early-upregulated genes encompass those encoding proinflammatory cytokines, and increased intrahepatic macrophages have been demonstrated to induce chronic hepatic inflammation[187]. Thus, my results established a novel oncogenic function of hepatocyte cytoplasmic p21 overexpression, which promotes the activation and infiltration of macrophage, leading to liver inflammation. This finding was later supported by a *Science* article, where an independent group of researchers found that cells with persistent p21 upregulation recruit macrophages and polarize them toward proinflammatory M1 phenotype[253]. A recent study also demonstrated that p21 knockout alleviates chronic lung inflammation in mice subjected to repetitive inhalations of LPS[254].

The cellular functions of p21 differ significantly depending on its localization and protein-protein interactions[255]. Although nuclear p21 inhibits cyclin-dependent kinases and functions as a tumor suppressor, p21 can be oncogenic in certain cellular contexts[255-258]. For example, in patient liver specimens and several mouse models of NAFLD, hepatic steatosis and chronic injuries have been shown to correlate with increased hepatic p21 expression[259,260]. Moreover, hepatocyte-specific overexpression of p21 increases the numbers of hepatic bipotential progenitors and hepatocyte nodules in mouse livers[261]. In my study, increased p21 expression in the cytoplasm of hepatocytes from *Ncoa5*$^{+/-}$ male mice positively correlates with HCC development, and *p21* knockout or deletion significantly reduces the HCC incidence of *Ncoa5*$^{+/-}$ male mice. Cytoplasmic p21 expression in hepatocytes correlating with HCC development was also reported in the HBx-expressing CD-1 transgenic mice[262]. Similarly, *p21* knockout impairs HPC proliferation and delays HCC formation in the *Mdr2*$^{-/-}$ mouse model of HCC with NF-κB signaling activation in hepatocytes[263]. In contrast, *p21* knockout promoted the HCC development of mice with hepatocyte-specific NEMO knockout that lack NF-κB signaling activation in hepatocytes[264]. Thus, the tumor-suppressing or oncogenic role of p21 in HCC development may depend on the activation of the NF-κB signaling pathway, where the NF-κB activation status might reflect the susceptibility of the disease models to severe chronic inflammation. My work supports this view because my results indicate that p21 overexpression is critical to the formation of a pro-tumorigenic microenvironment through altering the expression of a set of specific genes and increased immune cell infiltrations in the *Ncoa5*$^{+/-}$ mouse model of HCC, which also contains activated NF-κB signaling in the liver[187].

Indeed, the upregulation of p21 and the subsequent pro-tumorigenic hepatic microenvironment is critical to the HCC development of *Ncoa5*$^{+/-}$ male mice as *p21* deletion or knockout greatly reduced their HCC incidence. Interestingly, while heterozygous deletion of *Il6* reduced tumor size without altering HCC incidence in *Ncoa5*$^{+/-}$ male mice[187], *p21* heterozygous deletion or knockout significantly reduced HCC incidence but did not reduce tumor size of *Ncoa5*$^{+/-}$ male mice. In *Ncoa5*$^{+/-}$*p21*$^{+/-}$ and *Ncoa5*$^{+/-}$*p21*$^{-/-}$ male mice that developed HCC, a large amount of infiltrated immune cells is still present in the tumor-adjacent livers (Fig. 1.3C). These results indicate that other factors also promote the establishment of the pro-tumorigenic microenvironment, although upregulated p21 contributes significantly to the chronic inflammation and increased HPCs in the livers of *Ncoa5*$^{+/-}$ male mice. Nevertheless, by monitoring a large cohort of mice (mouse n>20 in each group), I observed that the HCC incidence of *Ncoa5*$^{+/-}$*p21*$^{+/-}$ male mice is sufficiently low, showing no significant difference compared to the HCC incidence of *p21*$^{+/-}$ male mice. Thus, p21 is likely the major player that creates the microenvironment for HCC development. Future studies investigating the HCC development of *Ncoa5*$^{+/-}$*p21*$^{+/-}$ and *Ncoa5*$^{+/-}$*p21*$^{-/-}$ male mice are warranted and will identify additional factors that promote HCC in *Ncoa5*$^{+/-}$ male mice.

Another interesting observation is that 16% of *p21*$^{+/-}$ male mice spontaneously developed HCC, while none of the *p21*$^{-/-}$ male mice had HCC by 18 months. Consistent with my results, a previous study reported that no HCC was found in a cohort of 151 *p21*-null 129Sv × C57BL/6 male and female mice monitored for 24 months[251]. Considering p21's dual roles in inhibiting and promoting HCC, I hypothesize that the homeostasis of p21 expression level plays different roles in different stages of

hepatocarcinogenesis. In the pre-cancer stage, increased p21 expression induces inflammation, subsequent hepatocyte damage, and increased HPCs to compensate for hepatocyte death. In contrast, in the stage of cell malignant transformation, decreased p21 expression fails to inhibit the cell cycle and promotes carcinogenesis. Thus, in mice with spontaneous inflammation and death of hepatocytes due to aging, decreased p21 expression by *p21* heterozygous deletion may promote the survival and proliferation of cells that accumulate genetic and epigenetic alterations and eventually result in malignant transformation. On the other hand, complete loss of p21 can protect mice from liver inflammation and cell damage, blocking hepatocarcinogenesis in the early steps. To validate this hypothesis, we have generated mice carrying the *p21* allele flanked by loxPs, and I have validated the Albumin-cre mediated *p21* deletion in these mice. Future studies will use the newly generated $p21^{flox}$ mice and inducible or deliverable cre to demonstrate the different effects of *p21* knockout in different stages of HCC development induced by genetic alterations, chemicals, or special diets.

My work also explored the mechanism underlying p21 upregulation in the hepatocytes of $Ncoa5^{+/-}$ male mice. I detected the association of NCOA5 with the p53 and NF-κB p65 binding sites of the *p21* promoter, and *NCOA5* knockdown increased *p21* mRNA level and augmented genotoxic agent camptothecin or IL-6-induced *p21* expression in human HCC cells. My results suggest that NCOA5 might co-repress *p21* transcription regulated by NF-κB and p53. This direct regulation of NCOA5 to *p21* transcription does not contradict possibly co-existing indirect mechanisms of *p21* transcription upregulation. One indirect mechanism is that NCOA5 deficiency in intrahepatic macrophages could release factors that activate the NF-κB and p53-

mediated *p21* transcription in hepatocytes. The results demonstrated in Chapter 3 support this hypothesis, as myeloid-specific deletion of *Ncoa5* significantly increased p21 mRNA and protein levels in the livers of male mice[265]. I also do not rule out the possibility that NCOA5 deficiency in hepatocytes influences other signaling pathways that regulate p21 expression. To further validate the direct regulation of *p21* transcription by NCOA5, investigators may perform luciferase reporter assays to show the functional association of NCOA5 to the p21 promoter. qChIP assays may also be performed in cells with or without activation of NF-κB and p53 to show that NCOA5's association with the *p21* promoter requires these transcription factors.

In summary, my work demonstrates that p21 upregulation is required for the formation of a unique pro-tumorigenic niche that promotes HCC development in *Ncoa5*$^{+/-}$ male mice and suggests NCOA5 regulates *p21* transcription as a corepressor. My findings highlight the importance of targeting the precancerous microenvironment for the treatment of HCC, and p21 is a potential target for chemo-preventive and therapeutic strategies against HCC development.

2.6 Materials and methods

2.6.1 Mice

C57BL/6 *Ncoa5*$^{+/-}$ mice were previously generated by backcrossing BALB/c *Ncoa5*$^{+/-}$ female mice with wild-type C57BL/6 male mice for seven generations. C57BL/6 *Ncoa5*$^{+/-}$ mice used in this study were further backcrossed with wild-type C57BL/6 mice for at least three generations. *p21*$^{-/-}$ C57BL/6 mice (B6.129S6(Cg)-*Cdkn1a*^{tm1Led}/J) were purchased from the Jackson Laboratory. *Ncoa5*$^{+/-}$*p21*$^{+/-}$ male mice were generated by crossing *Ncoa5*$^{+/-}$ female mice and *p21*$^{-/-}$ male mice. *Ncoa5*$^{+/-}$*p21*$^{-/-}$ male mice were

generated by crossing *Ncoa5*$^{+/-}$*p21*$^{+/-}$ female mice with *p21*$^{+/-}$ and *p21*$^{-/-}$ male mice. Female mice were excluded from experiments because only male *Ncoa5*$^{+/-}$ mice were previously reported to develop HCC in 10-18 months[187]. All mice were under a standard normal diet and 12 h light/12 h dark cycle at the Michigan State University animal facilities and housed in Optimice cages. All experimental procedures on mice were approved by the Michigan State University Institutional Animal Care and Use Committee and were performed in accordance with their regulatory standards.

2.6.2 Cell culture

The human liver cancer cell line HepG2 (derived from male) was purchased from the American Type Culture Collection (ATCC) and authenticated by the ATCC Cell line authentication service using short tandem repeat (STR) analysis. Cells were cultured using DMEM high glucose medium (Thermo Fisher) supplemented with 10% fetal bovine serum (FBS), 100 U/mL of penicillin, and 100 µg/mL of streptomycin. Lentiviral-induced knockdown with scramble shRNA or *NCOA5* shRNA was carried out as described previously[187]. Cells were treated in normal culture media with camptothecin (Sigma-Aldrich, #208925) for 24h. For IL-6 treatment, cells were first cultured in phenol red-free DMEM supplemented with 10% charcoal-stripped serum for 24h and then treated with recombinant IL-6 (PeproTech, #200-06) for 24h.

2.6.3 Quantitative real-time reverse transcription polymerase chain reaction

Total RNA was isolated using TRIzol (Thermo Fisher) according to the manufacturer's instructions. cDNA was generated using the SuperScript IV First-Strand Synthesis System (Thermo Fisher) according to the manufacturer's instructions. Quantitative real-time PCR was performed on a QuantStudio 3 Real-Time PCR

machine using TaqMan Gene Expression Master Mix and TaqMan probes in Custom TaqMan Array 96 Plates (Thermo Fisher, Custom Plate part number 4413264).

2.6.4 Tissue histology and immunohistochemistry assays

Neutrally buffered 10% formalin solution (Sigma-Aldrich) fixed mouse tissues were sent to the Investigative Histopathology Laboratory of Michigan State University and processed, embedded, sectioned, and H & E stained. IHC staining was performed using the VECTASTAIN ABC-HRP system (Vector Laboratories) according to the manufacturer's instructions. Quantification of EPCAM-positive, Keratin 19 (KRT-19)-positive, and MAC-2-positive cells and the IHC labeling score of p21 were determined in five random fields per slide. p21 IHC staining intensity was scored using the IRS system[266]. Antibodies used include anti-p21 (Santa Cruz Biotechnology, sc-6246), anti-EPCAM (Abcam, ab71916), anti-KRT-19 (Proteintech, 10712-1-AP), and anti-MAC-2 (Cedarlane Laboratories, CL8942AP).

2.6.5 Chromatin immunoprecipitation assay

ChIP was performed using the Imprint Chromatin Immunoprecipitation Kit (Sigma-Aldrich) according to the manufacturer's instructions. Chromatin was sheared using a Sonic Dismembrator Model 500 (Fisher Scientific). Antibodies other than the anti-IgG and anti-RPII supplied by the kit include anti-NCOA5 ab1 (Santa Cruz Biotechnology, sc-86178) and anti-NCOA5 ab2 (Bethyl, A300-789A). Primers used for amplifying DNA fragments: p65 binding site F: GGGCTGCCTCTGCTCAATAA; R: CCCAAGCCTGAAGAAGGAGG. p53 binding site F: ATCCCTATGCTGCCTGCTTC; R: TCCTGTCTCCTACCATCCCC.

2.6.6 Quantification and statistical analysis

All data are shown as mean ± SEM. Statistical significance of differences was determined by two-way ANOVA Tukey's multiple comparisons test, two-tailed unpaired Student's t test, Chi-squared test, and Fisher's exact test in GraphPad Prism 7 with details listed in the corresponding figure legends. ****$p<0.0001$, ***$p<0.001$, **$p<0.01$, *$p<0.05$.

CHAPTER 3: NCOA5 Haploinsufficiency in Myeloid-lineage Cells Sufficiently Causes Nonalcoholic Steatohepatitis and HCC through PF4 Upregulation in Liver Macrophages

3.1 Preface

This chapter is a modified version of a previously published article in *Cellular and Molecular Gastroenterology and Hepatology*, Volume 17, **Zhang, Y.**, Luo, Y., Liu, X., Kiupel, M., Li, A., Wang, H., Mi, Q.S. and Xiao, H., NCOA5 haploinsufficiency in myeloid-lineage cells sufficiently causes nonalcoholic steatohepatitis and hepatocellular carcinoma, pp.1-27, Copyright Elsevier (2024).

I performed most experiments and investigations, wrote the original manuscript, and edited and revised the article. Former visiting scholar Yue Luo performed the glucose and insulin tolerance tests, the peritoneal macrophage study, and the *in vitro* experiments of testing the effect of conditioned medium on the proliferation and migration of HCC cells and helped with the generation of *Ncoa5* knockout RAW 264.7 cells. Former visiting scholar Xinhui Liu helped generate and characterize the *Ncoa5*$^{\Delta M/+}$ mice. Dr. Matti Kiupel performed pathologic analyses and consultations.

We thank Dr. Myriam Aouadi for providing us with glucan shells and technical advice for this study. We thank Drs. Huirong Xie and Elena Demireva at the Transgenic and Genome Editing Facility of MSU for using the CRISPR/Cas9 method to generate *Ncoa5* floxed mice used in our pilot study, Dr. Feiye Liu for her initial effort in creating *Ncoa5* floxed mice, and Dr. Ying Qin for consultation on mouse liver histology.

3.2 Abstract

Molecular and cellular mechanisms triggering the onset and progression of NAFLD, NASH, and HCC remain incompletely understood. Here, we show that myeloid-cell-specific heterozygous deletion of *Ncoa5* (*Ncoa5*$^{\Delta M/+}$) sufficiently causes the development of NAFLD/NASH and HCC in male mice. The PF4 overexpressed in *Ncoa5*$^{\Delta M/+}$ intrahepatic macrophages is identified as a potent mediator to trigger lipid accumulation in hepatocytes via inducing the expression of lipogenesis-promoting genes. The transcriptome of intrahepatic macrophages from *Ncoa5*$^{\Delta M/+}$ male mice resembles that of obese human individuals. Moreover, in HCC patients, high PF4 expression correlates with poor prognosis and increased infiltrations of M2 macrophages, Tregs, and MDSCs in HCCs. Our results reveal a novel mechanism for the onset of NAFLD/NASH and HCC initiated by dysregulated macrophages, suggesting the NCOA5-PF4 axis in macrophages as a potential target for developing preventive and therapeutic interventions against NAFLD/NASH and HCC.

3.3 Introduction

NAFLD, consisting of non-alcoholic fatty liver, also known as hepatic steatosis, and NASH, affects approximately 25% of the world population[267]. Patients commonly develop NAFLD due to susceptible genetic and environmental factors, a substantial proportion of which progress to NASH. Some eventually advance to cirrhosis and HCC[268]. Cumulating evidence suggests that multiple parallel factors, including dietary factors, hormones, and gut microbiota, act together on genetically predisposed individuals, promoting the development of insulin resistance, endoplasmic reticulum stress, mitochondrial dysfunction, and release of proinflammatory cytokines, thereby

inducing NAFLD and NASH[24]. Human and animal studies have provided convincing data suggesting that intrahepatic resident macrophages and recruited macrophages play a crucial role in the pathogenesis of NAFLD/NASH and HCC via promoting chronic inflammation, lipogenesis, and the formation of an immunosuppressive microenvironment[269]. In response to extrinsic signals from the microenvironment, the intrahepatic macrophages were found to polarize towards a proinflammatory phenotype and release proinflammatory cytokines, nitric oxide, and ROS in the liver, leading to the recruitment of other immune cells such as B and T cells, DNA damage, and cell death of hepatocytes. The combination of these alterations in the liver results in chronic inflammation, hepatic fibrosis, and immunosuppression, eventually advancing to HCC. However, how distinct cellular factors and signal pathways that intrinsically regulate the polarization and functions of heterogeneous macrophages contribute to the pathogenesis of these diseases is incompletely understood. Moreover, whether genetic and epigenetic risk factors in macrophages can sufficiently cause the development of NAFLD and HCC remains unknown.

NCOA5 is a unique coactivator for several known nuclear receptors, including estrogen receptor α and liver X receptor, having both transcriptional coactivator and corepressor activities[178-180]. Analysis of SNPs in chromosome 20q12-13.1 region for associations with T2D and body mass index in European American case-control populations revealed that the *NCOA5* is a T2D susceptibility gene candidate[270]. We previously reported that heterozygous deletion of *Ncoa5* results in the development of hepatic steatosis, insulin resistance, and HCC in mice in a male-biased manner. The development of these diseases is accompanied by increased infiltrating immune cells,

including macrophages, and overexpressed proinflammatory cytokines in the liver[187,271]. While these observations indicate the importance of NCOA5 in suppressing hepatocarcinogenesis, it remains to be understood how NCOA5 regulates the development of hepatic steatosis and HCC, especially in macrophages. Here, we demonstrate that NCOA5 in intrahepatic macrophages plays a crucial role in regulating the interaction of macrophages with hepatocytes. Its haploinsufficiency in myeloid-lineage cells sufficiently induced the development of NAFLD/NASH and HCC in male mice, at least partially, through overexpression of PF4 in intrahepatic macrophages.

3.4 Results

3.4.1 Myeloid-lineage-specific heterozygous deletion of Ncoa5 results in spontaneous metabolic syndrome and HCC development in male mice fed a normal diet

To study the underlying mechanism and cell-specific impact of *Ncoa5* haploinsufficiency on NAFLD and HCC development, we generated C57BL/6 mice carrying the *Ncoa5* allele with loxP-flanked exons 3 and 4 (*Ncoa5*^{fl}), which are the identical targeted exons in *Ncoa5*$^{+/-}$ mouse[187] (Fig. 2.1A). We were particularly interested in the role of NCOA5 in regulating macrophage function. *Ncoa5*$^{\Delta M/+}$ (*Ncoa5*$^{fl/+}$/LysM$^{cre/+}$) mice were generated by crossing *Ncoa5*$^{fl/fl}$ mice with LysMcre mice (Jackson Lab) that allow for cre-mediated deletion in myeloid-lineage cells, including mature macrophages, some neutrophils and monocytes, and few dendritic cells[272]. Deletion of the *Ncoa5* gene in intrahepatic macrophages was confirmed by Western blotting using *Ncoa5*$^{\Delta M/+}$ (*Ncoa5*$^{fl/+}$/LysM$^{cre/+}$) and *Ncoa5*$^{\Delta M/\Delta M}$ (*Ncoa5*$^{fl/fl}$/LysM$^{cre/+}$) mice (Fig. 2.1B and 2.1C). Mice with cre-mediated cell-type-specific *Ncoa5* deletion in hepatocytes were also generated by crossing *Ncoa5*$^{fl/fl}$ mice with *Speer6-ps1*$^{Alb\text{-}cre/+}$

mice and confirmed by Western blotting (Fig. 2.1D). *Ncoa5*$^{\Delta M/+}$, *Ncoa5*$^{\Delta M/\Delta M}$, and *Ncoa5*$^{\Delta H/\Delta H}$ mice were viable and fertile with normal litter size.

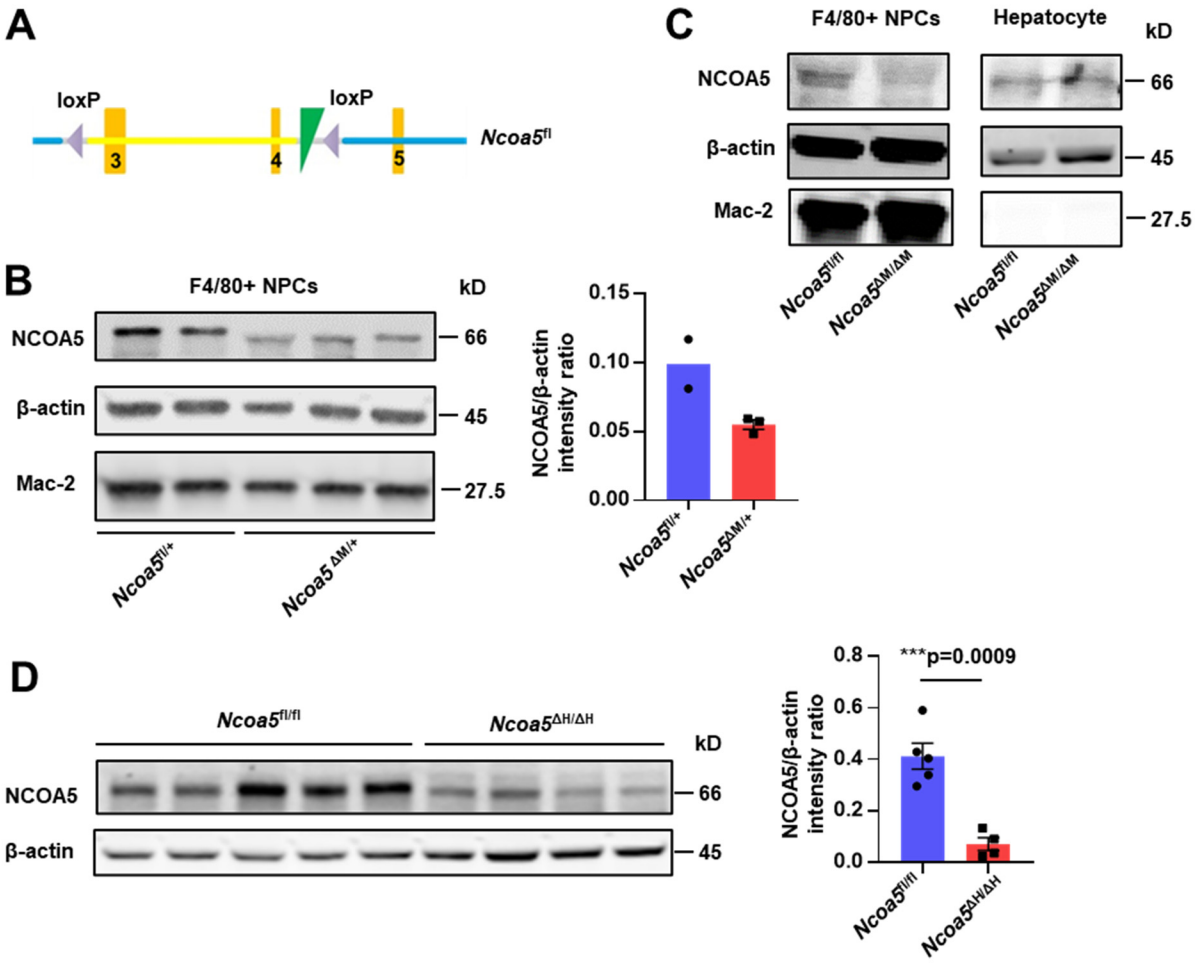

Figure 2.1. Validation of cell-type-specific *Ncoa5* deletion in mice. (A) The schematic representation of the floxed *Ncoa5* gene. (B and C) Western blot analysis of myeloid-lineage-specific *Ncoa5* heterozygous deletion or knockout in *Ncoa5*$^{\Delta M/+}$ or *Ncoa5*$^{\Delta M/\Delta M}$ males. Nonparenchymal cells (NPCs) and parenchymal cells (PCs, hepatocytes) were isolated from the mouse liver using a two-step perfusion method. F4/80+ cells were isolated using Anti-F4/80 MicroBeads from NPCs. The error bar represents SEM. (D) Western blot validation of reduced NCOA5 expression in the liver lysate of *Ncoa5*$^{\Delta H/\Delta H}$ males (n=4) compared to *Ncoa5*$^{fl/fl}$ males (n=5). Data represent mean ± SEM. Two-tailed unpaired Student's t test. ***p<0.001.

To circumvent the possible cell development defects associated with *Ncoa5* homozygous loss and better compare with the previous phenotypes in *Ncoa5*$^{+/-}$ mice, we focused on *Ncoa5*$^{\Delta M/+}$ mice. We examined the fasting serum glucose, glucose

tolerance, and insulin tolerance on 7- to 8-week-old *Ncoa5*$^{fl/+}$ and *Ncoa5*$^{\Delta M/+}$ mice fed a normal diet. While the fasting blood glucose level was comparable between the *Ncoa5*$^{\Delta M/+}$ and *Ncoa5*$^{fl/+}$ male mice, the glucose tolerance and insulin sensitivity were significantly decreased in *Ncoa5*$^{\Delta M/+}$ male mice compared to *Ncoa5*$^{fl/+}$ male mice (Fig. 2.2A). There was no significant difference in glucose tolerance and insulin sensitivity between the two groups of female mice (Fig. 2.2B). This result is consistent with the fact that no significant phenotypes were observed in *Ncoa5*$^{+/-}$ female mice[187]; thus, we focus our studies on *Ncoa5*$^{\Delta M/+}$ male mice.

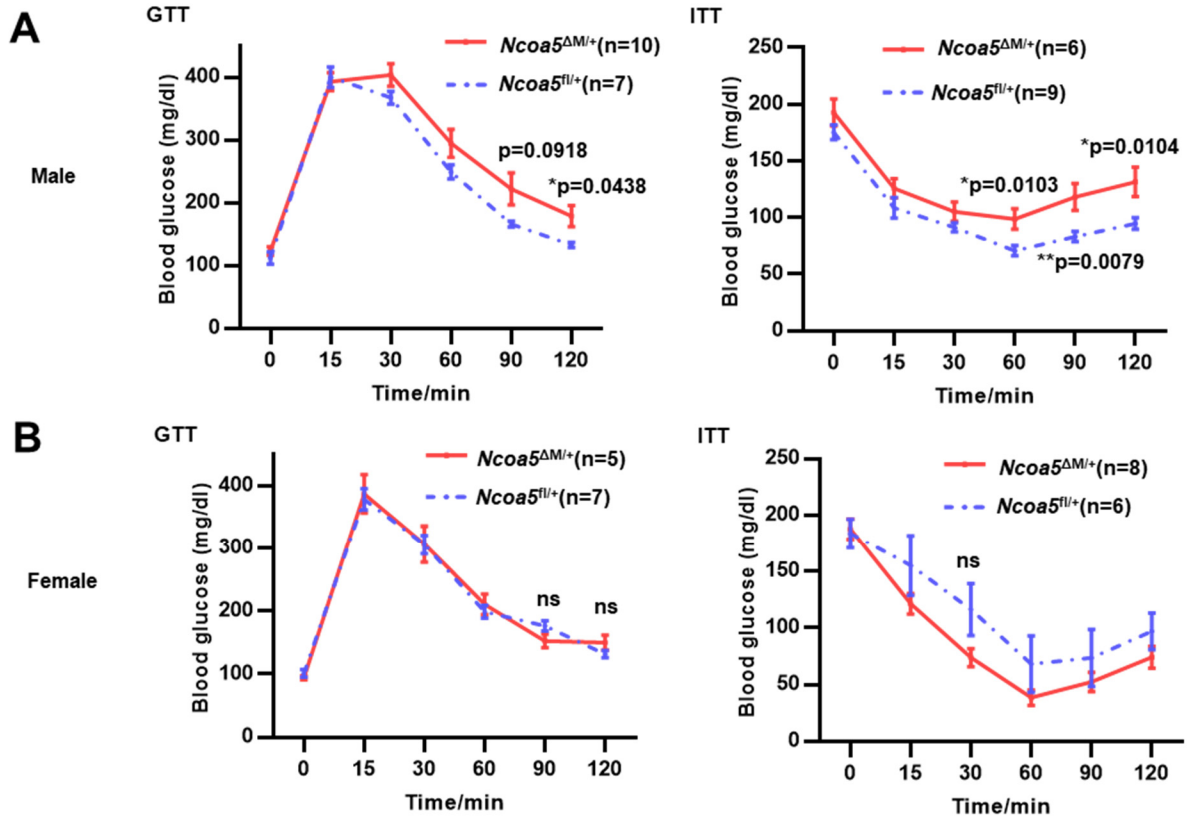

Figure 2.2. Glucose and insulin tolerance tests in *Ncoa5*$^{\Delta M/+}$ mice fed a normal diet. (A and B) Glucose tolerance test of 7-week-old (left) and insulin tolerance test of 8-week-old (right) *Ncoa5*$^{fl/+}$ and *Ncoa5*$^{\Delta M/+}$ male (A) and female (B) mice. The number of mice tested is labeled. Data represent mean ± SEM. Two-tailed unpaired Student's t test. *p<0.05. ns, not significant.

At five months of age, *Ncoa5*$^{\Delta M/+}$ male mice had significantly increased body weight compared to *Ncoa5*$^{fl/+}$ male mice (Fig. 2.3A), and some *Ncoa5*$^{\Delta M/+}$ male mice had mild microvesicular steatosis (Fig. 2.3B). Finally, spontaneous HCC was observed in *Ncoa5*$^{\Delta M/+}$ male mice starting at ten months of age. 25% of *Ncoa5*$^{\Delta M/+}$ male mice developed liver tumors. In contrast, no liver tumor was found in *Ncoa5*$^{fl/+}$ male mice over 18 months (Fig. 2.3C). The liver tumors in *Ncoa5*$^{\Delta M/+}$ male mice were well to moderately differentiated HCCs associated with hepatic steatosis (Fig. 2.3D). Altogether, these results suggest that myeloid-lineage-specific heterozygous deletion of *Ncoa5* is sufficient to induce the spontaneous development of the metabolic syndrome and a moderate incidence of HCC in mice in a male-biased manner.

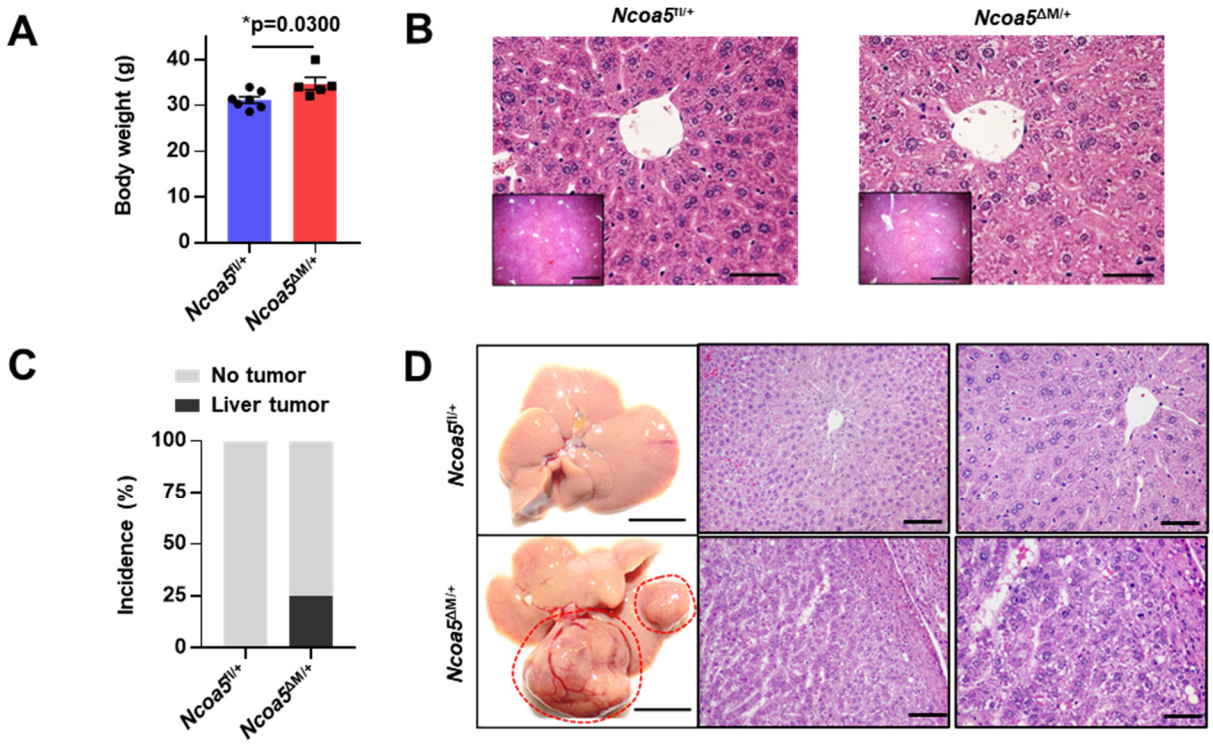

Figure 2.3. Metabolic-related phenotypes and spontaneous HCCs in *Ncoa5*$^{\Delta M/+}$ mice fed a normal diet. (A) Body weight of 5-month-old *Ncoa5*$^{fl/+}$ (n=7) and *Ncoa5*$^{\Delta M/+}$ (n=5) male mice. (B) Representative H & E staining photos of 5-month-old *Ncoa5*$^{fl/+}$ and *Ncoa5*$^{\Delta M/+}$ males showing mild microvesicular steatosis in some 5-month-old *Ncoa5*$^{\Delta M/+}$ male mice. Scale bars: 50 μm and 750 μm (insets). (C) Incidence of HCC in aged *Ncoa5*$^{fl/+}$ (n=12) and *Ncoa5*$^{\Delta M/+}$ (n=16) male mice monitored till 18-month-old. (D) Representative macroscopic photos and H & E-stained liver sections of 18-month-old

Figure 2.3 (cont'd)
Ncoa5$^{fl/+}$ or tumor-bearing *Ncoa5*$^{\Delta M/+}$ male mice. Red circles indicate HCCs. Scale bar: 1 cm, 100 µm, or 50 µm. Data represent mean ± SEM. Two-tailed unpaired Student's t test. *p<0.05.

3.4.2 Myeloid-lineage-specific heterozygous deletion of Ncoa5 results in the spontaneous development of NASH in aged male mice fed a normal diet

To evaluate the impact of myeloid-lineage-specific heterozygous deletion of *Ncoa5* on the liver at the preneoplastic step of hepatocarcinogenesis, we examined the post-mortem livers of 10 months *Ncoa5*$^{fl/+}$ and *Ncoa5*$^{\Delta M/+}$ mice. Most of the livers from

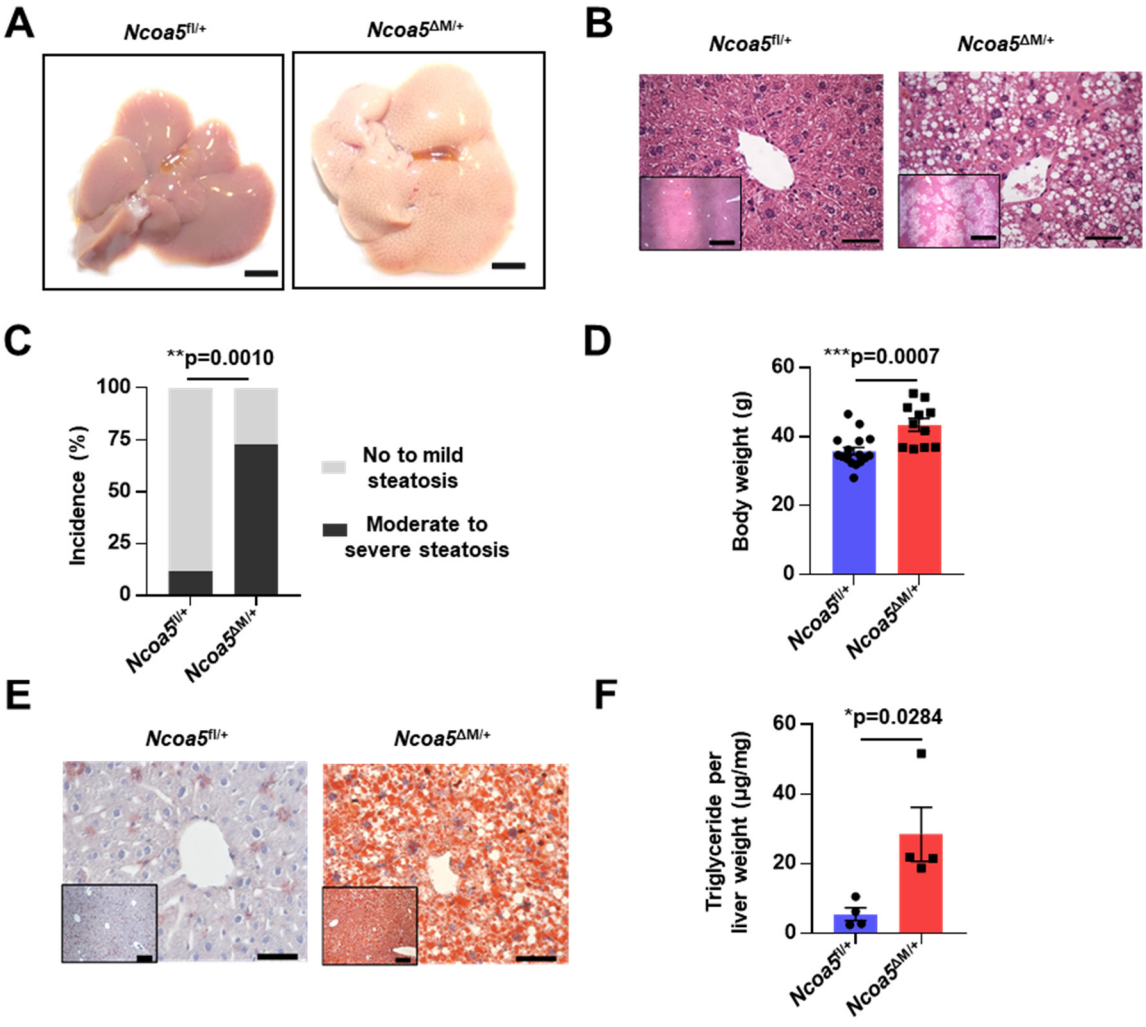

Figure 2.4. Steatosis phenotypes in livers of 10-month-old *Ncoa5*$^{\Delta M/+}$ male mice fed a normal diet. (A) Representative macroscopic images of livers from 10-month-old *Ncoa5*$^{fl/+}$ and *Ncoa5*$^{\Delta M/+}$ male mice. Scale bar: 0.5 cm. (B) Representative H & E staining

Figure 2.4 (cont'd)
of liver sections from 10-month-old *Ncoa5*$^{fl/+}$ and *Ncoa5*$^{\Delta M/+}$ male mice. Scale bar: 50 μm or 750 μm (insets). (C) Incidence of no to mild steatosis and moderate to severe steatosis in 10-month-old *Ncoa5*$^{fl/+}$ (n=17) and *Ncoa5*$^{\Delta M/+}$ (n=11) male mice. Chi-squared test. (D) Bodyweight of 10-month-old *Ncoa5*$^{fl/+}$ (n=17) and *Ncoa5*$^{\Delta M/+}$ (n=11) male mice. (E) Representative Oil-red-o staining of livers from 10-month-old *Ncoa5*$^{fl/+}$ and *Ncoa5*$^{\Delta M/+}$ male mice. Scale bar: 50 μm or 200 μm (insets). (F) Liver triglyceride concentration of mice as indicated. Mouse n=4 for each group. Data represent mean ± SEM. Two-tailed unpaired Student's t test was used if not otherwise specified. ***p<0.001, **p<0.01, *p<0.05.

Ncoa5$^{\Delta M/+}$ male mice have a much lighter color than control livers (Fig. 2.4A). 73% of *Ncoa5*$^{\Delta M/+}$ male mice exhibited moderate to severe steatosis as H & E staining showed moderate to marked centrilobular macrovesicular steatosis and was associated with mild to moderate inflammatory infiltrates in the liver (Fig. 2.4B and 2.4C). *Ncoa5*$^{\Delta M/+}$ male mice also had significantly increased body weight (Fig. 2.4D). Markedly increased hepatic lipid content in these mice was detected by oil-red-o staining and measured with triglyceride colorimetric assay (Fig. 2.4E and 2.4F). The number of macrophages significantly increased in the livers of *Ncoa5*$^{\Delta M/+}$ male mice, as shown in the IHC assay. The macrophages accumulated near ballooned hepatocytes and formed a crown-like structure[273] (Fig. 2.5A). Sirius red staining indicated that the NASH livers of *Ncoa5*$^{\Delta M/+}$ male mice also had fibrosis (Fig. 2.5B). I then examined the expression of the transcription factors PPARγ, SREBP-1c, and ChREBP, which are important in regulating hepatic glucose and lipid metabolisms and are often dysregulated in patients with NAFLD/NASH[274-276]. Among them, the mRNA level of *Pparg2* was significantly increased in the livers of 10-month-old *Ncoa5*$^{\Delta M/+}$ mice compared to age-matched *Ncoa5*$^{fl/+}$ male mice (Fig. 2.6A). The protein level of PPARγ was elevated considerably and translocated to the nuclei in hepatocytes of *Ncoa5*$^{\Delta M/+}$ mice (Fig. 2.6B). Consistent with this observation, the mRNA levels of the downstream targets of PPARγ2, including

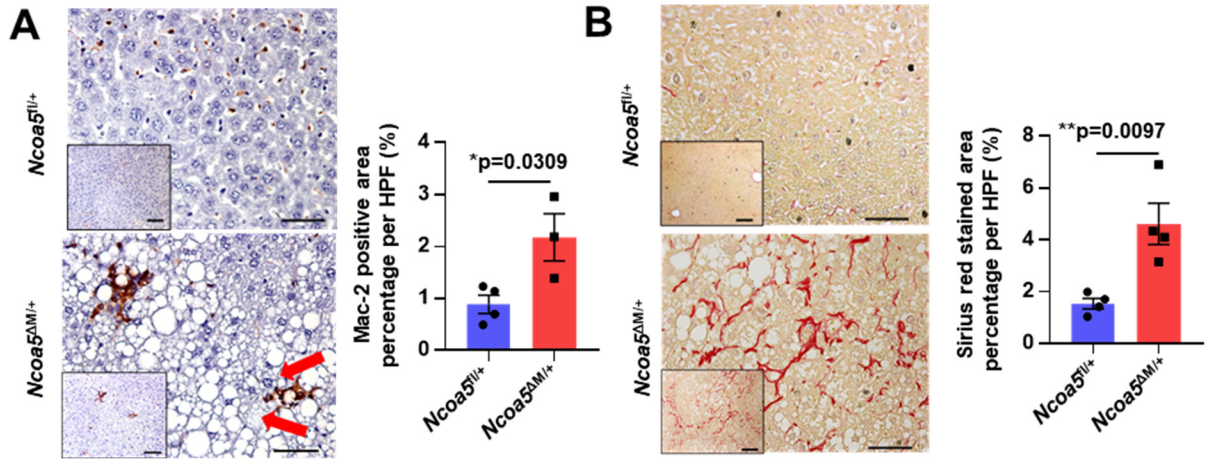

Figure 2.5. Inflammation and fibrosis phenotypes in livers of 10-month-old *Ncoa5*$^{\Delta M/+}$ male mice fed a normal diet. (A) Representative images of MAC-2 IHC liver sections from 10-month-old *Ncoa5*$^{fl/+}$ (n=4) and *Ncoa5*$^{\Delta M/+}$ (n=3) male mice and the quantification of stained area positive for MAC-2. Arrows indicate hepatocytes with ballooning. 5 high-power fields (HPFs) per mouse. Scale bar: 50 μm and 100 μm. (B) Representative images of Sirius red-stained liver sections from 10-month-old *Ncoa5*$^{fl/+}$ (n=4) and *Ncoa5*$^{\Delta M/+}$ (n=4) male mice and the quantification of stained areas. 5 HPFs per mouse. Scale bar: 50 μm and 100 μm. Data represent mean ± SEM. Two-tailed unpaired Student's t test. **p<0.01, *p<0.05.

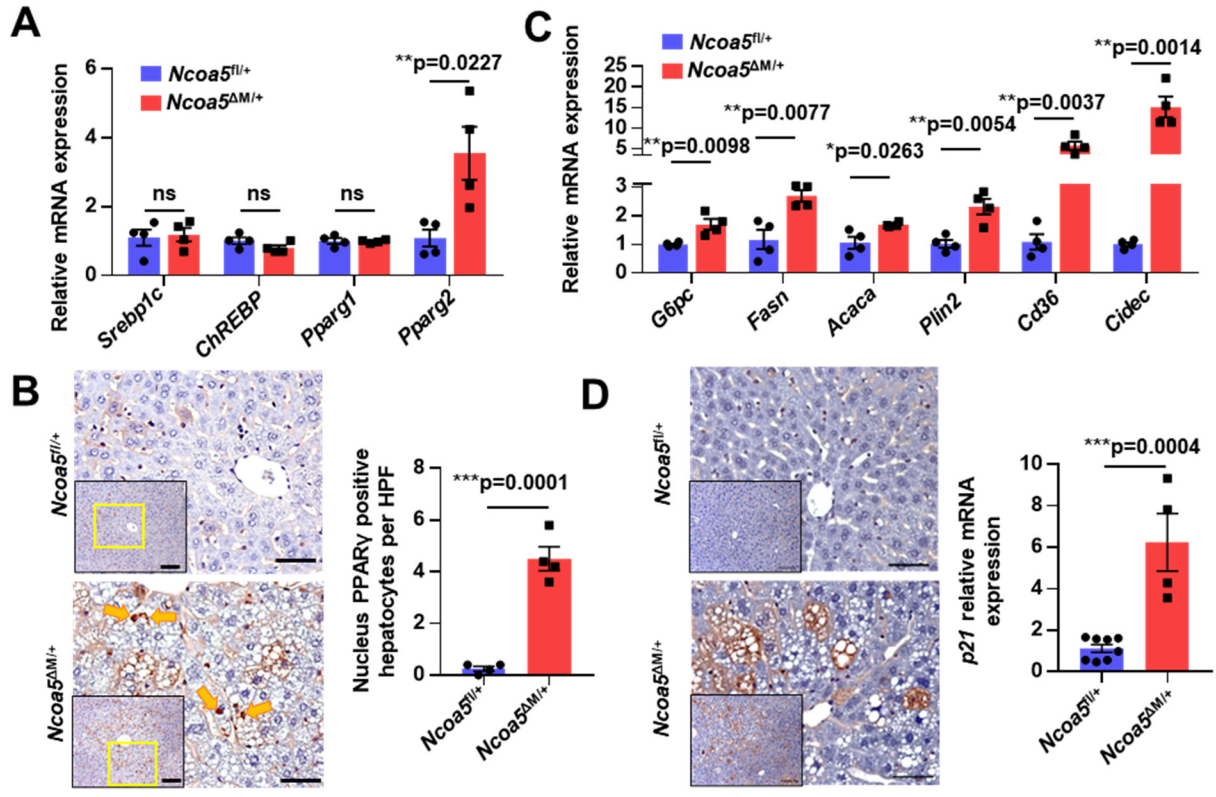

Figure 2.6. Steatosis-related gene expression in *Ncoa5*$^{\Delta M/+}$ male mice fed a normal

Figure 2.6 (cont'd)
diet. (A) RT-qPCR analysis of the mRNA levels of transcription factors related to liver lipid metabolism between livers of 10-month-old *Ncoa5*$^{fl/+}$ (n=4) and *Ncoa5*$^{\Delta M/+}$ (n=4) male mice. (B) Representative images of IHC for PPARγ in liver sections of 10-month-old *Ncoa5*$^{fl/+}$ (n=4) and *Ncoa5*$^{\Delta M/+}$ (n=4) male mice and the quantification of nucleus-positive cell numbers. Arrows indicate the nuclear localization of PPARγ. (C) RT-qPCR analysis of the mRNA levels of genes encoding critical enzymes in glucose and lipid metabolisms and genes regulated by PPARγ in the livers of 10-month-old *Ncoa5*$^{fl/+}$ (n=4) and *Ncoa5*$^{\Delta M/+}$ (n=4) male mice. (D) RT-qPCR analysis of the mRNA levels of *p21* in livers of 10-month-old *Ncoa5*$^{fl/+}$ (n=8) and *Ncoa5*$^{\Delta M/+}$ (n=4) male mice and the representative photos of IHC for p21. Data represent mean ± SEM. Two-tailed unpaired Student's t test. ***p<0.001, **p<0.01, *p<0.05. Scale bar: 50 μm and 100 μm (insets).

G6pc, *Fasn*, *Acaca*, *Plin2*, *Cd36*, and *Cidec*[277], were significantly increased in the livers of *Ncoa5*$^{\Delta M/+}$ male mice compared to *Ncoa5*$^{fl/+}$ male mice (Fig. 2.6C). Consistent with our previous report in *Ncoa5*$^{+/-}$ male mice[271], *p21* expression was also increased in *Ncoa5*$^{\Delta M/+}$ male mice (Fig. 2.6D). These results suggest that *Ncoa5*$^{\Delta M/+}$ male mice develop NASH at 10 months old.

3.4.3 Ncoa5-deficient macrophages trigger lipid accumulation in hepatocytes by inducing the expression of lipogenic genes, at least in part, via releasing PF4

To identify potential NCOA5 downstream targets and molecular factors in myeloid-lineage cells contributing to the development of NASH, we systematically examined genes and pathways altered in *Ncoa5* deficient mice by performing RNA-seq and transcriptome analysis on intrahepatic F4/80+ macrophages isolated from the pre-NASH livers of 6.5-month-old *Ncoa5*$^{\Delta M/+}$ and *Ncoa5*$^{fl/+}$ male mice (Fig. 2.7A and 2.7B). I found 207 differently expressed genes (DEGs) (fold change>2, padj<0.1) between these two macrophage groups (Fig. 2.7C) and that the genes encoding secretory proteins, including *Pf4*, *Angptl7*, and *Mmp13,* were upregulated in *Ncoa5*$^{\Delta M/+}$ intrahepatic macrophages. *Pf4*, also known as chemokine CXCL4, had the most

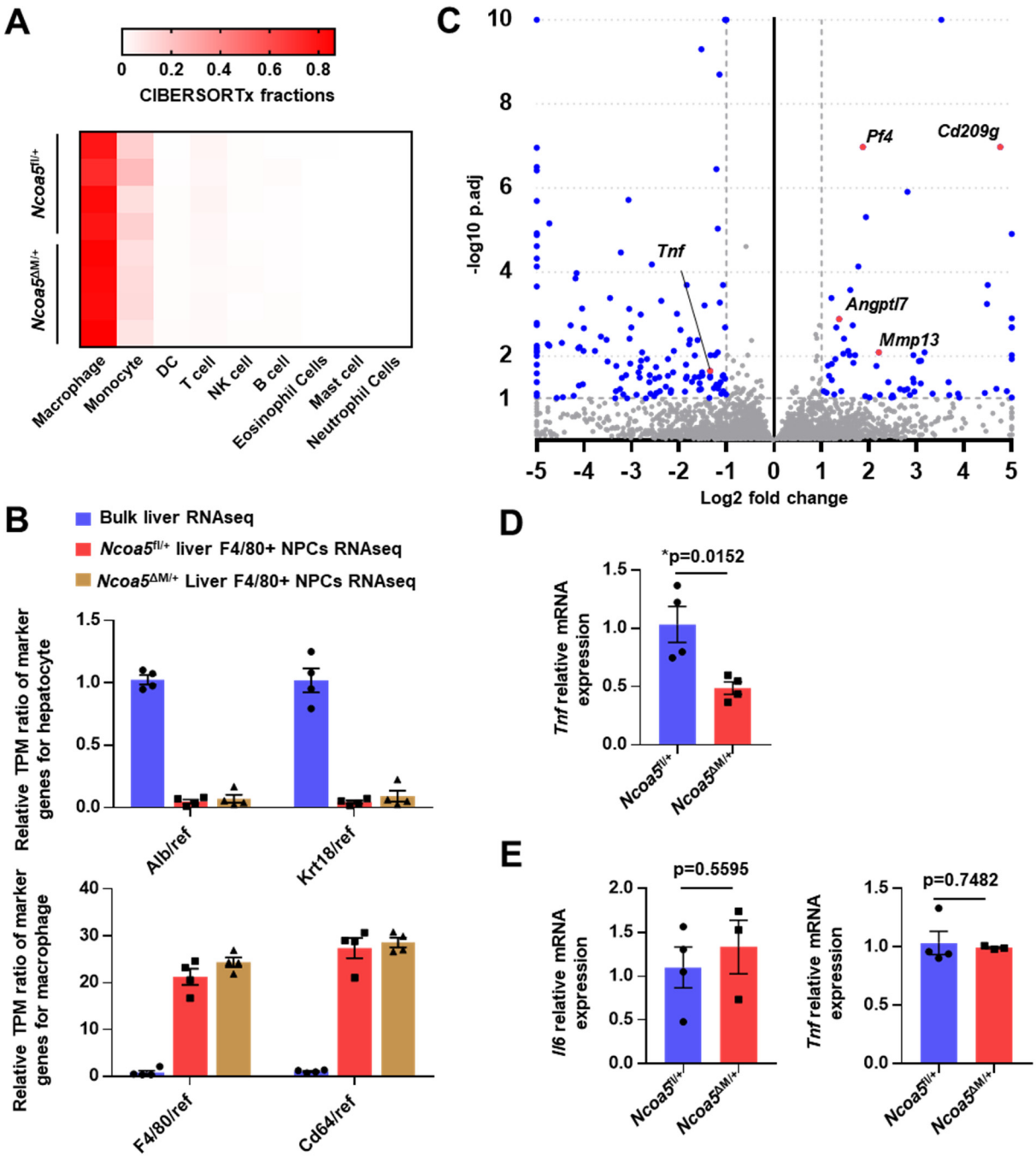

Figure 2.7 Expression differences of classical proinflammatory cytokines comparing *Ncoa5*$^{fl/+}$ and *Ncoa5*$^{\Delta M/+}$ intrahepatic macrophages. (A) Cell-type composition of isolated F4/80+ hepatic nonparenchymal cells from 6.5-month-old *Ncoa5*$^{fl/+}$ and *Ncoa5*$^{\Delta M/+}$ males inferred by CIBERSORTx using immuCC signature. (B) Relative expression of hepatocyte and macrophage markers in isolated F4/80+ hepatic nonparenchymal cells from 6.5-month-old *Ncoa5*$^{fl/+}$ and *Ncoa5*$^{\Delta M/+}$ males compared to bulk livers from 5-month-old wild-type C57BL/6 males (GSE110524). n=4 per mouse group. Relative expression of marker genes was calculated as the TPMs of markers divided by the TPMs of a group of housekeeping genes and then normalized to the

Figure 2.7 (cont'd)
result of bulk liver RNA-seq. (C) The volcano plot showing the DESeq2 differential gene expression analysis results comparing the intrahepatic macrophages from 6.5-month-old *Ncoa5*$^{fl/+}$ males versus *Ncoa5*$^{\Delta M/+}$ males. Genes with p.adj<0.1 and fold change >2 were labeled in blue and red. (D) RT-qPCR validation of *Tnf* mRNA expression in the intrahepatic macrophages from 6.5-month-old *Ncoa5*$^{fl/+}$ (n=4) and *Ncoa5*$^{\Delta M/+}$ (n=4) male mice. (E) RT-qPCR analysis of the mRNA levels of *Il6* and *Tnf* in livers of 3-month-old *Ncoa5*$^{fl/+}$ (n=4) and *Ncoa5*$^{\Delta M/+}$ (n=3) male mice. Data represent mean ± SEM in B, D, and E. Two-tailed unpaired Student's t test. *p<0.05.

significant increase among them. Interestingly, RNA-seq did not detect a significant change in the gene encoding the proinflammatory cytokine IL-6, which plays a critical role in the initiation and progression of HCC in several mouse models of NASH and HCC, including *Ncoa5*$^{+/-}$ male mice and diet- or chemical-induced mice[98,278]. Moreover, the mRNA level of *Tnf* encoding another proinflammatory cytokine, TNFα, was significantly reduced in the intrahepatic macrophages of *Ncoa5*$^{\Delta M/+}$ male mice, validated by RT-qPCR (Fig. 2.7D). The expression of *Il6* or *Tnf* was comparable in the livers of *Ncoa5*$^{\Delta M/+}$ male mice compared to *Ncoa5*$^{fl/+}$ mice at an earlier age (Fig. 2.7E), indicating that these two proinflammatory cytokines may not be involved in the initiation of hepatic steatosis in these mice.

Given the previous findings that CXCR3, a chemokine receptor for CXCL9, CXCL10, CXCL11, and PF4, is crucial in developing diet-induced NAFLD/NASH[279] and among these ligands, only PF4 was overexpressed in *Ncoa5*$^{\Delta M/+}$ macrophages in RNA-seq data analysis (Fig. 2.8A), we next focused on PF4. I confirmed that *Pf4* mRNA expression was increased in the intrahepatic macrophages of *Ncoa5*$^{\Delta M/+}$ male mice compared to age-matched *Ncoa5*$^{fl/+}$ male mice by RT-qPCR (Fig. 2.8B) and showed that the protein level of PF4 was also elevated in the NASH livers of *Ncoa5*$^{\Delta M/+}$ male mice compared to age-matched *Ncoa5*$^{fl/+}$ male mice by western blotting (Fig. 2.8C). In

contrast, PF4 expression was seemingly not elevated as it is undetectable in the livers of age-matched *Ncoa5*$^{\Delta M/+}$ and *Ncoa5*$^{fl/+}$ female mice (Fig. 2.8D). Interestingly, the

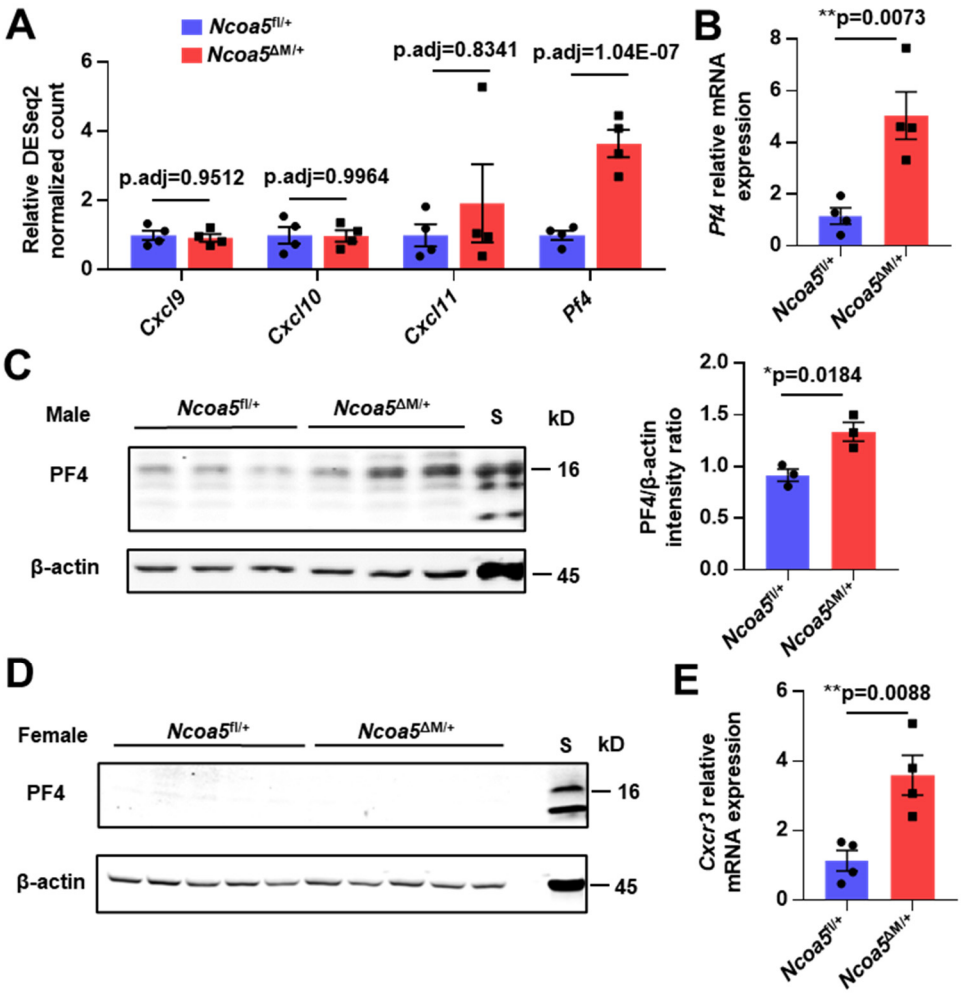

Figure 2.8 Expression changes of CXCR3 and its ligands in *Ncoa5*$^{\Delta M/+}$ male mice fed a normal diet. (A) The mRNA levels of genes encoding CXCR3 ligands in intrahepatic macrophages from 6.5-month-old *Ncoa5*$^{fl/+}$ and *Ncoa5*$^{\Delta M/+}$ males. They were assessed by RNA-seq and shown as DESeq2 normalized counts relative to the average counts of *Ncoa5*$^{fl/+}$ male mice (as 1). p.adj calculated by DESeq2. (B) RT-qPCR validation of *Pf4* mRNA expression in the intrahepatic macrophages from 6.5-month-old *Ncoa5*$^{fl/+}$ (n=4) and *Ncoa5*$^{\Delta M/+}$ (n=4) male mice. (C) Western blotting and the quantification of PF4 protein level in liver lysates of 10-month-old *Ncoa5*$^{fl/+}$ (n=3) and *Ncoa5*$^{\Delta M/+}$ (n=3) male mice. S: Spleen lysate from wild-type mice. (D) Western blotting of PF4 protein level in liver lysates of 5-month-old *Ncoa5*$^{fl/+}$ (n=5) and *Ncoa5*$^{\Delta M/+}$ (n=5) female mice. S: Spleen lysate from wild-type mice. (E) RT-qPCR validation of *Cxcr3* mRNA expression in the intrahepatic macrophages from 6.5-month-old *Ncoa5*$^{fl/+}$ (n=4) and *Ncoa5*$^{\Delta M/+}$ (n=4) male mice. Data represent mean ± SEM. Two-tailed unpaired Student's t test if not otherwise specified. **p<0.01, *p<0.05.

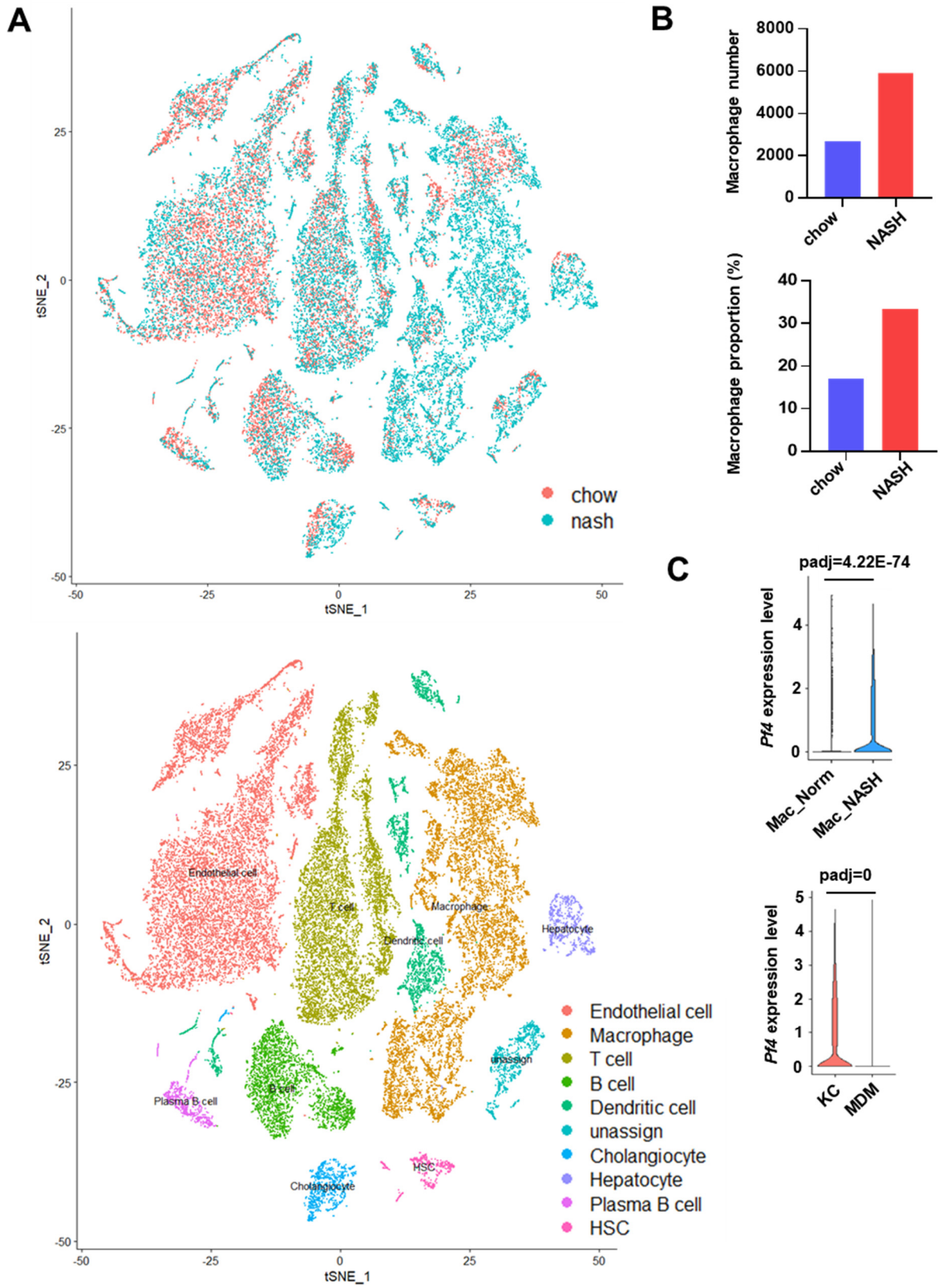

Figure 2.9 Difference in *Pf4* expression between AMLN diet and control diet mice

Figure 2.9 (cont'd)
assessed by single-cell RNA-seq. (A) t-SNE plot visualizing the single-cell transcriptome clustering of liver cells from mice fed a control diet (chow) and mice fed an AMLN diet (nash). Top: cells labeled according to mouse diets. Bottom: cells labeled according to inferred cell types. (B) Cell number and proportion of inferred macrophage cell type in mice fed a control diet (chow) and an AMLN diet (nash). They were produced in my re-analysis of the NCBI Sequence Read Archive PRJNA531644 raw data (GSE129516). (C) *Pf4* expression in intrahepatic macrophages of ALMN-induced NASH livers and control livers. Seurat reported adjusted p-values. Mac: intrahepatic macrophage, KC: Kupffer cell, MDM: monocyte-derived macrophage.

expression of *Cxcr3* was also increased in the intrahepatic macrophages of *Ncoa5*$^{\Delta M/+}$ male mice (Fig. 2.8E).

Pf4 was previously revealed as a continuously upregulated gene in intrahepatic macrophages of NAFLD mice induced by a westernized and sucrose/fructose-supplemented diet[280]. To determine whether *Pf4* is also upregulated in other mouse models of NAFLD/NASH, I reanalyzed a published single-cell RNA-seq dataset of nonparenchymal cells from Amylin liver NASH (AMLN) diet-induced NASH livers and normal diet-fed mouse livers[281]. The t-SNE plots showed a liver cell clustering pattern and increased macrophage proportion in NASH livers similar to the previous reports (Fig. 2.9A and 2.9B). Indeed, *Pf4* expression was significantly upregulated in the intrahepatic macrophages from NASH livers compared to those from normal livers (Fig. 2.9C). The high *Pf4* expression was found in Kupffer cells rather than monocyte-derived macrophages (Fig. 2.9C).

To determine the role of PF4 secreted from intrahepatic macrophages in hepatic lipogenesis regulation, we assess the effect of macrophage PF4 on hepatocytes *in vitro* and *in vivo*. Firstly, we demonstrated that *Ncoa5*-null macrophage-like RAW 264.7 cells displayed an increased PF4 expression compared to control RAW264.7 cells (Fig. 2.10A). Media conditioned by different RAW264.7 cells containing various secreted

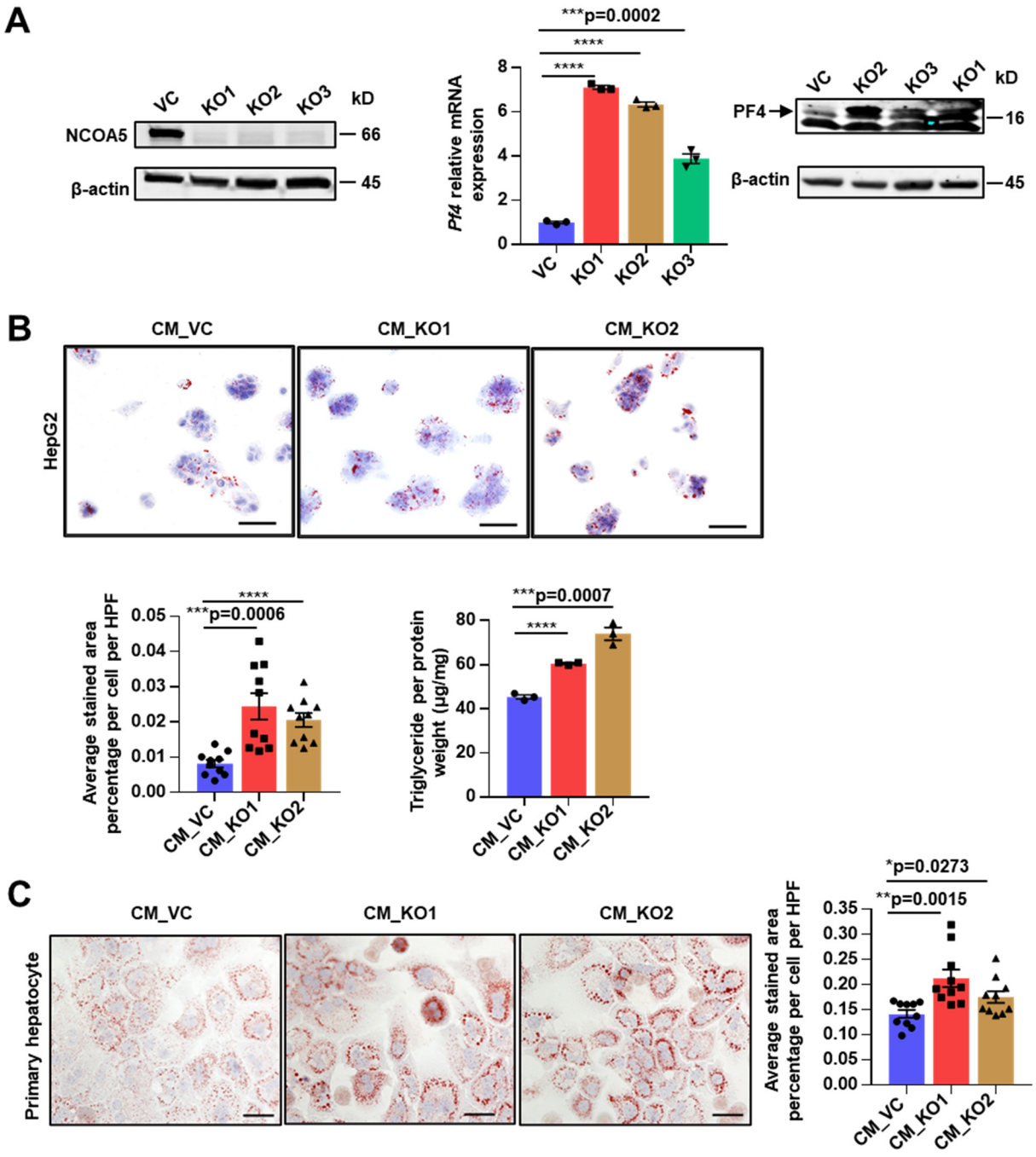

Figure 2.10 Effect of *Ncoa5* knockout on PF4 expression in macrophage-like RAW 264.7 cells and the influence of their conditioned medium on lipid accumulation in hepatocytes. (A) Left: Western blot validation of *Ncoa5* knockout in RAW 264.7 cells. VC: vector control. KO1-3: 3 independent clones. Mid and right: RT-qPCR showing *Pf4* mRNA levels (mid) and Western blotting analyzing PF4 protein (right) in RAW 264.7 cells with or without *Ncoa5* knockout. PF4 is indicated with an arrow. (B) Top: Representative Oil-red-o staining of human HCC HepG2 cells treated with CM from RAW 264.7 cells with or without *Ncoa5* knockout for one day. Bottom left: Quantification of Oil-red-o-stained area per cell treated with indicated CM, 5 HPFs were captured in

Figure 2.10 (cont'd)
each condition, combined results from two experiments. Bottom right: Cell triglyceride concentration of HepG2 cells treated with indicated CM, Representative data of three repeats. Data were quantitated and expressed as micrograms of triglyceride per milligram of protein. (C) Representative Oil-red-o staining and the quantification of stained area per cell for mouse primary hepatocytes treated with CM from RAW 264.7 cells with or without *Ncoa5* knockout for one day. 5 HPFs were captured in each condition, combining results from two experiments. Scale bar: 50 μm. Data represent mean ± SEM. Two-tailed unpaired Student's t test. *p<0.05, **p<0.01, ***p<0.001, ****p<0.0001.

factors were collected to treat hepatocytes. I showed that cellular lipids were significantly increased in primary mouse hepatocytes and human HepG2 cells treated with the conditioned medium (CM) of *Ncoa5*-null RAW 264.7 cells compared to those treated with the CM of vector-control RAW 264.7 cells (Fig. 2.10B and 2.10C).

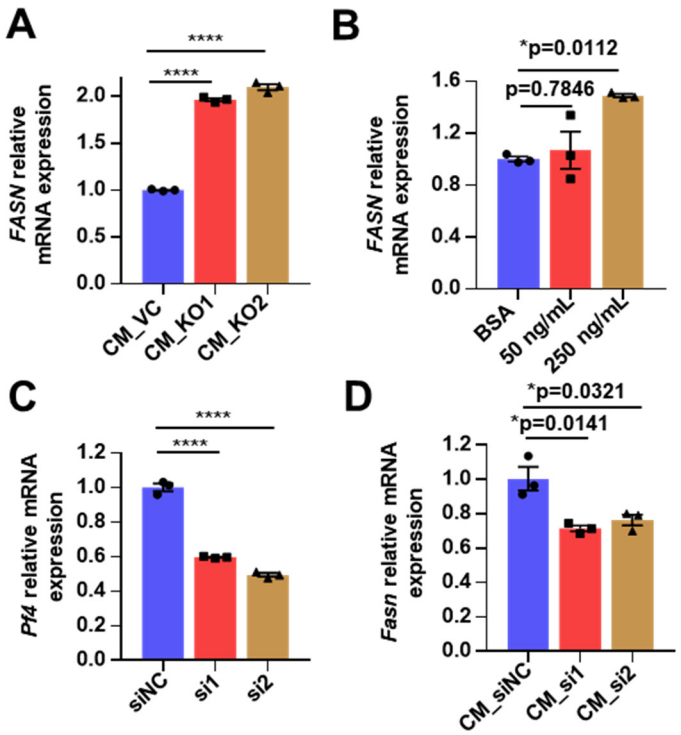

Figure 2.11 Effect of conditioned medium and PF4 on *FASN* expression in hepatocytes. (A) RT-qPCR analysis of the mRNA levels of *FASN* in HepG2 cells treated with CM from RAW 264.7 cells with or without *Ncoa5* knockout. (B) RT-qPCR analysis of the mRNA levels of *FASN* in HepG2 cells treated with BSA or recombinant mouse PF4 in low glucose 5% FBS medium for three days. One-way ANOVA Dunnett's multiple comparisons test. (C) RT-qPCR analysis of *Pf4* mRNA levels in *Ncoa5*-null RAW 264.7 cells transfected with siRNAs for *Pf4* or negative control siRNA (siNC). (D)

Figure 2.11 (cont'd)
RT-qPCR analysis of *Fasn* mRNA levels in mouse primary hepatocytes treated with CM from *Ncoa5*-null RAW 264.7 cells with or without *Pf4* knockdown. Data represent mean ± SEM. Two-tailed unpaired Student's t test was used if not otherwise specified. ****p<0.0001, *p<0.05.

Next, I demonstrated that treating HepG2 cells with the CM of *Ncoa5*-null RAW 264.7 cells significantly increased expression of *FASN*, which encodes the key enzyme fatty acid synthase in lipogenesis, compared to those treated with the CM of vector-control RAW 264.7 cells (Fig. 2.11A). Importantly, treating HepG2 cells with recombinant mouse PF4 had a similar effect (Fig. 2.11B). To determine if the effect of CM treatment on *FASN* expression was due to PF4 overexpression, I generated *Ncoa5*-null RAW 264.7 cells with or without *Pf4* knockdown (Fig. 2.11C). Mouse primary hepatocytes treated with the CM from the *Ncoa5*-null RAW 264.7 cells with *Pf4* knockdown had significantly lower *Fasn* expression than those treated with the CM from the *Ncoa5*-null cells transfected with a control siRNA (Fig. 2.11D).

Moreover, I ectopically overexpressed human or mouse *PF4* in RAW 264.7 cells and used their CM to treat mouse primary hepatocytes (Fig. 2.12A). The CM from either mouse or human PF4-overexpressed cells was able to increase lipid content and the mRNA levels of *G6pc* and *Acaca*, encoding key enzymes in glucose neogenesis and lipogenesis, in primary mouse hepatocytes (Fig. 2.12B and 2.12C) and increased the triglyceride concentration in HepG2 cells (Fig. 2.12D) compared to CM from RAW 264.7 cells that express GFP control. Mouse primary hepatocytes treated with recombinant mouse PF4 significantly increased the mRNA expressions of *G6pc*, *Cyp2e1*, *Fasn*, *p21*, and *Acaca* and trended to increase the triglyceride content (Fig. 2.12E and 2.12F).

Finally, I used a glucan-encapsulated siRNA particle (GeRP) approach[30,31,282] to

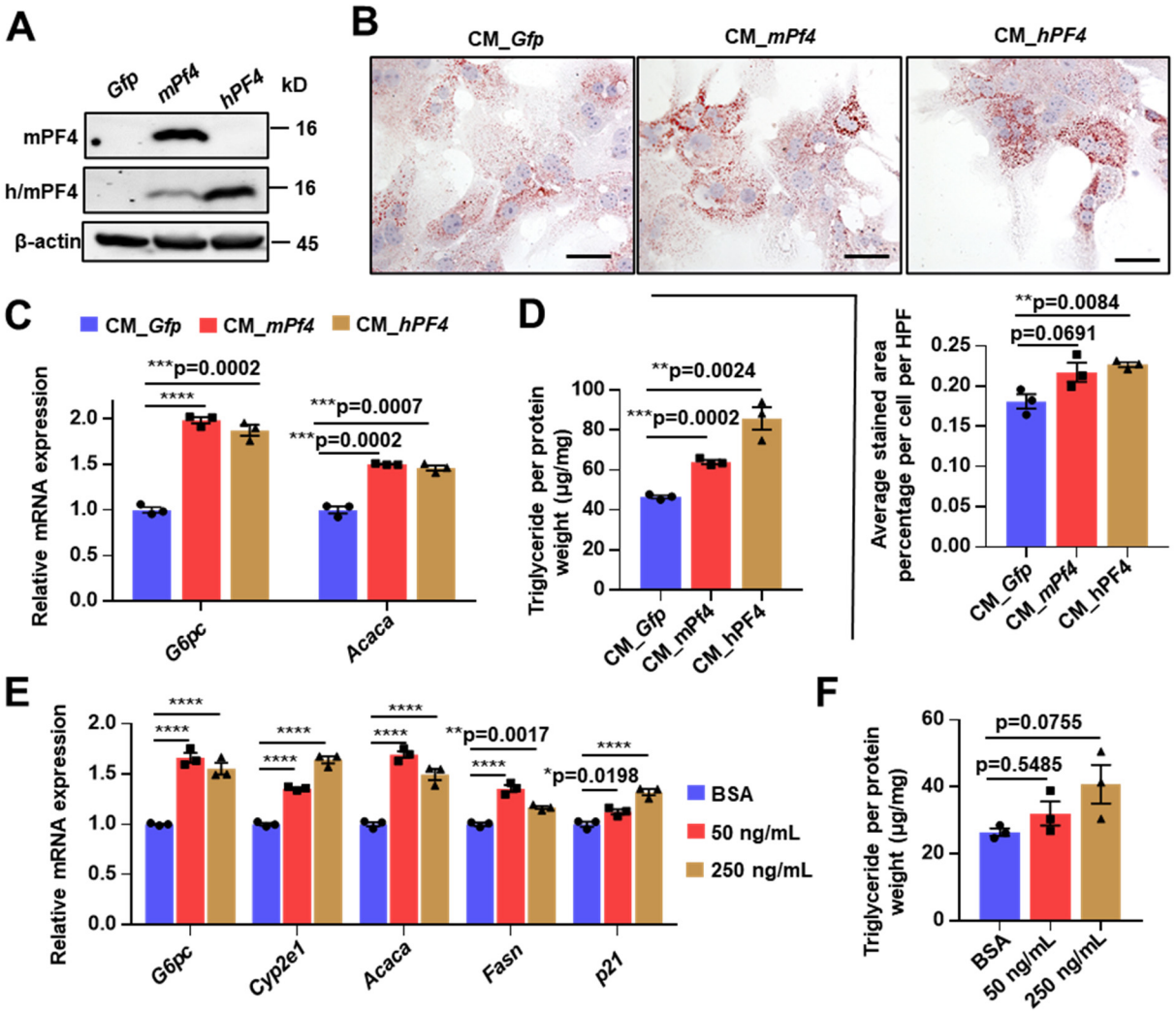

Figure 2.12 Effects of PF4 on lipid accumulation and lipogenic gene expression in hepatocytes. (A) Western blotting validation of mouse PF4 overexpression or human PF4 ectopic expression in lentivirus-transformed RAW 264.7 cells. h/mPF: an antibody that recognizes both human and mouse PF4. (B) Top: Representative Oil-red-o staining images of mouse primary hepatocytes treated with CM from RAW 264.7 cells with or without PF4 overexpression. Bottom: The quantification of stained area per cell. 5 HPFs were captured in each condition, summarized from three repeats. (C) RT-qPCR analysis of *G6pc* and *Acaca* mRNA levels in mouse primary hepatocytes treated with CM from RAW 264.7 cells with PF4 ectopic expression. Representative data from three repeats. (D) Cell triglyceride concentration per protein weight of HepG2 cells treated with different CM. Representative data from three repeats. Data were quantitated and expressed as micrograms of triglyceride per milligram of protein. (E) RT-qPCR analysis of the mRNA levels of glucose and lipid metabolism genes in mouse primary hepatocytes treated with recombinant mouse PF4. Two-way ANOVA Dunnett's multiple comparisons test. (F) Cell triglyceride concentrations in mouse primary hepatocytes treated with recombinant mouse PF4. Data were quantitated and expressed as micrograms of triglyceride per milligram of protein. Data represent mean ± SEM. Two-

Figure 2.12 (cont'd)
tailed unpaired Student's t test was used if not otherwise specified. ****p<0.0001, ***p<0.001, **p<0.01. Scale bar: 50 μm.

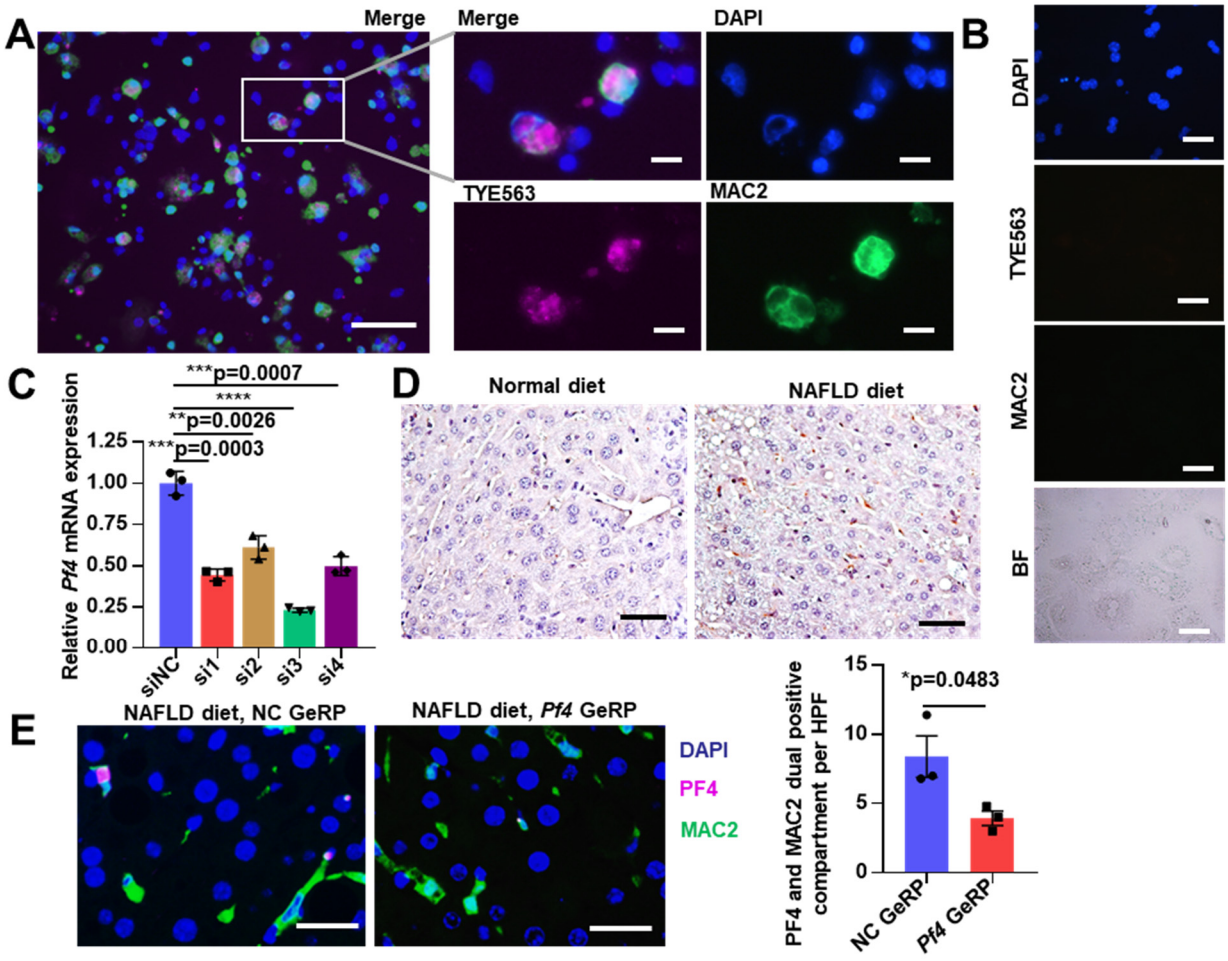

Figure 2.13 Intrahepatic-macrophage-specific *Pf4* knockdown mediated by GeRPs. (A and B) Representative immunofluorescence staining of MAC-2 in isolated hepatic non-parenchymal cells (A) or parenchymal cells (B) from mice injected with GeRPs containing TYE563-labeled siRNA. Blue: DAPI. Purple: TYE563. Green: MAC-2. Scale bar in (A) left: 50 μm, middle and right: 10 μm. Scale bar in (B): 50 μm. (C) RT-qPCR analysis of the *Pf4* mRNA expression in RAW 264.7 *Ncoa5* knockout clone 1 treated with four different Dharmacon siRNAs targeting mouse *Pf4* (si1-si4) or a non-targeting siRNA (siNC). (D) Representative IHC staining of PF4 in livers of wild-type male mice fed a normal or NAFLD diet for three months. Scale bar: 50 μm. (E) Representative dual-immunofluorescence staining of PF4 and MAC-2 in livers of wild-type male mice (n=3 per group) fed a NAFLD diet injected with siNC- or si3-containing GeRPs and the quantification of dual-stained compartments. Blue: DAPI. Purple: PF4. Green: MAC-2. Scale bar: 25 μm. Data represent mean ± SEM. Two-tailed unpaired Student's t test. ****p<0.0001, ***p<0.001, **p<0.01, *p<0.05.

specifically target intrahepatic macrophages in mice (Fig. 2.13A and 2.13B), using a siRNA that efficiently knocks down *Pf4* expression *in vitro* (si3 in Fig. 2.13C). PF4 overexpression was confirmed in the intrahepatic macrophages of mice fed the aforementioned westernized diet[280] (Fig. 2.13D). Specific *Pf4* knockdown in intrahepatic macrophages (Fig. 2.13E) reduced the lipid accumulation and the mRNA levels of *Pparg2* and its downstream targets in the livers of mice fed the westernized diet (Fig. 2.14A - 2.14D). The reduction in the mRNA levels of *Pparg2* and its downstream targets by the *Pf4* knockdown was also observed in the livers of male *Ncoa5*$^{\Delta M/+}$ mice (Fig.

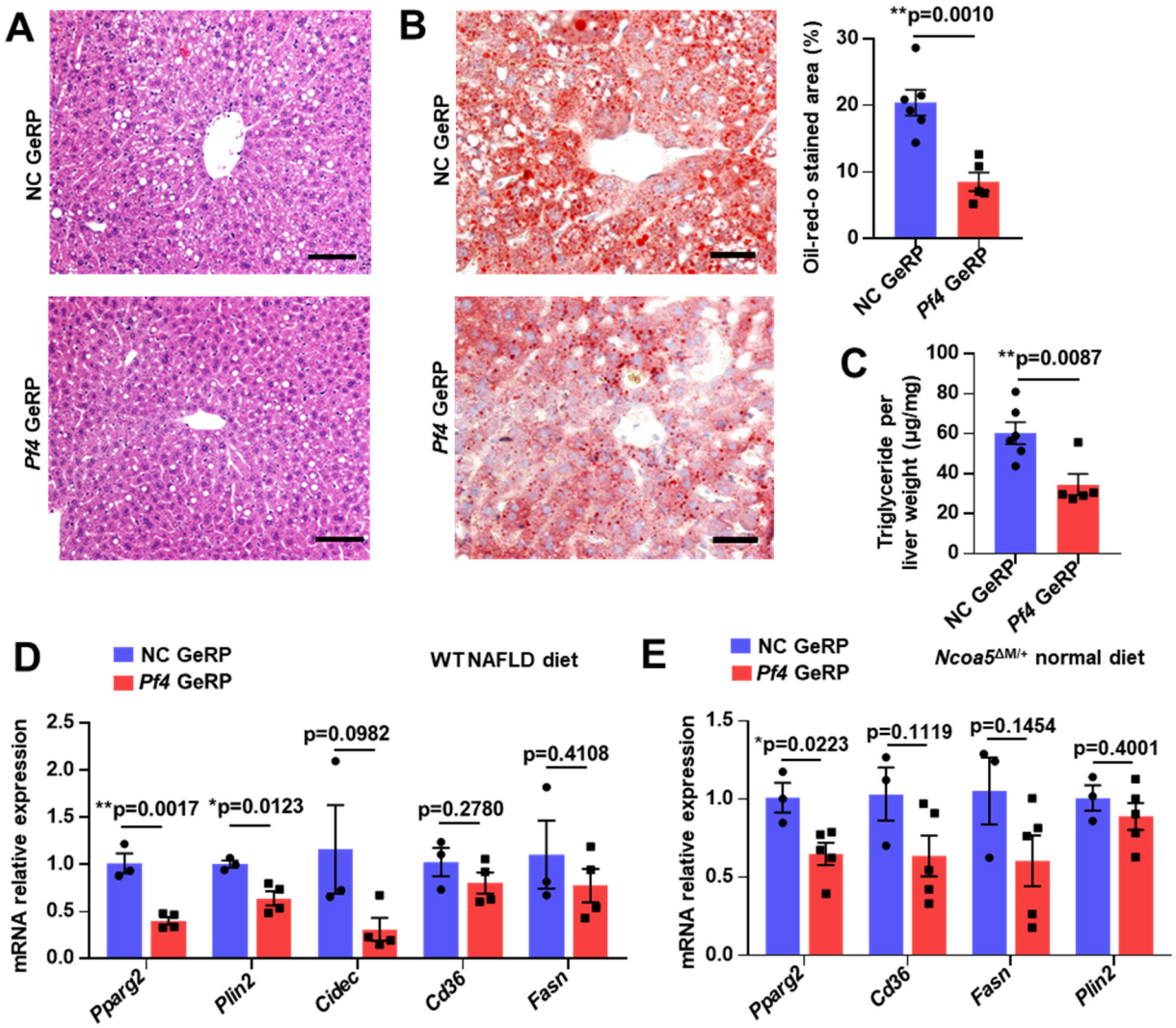

Figure 2.14 Effect of intrahepatic-macrophage-specific *Pf4* knockdown on hepatic

Figure 2.14 (cont'd)
steatosis in wild-type mice fed a NAFLD diet and *Ncoa5*$^{\Delta M/+}$ fed a normal diet. (A) Representative H & E staining of livers from wild-type male mice fed a NAFLD diet injected with siNC or si3-containing GeRPs. Scale bar: 100 μm. (B) Representative Oil-red-o staining of livers from siNC (n=6) or si3-containing (n=5) GeRPs injected wild-type male mice fed a NAFLD diet and the quantification of Oil-red-o-stained area. Scale bar: 50 μm. (C) Triglyceride concentration of livers from siNC (n=6) or si3-containing (n=5) GeRPs injected wild-type male mice fed a NAFLD diet. (D) RT-qPCR analysis of the mRNA expression of *Pparg2* and its target genes in livers of wild-type male mice fed a NAFLD diet injected with siNC (n=3) or si3-containing (n=4) GeRPs. (E) RT-qPCR analysis of the mRNA expression of *Pparg2* and its target genes in livers of 7.5-month-old *Ncoa5*$^{\Delta M/+}$ male mice fed a normal diet injected with siNC (n=3) or si3-containing (n=5) GeRPs. Data represent mean ± SEM. Two-tailed unpaired Student's t test. **p<0.01, *p<0.05.

2.14E). Altogether, these results suggest that increased PF4 from intrahepatic macrophages triggers the onset of hepatic steatosis via increasing expression of lipogenic genes in male *Ncoa5*$^{\Delta M/+}$ mice and a diet-induced model of NAFLD with reported *Pf4* upregulation specifically in intrahepatic macrophages.

3.4.4 Dysregulated intrahepatic macrophages from Ncoa5$^{\Delta M/+}$ male mice highly resemble the intrahepatic macrophages from NAFLD humans

To determine the clinical relevance of our findings, I compared the dysregulated transcriptomes between intrahepatic macrophages from *Ncoa5*$^{\Delta M/+}$ mice and humans with obesity or NAFLD. Generally Applicable Gene-set Enrichment (GAGE) analysis[283] revealed 47 upregulated and 41 downregulated KEGG (Kyoto Encyclopedia of Genes and Genomes) pathways (q<0.1), including upregulated fatty acid metabolism and fatty acid elongation pathways, in *Ncoa5*$^{\Delta M/+}$ intrahepatic macrophages (Fig. 2.15A). When applying the same pathway analysis to the transcriptome data of human intrahepatic macrophages from non-obese and obese individuals[30], I found that 60.2% of dysregulated KEGG pathways in *Ncoa5*$^{\Delta M/+}$ intrahepatic macrophages were also dysregulated in the intrahepatic macrophages of obese humans in the same direction

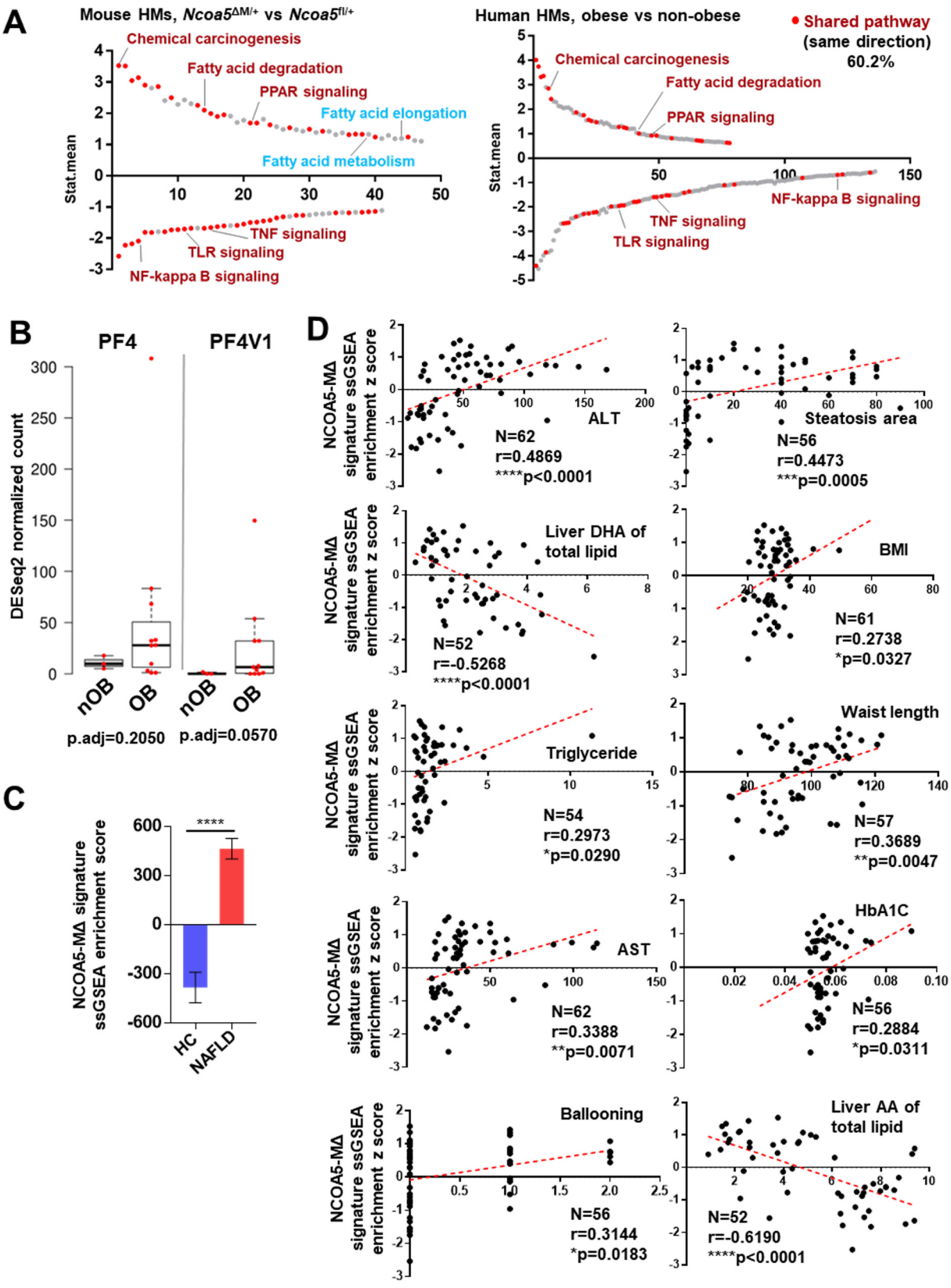

Figure 2.15 Comparison of the transcriptome changes in intrahepatic

Figure 2.15 (cont'd)
macrophages between *Ncoa5*$^{\Delta M/+}$ male mice and obese humans or NAFLD patients. (A) KEGG pathway analysis results comparing intrahepatic macrophages of *Ncoa5*$^{\Delta M/+}$ vs. *Ncoa5*$^{fl/+}$ male mice (n=4 each) (left) and obese humans (n=11) vs. non-obese humans (n=3) (right) (PRJNA491664) using GAGE. Each dot represents a dysregulated KEGG pathway (q<0.1). A red dot indicates that the same KEGG pathway is shared in both human and mouse analyses with the same direction in regulation. HM: intrahepatic macrophage. (B) The mRNA expression of PF4 and its non-allelic variant PF4V1 in intrahepatic macrophages from non-obese (nOB) and obese (OB) individuals. It was assessed by RNA-seq. p.adj calculated by DESeq2. Box and whisker were drawn using the Tukey method drawing all data points. (C) ssGSEA enrichment scores of NCOA5-MΔ signature in liver transcriptomes of health control people (n=24) and NAFLD patients (steatosis and NASH, n=39) (GSE89632). Data represent mean ± SEM. Two-tailed unpaired Student's t test. (D) Correlations between NCOA5-MΔ enrichment z score and NAFLD clinical parameters, including alanine aminotransferase (ALT) level, steatosis area, liver docosahexaenoic acid (DHA) level of total lipid, body mass index (BMI), triglyceride, waist length, aspartate transferase (AST), hemoglobin A1C (HbA1C), ballooning of hepatocyte, and liver arachidonic acid (AA) level of total lipid (GSE89632). Each dot represents one patient. Pearson's r and p-values are indicated. ****p<0.0001, ***p<0.001, **p<0.01, *p<0.05.

(q<0.1) (Fig. 2.15A). Unlike mouse cells, human cells also express a PF4 variant 1 gene (*PF4V1*) that encodes a protein in the mature form 96% identical to mature PF4. I found that most obese individuals had highly upregulated PF4 or PF4V1 mRNA expression in their intrahepatic macrophages compared to non-obese individuals (Fig. 2.15B). Next, I generated the NCOA5-MΔ signature using the high-confidential human homologs (156 genes, Table 1.1) converted from *Ncoa5*$^{\Delta M/+}$ intrahepatic macrophage DEGs (171 genes with Entrez Gene ID within the 207 DEGs) and applied this signature to human NAFLD patient and healthy control liver transcriptome data using ssGSEA (single-sample Gene Set Enrichment Analysis) analysis[284,285]. The enrichment score of this signature was significantly higher in NAFLD patient livers (Fig. 2.15C). It significantly correlated with most NAFLD clinical parameters, including ALT, steatosis area, liver docosahexaenoic acid of total lipid, and others (Fig. 2.15D). These data indicated that dysregulated intrahepatic macrophages from *Ncoa5*$^{\Delta M/+}$ male mice resembled those from obese

people or NAFLD patients. We also found that NAFLD patients, including those with NASH, did not have apparent hepatic inflammation in this human liver gene expression dataset (Fig. 2.16).

Table 1.1 NCOA5-MΔ gene signature

UP	ANGPTL7, BMP7, C20orf173, C8orf34, CACNG7, CCT6B, CD209, CD4, PF4, PF4V1, CIDEA, CLSTN3, DCT, FAM241B, FITM1, FRS3, GPRC5B, GSTM3, KLHL32, MMP13, MT-ATP6, NAT8, NAT8B, PIANP, POMGNT2, PTPRT, PXDC1, RAB34, RGS11, RIMKLB, SEMA5B, SGCE, SLC12A5, SLC1A2, SLC22A3, SMIM1, SPTLC3, SYNGAP1, TENM2, THRSP, TLX1, TPPP, UNC13B, ZNF627
DOWN	ABCB1, AC008012.1, AC010616.1, ACE, ADORA2B, AGPAT4, AL049634.2, AL357075.4, ANKDD1A, AP000781.2, ATP1A3, BCAS1, BCL2, BCL2A1, C3orf80, CCL18, CCL3, CCL3L3, CCND2, CD177, CD244, CD300E, CD79B, CLEC4E, CNN2, CORO1A, CYFIP2, DGKG, DNAH12, DUSP2, DUSP5, EGR3, EPHA4, FAM217B, FCGR3A, FCGR3B, FCRL5, FNDC1, FUT7, GDA, GFI1B, GLIPR1, GPR171, GPR18, GPR31, GRAP2, GRHL1, HCCS, IFIT1B, IGSF9, IKZF3, IL12B, IL21R, IPCEF1, ITGAD, ITGAX, KCNA3, KCNG3, KCNN4, KLRB1, KLRG2, KRT80, LAT2, LTBP2, MAP3K19, MBP, MCUB, MMP8, MSL3, MYO1E, NAPSA, NAT8L, NEGR1, NR4A2, NUPR1, NXPE3, NXPE4, PBXIP1, PCDHGA10, PDCD1, PECAM1, PLAUR, PPP1R3D, PRG2, PRPS2, PSTPIP1, RADX, RNF144A, RUNX2, RYR1, SCD, SCEL, SH2D1B, SH3PXD2B, SIRPA, SIRPB1, SIRPG, SLAMF9, SLC2A6, SLC4A1, SLC9A7, SOCS3, SORT1, SPN, SYCP2, TLR7, TLR8, TMEM121B, TMSB4Y, TNF, TRAF1, TREML2

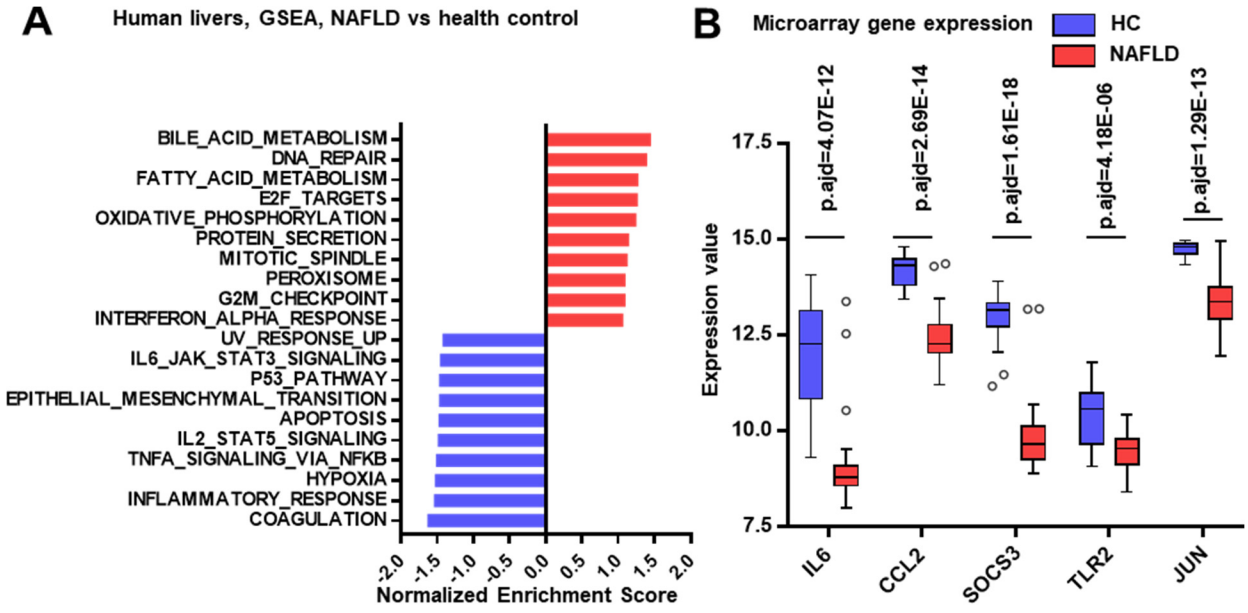

Figure 2.16 Pathway enrichments and expression of proinflammatory cytokines in liver samples from NAFLD patients and healthy controls. (A) Gene Set Enrichment Analysis (GSEA) result of the hallmark gene set enrichment comparing the liver

Figure 2.16 (cont'd)
microarray data from healthy control (HC) people (n=24) and NAFLD patients (steatosis and NASH, n=39) (GSE89632). The top 10 positively and negatively enriched signatures in NAFLD patient samples compared to healthy controls were shown. (D) Expression of selected inflammation-related genes from health control people (n=24) and NAFLD patients (including patients with steatosis or NASH, n=39) (GSE89632). Differential expression analysis with limma. Box and whisker were drawn using the Tukey method.

3.4.5 Ncoa5 deficiency promotes the differentiation of macrophages toward M2-like

We previously reported increased M2 macrophage infiltration in the preneoplastic liver of *Ncoa5*$^{+/-}$ male mice[187,271]. Consistently, my pathway analysis revealed that proinflammatory pathways, including TNF signaling, NF-κB signaling, and Toll-like receptor signaling, were downregulated in *Ncoa5*$^{\Delta M/+}$ intrahepatic macrophages. In contrast, anti-inflammatory PPAR signaling[286] was upregulated (Fig. 2.15A). These results agree with the aforementioned observation that the expression of TNFα, an M1 macrophage marker, was significantly reduced in the intrahepatic macrophages of *Ncoa5*$^{\Delta M/+}$ male mice (Fig. 2.7D), indicating a transition to M2-like differentiation. M2-like macrophages have a repertoire of tumor-promoting capabilities, such as inducing an immunosuppressive microenvironment and promoting the growth and metastatic potential of cancer cells. We sought to determine if myeloid-lineage-specific heterozygous deletion of *Ncoa5* in mice is sufficient to increase the intrahepatic M2-like macrophage population observed previously in *Ncoa5*$^{+/-}$ male mice[271], which might contribute to the formation of the hepatic immunosuppressive microenvironment in *Ncoa5*$^{\Delta M/+}$ male mice. Transcriptome analysis indicated that the intrahepatic macrophages of pre-NASH *Ncoa5*$^{\Delta M/+}$ male mice expressed significantly higher levels of Cd209 family genes, markers for M2 macrophages (Fig. 2.17A). The increased M2-like macrophages in the livers of *Ncoa5*$^{\Delta M/+}$ male mice were confirmed by IHC using an

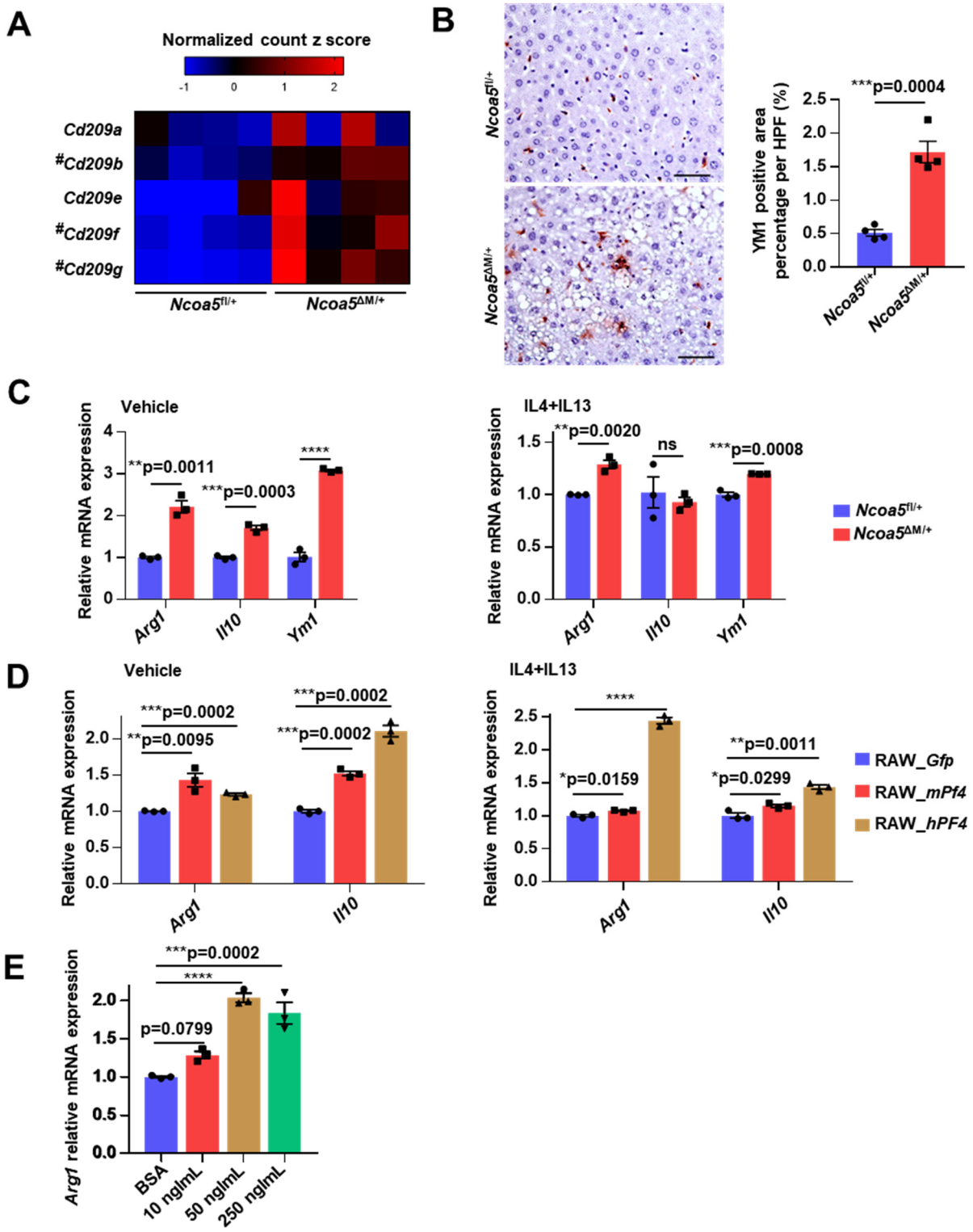

Figure 2.17 Effects of myeloid-lineage-specific *Ncoa5* heterozygous deletion on macrophage M2-like polarization. (A) Differences in mRNA expression of Cd209 family genes between intrahepatic macrophages from 6.5-month-old *Ncoa5*$^{fl/+}$ (n=4) and *Ncoa5*$^{\Delta M/+}$ (n=4) male mice. Gene expression was visualized as z scores within each

Figure 2.17 (cont'd)
gene comparison using DESeq2 normalized counts. # sign represents adjusted p-value <0.01 reported by DESeq2 DEG analysis. (B) Representative photos of YM1 IHC staining in liver sections of 10-month-old *Ncoa5*$^{fl/+}$ (n=4) and *Ncoa5*$^{\Delta M/+}$ (n=4) male mice and the quantification of stained area positive for YM1. 5 HPFs per mouse. (C) RT-qPCR analysis of the mRNA levels of M2-macrophage markers in mouse peritoneal macrophages isolated from 6-week-old *Ncoa5*$^{fl/+}$ and *Ncoa5*$^{\Delta M/+}$ male mice treated with vehicle (left) or mouse IL-4 and IL-13 (right) for one day. Pooled RNA from 2 or 3 mice in each group. (D) RT-qPCR analysis of the mRNA levels of M2-macrophage markers in RAW 264.7 cells with ectopic PF4 expression treated with vehicle (left) or 20 ng/mL of mouse IL-4 and IL-13 (right). (E) RT-qPCR showing *Arg1* mRNA levels in RAW 264.7 cells treated with vehicle or mouse PF4 for one day. Representative data of three repeats. One-way ANOVA Dunnett's multiple comparisons test. Data represent mean ± SEM. Two-tailed unpaired Student's t test was used if not otherwise specified. ****p<0.0001, ***p<0.001, **p<0.01, *p<0.05. Scale bar: 50 μm.

antibody against mouse M2 macrophage marker YM1 (Fig. 2.17B). To verify that the transition to M2-like macrophages was caused by *Ncoa5* deficiency intrinsically, we isolated peritoneal macrophages from 6-week-old *Ncoa5*$^{fl/+}$ and *Ncoa5*$^{\Delta M/+}$ male mice and assessed the expression of M2 macrophage markers. Without external stimulation, elevated expression of *Arg1*, *Il10*, and *Ym1* was already evident in peritoneal macrophages from *Ncoa5*$^{\Delta M/+}$ male mice compared to *Ncoa5*$^{fl/+}$ male mice (Fig. 2.17C left). When treated with IL4 and IL13 to induce M2 differentiation, the peritoneal macrophages from *Ncoa5*$^{\Delta M/+}$ male mice expressed higher *Arg1* and *Ym1* mRNA than those from *Ncoa5*$^{fl/+}$ male mice (Fig. 2.17C right).

Since PF4 treatment could induce monocyte differentiation into macrophages and reduce the M1 activation of mouse macrophages[287-289], we asked if *Pf4* overexpression affects M2-like differentiation of macrophages. RAW 264.7 cells with *Pf4* overexpression or ectopic human *PF4* expression had significantly increased expression of *Arg1* and *Il10*, two M2 markers, while treating cells with M2-inducers resulted in higher *Arg1* and *Il10* expression in cells with PF4 overexpression (Fig.

2.17D). Treating RAW 264.7 cells with recombinant mouse PF4 significantly increased *Arg1* expression (Fig. 2.17E). These results suggest a role of PF4 in inducing macrophage M2-like differentiation.

3.4.6 Macrophages lacking NCOA5 affect HCC cell growth and invasion potential in vitro

M2-like macrophages can promote tumor cell proliferation and metastasis potential[290,291]. We then examined the effect of *Ncoa5*-deficient macrophages on HCC cell growth and invasion potential *in vitro* by treating HepG2 cells with CM of RAW 264.7 cells with or without *Ncoa5* knockout. HepG2 cells treated with CM of *Ncoa5*-null RAW 264.7 cells had increased cell growth compared to cells treated with CM of control RAW 264.7 cells (Fig. 2.18A). CM of *Ncoa5*-null RAW 264.7 cells could promote HepG2

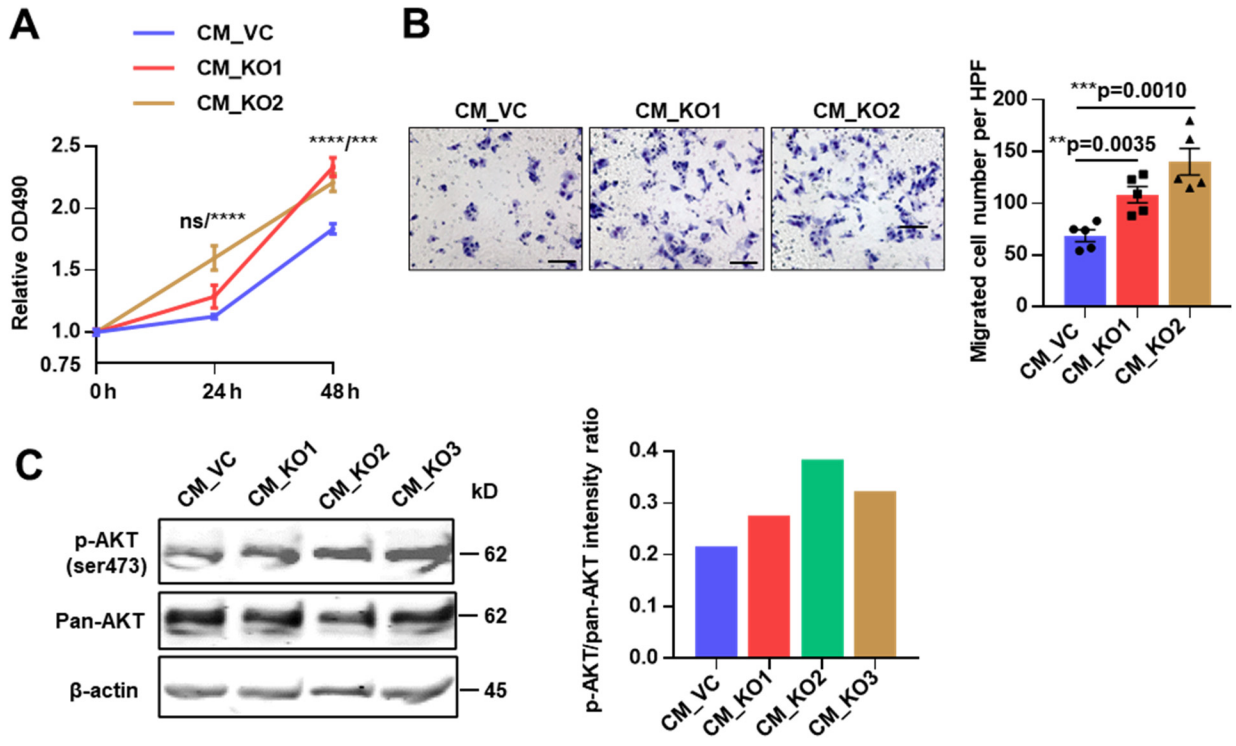

Figure 2.18 Effect of conditioned medium of *Ncoa5* knockout RAW 264.7 cells on proliferation and migration of HCC cells. (A) CCK8 assay of the proliferation of HepG2 cells cultured with CM from RAW 264.7 cells with or without *Ncoa5* knockout

Figure 2.18 (cont'd)
with a final concentration of 2% FBS. Representative data of two repeats. Two-way ANOVA Dunnett's multiple comparisons test. (B) Representative photos and the quantification of migrated cells for HepG2 cell transwell migration assay using CM from RAW 264.7 cells with or without *Ncoa5* knockout. 5 HPFs in each condition, representative result of two repeats. Two-tailed unpaired Student's t test. (C) Western blotting analysis of AKT ser-473 phosphorylation in starved HepG2 cells treated with CM from RAW 264.7 cells with or without *Ncoa5* knockout. HepG2 cells were serum-starved for 24 hours and then treated with different CM for 20 minutes. Data in A and B represent mean ± SEM. ****p<0.0001, ***p<0.001, **p<0.01. Scale bar: 50 μm.

cell migration compared to CM of control RAW 264.7 cells (Fig. 2.18B). CM of *Ncoa5*-null RAW 264.7 cells increased the AKT phosphorylation in HepG2 cells compared to CM of control RAW 264.7 cells, suggesting that the increased growth and migration might be related to AKT activation (Fig. 2.18C). Together, these results indicate that macrophages with NCOA5 loss promote HCC cell growth and invasion *in vitro*.

3.4.7 High PF4 expression in human HCC samples correlates with poor overall survival and increased M2 macrophages, Tregs, and MDSCs in HCCs

PF4 was demonstrated to stimulate the proliferation of Tregs and induce the tumor-infiltrated population of MDSCs, which could suppress the activation, proliferation, and cytokine production of CD4+ and CD8+ T cells and correlate negatively with cancer patient survival[292-294]. To assess the clinical relevance of PF4 high expression in HCC, I analyzed the TCGA LIHC cohort and used the mRNA levels of PF4 and its non-allelic variant PF4V1 to segregate TCGA HCC patients. Kaplan-Meier analysis revealed that HCC patients with high tumoral combined PF4 and PF4V1 mRNA expression had a significantly worse overall survival than the rest of the HCC patients (Fig. 2.19A). Next, CIBERSORTx was used to infer immune cell type proportions in HCCs from the same HCC patient cohort using the default LM22 signature[295]. I found that the HCC samples with high combined expression of PF4 and

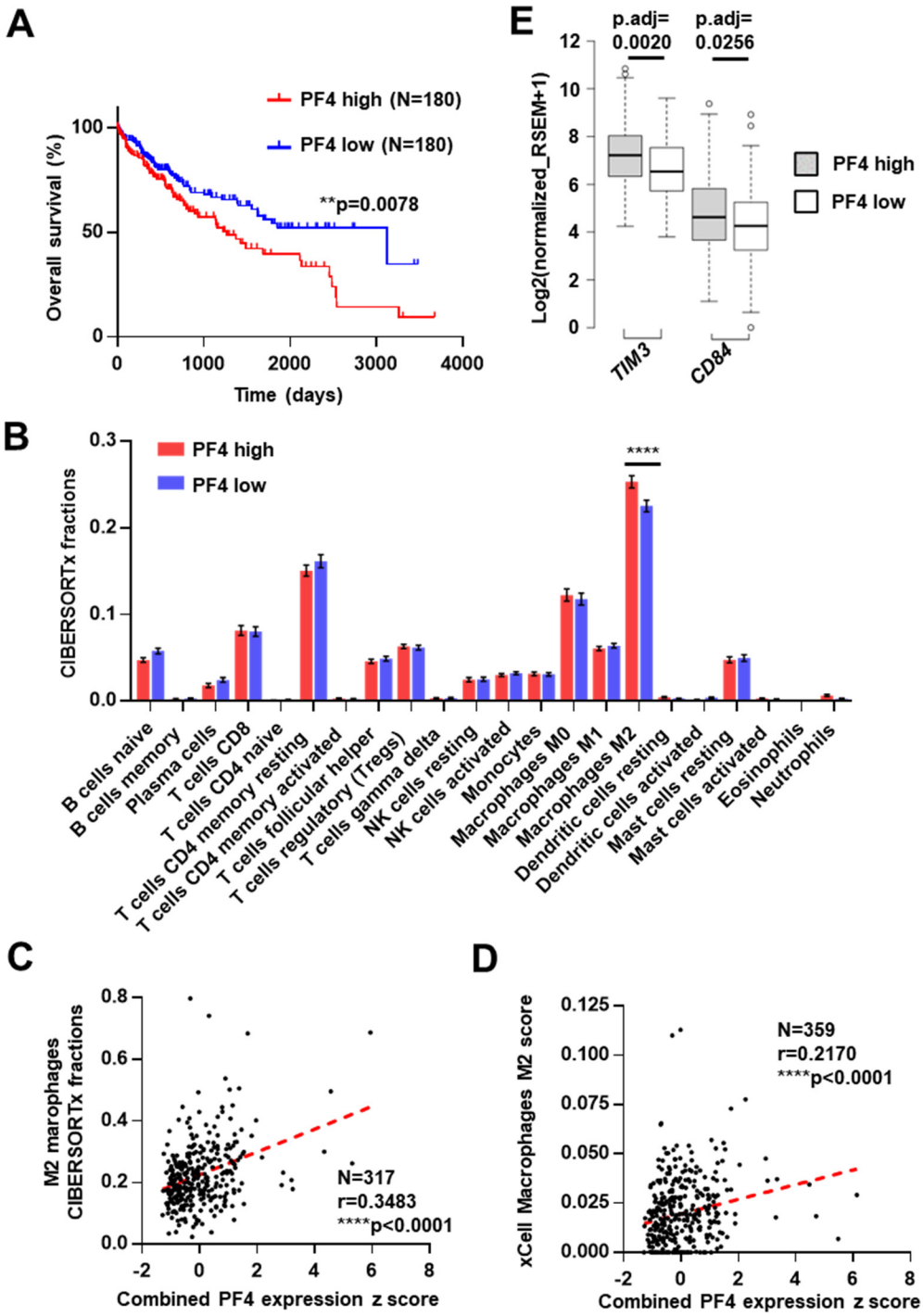

Figure 2.19 Relationships between PF4 expression and survival, M2 macrophage population, and expression of immunosuppression-related genes in TCGA HCC patients. (A) Kaplan Meier plot of overall survival for TCGA primary HCC patients with high (n=180) or low (n=180) combined PF4 and PF4V1 expression in the tumor (referred to as PF4 high or low groups in the following figures). Log-rank test. Combined PF4 and PF4V1 expressions were ranked by ssGSEA. PF4 high group includes patients with the top 50% of combined expression, while the low group includes the rest.

Figure 2.19 (cont'd)
**p<0.01. (B) Predicted immune cell fractions in HCCs of combined PF4 and PF4V1 high or low TCGA patients by CIBERSORTx absolute mode. Samples with p>0.05 were filtered. Patients n=165 and 152. Two-way ANOVA Sidak's multiple comparisons test was used for statistical analysis. Data represent mean ± SEM. ****p<0.0001. (C) Correlation between combined tumoral PF4 and PF4V1 expression and predicted M2 macrophage fractions in TCGA patients. Pearson's r and p-values and patient numbers are indicated. The patient separation was done in B and C as described in A, except 43 patient samples were filtered because of their CIBERSORTx p>0.05. (D) Correlation between combined tumoral PF4 and PF4V1 expression and xCell Macrophages M2 score in TCGA patients. Pearson's r and p-values and patient numbers are indicated. The same patient cohort as in (A) – (C) was used, but data for two patients were missing in the original xCell analysis performed by the authors of the tool. (E) Expression of immunosuppression-related genes in HCCs from TCGA patients with high or low combined PF4 and PF4V1 expression. Welch's t test with the FDR method of Benjamini-Hochberg. Box and whisker are drawn using the Tukey method.

PF4V1 had significantly higher M2 macrophage fractions (Fig. 2.19B). Moreover, the positive correlation of combined PF4 and PF4V1 mRNA expression with M2 macrophage fractions was shown using CIBERSORTx (Fig. 2.19C) and the xCellmethod (Fig. 2.19D)[296]. While having a similar proportion of CD8 T cell fraction (Fig. 2.19B), HCCs with high PF4 and PF4V1 mRNA expression expressed higher immune checkpoint molecule *TIM3* and MDSC marker *CD84*[297] compared to the rest of tumors (Fig. 2.19E). The signatures of Treg[298] and MDSC[297] were enriched in HCCs with high PF4 and PF4V1 expression compared to the rest of the HCC samples[299] (Fig. 2.20A and 2.20B).

In the LCI HCC cohort, an HCC cohort with a different patient ethnicity and etiology compared to the TCGA cohort[300], high tumoral PF4 and PF4V1 mRNA expression also correlated with poor overall survival and recurrence-free survival (Fig. 2.21A) and tumors with high PF4 and PF4V1 expression also had increased *CD84* expression (Fig. 2.21B). Furthermore, I found that HCC patients with high tumoral PF4 protein expression had poor recurrence-free survival compared to other patients by

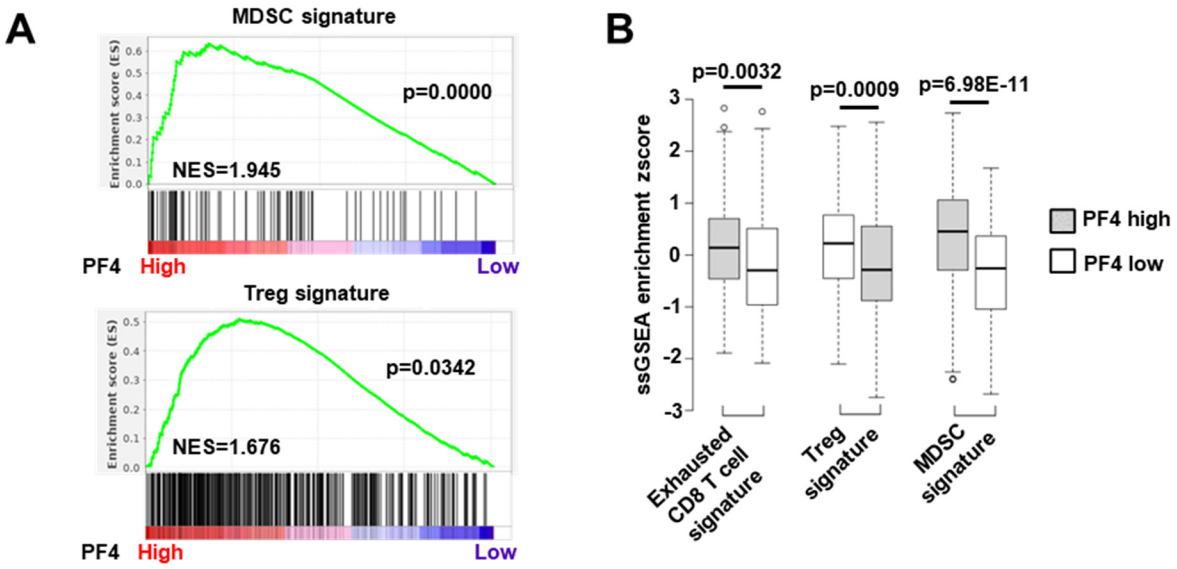

Figure 2.20 Relationships between PF4 expression and the enrichment of immunosuppression-related gene signatures in TCGA HCC patients. (A) GSEA analysis result using indicated signatures comparing HCCs from TCGA patients with high or low combined PF4 and PF4V1 expression. Normalized enrichment scores and p-values are shown. (B) ssGSEA result of published gene sets as indicated in TCGA patients with high or low PF4 and PF4V1 mRNA expression. Two-tailed unpaired Student's t test. Box and whisker were drawn using the Tukey method.

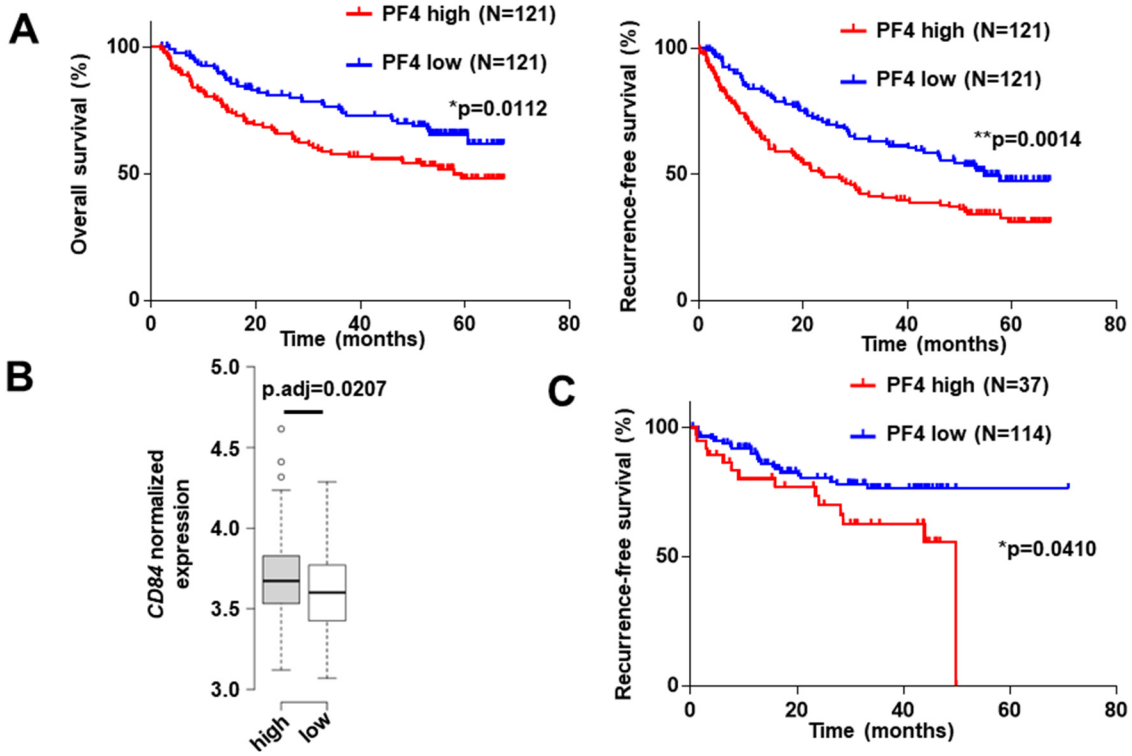

Figure 2.21 Relationships between tumoral PF4 expression and HCC patient

Figure 2.21 (cont'd)
prognosis in the LCI and proteomic study cohorts. (A) Kaplan Meier plot of overall survival and recurrence-free survival for LCI primary HCC patients with high (n=121) or low (n=121) combined PF4 and PF4V1 expression in the tumor. Log-rank test. (B) Expression of CD84 in HCCs from LCI patients with high or low PF4 expression. p.adj calculated using limma. Box and whisker were drawn using the Tukey method. (C) Kaplan Meier plot of recurrence-free survival for PDC000198 primary HCC patients with PF4 protein expression in the top quartile and the rest of patients. Log-rank test. **p<0.01, *p<0.05.

analyzing a proteomic dataset[301] (Fig. 2.21C). These results suggest that PF4 is involved in the formation of the immunosuppressive microenvironment and the progression of HCC.

3.5 Discussion

Myeloid-lineage cells, especially intrahepatic macrophages, are central to NASH and HCC development[269]. The action of intrahepatic macrophages involved in the pathogenesis of these diseases has been known to be secondary to external factors such as excessive nutrition, endotoxin influx, and hepatocyte damage, which induce macrophage differentiation and subsequent production of proinflammatory cytokines. Indeed, current animal models of NAFLD/NASH and HCC were generated mainly by applying nutrient-excessive or nutrient-deficient diet, chemical insults, spontaneous gene mutations, or gene-targeting to the whole body or liver parenchymal cells[302-304]. In this study, we discovered for the first time that a myeloid-lineage-specific *Ncoa5* heterozygous deletion sufficiently causes insulin insensitivity, weight gain, NASH, and a moderate incidence of HCC in male mice fed a normal diet. These unexpected findings suggest that a genetic predisposition factor in myeloid-lineage cells can sufficiently induce the development of NAFLD, NASH, and HCC and highlight the importance of dysregulated myeloid cells that can promote the development of NAFLD, NASH, and

HCC.

We focused on the *Ncoa5*$^{\Delta M/+}$ mice in this study because *Ncoa5*$^{\Delta M/\Delta M}$ mice exhibited less severe hepatic steatosis compared to *Ncoa5*$^{\Delta M/+}$ male mice and did not have increased body weight until 18 months of age. The lessened effect of *Ncoa5*-null myeloid-lineage cells on the hepatocytes could be due to the impact of *Ncoa5* knockout on the cell proliferation or development, as *Ncoa5*-null RAW 264.7 cells were less proliferative than the vector control cells (Fig. 2.22A and 2.22B). Nevertheless, elucidating why *Ncoa5*$^{\Delta M/\Delta M}$ mice exhibited less severe hepatic steatosis requires further experimentation. Moreover, *Ncoa5*$^{\Delta M/+}$ mice allow a more precise comparison with *Ncoa5*$^{+/-}$ mice and better replicate the pathogenesis of humans containing heterozygous mutation or reduced cellular expression of NCOA5.

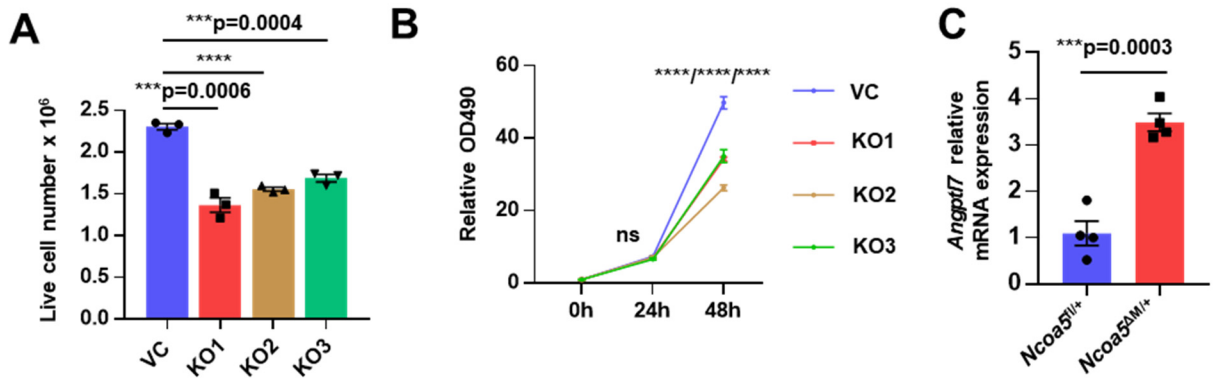

Figure 2.22 The role of NCOA5 in macrophage proliferation and *Angptl7* expression. (A) Live cell number of the same initial amount of RAW 264.7 cells with or without *Ncoa5* knockout after 48-hour culture. Representative data of three repeats. Data represent mean ± SEM. Two-tailed unpaired Student's t test. (B) CCK8 assay of the proliferation of RAW 264.7 cells with or without *Ncoa5* knockout. Representative data of three repeats. Data represent mean ± SEM. Two-way ANOVA Dunnett's multiple comparisons test. (C) The mRNA levels of *Angptl7* in intrahepatic macrophages from 6.5-month-old *Ncoa5*$^{fl/+}$ and *Ncoa5*$^{\Delta M/+}$ male mice tested by RT-qPCR. Two-tailed unpaired Student's t test. Data represent mean ± SEM. ns: not significant, ****p<0.0001, ***p<0.001.

By combining cell-specific genetic and CRISPR/Cas9-knockout cells with transcriptomic studies, we found that prior to the advanced NASH in *Ncoa5*$^{\Delta M/+}$ male mice, their intrahepatic macrophages had already exhibited a more M2-like phenotype in the intrahepatic macrophages rather than a proinflammatory phenotype that is often described as critical to their contribution to insulin resistance, hepatic steatosis, inflammation, and liver injury[305,306]. The dysregulated pathways in these *Ncoa5*$^{\Delta M/+}$ macrophages in the pre-NASH mouse livers were similar to those of obese humans who did not have a proinflammatory phenotype in their intrahepatic macrophages[30]. Moreover, the NCOA5-MΔ signature consisting of DEGs in *Ncoa5*$^{\Delta M/+}$ intrahepatic macrophages can separate the NAFLD livers from the health control livers in the liver transcriptome dataset. These results indicated that intrahepatic macrophages might promote the initiation and progression of hepatic steatosis through an inflammation-independent pathway, which aligns with several recent studies[30,31].

Our findings raise the question of how NCOA5-deficient macrophages trigger the onset of hepatic steatosis. We hypothesized that NCOA5-deficient intrahepatic macrophages initiate hepatic steatosis, at least in part, by releasing excessive PF4. In support of this hypothesis, we found that *Pf4* was the most significantly upregulated gene among the genes encoding secretory proteins in the intrahepatic macrophages of pre-NASH livers of *Ncoa5*$^{\Delta M/+}$ male mice and was continuously increased in the NASH livers of *Ncoa5*$^{\Delta M/+}$ male mice. Moreover, we observed that *Ncoa5*-null RAW 264.7 cells overexpressed PF4, and the conditioned medium from these cells and recombinant PF4 protein directly stimulated lipid accumulation and lipogenic gene expression in hepatocytes. Our data from the experiment of *in vivo* knockdown of PF4 expression,

specifically in intrahepatic macrophages, also indicate a critical role of PF4 secreted from intrahepatic macrophages in upregulating lipogenic gene expression in livers of *Ncoa5*$^{\Delta M/+}$ male mice (Fig. 2.13 and 2.14). Increased hepatic PF4 has been reported in the livers of rats fed a westernized diet[307], human alcoholic hepatitis patients[308], and HCV-infected patients with liver fibrosis[309]. Although resident macrophages are known to express PF4[310], increased PF4 expression in macrophages has seldom been reported to be associated with NASH or NAFLD. Nevertheless, our studies found increased *Pf4* expression in the Kupffer cells of NASH livers in a published single-cell RNA-seq dataset of an AMLN diet-induced mouse model of NASH[281]. Additionally, a study using a westernized, sucrose/fructose-supplemented diet also identified *Pf4* as a continuously upregulated gene in intrahepatic macrophages of NAFLD mice[280]. Importantly, our results demonstrated that PF4 overexpression in intrahepatic macrophages is critical for the upregulation of lipogenic genes and lipid accumulation in this diet-induced mouse model of NAFLD (Fig. 2.13 and 2.14).

PF4 was reported to interact with various receptors that mediate diverse signaling pathways in several cell types[311]. One of the receptors for PF4, CXCR3, is expressed in various liver cells, including hepatocytes, and has been shown to play a crucial role in obesity and NASH development by inducing actions including fatty acid synthesis[279,312]. The functional binding of PF4 to CXCR3 has been well established. The published evidence includes results of binding assay of radiolabeled PF4 to CXCR3 and using CXCR3 inhibitor (±)-AMG487, CXCR3-specific siRNA, and anti-CXCR3 antibodies to block the functional binding of PF4 to CXCR3[313,314]. CXCR3 regulates multiple signaling pathways that include PI3K/Akt and mTOR signaling, which could, in

turn, alter the expression of lipogenic genes including *Pparg2*[277,315]. Thus, the newly discovered pro-steatosis action of PF4 might be exerted by signaling the CXCR3 receptor. Nevertheless, our data do not rule out other mechanisms that may also contribute to the development of insulin resistance and hepatic steatosis in *Ncoa5*$^{\Delta M/+}$ male mice initially. For example, another identified upregulated gene in the intrahepatic macrophages of *Ncoa5*$^{\Delta M/+}$ male mice, *Angptl7* (Fig. 2.22C), encodes a secreted protein that has been recently reported to promote insulin resistance and type 2 diabetes[316]. Moreover, proinflammatory cytokines might contribute to the progression of simple hepatic steatosis to NASH and HCC after the onset of fat accumulation in hepatocytes in *Ncoa5*$^{\Delta M/+}$ male mice. Regardless of whether other factors contributed to the pathogenesis of NAFLD in *Ncoa5*$^{\Delta M/+}$ male mice, the finding that *Pf4* overexpression in intrahepatic macrophages can signal to hepatocytes and increase the expression of lipogenic genes is both significant and innovative.

The precise mechanism for the spontaneous HCC development in *Ncoa5*$^{\Delta M/+}$ male mice remains unclear. Although the links between NAFLD and HCC remain to be fully elucidated, previous data have suggested several underlying mechanisms[317,318]. Since the immunosuppressive hepatic microenvironment is pivotal to the transition from NAFLD/NASH to HCC[319], it is conceivable that intrahepatic immunosuppressive immune cells contribute to hepatocarcinogenesis in *Ncoa5*$^{\Delta M/+}$ male mice having NASH. Consistent with this model, we found that *Ncoa5*$^{\Delta M/+}$ male mice had increased M2-like intrahepatic macrophages that transcriptomically differ from M0, M1, or M4 macrophages[320,321], and recombinant PF4 treatment or ectopic *Pf4* overexpression in RAW 264.7 cells could induce an M2-like phenotype. PF4 was reported to induce Treg

proliferation while inhibiting nonregulatory T cell proliferation[293] and promote breast tumor progression and metastasis by regulating MDSCs and inhibiting CD8+ T cells[294]. Interestingly, when we analyzed the TCGA HCC cohort for the association of tumor PF4 mRNA expression (possibly from tumor-associated macrophages) with patient survival or immunosuppressive cells, we not only found that high PF4 expression is associated with poor overall survival but also saw increased inferred M2 macrophage fractions. Moreover, enriched Treg and MDSC signatures in the tumor were associated with high PF4 expression. In line with our findings, the upregulation of PF4 and its impact on cell proliferation and metastatic potential were also found in other solid tumors, including pancreatic and lung cancers[322]. These data support the role of PF4 in HCC immunosuppression, and therefore, future work exploring the use of PF4 signaling inhibitors in HCC immunotherapy is warranted.

The relatively low HCC incidence in the NASH liver of *Ncoa5*$^{\Delta M/+}$ male mice compared to *Ncoa5*$^{+/-}$ male mice suggests the contributions of other NCOA5-deficient cells, such as hepatocytes and pancreatic islet cells, to the higher HCC incidence in *Ncoa5*$^{+/-}$ male mice. Nevertheless, NASH patients also have a moderate incidence and prolonged latency of human HCC, which *Ncoa5*$^{\Delta M/+}$ mice can model. We expect that additional genetic modification in the *Ncoa5*$^{\Delta M/+}$ mice or feeding them special diets can accelerate the NASH establishment and HCC development, enabling us to study further the mechanisms underlying NASH to HCC transition.

In summary, we establish a novel genetic mouse model of NASH generated by myeloid-lineage-specific heterozygous deletion of *Ncoa5*, uncovering a molecular mechanism in which NACA5 haploinsufficiency in myeloid cells triggers and propagates

NASH development through PF4 overexpression in intrahepatic macrophages, leading to HCC development (Fig. 2.23). *Ncoa5*$^{\Delta M/+}$ mice may provide a useful preclinical tool for NASH research. We anticipate that this work will lead to further insights into the pathogenesis of NASH to advance the development of treatments for NASH and HCC.

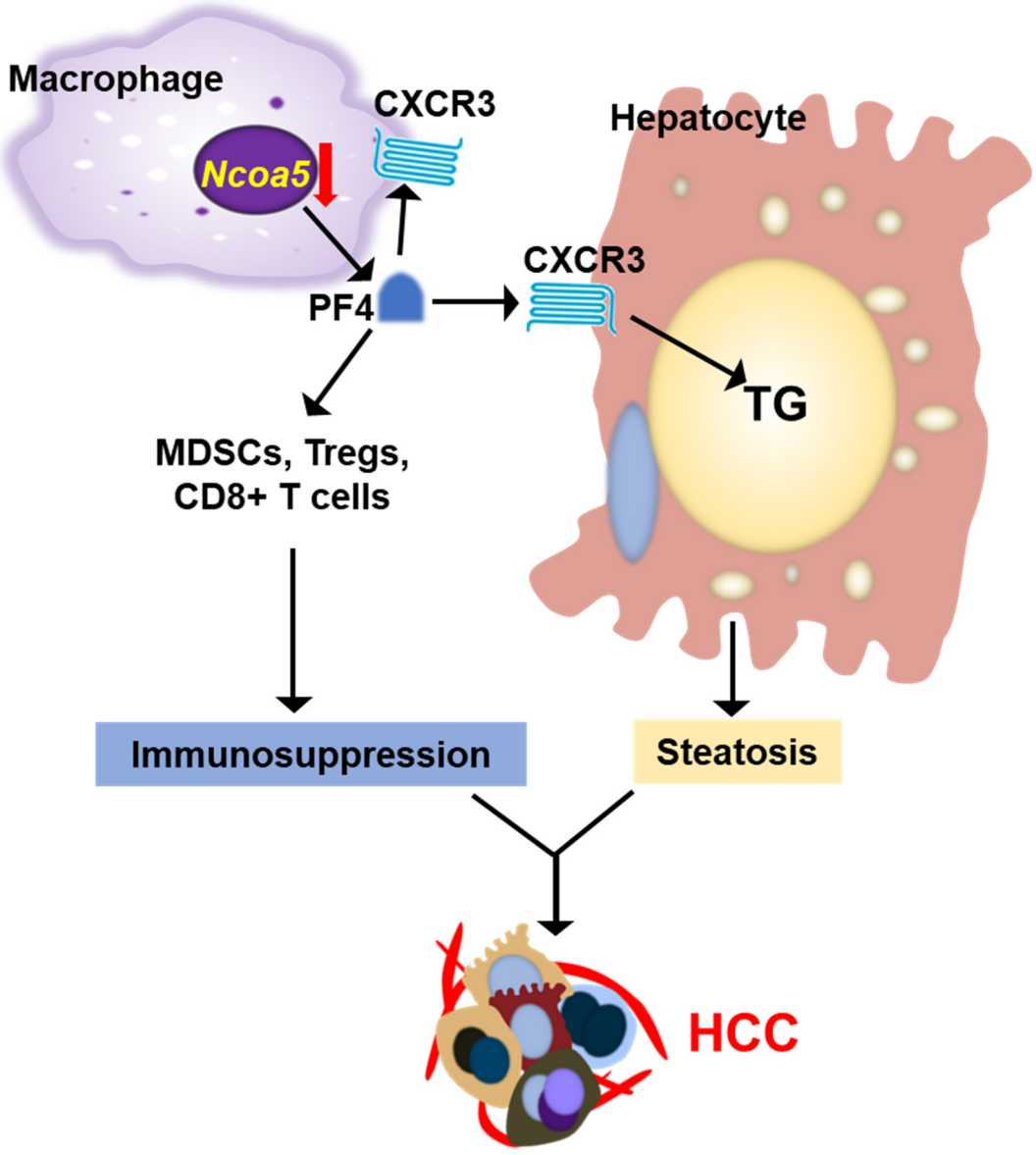

Figure 2.23 A graphical summary of the study.

3.6 Materials and methods

3.6.1 Generation of Ncoa5$^{fl/+}$, Ncoa5$^{fl/fl}$, Ncoa5$^{\Delta M/+}$, Ncoa5$^{\Delta M/\Delta M}$, and Ncoa5$^{\Delta H/\Delta H}$ mice

The *Ncoa5*$^{fl/+}$ mice were generated by Cyagen (Santa Clara, California). The targeting vector for LoxP site insertions contains homology arms flanking exons 3 and 4 of the *Ncoa5* gene, LoxP sites, and *neo*-gene flanked by Rox sites. The correctly targeted C57BL/6 embryonic stem (ES) cell clones were confirmed by Southern Blotting. ES cells were then transfected with a Dre expression vector to remove the neomycin cassette. Correct clones were then subjected to blastocyst microinjection, and chimeras were produced. Crossbreeding the chimeras with wild-type C57BL/6 mice obtained founders that were transmitted in the germline. Genotyping for LoxP sites flanking the *Ncoa5* gene was performed using primers: Forward: GATTCAGCCAGGCAGTCCACAGAT; Reverse: AATGGGCAAGAGTAGATGAGTTTCC. *Ncoa5*$^{flox/flox}$ mice were generated by mating *Ncoa5*$^{flox/+}$ mice. LysMcre mice were purchased from the Jackson Laboratory. *Ncoa5*$^{\Delta M/+}$ mice were generated by crossing *Ncoa5*$^{flox/flox}$ mice with heterozygote LysMcre mice. *Ncoa5*$^{\Delta M/\Delta M}$ mice were first generated by mating *Ncoa5*$^{\Delta M/+}$ mice and then by crossing *Ncoa5*$^{\Delta M/\Delta M}$ mice with *Ncoa5*$^{flox/flox}$ mice. Genotyping for LysMcre was carried out using primers suggested by Jackson Laboratory. *Speer6-ps1*$^{Alb\text{-}cre/+}$ mice were purchased from the Jackson Laboratory, and *Ncoa5*$^{\Delta H/\Delta H}$ mice were generated using the same strategy as the *Ncoa5*$^{\Delta M/\Delta M}$ mice. All mice except those wild-type C57BL/6 male mice enrolled for diet-induced NAFLD were housed in Optimice cages under a regular 12 h light/12 h dark cycle and standard normal diet at the Michigan State University animal facility. All experimental procedures on mice were approved by the Michigan State

University Institutional Animal Care and Use Committee and were performed in accordance with their regulatory standards.

3.6.2 Glucose tolerance test (GTT) and insulin tolerance test (ITT)

GTT and ITT were performed as previously described[187]. Briefly, mice were fasted for 12 or 6 hours before the intraperitoneal injection of 2 g/kg D(+)-glucose or 1U/kg insulin (Sigma-Aldrich) for GTT or ITT. A glucometer and Accu-check active test strips (Roche) were used to measure blood glucose from blood drops from the tail vein.

3.6.3 Western blotting

Western blotting was performed as previously described[187]. Generally, the protein was isolated from tissue or cell samples using RIPA buffer (Thermo Fisher). Total protein concentration was measured by Biorad Protein Assay (Biorad), and SDS-PAGE was carried out on Biorad Mini-protein TGX Gels. LICOR IRDye secondary antibodies were used for fluorescent detection, and photos were captured using the LICOR Odyssey Imaging system. Quantification was performed using LICOR Odyssey and Image Studio software.

3.6.4 Antibodies and recombinant protein

Antibodies used in this study include β-Actin (sc-47778), p21 (sc-6246), and PPARγ (sc-7273) by Santa Cruz Biotechnology; MAC-2 (Galectin-3, CL8942AP) by Cedarlane Labs; NCOA5 (A300-790A) by Bethyl Laboratories; YM1 (AF-2446) by R&D Systems; PF4 (500-P05) by PeproTech; Akt (pan) (C67E7, #4691) and Phospho-Akt (Ser473) (#9271) by Cell Signaling Technology. Recombinant murine PF-4 (250-39), murine IL-4 (214-14), and murine IL-13 (210-13) were purchased from PeproTech.

3.6.5 Histological and immunohistochemistry analysis

Mouse tissues were fixed in neutrally buffered 10% formalin solution (Sigma-Aldrich). Fixed tissues were then submitted to the Investigative Histopathology Laboratory of Michigan State University for embedding, sectioning, and H & E staining. A board-certified pathologist reviewed the histopathology of mouse liver sections. Oil-red-o staining and Sirius red staining were performed according to published protocols[323,324]. Immunohistochemistry analysis was performed using the VECTASTAIN ABC-HRP system (Vector Laboratories) according to the protocol supplied by the manufacturer.

Microscopic photos were captured using a Nikon ECLIPSE E600 microscope with a QImaging MicroPublisher 6 camera (TELEDYNE PHOTOMETRICS). Macroscopic photo images were captured using a Nikon COOLPIX L340 camera.

3.6.6 RNA preparation, reverse transcription, and quantitative real-time PCR

Total RNA from mouse tissues, isolated cells, or cultured cells was isolated using TRIzol reagent (Thermo Fisher) or combined TRIzol and RNeasy Mini Kit (Qiagen) method according to manufacturers' instructions. Reverse transcription was performed using the SuperScript IV First-Strand Synthesis System (Thermo Fisher) and PrimeScript RT Reagent Kit (TAKARA) according to manufacturers' instructions. Quantitative real-time PCR was carried out on a QuantStudio 3 Real-Time PCR machine using the PowerUp SYBR Green reagent (Thermo Fisher). Oligonucleotide sequences for the primers are described in Table 1.2.

Table 1.2 Oligos used in the study

Genes	Forward	Reverse
Polr2a	GCGGTTGACCCCATGACGAGTGAT	GCCTGATGCGGGTGCTGAGTGAG
Srebp1c	GGAGCCATGGATTGCACATT	GGCCCGGGAAGTCACTGT
ChREBP	AATGGGATGGTGTCTACCGC	GGCGAAGGGAATTCAGGACA
Pparg1	TGAAAGAAGCGGTGAACCACTG	TGGCATCTCTGTGTCAACCATG
Pparg2	GCATGGTGCCTTCGCTGA	TGGCATCTCTGTGTCAACCATG
G6pc	TGGTAGCCCTGTCTTTCTTTG	TTCCAGCATTCACACTTTCCT
Fasn	CCTCAAGGCCTGCGTAGACAC	GCCACATCATGCTGCTGCAGT
Acaca	GTCCCCAGGGATGAACCAATA	GCCATGCTCAACCAAAGTAGC
Plin2	AAGAGAAGCATCGGCTACGA	GGCGATAGCCAGAGTACGTG
Cd36	GATGACGTGGCAAAGAACAG	TCCTCGGGGTCCTGAGTTAT
Cidec	AGGCCCTGTCGTGTTAGCAC	CATGATGCCTTTGCGAACCT
p21	CAGATCCACAGCGATATCC	ACGGGACCGAAGAGACAAC
Pf4	TGCACTTAAGAGCCCTAGACCCAT	AGATCTCCATCGCTTTCTTCGGGA
Tnf	GCCTATGTCTCAGCCTCTTCT	TTGAGATCCATGCCGTTGGCC
Cxcr3	CAGCCTGAACTTTGACAGAACCT	GCAGCCCCAGCAAGAAGA
Gas6	TGCTGGCTTCCGAGTCTTC	CGGGGTCGTTCTCGAACAC
Arg1	CTTGCGAGACGTAGACCCTG	TCCATCACCTTGCCAATCCC
Ym1	GTACCCTGGGTCTCGAGGAA	CCTTGGAATGTCTTTCTCCACAG
Il10	CCAGGGAGATCCTTTGATGA	AACTGGCCACAGTTTTCAGG

3.6.7 Cell culture, CRISPR, gene silencing, and lentiviral gene expression

Mouse macrophage RAW 264.7 (derived from male) and human liver cancer cell line HepG2 (derived from male) were purchased from ATCC and cultured in DMEM medium (Thermo Fisher) supplemented with 10% fetal bovine serum and 100 U/mL of penicillin and 100 µg/mL of streptomycin at 37 °C in 5% CO_2. For the collection of conditioned medium, 4 x 10^6 RAW 264.7 cells were plated in a 100 mm plate and cultured in the serum-free DMEM medium for 24 hours. The medium was collected and centrifuged to remove cells and debris. The conditioned medium was centrifuged and mixed with the complete medium in a 1:1 ratio when treating cells with a conditioned medium.

CRISPR knockout of *Ncoa5* gene was achieved using pSpCas9(BB)-2A-Puro

(PX459) V2.0 plasmid purchased from Addgene[325], and the guide target sequences are the following: target1 (exon 3): CTGCGGTCCCGCAAATCCCG; target2 (exon 3): CGTGATCGCTCTCCAATTCG; target3 (exon 4): ATATGACCGTTATCTGAGGG. The target sequences and PAMs were cloned into the PX459 V2.0 plasmid according to the target sequence cloning protocol described on Addgene. RAW 264.7 cells were transiently transfected with vector control or constructs using Lipofectamine 3000 (Thermo Fisher) and selected with 5 μg/mL puromycin. Single clones were picked and cultured. Genomic DNA was extracted with QuickExtract (Lucigen), and PCR amplification and sequencing validation were performed. Finally, Western blotting was performed to validate the loss of NCOA5 protein.

RNA-induced gene silencing was performed using DsiRNAs purchased from Integrated DNA Technologies according to the protocol supplied by the manufacturer. siRNA sequences are: mm. Ri.Pf4.13.1-SEQ1/2: rGrGrGrCrArGrGrCrArGrUrGrArArGrArUrArArArArCrGTG/rCrArCrGrUrUrUrUrArUrCrUrUrCrArCrUrGrCrCrUrGrCrCrCrArG; mm.Ri.Pf4.13.2-SEQ1/2: rCrCrGrArUrGrUrUrUrArUrArUrUrArUrCrCrUrUrCrArAGA/rUrCrUrUrGrArArGrGrArUrArArUrArUrArArArCrArUrCrGrGrArA.

The double-stranded DNA fragments of consensus coding sequences of mouse and human *PF4* genes (CCDS 19416.1 and 3562.1) were synthesized by Integrated DNA Technologies and were cloned into the pSin-EF2-Pur vector (Addgene). Lentivirus was produced by polyethyleneimine-mediated transfection of HEK293T (ATCC) cells with pCMV delta R8.2 packaging plasmid (Addgene), pMD2.G envelope plasmid (Addgene), and pSin-EF2-PF4-Pur expression plasmid.

3.6.8 Mouse liver hepatocyte, nonparenchymal cell, F4/80+ nonparenchymal cell, and peritoneal macrophage isolation

Primary hepatocytes were isolated from wild-type male mice and cultured according to a published protocol[326] with the following modifications: the portal vein was cannulated instead of the inferior vena cava, and the inferior vena cava was cut after the initial perfusion; plates/wells were prepared with 0.01% w/v rat-tail collagen (Sigma-Aldrich). Liver nonparenchymal cells were isolated in a two-step perfusion procedure similar to the isolation of mouse hepatocytes. The F4/80+ cells were isolated from nonparenchymal cells using Anti-F4/80 MicroBeads (130-110-443, Miltenyi Biotec) according to the manufacturer's instructions. Peritoneal macrophages were isolated from mice using ice-cold phosphate-buffered saline containing 3% FBS.

3.6.9 RNA-sequencing and mouse transcriptome analysis

High-quality RNA was prepared from F4/80+ nonparenchymal cells using a combined TRIzol and RNeasy Mini Kit (Qiagen) method. RNA quality control was performed using the Nanodrop Spectrophotometer (Thermo Fisher) and TapeStation System (Agilent). cDNA library construction from mRNA, RNA-sequencing on a NovaSeq 6000 (Illumina), raw data quality control, and data delivery were carried out by Novogene. Approximately 90 million reads were generated for each sample. The raw data was filtered and quality-controlled using fastp[327]. The data quantification was performed using Salmon[328] with the mapping-based mode and a salmon index built using Gencode mouse release M25 (GRCm38.p6). The gene expression analysis was performed using DESeq2[329]. KEGG pathway analysis was carried out using GAGE[283].

3.6.10 Transcriptomic and proteomic analyses of human samples

RNA-seq raw data of human liver macrophages were downloaded from NCBI Sequence Read Archive PRJNA491664[30]. The data analysis procedure was the same as the mouse F4/80+ cells analysis, except that the reads were mapped using STAR[330], where higher mapping rates were achieved in this instance. The STAR index was built using Gencode human release 35 (GRCh38.p13). Human liver microarray data of NAFLD patients and healthy controls were downloaded from NCBI Gene Expression Omnibus (GSE89632)[284]. Processed expression and clinical data of patients in the TCGA LIHC cohort were retrieved from UCSC Xena. Processed microarray expression and clinical data of the LCI HCC cohort were downloaded from NCBI Gene Expression Omnibus (GSE14520)[300]. Gene expression difference between TCGA LIHC patient subgroups was determined with cBioportal[331]. Differential expression analysis for microarray data was performed using limma[332]. GSEA version 4.2.1 and ssGSEA v10 were used[285,299], and the analysis was carried out on GenePattern. CIBERSORTx was run in absolute mode according to the published instructions[333,334]. xCell cell types enrichment analysis for TCGA patients was pre-calculated by the authors of xCell and retrieved from the xCell website[296].

Processed protein quantitation and clinical data from a published HCC proteogenomic study were downloaded from the NIH Proteomic Data Commons (PDC000198)[301].

In the TCGA LIHC cohort, 12% of patients had low NCOA5 mRNA expression (z<-1 relative to diploid samples) and 3.6% had NCOA5 shallow deletion, missense mutation, or truncating mutation in their tumors.

3.6.11 Single-cell transcriptomic analysis of diet-induced NASH mouse livers

Single-cell sequencing raw data of nonparenchymal cells from control and diet-induced NASH mouse livers were downloaded from NCBI Sequence Read Archive PRJNA531644. The data analysis procedure was the same as in the original publication[281]. Our analysis revealed ten major cell clusters similar to the original publication (Fig. 2.9A).

3.6.12 Intrahepatic-macrophage-specific gene knockdown mediated by glucan-encapsulated siRNA particle (GeRP)

GeRPs were prepared according to published protocols[30,31,282] with the modification of no FITC labeling steps. Wild-type C57BL/6 male mice were fed with a westernized and sucrose/fructose supplemented diet (D09061704i, Research Diets, Inc.) starting at six weeks of age for three months to induce NAFLD with a concurrent *Pf4* upregulation specifically in intrahepatic macrophages[280]. GeRP administration was carried out according to published articles with slight modifications[30,31]. Mice fed the special diet were randomized according to body weight and intravenously injected with a dose of 6.25 mg/kg GeRPs loaded with 247 μg/kg siRNA and 1.135 mg/kg Endo-Porter (EP, Gene Tools, LLC). Mice were switched to a normal diet 24 hours after GeRP administration, and samples were collected one week after GeRP administration. 7-month-old *Ncoa5*$^{\Delta M/+}$ male mice fed a normal diet were randomized according to body weight and intravenously injected with seven doses of 3.125 mg/kg GeRPs loaded with 123.5 μg/kg siRNA and 0.5675 mg/kg EP over two weeks and samples were collected 24h after the last injection. siRNAs used in this study are proprietary Dharmacon D-001810-01-50 ON-TARGETplus Nontargeting siRNA #1 and J-063518-11-0050 ON-

TARGETplus Mouse Pf4 (56744) siRNA (Horizon Discovery). The LQ-063518-01-0002 ON-TARGETplus Mouse Pf4 (56744) siRNA - Set of 4 was initially tested, and the siRNA with the highest efficiency was identified and used in formal experiments.

3.6.13 Cell proliferation and colorimetric assays

1 x 10^5 RAW 264.7 cells were seeded in 12-well plates and cultured for 48 hours in the DMEM complete medium. Cell numbers were then counted using a Countess II FL hemocytometer with an automated cell counter (Thermo Fisher). For the colorimetric cell proliferation assay, 1500 RAW 264.7 cells or 4000 HepG2 cells were seeded in 96-well plates, and CCK-8 (Dojindo) was used to determine the cell number according to the protocol supplied by the manufacturer. Triglyceride levels in liver homogenates and cell lysates were measured using the Triglyceride Colorimetric Assay Kit (Cayman Chemical) according to the protocol provided by the manufacturer. Absorbance was read by a FLUOstar OPTIMA microplate reader (BMG LABTECH).

3.6.14 Transwell migration assay

Transwell permeable support (Ref 3422, Costar) plated with 1 x 10^5 HepG2 cells in serum-free DMEM medium was inserted into a 24-well plate containing medium conditioned by RAW 264.7 cells mixed with DMEM medium with 2.5% FBS. After 24 hours, the membranes were stained with Giemsa stain (Sigma-Aldrich).

3.6.15 Quantification and statistical analyses

All data represent ± SEM from the mean if not otherwise specified. Statistical differences were determined with one-way ANOVA Dunnett's multiple comparisons test, two-way ANOVA Dunnett's multiple comparisons test and Sidak's multiple comparisons

test, two-tailed Student's t test, Welch's t test, chi-squared test, Pearson's correlation two-tailed significance test, or log-rank test by GraphPad Prism 7 with details listed in the corresponding figure legends. ****p<0.0001, ***p<0.001, **p<0.01, *p<0.05, ns = not significant.

3.6.16 Deposited data

Raw and processed RNA-sequencing data were deposited in NCBI's Gene Expression Omnibus and are accessible through GEO Series accession number GSE192554.

CHAPTER 4: Hyperpolarization-activated Cyclic Nucleotide-gated Cation Channel 3 Promotes HCC Development in a Female-biased Manner

4.1 Preface

This chapter is a modified version of a previously published article in *Cell Reports*, Volume 42, **Zhang, Y.**, Liu, X., Sun, K., Luo, Y., Yang, J., Li, A., Kiupel, M., Fenske, S., Biel, M., Mi, Q.S., Wang, H. and Xiao, H., Hyperpolarization-activated cyclic nucleotide-gated cation channel 3 promotes HCC development in a female-biased manner, Copyright Elsevier (2023).

I performed most experiments and investigations, wrote the original manuscript, and edited and revised the article. Former visiting scholars Xinhui Liu and Aimin Li helped with the generation and the initial characterization of the *Ncoa5*$^{+/-}$*Tip30*$^{+/-}$ mice. Xinhui Liu performed serological assays and characterized *Il6* and *Tnf* mRNA expression in younger mice. Medical student volunteer Kairui Sun helped study the transcriptional regulation of HCN3. Former visiting scholar Yue Luo helped with the hydrodynamic tail-vein injection procedure. Former undergraduate volunteer Jack Yang helped with the generation of HCN3 knockout cell clones. Dr. Matti Kiupel performed pathologic analyses and consultations. Drs. Stefanie Fenske and Martin Biel provided the *Hcn3* knockout mice. We thank Dr. Xin Chen for the gifts of pt3 and SB vectors.

4.2 Abstract

Sex differences in HCC development are regulated by sex and non-sex chromosomes, sex hormones, and environmental factors. We previously reported that *Ncoa5*$^{+/-}$ mice develop HCC in a male-biased manner. Here, we show that NCOA5 expression is reduced in male patient HCCs while the expression of an NCOA5-interacting tumor suppressor, TIP30, is lower in female HCCs. *Tip30* heterozygous deletion does not change HCC incidence in *Ncoa5*$^{+/-}$ male mice but dramatically increases HCC incidence in *Ncoa5*$^{+/-}$ female mice, accompanied by hepatic HCN3 overexpression. HCN3 overexpression cooperates with MYC to promote mouse HCC development, whereas *Hcn3* knockout preferentially hinders HCC development in female mice. Furthermore, HCN3 amplification and overexpression occur in human HCCs and correlate with a poorer prognosis of patients in a female-biased manner. Our results suggest that TIP30 and NCOA5 protect against female liver oncogenesis and that HCN3 is a female-biased HCC driver.

4.3 Introduction

Liver cancer is the 9th most common cancer in women and the 5th in men in the US and is the third leading cause of cancer death worldwide. Despite the decline in incidence and mortality rates of most cancer types over the last decade, liver cancer incidence and mortality have steadily increased in the United States[5,335]. Notably, liver cancer incidence and mortality rates have risen faster in women than men[335,336]. HCC is the most common type of primary liver cancer, and its incidence in men is two to four times higher than in women[88]. A similar male predominance of liver tumor development has also been observed in rodent models of HCC[16,187,337,338]. Previous studies have

suggested that sex differences in HCC risk can be partly attributed to sex disparities in environmental exposures such as HBV infection and alcohol consumption[155,339-341]. However, a recent prospective cohort analysis on cancer risk for 21 cancer types, including HCC, suggests that genetic and epigenetic differences between men and women affect susceptibility to cancer and that environmental exposures alone may only explain some of the sex disparities in cancer[95]. Thus, understanding the molecular mechanisms underlying sex differences in HCC development will improve the prevention, treatment, and outcome for male and female patients with HCC.

HCC has the most significant sex differences in autosomal mutational profiles among cancers of non-reproductive tissues among 18 tumor types examined[94], suggesting etiological differences between male and female HCC. There is growing evidence of sex-biased mechanisms driving HCC initiation and progression in males and females[93,342,343], which are influenced by hormones and lifestyle[17,98,344]. The β-catenin encoded by *CTNNB1*, a well-known liver cancer driver, is a male-biased HCC driver with a higher mutation frequency in male HCC specimens. *CTNNB1* mutations also affect patient outcomes in both sexes but have a male-biased preference[94]. Identifying sex-biased liver cancer drivers may allow us to discover new opportunities for developing sex-specific anti-HCC therapies. Although extensive studies on hepatocarcinogenesis have uncovered protective or promotive mechanisms related to sex hormones[98,345] and non-sex hormone factors[134,135], most studies have primarily used male subjects due to the prevalence of HCC in males, resulting in a female patient and animal underrepresentation. Consequently, those identified sex-biased liver cancer drivers tend to promote cancer development in a male-biased manner. Recently,

several female-preferentially expressed factors such as miR26s and CYP39A1 have been reported to suppress HCC development[136-138]. Furthermore, four genes with a higher mutation frequency in female HCCs were identified in HBV-related and aflatoxin-exposed HCC patients[346]. However, none of these genes have been reported as HCC drivers for promoting malignant transformation, and the mechanisms driving HCC development in females remain poorly understood.

NCOA5 is a unique nuclear receptor coactivator with both coactivator and corepressor functions. It cooperates with TIP30, a known tumor suppressor[208,347], to repress ERα-activated c-*myc* gene transcription in estrogen-dependent and independent ways[180]. NCOA5 plays a critical role in the sex differences in HCC development, as its haploinsufficiency leads to spontaneous HCC development in a male-biased manner through increased proinflammatory cytokine expression, p53-p21 pathway activation, and increased populations of immunosuppressive cells[187,250,271,348]. To investigate the mechanism preventing HCC development in female *Ncoa5*$^{+/-}$ mice, we generated mice carrying dual *Ncoa5* and *Tip30* heterozygous deletions for genetic and biochemical analyses. Our results demonstrate that TIP30 is critical in suppressing HCC development in *Ncoa5*$^{+/-}$ female mice, and HCN3, whose expression is significantly increased in the livers of *Ncoa5*$^{+/-}$*Tip30*$^{+/-}$ female, is a female-biased cancer driver for promoting HCC development.

4.4 Results

4.4.1 NCOA5 and TIP30 are differentially expressed in male and female HCCs and are interrelated in expression levels

We previously reported that NCOA5 haploinsufficiency resulted in a high

incidence of HCC in aged male mice but rarely in female mice[187]. To explore if there are sex-different roles of NCOA5 in human hepatocarcinogenesis, I first determine the levels of NCOA5 expression in HCCs from male and female patients of the TCGA cohort. I found that HCC specimens from male patients had significantly lower *NCOA5* mRNA than female patients (Fig. 3.1A and 3.1B left). Through protein-protein interaction networks, I identified NCOA5 interacting proteins with differential expression levels between HCCs from male and female patients (Fig. 3.1C). One of these proteins is TIP30/HTATIP2, which can cooperate with NCOA5 to regulate ERα-mediated c-*myc* gene transcription[180]. TIP30 mRNA levels in HCCs from female patients were significantly lower compared to HCCs from male patients (Fig. 3.1B right). Intriguingly, the mRNA levels of *NCOA5* and *TIP30* negatively correlated with each other in HCCs from the TCGA cohort (Fig. 3.1D). This negative correlation was also observed in younger female and older male and female mice, as *Tip30* mRNA levels were increased in the livers of 2 and 5-month-old *Ncoa5*$^{+/-}$ female mice but not in age-matched *Ncoa5*$^{+/-}$ male mice (Fig. 3.2A). In contrast, *Tip30* mRNA levels were increased in the livers of *Ncoa5*$^{+/-}$ male mice at an older age (Fig. 3.2B). These results indicate that NCOA5 and TIP30 expressions are sex-dependent and interrelated in both mouse and human livers. Given its tumor-suppressive role[347], we hypothesize that *Tip30* is critical in suppressing hepatocarcinogenesis in females with NCOA5 deficiency.

4.4.2 Tip30 heterozygous deletion promotes the HCC development of Ncoa5-deficient mice in a female-biased manner

To test the hypothesis above, we sought to determine if the downregulation of TIP30 increases liver tumor incidence in the *Ncoa5*$^{+/-}$ mouse model of HCC. Since a

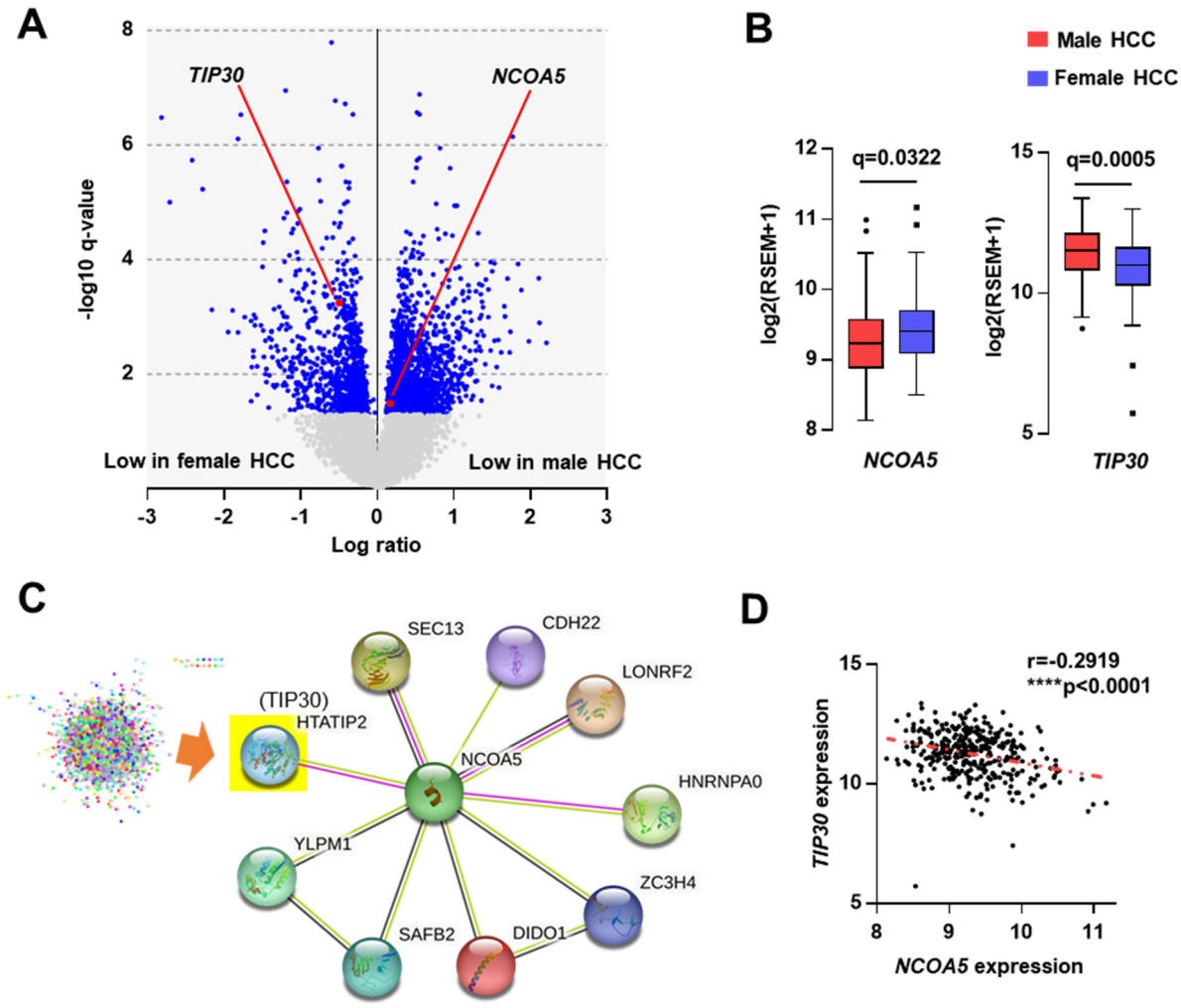

Figure 3.1 Gene expression differences between male and female HCC samples from the TCGA cohort and the correlation between NCOA5 and TIP30 expression in human HCC. (A) Volcano plot showing differentially expressed genes between primary HCC samples from female (n=117) and male (n=244) patients in the TCGA cohort. Welch's t test with the FDR method of Benjamini-Hochberg. q cutoff at 0.05. Genes on XY chromosomes are not included in the graph. (B) Box plots showing mRNA levels of *NCOA5* and *TIP30* in male and female primary HCC samples. q values are from the result shown in Figure A. Box and whisker were drawn using the Tukey method. (C) Graph showing protein interaction network of NCOA5. Differentially expressed genes between male and female primary HCCs in the TCGA cohort were used to generate the network. The node centered by NCOA5 containing its first interacting neighbors was extracted and shown. (D) Correlation between NCOA5 and TIP30 mRNA levels in primary HCC samples from male and female patients in the TCGA cohort. n=361. Pearson correlation. ****p<0.0001.

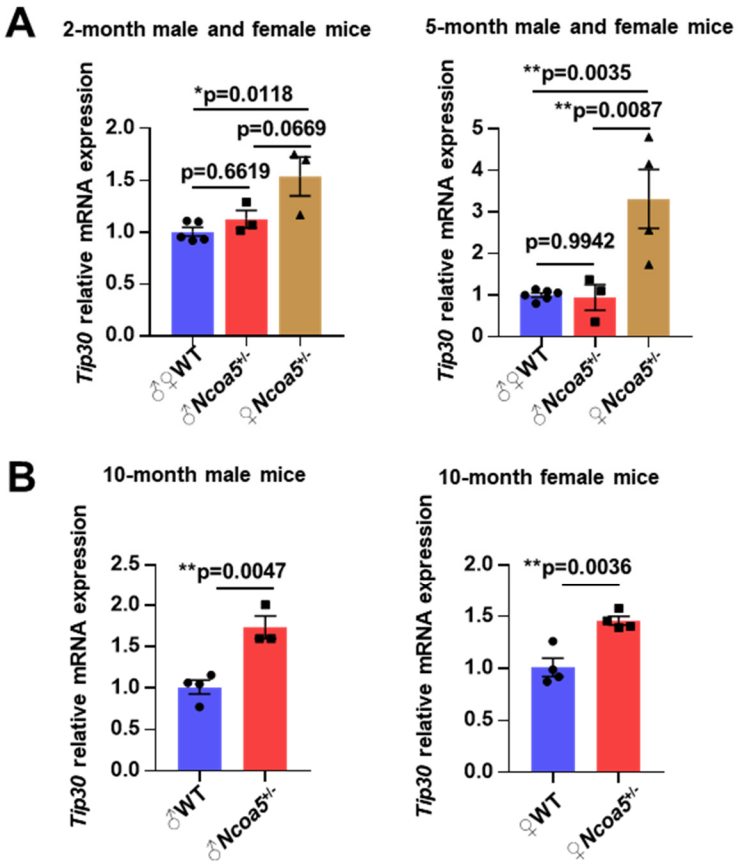

Figure 3.2 *Tip30* mRNA levels in livers of male and female mice with and without *Ncoa5* deletion at different ages. (A) RT-qPCR analysis of the *Tip30* mRNA levels in the livers of mice. Left: 2-month-old wild-type male (n=3) and female (n=2) mice, *Ncoa5*$^{+/-}$ male (n=3) and female mice (n=3). Right: 5-month-old wild-type male (n=4) and female (n=2) mice, *Ncoa5*$^{+/-}$ male (n=3) and female (n=4) mice. One-way ANOVA Tukey's multiple comparisons test. (B) RT-qPCR analysis of the *Tip30* mRNA levels in left: 10-month-old wild-type (n=4) and *Ncoa5*$^{+/-}$ (n=3) male mice; right: 10-month-old wild-type (n=4) and *Ncoa5*$^{+/-}$ (n=4) male mice. Two-tailed unpaired Student's t test. **p<0.01, *p<0.05. Data represent mean ± SEM.

high incidence of lung and mammary gland tumors in *Tip30*$^{-/-}$ mice[208,227] might complicate the results, we monitored liver tumor development in a cohort of wild-type, *Tip30*$^{+/-}$, *Ncoa5*$^{+/-}$, and *Ncoa5*$^{+/-}$*Tip30*$^{+/-}$ female and male mice. Mice were euthanized and subject to complete necropsy when moribund or at the age of 18 months. Liver, lung, and mammary tumors were detected at the surface of the organs in mice older than 10 months. Interestingly, a liver tumor incidence of 80% was observed in *Ncoa5*$^{+/-}$

Tip30$^{+/-}$ female mice, whereas only 10% of *Ncoa5*$^{+/-}$ female mice developed liver tumors. No liver tumor was detected in wild-type or *Tip30*$^{+/-}$ female mice (Fig. 3.3A). In contrast, liver tumor incidence was not increased in *Ncoa5*$^{+/-}$*Tip30*$^{+/-}$ male mice compared to *Ncoa5*$^{+/-}$ male mice (Fig. 3.3A). 26.7% of *Tip30*$^{+/-}$ female mice developed lung tumors and 13.3% developed mammary gland tumors. For *Ncoa5*$^{+/-}$*Tip30*$^{+/-}$ female mice, 10% of mice developed lung tumors, and another 10% developed mammary gland tumors without comorbidities with liver tumors. No lung or mammary gland tumors were observed in *Ncoa5*$^{+/-}$ female mice. All liver tumors from female and male *Ncoa5*$^{+/-}$ *Tip30*$^{+/-}$ mice were well to moderately-differentiated HCCs[349] with similar histological features (Fig. 3.3B) and the livers of 10-month-old *Ncoa5*$^{+/-}$*Tip30*$^{+/-}$ female mice displayed moderate to severe steatosis compared to the livers of age-matched *Ncoa5*$^{+/-}$ female mice (Fig. 3.3C), similar to those previously described in *Ncoa5*$^{+/-}$ male mice[187]. Heterozygous deletion of *Tip30* alone did not result in any case of HCC, nor did it change the liver histology[350] significantly in female mice (Fig. 3.3A, 3.3D, and 3.3E). Notably, heterozygous deletion of *Ncoa5* resulted in moderately disrupted liver architecture and vacuolated hepatocytes in aged female mice (Fig. 3.3D and 3.3E), even though the severities were much less compared to that in age-matched male mice.

In line with these results, both α-fetoprotein (AFP) levels and ALT activity were significantly increased in the serum of *Ncoa5*$^{+/-}$*Tip30*$^{+/-}$ female mice at the age of 18 months compared to age-matched female mice in other genotypical groups, confirming the severe liver damage and liver malignancy in dual mutant female mice (Fig. 3.4A). ALT activity was also increased in the serum of 18-month-old *Ncoa5*$^{+/-}$ female mice compared to wild-type mice (Fig. 3.4A). IHC staining of macrophage marker MAC-2

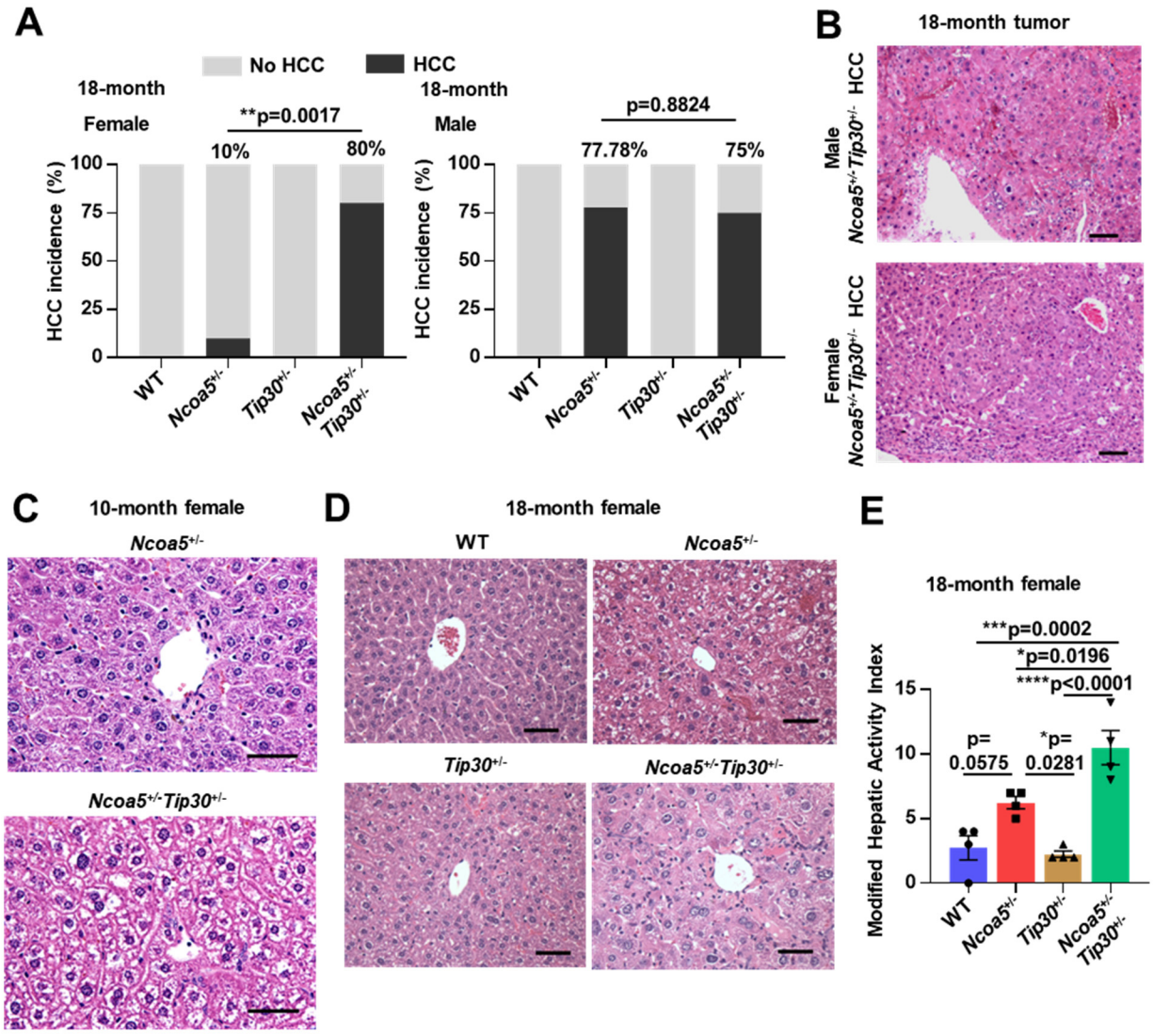

Figure 3.3 HCC incidence and histopathology features in 18-month-old male and female mice with *Ncoa5* and/or *Tip30* deficiency. (A) HCC incidence in 18-month-old female and male mice with indicated genotype. Female mice (left) n=12, 10, 15, or 10; male mice (right) n=6, 9, 11, or 12. Chi-squared test. (B) Representative H & E staining photos of moderately differentiated HCCs from *Ncoa5*$^{+/-}$*Tip30*$^{+/-}$ male or female mice. Grading was according to the WHO classification. Scale bar: 100 μm. (C) Representative H & E staining photos of livers of 10-month-old *Ncoa5*$^{+/-}$ and *Ncoa5*$^{+/-}$ *Tip30*$^{+/-}$ female mice. Scale bar: 50 μm. (D) Representative H & E staining photos of non-tumor adjacent liver from 18-month-old female mice as indicated. Scale bar: 50 μm. (E) Modified Hepatic Activity Index of 18-month-old female mice with the corresponding genotypes (n=4 per group), scored with H & E staining. One-way ANOVA Tukey's multiple comparisons test. ****p<0.0001, ***p<0.001, **p<0.01, *p<0.05. Data represent mean ± SEM.

revealed increased macrophage infiltration to the livers of 18-month-old *Ncoa5*$^{+/-}$*Tip30*$^{+/-}$ female mice compared to *Ncoa5*$^{+/-}$ or wild-type age-matched female mice (Fig. 3.4B). Together, these data demonstrated that heterozygous *Tip30* deletion preferentially promotes HCC development in *Ncoa5*$^{+/-}$ female mice.

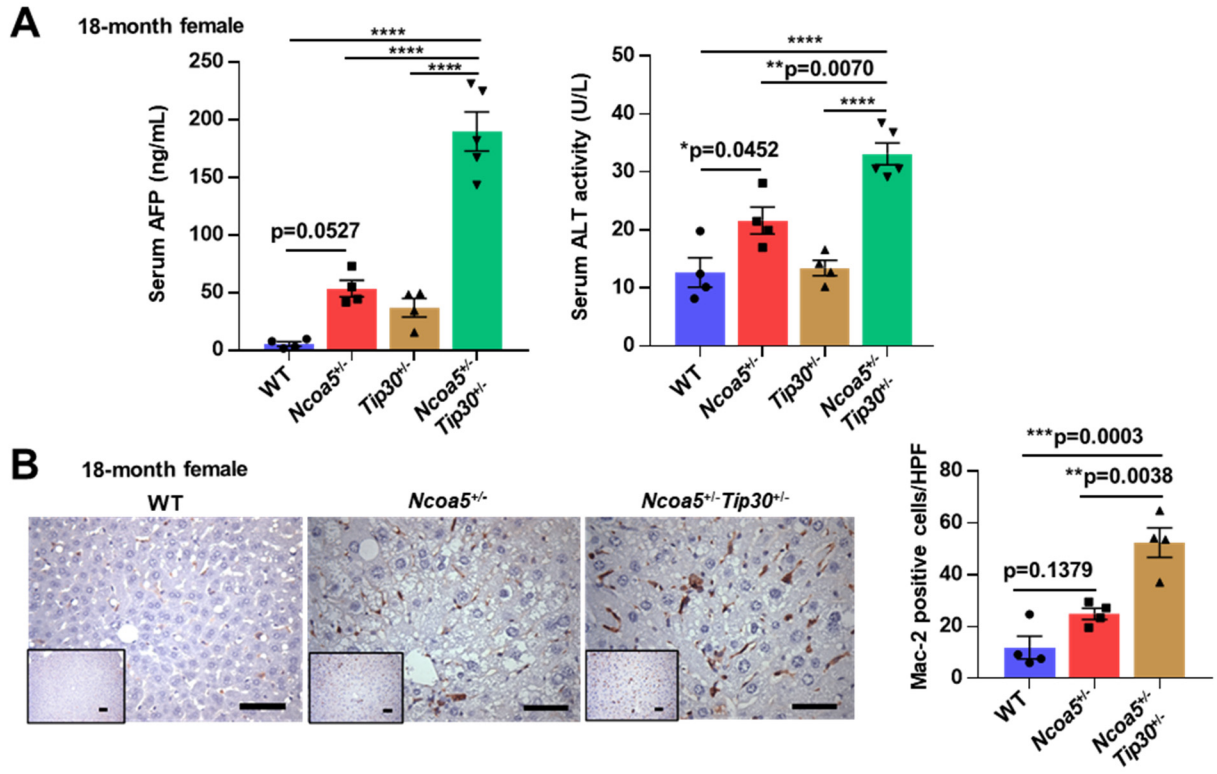

Figure 3.4 AFP, ALT, and liver MAC-2 IHC assays of 18-month-old female mice with or without *Ncoa5* and/or *Tip30* deficiency. (A) Serum AFP level and ALT activity in 18-month-old female mice as indicated. Mouse n=4 per group.One-way ANOVA Tukey's multiple comparisons test. (B) Representative MAC-2 IHC staining photos and analysis of livers from 18-month-old female mice as indicated. Mouse n=4 per group. One-way ANOVA Tukey's multiple comparisons test. Scale bar: 50 μm. ****p<0.0001, ***p<0.001, **p<0.01, *p<0.05. Data represent mean ± SEM.

4.4.3 Deletion of Tip30 in Ncoa5$^{+/-}$ *female mice upregulates pathways in cation transport and cell cycle and HCN3 expression*

To identify genes and signaling pathways that promote the hepatocarcinogenesis in *Ncoa5*$^{+/-}$*Tip30*$^{+/-}$ female mice, we performed RNA sequencing and transcriptome

analysis on isolated RNA from the livers of 5-month-old wild-type, *Ncoa5*$^{+/-}$, *Tip30*$^{+/-}$, and *Ncoa5*$^{+/-}$*Tip30*$^{+/-}$ female mice. Gene Ontology (GO) enrichment analysis revealed that the top five GO.bp pathways uniquely upregulated in *Ncoa5*$^{+/-}$*Tip30*$^{+/-}$ female livers included cycle G2/M phase transitions and multiple pathways related to the regulation of transport of calcium and other cations (Fig. 3.5). The bile acid metabolism and vesicle transport associated with the endoplasmic reticulum and Golgi apparatus were uniquely downregulated in the livers of *Ncoa5*$^{+/-}$*Tip30*$^{+/-}$ female mice. Unexpectedly, *Tip30*

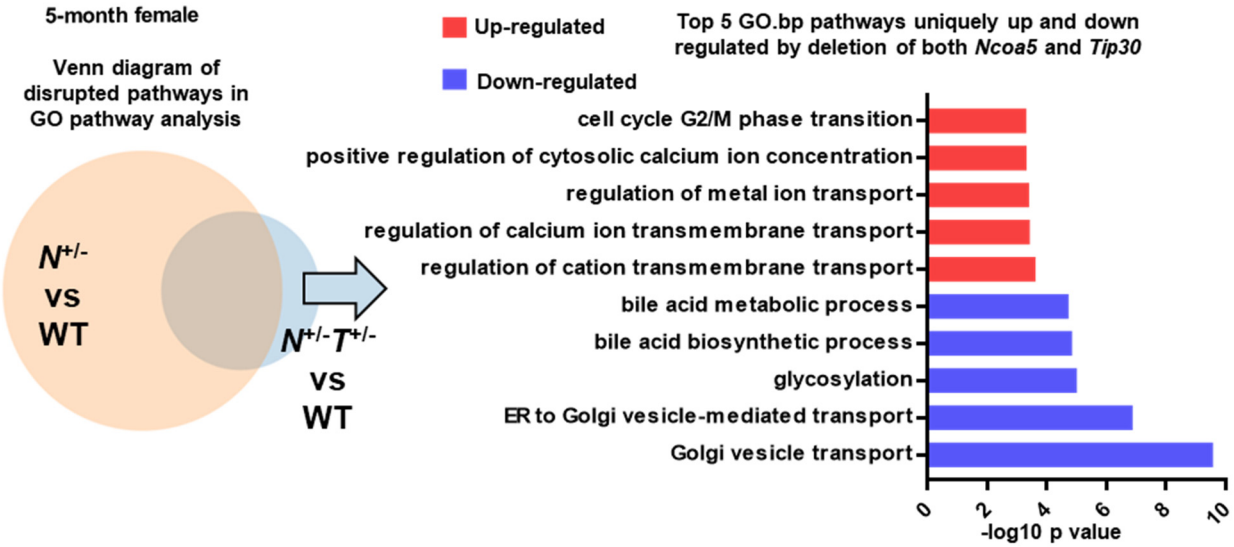

Figure 3.5 GO.bp pathways uniquely disrupted in *Ncoa5*$^{+/-}$*Tip30*$^{+/-}$ female livers. Disrupted pathways in GO.bp pathway analyses comparing liver transcriptomes of *Ncoa5*$^{+/-}$ or *Ncoa5*$^{+/-}$*Tip30*$^{+/-}$ female mice vs. wild-type female mice. n=4 in each group. Left: Venn diagram. Pathways with q<0.05 were recognized as significantly disrupted pathways. Right: Top 5 GO.bp pathways uniquely up and downregulated by deletion of both *Ncoa5* and *Tip30*, but not by deletion of *Ncoa5* or *Tip30* alone.

deletion did not further activate inflammatory pathways that were upregulated in *Ncoa5*$^{+/-}$ female mice livers, nor did it further activate p53-p21 signaling pathways (Fig. 3.6). Consistently, the mRNA levels of IL-6 and TNF-α were not increased in the livers of 5-month-old *Ncoa5*$^{+/-}$*Tip30*$^{+/-}$ female mice compared to age-matched *Ncoa5*$^{+/-}$ or *Tip30*$^{+/-}$ female mice nor were they raised in the HCCs or adjacent normal liver tissues

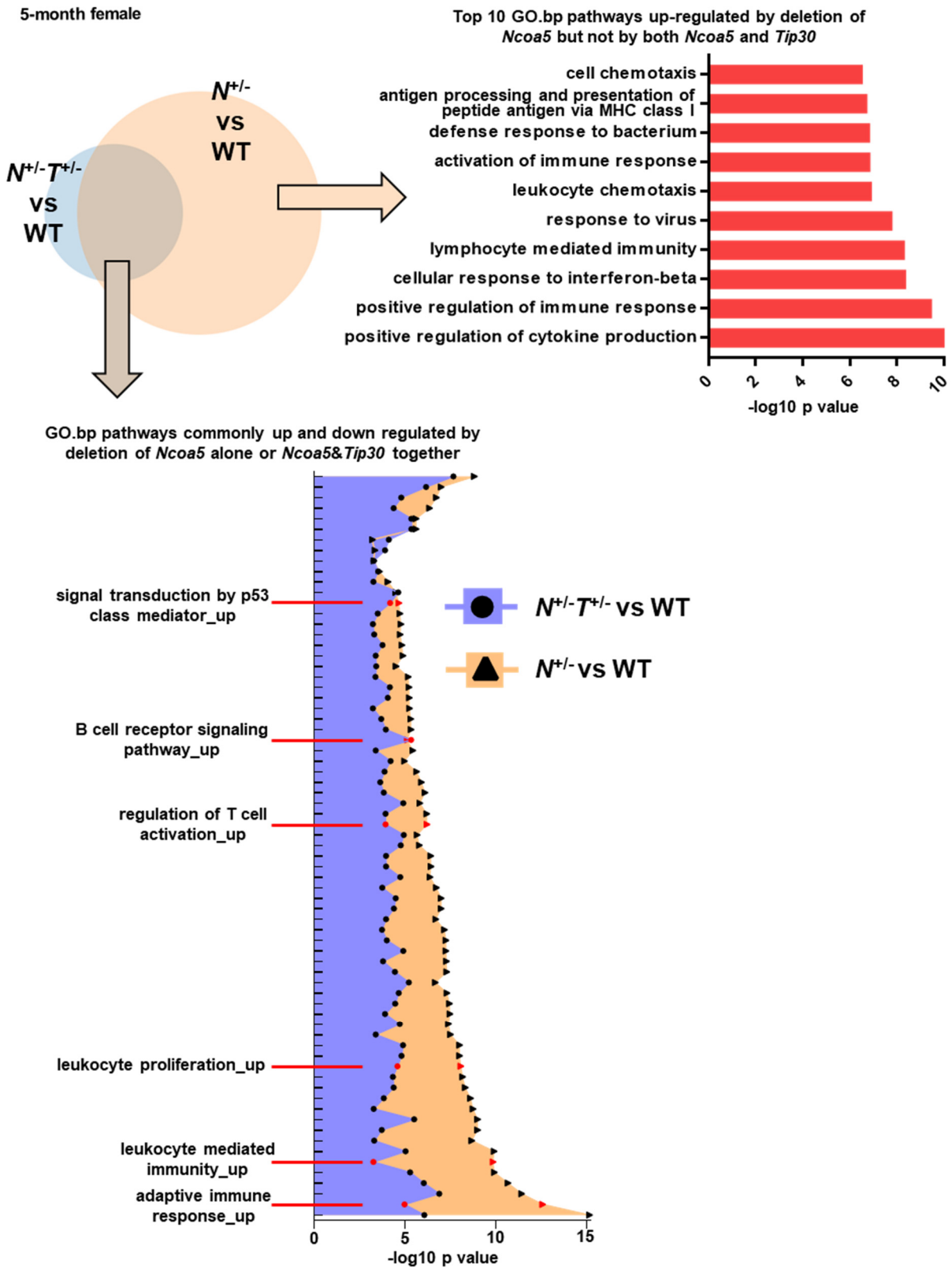

Figure 3.6 GO.bp pathways that were disrupted by *Ncoa5* deletion and not further

Figure 3.6 (cont'd)
disrupted by *Tip30* deletion. GO.bp pathway analysis results comparing the transcriptome of *Ncoa5*$^{+/-}$ and *Ncoa5*$^{+/-}$*Tip30*$^{+/-}$ female livers vs. wild-type livers. Top left is the Venn diagram showing GO.bp pathways disrupted by *Ncoa5* deletion in livers of female mice, including pathways upregulated by deletion of *Ncoa5* but not by deletions of *Ncoa5* and *Tip30* (top right) and pathways commonly up and downregulated by deletion of *Ncoa5* alone or *Ncoa5*&*Tip30* together (bottom). Examples of pathways related to immune response and p53 were highlighted in the bottom figure.

of 18-month-old *Ncoa5*$^{+/-}$*Tip30*$^{+/-}$ female mice compared to *Ncoa5*$^{+/-}$ female mice (Fig. 3.7A and 3.7B). IHC staining and enzyme-linked immunosorbent assay (ELISA) confirmed no increased IL-6 expressing cells and protein levels in the livers of 18-month-old *Ncoa5*$^{+/-}$*Tip30*$^{+/-}$ female mice compared to those of *Ncoa5*$^{+/-}$ female mice (Fig. 3.7C and 3.7D).

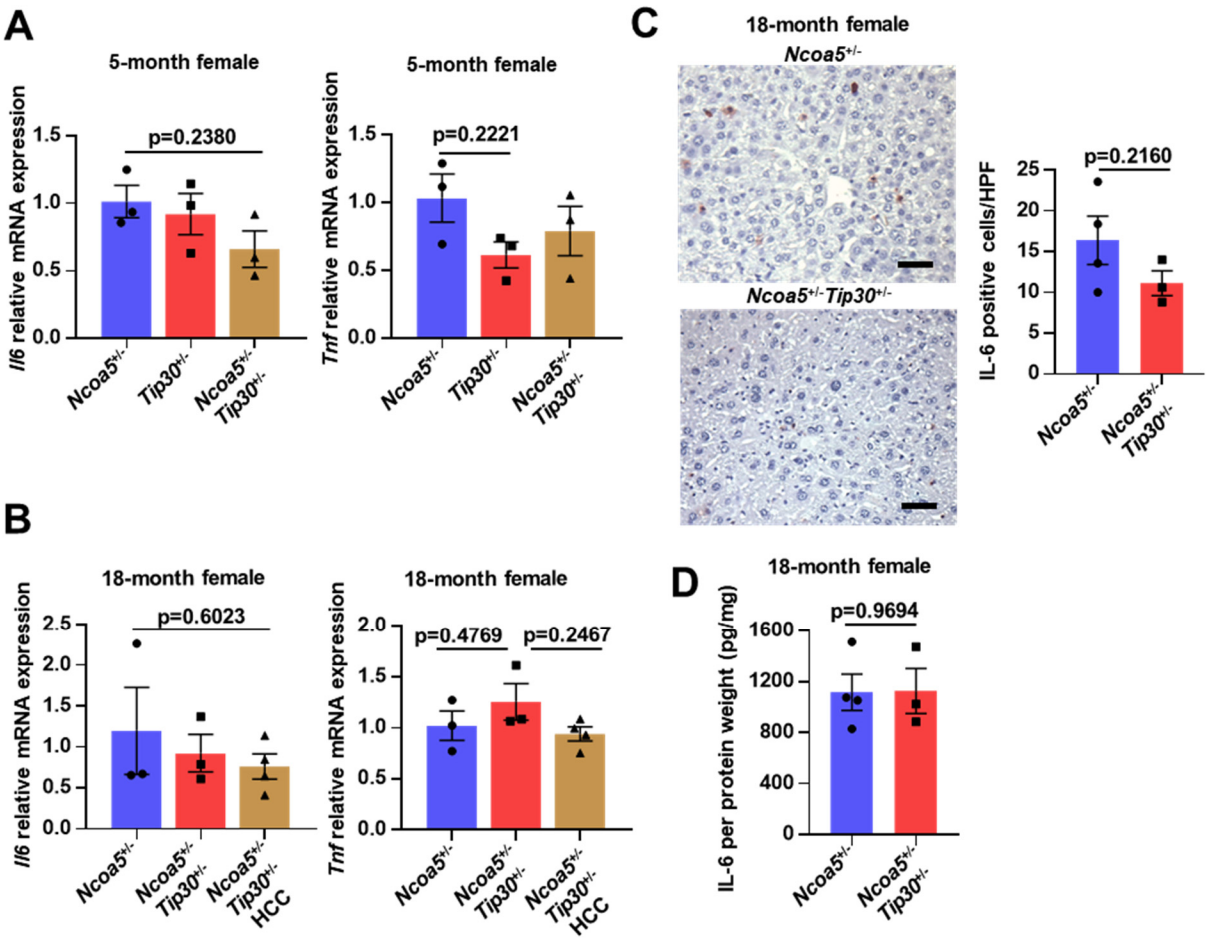

Figure 3.7 Expressions of IL-6 and TNF-α in livers of female *Ncoa5*$^{+/-}$ mice with

Figure 3.7 (cont'd)
and without *Tip30* deletion. (A and B) RT-qPCR analysis of mRNA levels of *Il6* and *Tnf* in livers of 5-month-old female mice (A) and in livers and HCCs of 18-month-old female mice (B) as indicated. One-way ANOVA Tukey's multiple comparisons test. (C) Representative IL6 IHC staining photos and analysis of livers from 18-month-old female mice as indicated. n=4 or 3. Two-tailed unpaired Student's t test. (D) Liver IL-6 level per total protein weight of 18-month-old female mice (n=4 or 3) measured by ELISA. Two-tailed unpaired Student's t test. Data represent mean ± SEM.

Next, I analyzed the DEGs between wild-type and three types of mutant livers (adjusted $p<0.05$). Dual *Ncoa5* and *Tip30* heterozygous deletions resulted in the highest number of DEGs (1099), while *Ncoa5* heterozygous deletion alone significantly changed the expression of 250 genes, and *Tip30* heterozygous deletion alone only changed 43 gene expression significantly (Fig. 3.8A). Only two DEGs, upregulated *Hcn3,* encoding a cation channel known to mediate the transport of potassium, sodium, and calcium[351,352], and downregulated *Wnt5a*, are shared by all three mutant liver groups (Fig. 3.8A and 3.8B). Notably, the proto-oncogene *Mycn* was significantly upregulated only in the dual mutant livers (Fig. 3.8A and 3.8C). When comparing gene expression profiles between livers of *Ncoa5*$^{+/-}$*Tip30*$^{+/-}$ and *Ncoa5*$^{+/-}$ female mice, the most significantly upregulated protein-coding gene in livers of *Ncoa5*$^{+/-}$*Tip30*$^{+/-}$ female mice was *Hcn3* (Fig. 3.8D). Moreover, the dual heterozygous deletions did not increase *Hcn3* mRNA in the livers of male mice (Fig. 3.8E). In wild-type mice, liver *Hcn3* mRNA level is higher in females than in males (Fig. 3.8F). Protein expression[266,353] of HCN3 was also increased in the livers of *Ncoa5*$^{+/-}$*Tip30*$^{+/-}$ female mice (Fig. 3.8G). Collectively, these results suggest that hepatic HCN3 overexpression is associated with HCC development in *Ncoa5*$^{+/-}$*Tip30*$^{+/-}$ female mice.

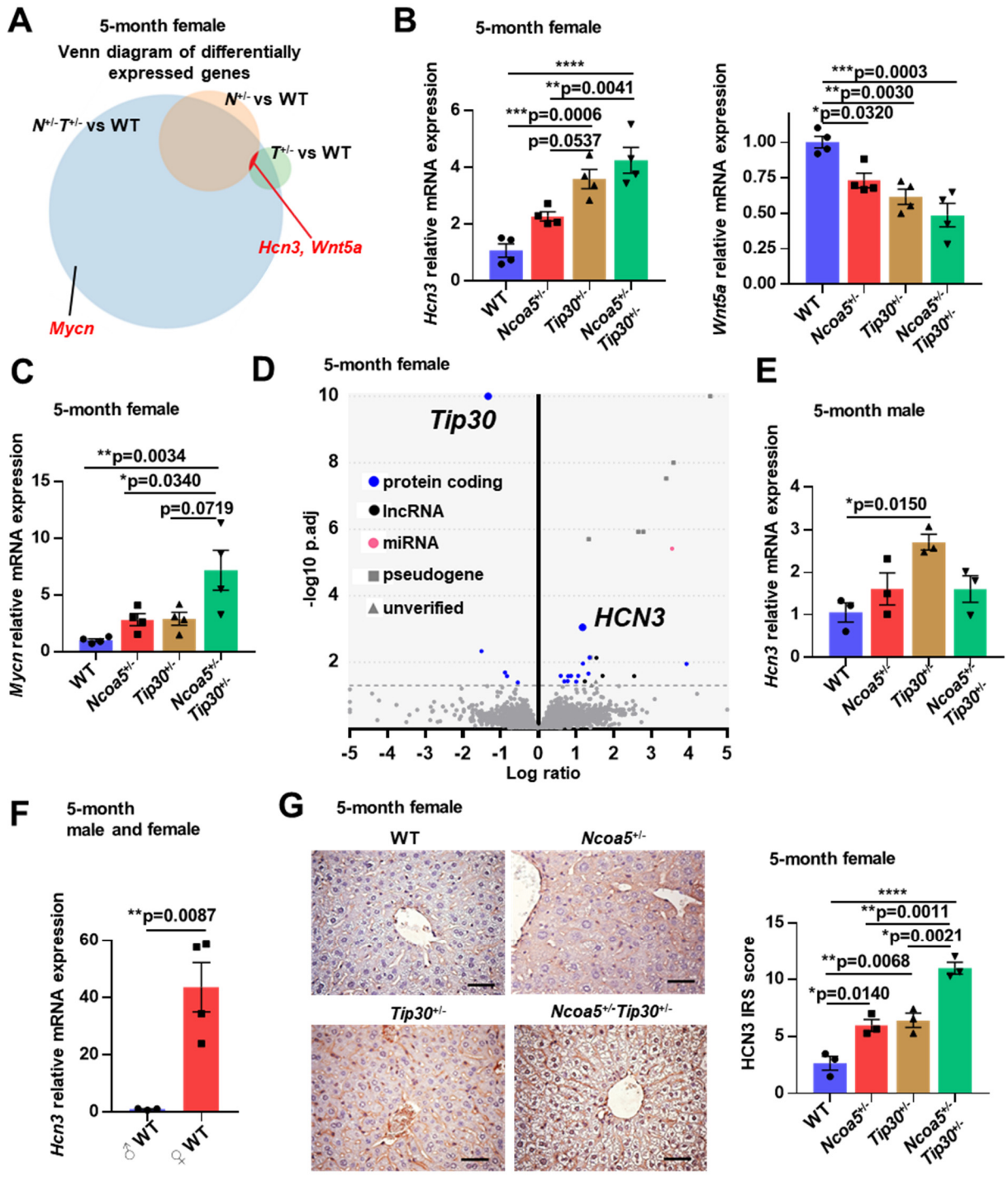

Figure 3.8 Transcriptome analysis of livers of 5-month-old wild-type, *Ncoa5*$^{+/-}$, *Tip30*$^{+/-}$, and *Ncoa5*$^{+/-}$*Tip30*$^{+/-}$ female mice and the expression of HCN3 in male and female mice. (A) Venn diagram of differentially expressed genes between liver transcriptomes of *Ncoa5*$^{+/-}$, *Tip30*$^{+/-}$, or *Ncoa5*$^{+/-}$*Tip30*$^{+/-}$ female mice and wild-type female mice. n=4 in each group. (B) RT-qPCR analysis of the mRNA levels of identified commonly upregulated gene *Hcn3* (left) and commonly downregulated gene *Wnt5a* (right) in livers of 5-month-old female mice as indicated. n=4 per group. One-way

Figure 3.8 (cont'd)
ANOVA Tukey's multiple comparisons test. (C) RT-qPCR analysis of the mRNA levels of *Mycn* in livers of 5-month-old female mice as indicated. n=4 in each group. One-way ANOVA Tukey's multiple comparisons test. (D) Volcano plot showing differentially expressed genes between livers of 5-month-old *Ncoa5*$^{+/-}$ and *Ncoa5*$^{+/-}$*Tip30*$^{+/-}$ female mice and their gene classes. Differentially expressed genes with adjusted p<0.05 were recognized as significant. -log10padj values larger than ten were drawn as 10, and log2fold-change values larger than five were drawn as 5. (E) RT-qPCR analysis of *Hcn3* mRNA levels in livers of 5-month-old male mice. n=3 per group. One-way ANOVA Tukey's multiple comparisons test. (F) RT-qPCR analysis of *Hcn3* mRNA levels in livers of 5-month-old male and female wild-type mice. n=3 or 4. Two-tailed unpaired Student's t test. (G) Left: Representative HCN3 IHC in livers of 5-month-old female mice. n=3 per group. Right: HCN3 IHC staining scores in livers of 5-month-old female mice as indicated. n=3 per group. One-way ANOVA Tukey's multiple comparisons test. Scale bar: 50 μm. ****p<0.0001, ***p<0.001, **p<0.01, *p<0.05. Data represent mean ± SEM.

4.4.4 HCN3 expression is regulated by the female hormone progesterone (Pg) and progesterone receptors (PRs)

Since multiple progesterone response elements (PREs) were predicated in the putative promoter region of *HCN3* using PROMO (Fig. 3.9A)[354,355], we tested if PRs and Pg transcriptionally regulated HCN3. Human PLC/PRF/5 HCC cells with endogenous expression of NCOA5 and TIP30 (Fig. 3.9B) were co-transfected with human progesterone receptor A (PRA) or B (PRB) expression vectors and a luciferase-reporter plasmid containing a promoter region with 9 PREs of the *HCN3* gene (Fig. 3.9A). Co-transfection of PRB-expressing vectors, but not PRA-expressing vectors, increased luciferase activities in cells without Pg. Treating cells with Pg produced 2.6- or 3.6-fold increases in luciferase activities in cells transfected with PRA or PRB, respectively (Fig. 3.9C). Consistently, treatment of HCC cells transfected with PRA or PRB expression vector with Pg increased the mRNA levels of HCN3. PRB expression increased HCN3 mRNA levels in the absence of Pg (Fig. 3.9D). Of note, HCC cells transfected with an empty vector also had increased HCN3 mRNA in response to Pg, which might be due to

the activation of endogenous PRs by Pg. Low levels of endogenous PRB protein in PLC/PRF/5 cells were detected (Fig. 3.9B), especially in the presence of proteasome inhibitor[226]. Co-transfection of the TIP30 expression vector reduced the luciferase activities in HCC cells with or without transfected PRA/PRB expression or Pg treatment (Fig. 3.9E and 3.9F). These results suggest that the HCN3 expression is activated by the female hormone Pg and its receptors and repressed by TIP30.

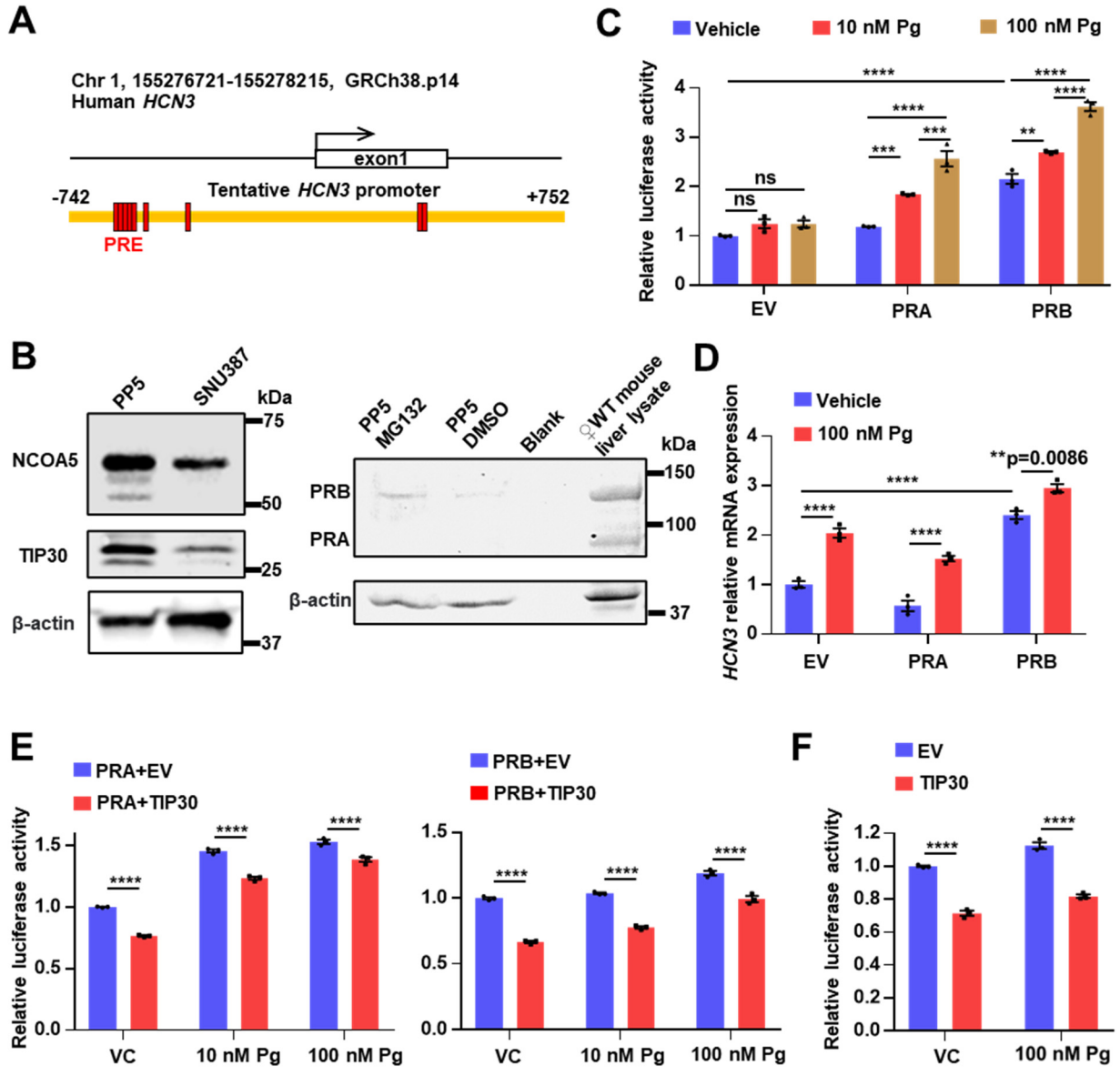

Figure 3.9 Transcriptional regulation of *HCN3* by Pg and PRs. (A) Diagram of the

Figure 3.9 (cont'd)
putative promoter region of human *HCN3* and the relative locations of predicted PREs in the HCN3 promoter-luciferase reporter plasmid. (B) Western blots of NCOA5 and TIP30 in HCC cell lines as indicated (left), and PRA and PRB in PLC/PRF/5 HCC cells treated with proteasome inhibitor MG-132 or DMSO and the liver lysate of a 5-month-old female wild-type mouse (right). (C) Relative luciferase activity of the *HCN3* promoter in PLC/PRF/5 HCC cells transfected with empty vector (EV), PRA expressing vector, or PRB expressing vector with or without Pg treatment. Two-way ANOVA Tukey's multiple comparisons test. (D) RT-qPCR analysis of *HCN3* mRNA levels in PLC/PRF/5 cells transfected with EV, PRA expressing vector, or PRB expressing vector with or without Pg treatment. Two-way ANOVA Tukey's multiple comparisons test. (E) Relative luciferase activity of the HCN3 promoter in PLC/PRF/5 cells transfected with PRA (left) or PRB (right) expressing vector together with EV or TIP30 expressing vector with or without Pg treatment. VC: Vehicle Control. Two-way ANOVA Sidak's multiple comparisons test. (F) Relative luciferase activity of the HCN3 promoter in PLC/PRF/5 cells transfected with EV or TIP30 expressing vector with or without Pg treatment. Two-way ANOVA Sidak's multiple comparisons test. Representative data of 3 repeats. ****p<0.0001, ***p<0.001, **p<0.01. Data represent mean ± SEM.

4.4.5 HCN3 promotes HCC cell proliferation and protects HCC cells from ER stress

Ion channels have been known to play essential roles in cell cycle progression[356-358], and HCN3 was reported to promote breast cancer progression[352]. To test if overexpressed HCN3 has oncogenic activity in the liver, I first confirmed the endogenous HCN3 expression in two different sex HCC cell lines, PLC/PRF/5 derived from a male patient and SNU-387 derived from a female patient that also express NCOA5 and TIP30 (Fig. 3.9B), as well as in the mouse immortal NIH/3T3 fibroblast cells (Fig. 3.10A). The cell growth was examined in media with either high or low serum concentrations to minimize influences from nutrients, growth factors, and inhibitors in the serum. Ectopic expression of HCN3 could promote the growth of all three cell lines in the low serum condition and NIH/3T3 and PLC/PRF/5 cells in the higher serum conditions (Fig. 3.10B). It also increased the soft agar colony formation ability of PLC/PRF/5 cells (Fig. 3.10C).

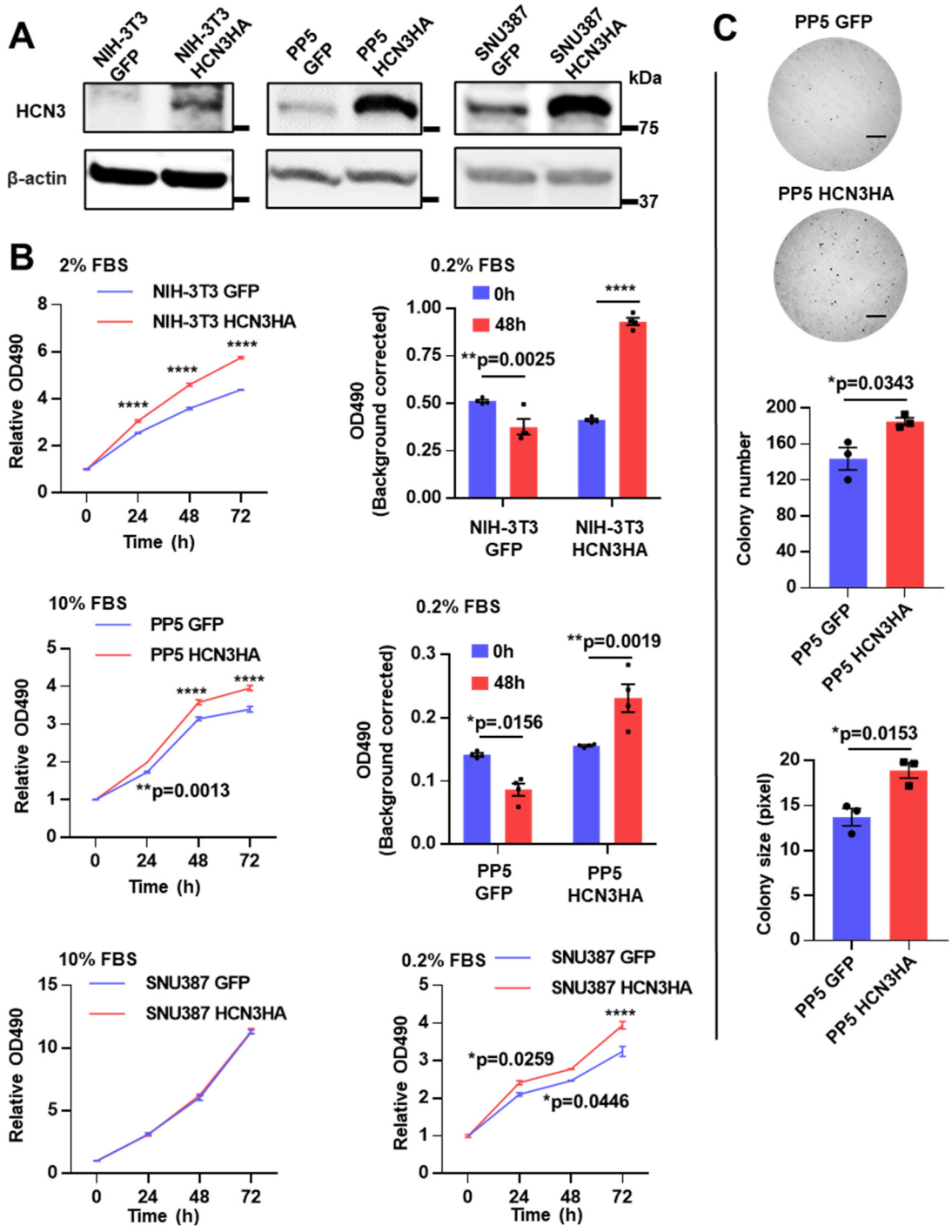

Figure 3.10 Effects of HCN3 overexpression on cell proliferation and survival *in vitro*. (A) Western blot of HCN3 overexpression in cell lines as indicated. (B) Effect of HCN3 overexpression on cell proliferation of NIH-3T3 (top), PLC/PRF/5 (PP5) (middle), and SNU-387 (bottom) cells. Cells were grown in a medium supplemented with FBS in concentration as indicated. Two-way ANOVA Sidak's multiple comparisons test. (C) Representative photos (top) of soft agar colony formation assays on PLC/PRF/5 cells with or without HCN3 overexpression and the quantifications of colony number (middle)

Figure 3.10 (cont'd)

and colony size (bottom). Two-tailed unpaired Student's t test. Scale bar: 2.5 mm. Representative data of 3 repeats. ****p<0.0001, **p<0.01, *p<0.05. Data represent mean ± SEM.

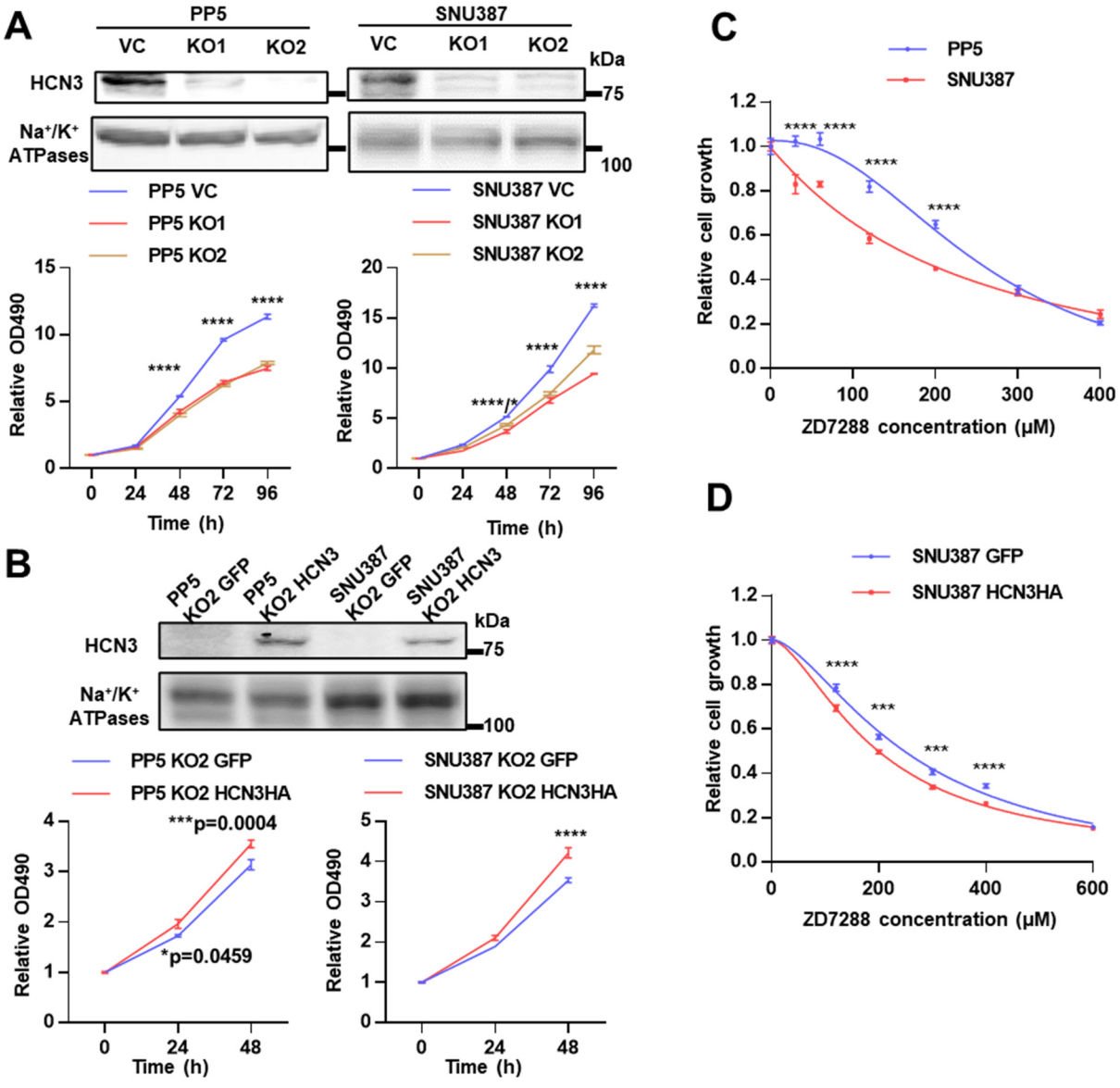

Figure 3.11 Effects of HCN3 knockout or inhibition on the growth of HCC cells *in vitro*. (A) Effect of HCN3 knockout on cell proliferation. Western blot validation of HCN3 CRISPR knockout in cell lines as indicated. VC: Vector Control. Cells were grown in medium with 10% FBS. Two independent single clones for each cell line were analyzed. (B) Effect of HCN3 compensation on cell proliferation of HCN3 knockout cells. Top: Western blot of HCN3 compensation in HCN3 knockout cells as indicated. Bottom: The proliferation of HCN3 knockout cells with HCN3 compensation. (C) Effect of HCN inhibition by ZD7288 on the growth of cell lines as indicated. (D) Effect of HCN inhibition

Figure 3.11 (cont'd)
by ZD7288 on the growth of SNU-387 cells with HCN3 or GFP overexpression. Two-way ANOVA Sidak's multiple comparisons test. Representative data of 3 repeats. ****p<0.0001, ***p<0.001, *p<0.05. Data represent mean ± SEM.

Consistently, the CRISPR-knockout of the *HCN3* gene in PLC/PRF/5 and SNU-387 cells significantly decreased the growth of both cell lines compared to vector control cells (Fig. 3.11A). The re-expression of HCN3 in the knockout cells could complement the cell growth inhibition (Fig. 3.11B). Moreover, the selective inhibitor for HCN channels, ZD7288[351], inhibited the cell proliferation of both PLC/PRF/5 and SNU-387 cells in a dosage-dependent manner. However, the female-derived SNU-387 cells were more sensitive than the male-derived PLC/PRF/5 cells to ZD7288 treatment (Fig. 3.11C). HCN3 overexpression also further increased the sensitivity of SNU-387 cells to HCN inhibition (Fig. 3.11D).

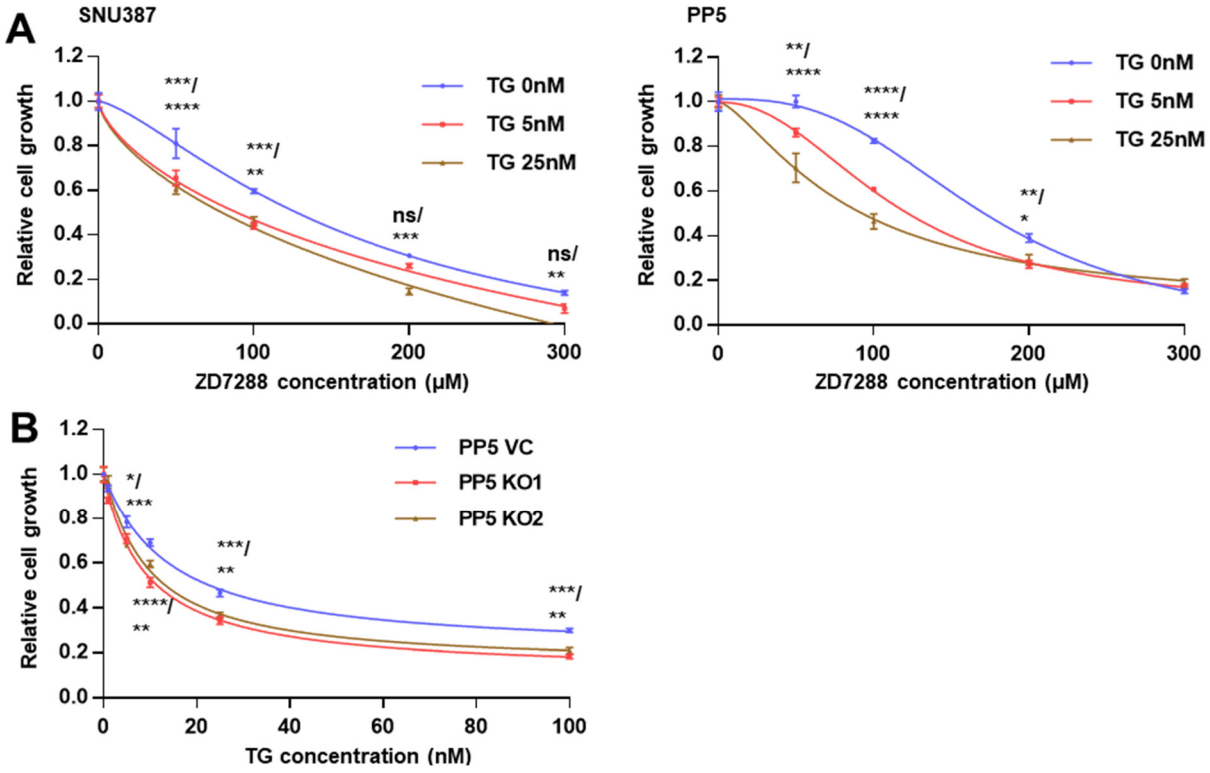

Figure 3.12 HCN3 and ER stress in HCC cell lines. (A) Effect of ER stressor thapsigargin treatment on the sensitivity of SNU-387 (left) and PLC/PRF/5 (right) HCC

Figure 3.12 (cont'd)
cells to the growth inhibition induced by HCN inhibition. Two-way ANOVA Sidak's multiple comparisons test. (B) Effect of *HCN3* knockout on the sensitivity of PLC/PRF/5 HCC cells to the growth inhibition induced by ER stressor thapsigargin. Two-way ANOVA Sidak's multiple comparisons test. Representative data of 3 repeats. ****p<0.0001, ***p<0.001, **p<0.01, *p<0.05. Data represent mean ± SEM.

HCN3 was previously reported to affect the cell cycle and apoptosis by inhibiting ER stress in breast cancer cells[352]. To assess the similar impact of HCN3 on HCC cells, we treated the HCC cells with ER-stress inducer thapsigargin (TG) in combination with ZD7288. In ER-stressed conditions, the sensitivity to ZD7288 was significantly increased in both cell lines (Fig. 3.12A). HCN3 knockout in PLC/PRF/5 cells also sensitized the cell to ER-stress-induced cell growth suppression (Fig. 3.12B).

Together, these results indicated that HCN3 promotes cell proliferation and protects against ER stress in HCC cells with a female preference *in vitro*.

4.4.6 HCN3 cooperates with MYC to promote the initiation and progression of HCC, and Hcn3 knockout preferentially hinders MYC/MCL1-induced HCC development in female mice

To examine the oncogenic role of HCN3 overexpression *in vivo*, we used the sleeping beauty transposon system and the hydrodynamic tail vein injection technique to achieve stable overexpression of genes, specifically in the hepatocyte of mice[359]. As *MYC* overexpression alone was shown to be insufficient to induce liver cancer in BALB/c genetic background[360], we chose to overexpress human *MYC* and *HCN3* simultaneously to induce oncogenesis. Injection of *MYC* and *HCN3* expressing vectors increased the incidence and volume of liver tumors compared to injection of the MYC expressing vector and the empty vector in female BALB/c mice (although not statistically significant) (Fig. 3.13A and 3.13B). Histology analysis revealed that all liver

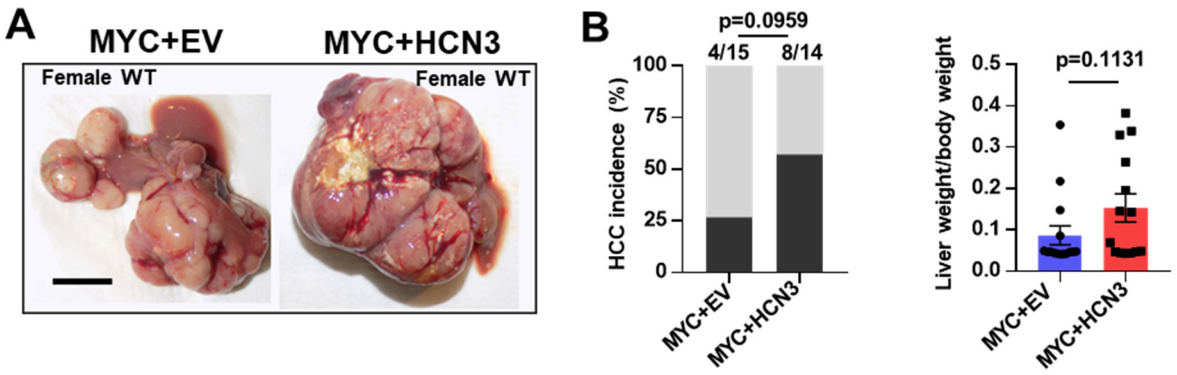

Figure 3.13 Formation of liver tumors induced by overexpression of *MYC* and *HCN3* in wild-type female mice. (A) Representative macroscopic photos of liver tumor formed in WT female mice injected with MYC expressing vector + empty vector (EV) (n=15) or MYC + HCN3 expressing vectors (n=14). Scale bar: 1 cm. (B) Liver tumor incidence and liver/body weight ratio of WT female mice injected with MYC + EV or MYC + HCN3 expressing vectors. Chi-squared test and two-tailed unpaired Student's t test. Data represent mean ± SEM.

tumors were moderately or poorly differentiated HCC. Remarkably, at least 50% of the tumors from female mice injected with *MYC* and *HCN3* expressing vectors were collision-type tumors consisting of moderately or poorly differentiated HCC and small-round undifferentiated cancer cells (Fig. 3.14A). Two out of eight HCC-bearing mice injected with *MYC* and *HCN3* expressing vectors had metastatic diseases, one of which had those small-round undifferentiated cells metastasized to the ovaries of both sides, and the other had metastasis in the pancreas (Fig. 3.14A and Fig. 3.14B). In contrast, liver tumors with *MYC* overexpression alone were all moderately differentiated HCC (Fig. 3.14A), and no collision tumor or metastasis was detected in those mice. In mice injected with *MYC* and *HCN3* expressing vectors, HCC and small round undifferentiated cells in the liver collision tumors and small round undifferentiated cells in the ovary expressed ectopic HCN3, Albumin, and AFP, indicating the cell origins of these collision tumors are possibly the hepatocyte or liver progenitor (Fig. 3.14A). These tumors also expressed more proliferation marker Ki-67 than liver HCCs from mice injected with *MYC*

expressing vector only (Fig. 3.14A).

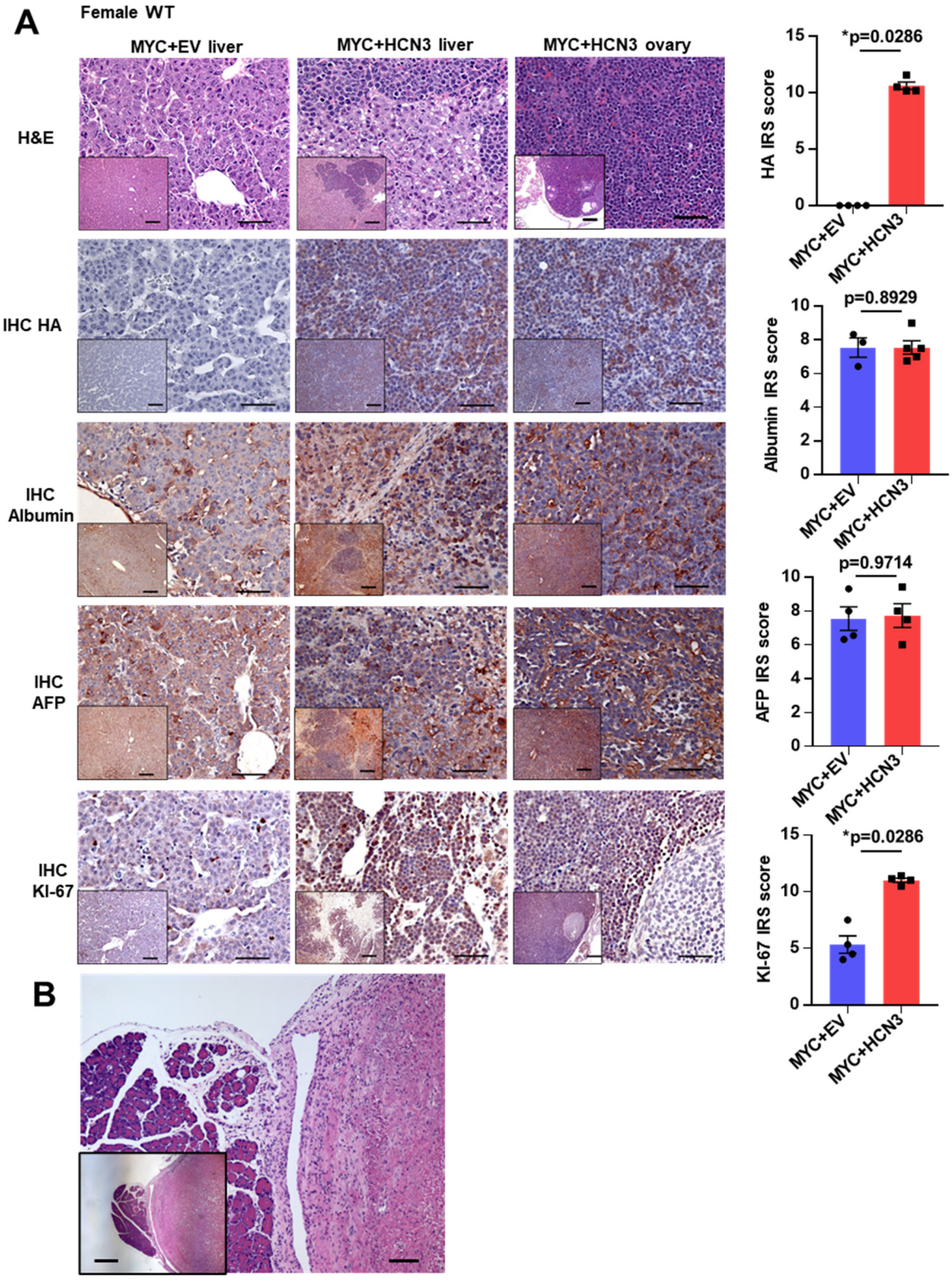

Figure 3.14 Histopathological features of liver tumors induced by overexpression

Figure 3.14 (cont'd)
of *MYC* and *HCN3* in wild-type female mice. (A) Left: Representative H & E staining, IHC for HA that tags HCN3, IHC for hepatocyte marker Albumin and AFP, and IHC for the proliferation marker Ki-67 in MYC-induced and MYC + HCN3-induced HCCs in female mice. Scale bar: 50 μm and 100 μm (insets). Right: IHC staining scores for antigens as indicated in female mice injected with MYC+EV or MYC+HCN3 (n=4 in each group except that for the albumin staining n=3 or 5). Mann-Whitney U test. Data represent mean ± SEM. *p<0.05. (B) H & E staining photos of a case of pancreas metastasis of HCC induced by overexpression of *MYC* and *HCN3* in a female wild-type mouse. Scale bar: 100 μm and 500 μm (insets).

Hydrodynamic injection of *MYC* and *MCL1* expressing vectors were reported to induce 100% penetrant multiple liver tumors in female FVB/N mice[138] and mice with different genetic backgrounds, including the BALB/c strain[360]. Consistently, I observed liver tumors with 100% penetrance and similar tumor volumes between male and female wild-type BALB/c mice injected with *MYC* and *MCL1* expressing vectors (Fig. 3.15). Hepatic *MYC* and *MCL1* overexpression in the same way resulted in 100% or

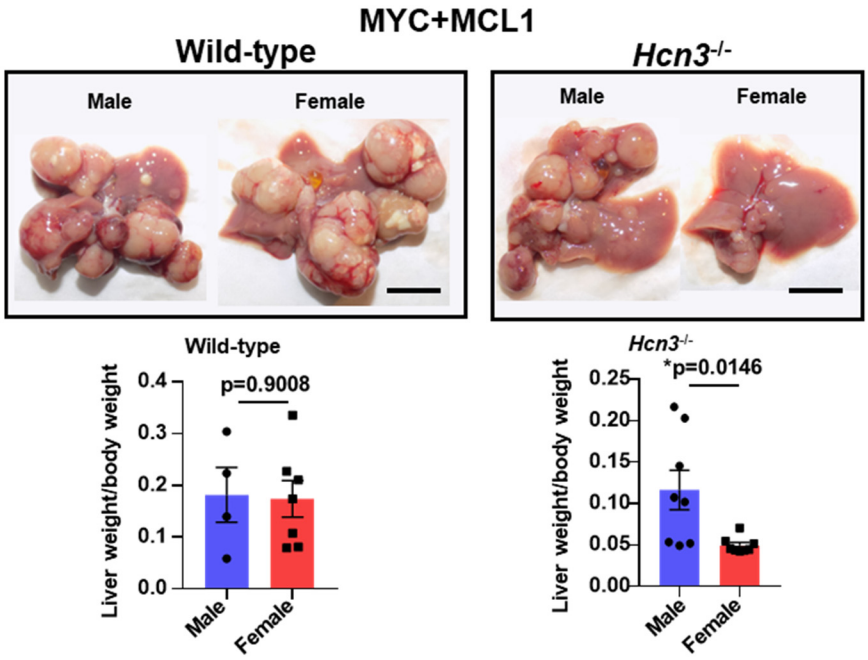

Figure 3.15 Formation of liver tumors induced by overexpression of *MYC* and *MCL1* in wild-type and *Hcn3*$^{-/-}$ male and female mice. Representative macroscopic photos and analysis of liver/body weight ratio of wild-type (left, n=4 or 7) or *Hcn3*$^{-/-}$ (right, n=8 per group) male and female mice injected with MYC + MCL1 vectors. Scale bar: 1 cm. Two-tailed unpaired Student's t test. Data represent mean ± SEM. *p<0.05.

75% liver tumor penetrance in male or female BALB/c *Hcn3*$^{-/-}$ mice[361], respectively. Importantly, liver tumor number and size were dramatically lower in *Hcn3*$^{-/-}$ female mice compared to *Hcn3*$^{-/-}$ male mice (Fig. 3.15). Collectively, these results suggest that HCN3 is a cancer driver that can cooperate with MYC to promote the initiation and progression of poorly differentiated HCC, and the lack of HCN3 preferentially hinders the hepatic tumorigenesis in female mice.

4.4.7 HCN3 is amplified and overexpressed in human HCC and correlated with poor survival, especially in female patients

To determine the clinical relevance of our findings on the upregulated cation transport pathways and HCN3 overexpression in the mice, I first used ssGSEA[284] to compare the enrichment of GO.bp pathways in HCC samples from male and female patients in the TCGA cohort[285]. Strikingly, 33 GO.bp pathways related to cation transport are significantly more enriched in HCC specimens from female patients than in male patients (Fig. 3.16).

Next, I examined the protein expression of HCN3 in primary HCC samples from male and female patients using IHC staining on a tissue microarray. HCN3 expression was significantly higher in female HCCs than in male HCCs (Fig. 3.17A). In the TCGA LIHC cohort, HCN3 mRNA expression was significantly upregulated in HCCs compared to adjacent noncancerous liver tissues (Fig. 3.17B). Its mRNA levels appeared to be higher in female HCC adjacent liver tissues compared to male tissues (Fig. 3.17C). Up to 24% of HCC samples (28% or 22% of female or male samples, respectively) had HCN3 alterations that were HCN3 gene amplification and mRNA overexpression (Fig.

Figure 3.16 Differentially enriched ion transport-related GO.bp pathways between HCCs from male and female patients of the TCGA cohort. ssGSEA enrichment score of GO.bp pathways in primary HCC samples from male (n=244) or female patients (n=117) from the TCGA cohort. Welch's t test with two-stage step-up FDR method. Pathways related to ion transport with $q<0.05$ were plotted. Data represent mean ± SEM.

3.17D). Interestingly, HCC samples with HCN3 alterations had significantly lower TIP30 mRNA levels compared to samples without HCN3 alterations (Fig. 3.17E). These alterations were mutually exclusive to *CTNNB1* mutation, amplification, or high expression in HCC (Fig. 3.17D and Table 2.1). In those HCC samples with *HCN3* alterations, female HCC samples appeared to have higher HCN3 mRNA levels than those from males (Fig. 3.17F).

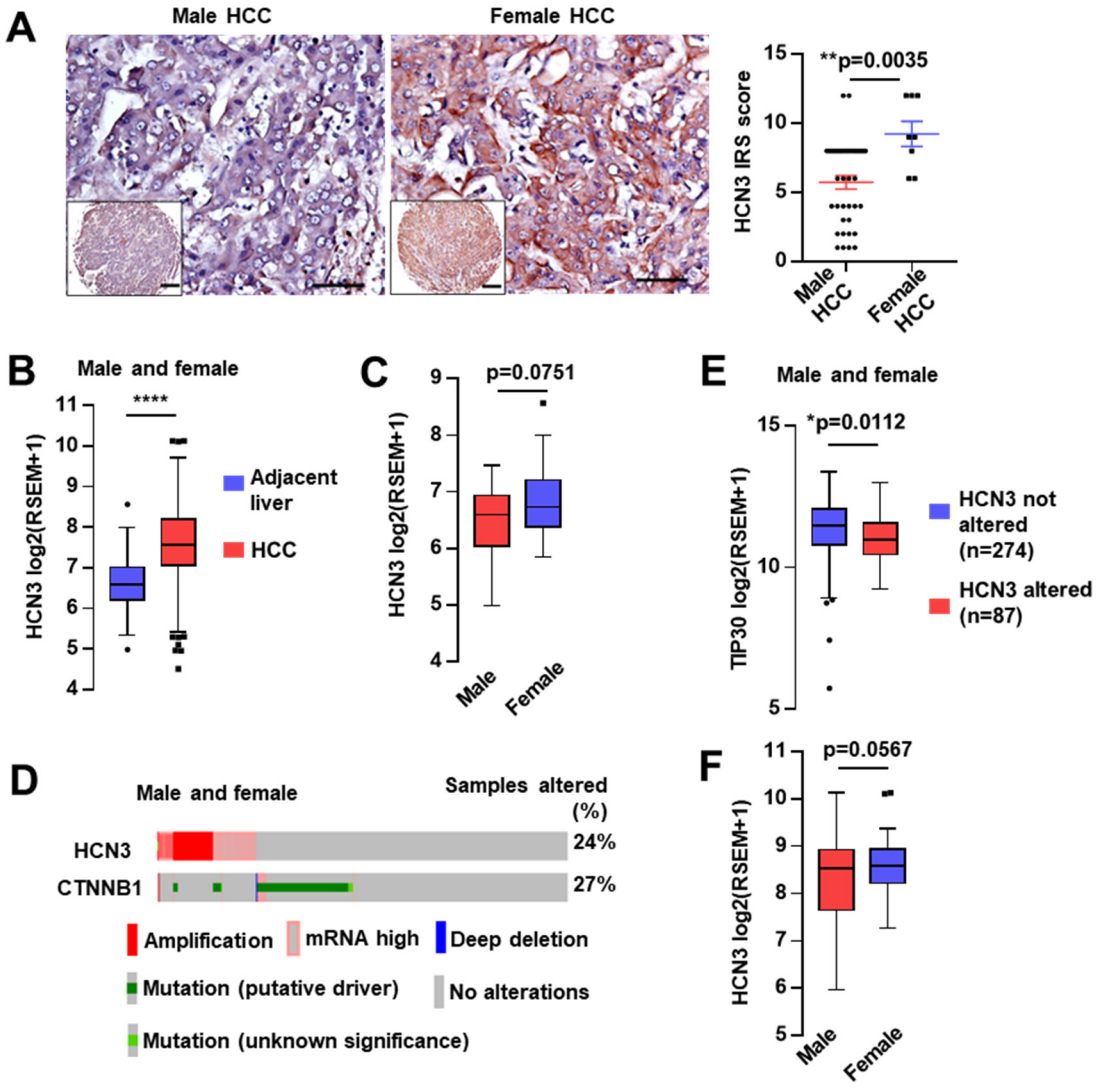

Figure 3.17 HCN3 expression and copy number variation in TCGA HCC patients. (A) Representative IHC staining photos and analysis of staining score of HCN3 in primary HCCs from male (n=38) and female (n=8) patients. HCN3 staining was scored according to the IRS system. Mann-Whitney U test. Data represent mean ± SEM. (B)

Figure 3.17 (cont'd)
mRNA expression of *HCN3* in adjacent non-tumor livers (n=49) and primary HCCs (n=361) from the TCGA cohort. Two-tailed unpaired Welch's t test. (C) mRNA expression of *HCN3* in non-tumor adjacent livers from the male (n=28) or female (n=22) primary HCC patients in the TCGA cohort. Two-tailed unpaired Welch's t test. (D) Genetic alterations and gene expression changes relative to diploid samples of *HCN3* and *CTNNB1* in primary HCC samples of TCGA cohorts. Samples with gene mRNA expression z score >3 or <-3 were recognized as having high or low expression. (E) mRNA expression of *TIP30* in primary HCC samples without (n=274) or with (n=87) HCN3 amplification and/or overexpression (regarded as HCN3 alterations) in the TCGA cohort. Two-tailed unpaired Welch's t test. (F) mRNA expression of *HCN3* in HCCs from the male (n=54) or female (n=33) patients with HCN3 alterations in the TCGA cohort. Two-tailed unpaired Welch's t test. Box plots were drawn using the Tukey method. ****p<0.0001, **p<0.01, *p<0.05.

Table 2.1 Test of mutual exclusivity and co-occurrence of HCN3 and CTNNB1 alteration events in HCC

Total	Number of samples with HCN3 or CTNNB1 alterations				Log2 Odds Ratio	p-Value
	Neither	Only HCN3	Only CTNNB1	Both		
361	188 (52.1%)	74 (20.5%)	86 (23.8%)	13 (3.6%)	-1.3807	0.0024

I then compared the transcriptome between HCCs with and without HCN3 alterations by assessing the enrichment of Hallmark pathways using GSEA[299]. Pathways of the G2M checkpoint, E2F targets, and mitotic spindle were highly enriched in HCC samples with HCN3 alterations, suggesting an increased cell proliferation in HCCs with HCN3 alterations, consistent with our *in vitro* and *in vivo* results (Fig. 3.18A). When comparing the enrichment of Hallmark pathways in HCC samples with and without HCN3 alterations using ssGSEA, I observed decreased inflammatory, ROS, and androgen response pathways in HCC specimens with HCN3 alterations, beside the same upregulated pathways as suggested by GSEA analysis (Fig. 3.18B). Patients with HCN3 alterations had higher AFP levels at procurement (Fig. 3.18C). Notably, female

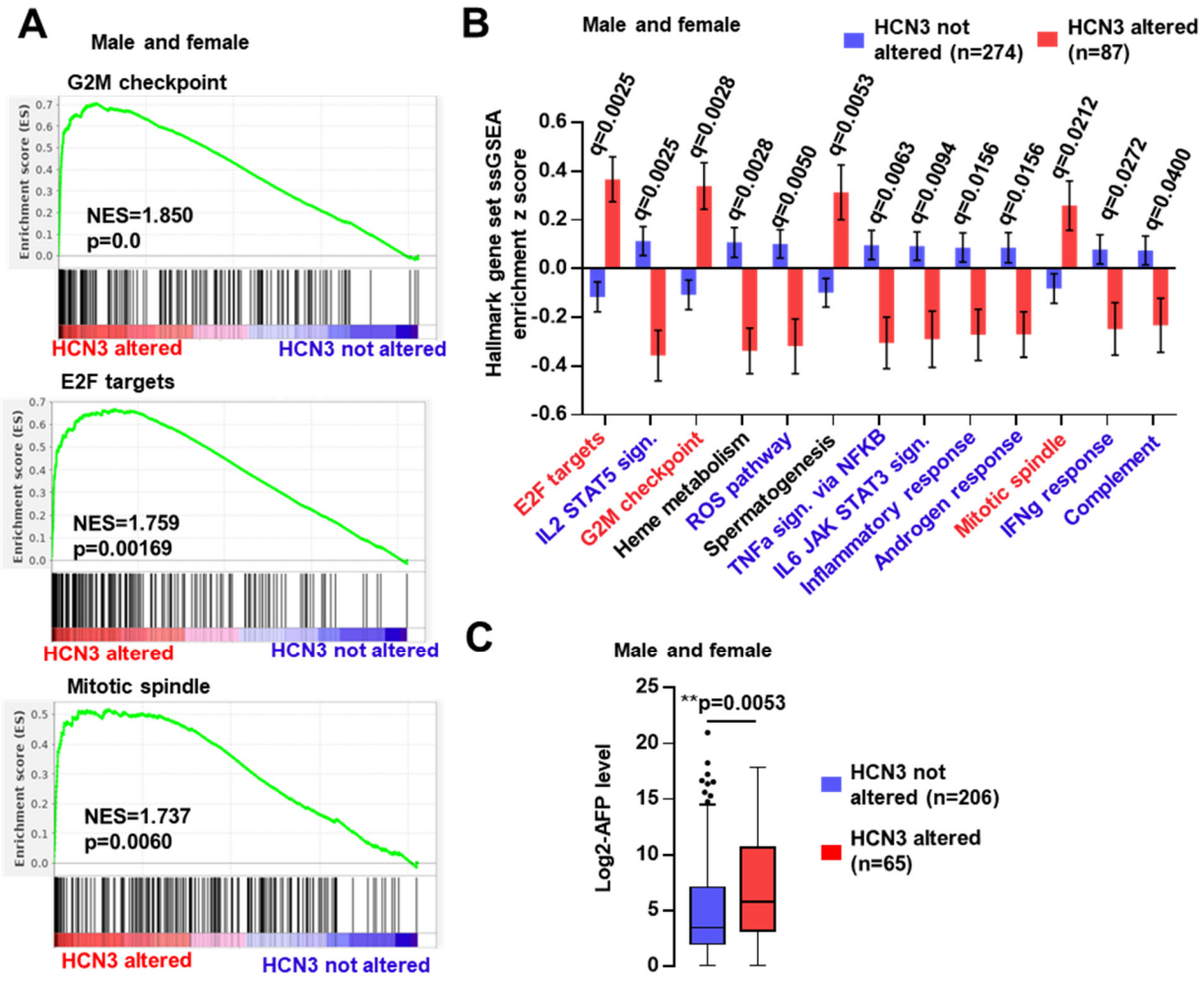

Figure 3.18 The relationship of HCN3 expression and copy number variation with hallmark pathway enrichment. (A) GSEA analysis results showing significantly differentially enriched hallmark pathways (FDR<0.1) between the transcriptome of HCCs with and without HCN3 alterations (n=87 or 274). Normalized enrichment score and p-value were shown. (B) ssGSEA enrichment score of hallmark pathways in primary HCC samples with or without HCN3 alterations (n=87 or 274). Welch's t test with two-stage step-up FDR method for 52 comparisons. Pathways with q<0.05 were recognized as significantly different and shown. (C) AFP levels at the procurement of primary HCC patients without (n=206) or with (n=65) HCN3 alterations in the TCGA cohort. Two-tailed unpaired Welch's t test. **p<0.01. Box plots were drawn using the Tukey method.

patients with HCN3 alterations had significantly poorer overall survival[362] and disease-free survival than those without HCN3 alterations. At the same time, such differences were insignificant in male patients (Table 2.2, Fig. 3.19A and 3.19B). Although the HCN3 alteration was associated with poorer HCC-specific survival and progression-free

survival in both sexes, the associations were more significant and had a higher predicted hazard ratio in female patients (Fig. 3.19C and 3.19D). Together, these results suggest that HCN3 amplification and overexpression predict a poorer prognosis for HCC patients with a female preference, and HCN3 is a potential therapeutic target for personalized anti-HCC therapy.

Table 2.2 Demographic data for each patient group

Category	Female			Male		
	HCN3 altered (n=33)	HCN3 not altered (n=84)	q value[a,b]	HCN3 altered (n=54)	HCN3 not altered (n=190)	q value[a,b]
Diagnosis age (Q3/median/Q1)	72/64/51	71/63/53	[a]0.9582	68/58/50	68/61/51	[a]0.2084
Patient height (Q3/median/Q1)	165/159/153	165/160.5/155	[a]0.9582	174/169/163	176/171/166	[a]0.1648
Patient weight (Q3/median/Q1)	78/62/51	78/63/55	[a]0.9582	77/68/58	89/73/62	[a]0.1221
Race (NA/American Indian or Alaska native/Asian/Black or African American/White)	0/0/9/0/24	3/0/25/3/53	[b]0.9582	2/0/36/3/13	5/2/86/11/86	[b]0.1221
Family History of Cancer (NA/YES/NO)	4/16/13	8/32/44	[b]0.9582	7/8/39	30/53/107	[b]0.1221
Prior Cancer Diagnosis Occurrence (YES/NO)	2/31	11/73	[b]0.9582	3/51	19/171	[b]0.5512
Neoadjuvant Therapy Type Administered Prior To Resection (YES/NO)	0/33	1/83	[b]0.9582	0/54	1/189	[b]0.5512
History hepatocarcinoma risk factor-Alcohol consumption (NA/YES/NO)	2/3/28	6/11/67	[b]0.9582	1/23/30	10/78/102	[b]0.9935
History hepatocarcinoma risk factor-Hepatitis B (NA/YES/NO)	2/6/25	6/13/65	[b]0.9582	1/25/28	10/59/121	[b]0.1515
History hepatocarcinoma risk factor-Hepatitis C (NA/YES/NO)	2/2/29	6/8/70	[b]0.9582	1/7/46	10/35/145	[b]0.4114
History hepatocarcinoma risk factor-NAFLD (NA/YES/NO)	2/2/29	6/5/73	[b]0.9582	1/0/53	10/13/167	[b]0.1729

[a]Mann-Whitney U test.
[b]Chi-squared test. "NA" subcategories were not included in statistical tests. In testing for each gender, if a subcategory has numbers 0 for both the HCN3 altered and not altered groups, the subcategory is removed. For 2x2 contingency tables with any number in cells <5, Chi-squared test with Yates' correction was performed.
[a,b]FDR method of Benjamini-Hochberg was used to correct for multiple comparisons.

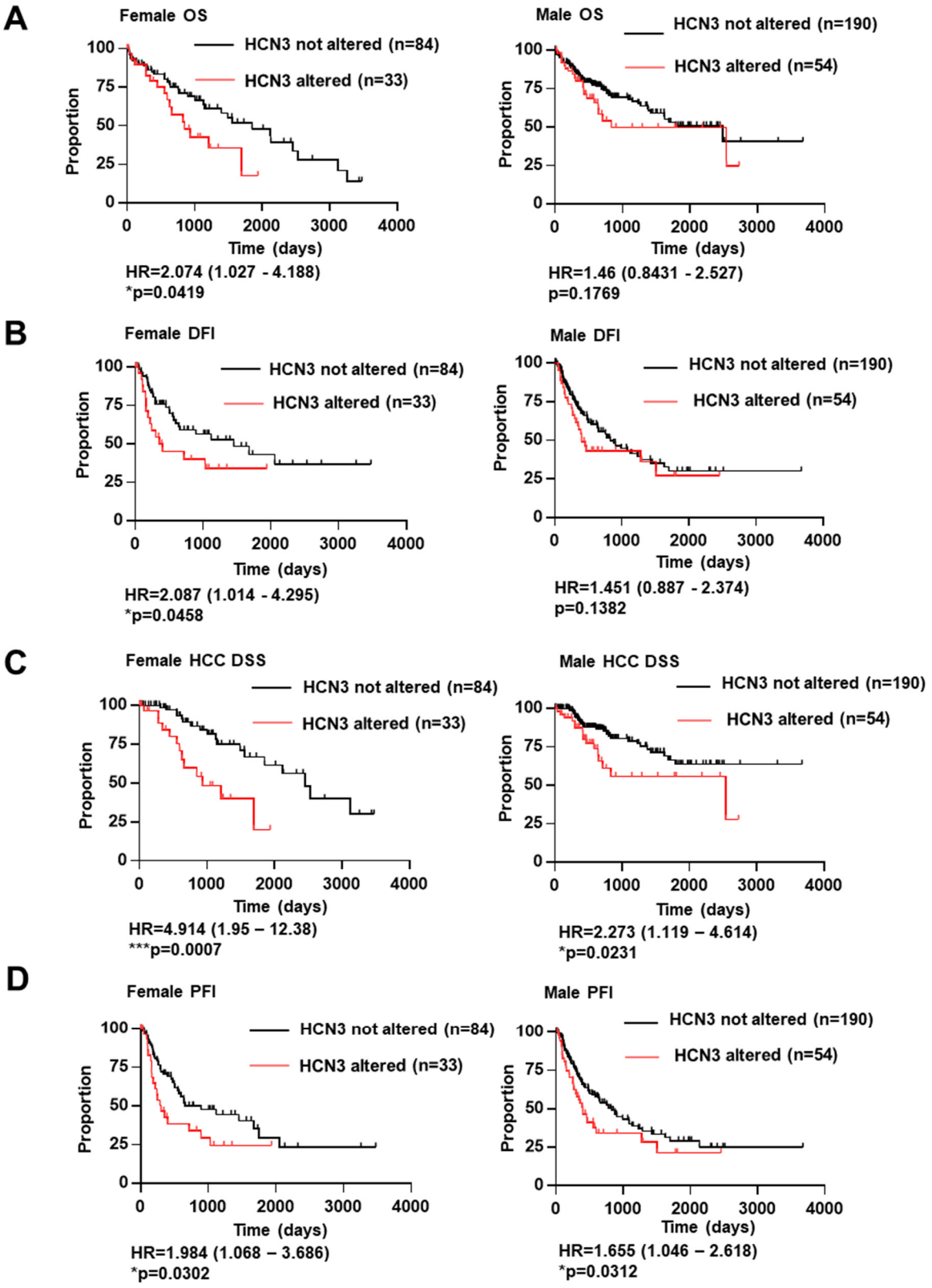

Figure 3.19 Survival curves for female and male HCC patients grouped by *HCN3* alteration status of their HCCs. Kaplan-Meier plots of overall survival (OS) (A),

Figure 3.19 (cont'd)
disease-free survival/interval (DFI) (B), HCC disease-specific survival (DSS) (C), and progression-free survival/interval (PFI) (D) of female (left) or male (right) patients with or without HCN3 alterations. TCGA survival data curated by a published article: DFI: the period from the date of diagnosis until the date of the first new tumor progression event subsequent to the determination of a patient's disease-free status after their initial diagnosis and treatment; HCC DSS: the period from the date of diagnosis until death from HCC; PFI: the period from the date of diagnosis until the date of the first occurrence of a new tumor event (NTE), which includes progression of the disease, locoregional recurrence, distant metastasis, new primary tumor, or death with tumor whether an NTE was reported or not. Log-rank test, HR calculated using the Mantel-Haenszel method. ***p<0.001, *p<0.05.

4.5 Discussion

In this study, we show for the first time that heterozygous deletion of *Tip30*, in the context of *Ncoa5* heterozygous deletion, preferentially promotes mouse HCC development in a female-biased manner. Unexpectedly, *Tip30* deletion did not cause further activation of proinflammatory and p53 pathways in the preneoplastic liver of *Ncoa5*$^{+/-}$ female mice, unlike what was observed in the preneoplastic liver of *Ncoa5*$^{+/-}$ male mice, suggesting that TIP30 does not inhibit proinflammatory and p53-p21 pathways. Instead, we found significant overexpression of HCN3 in the livers of dual-mutant female mice compared to single-mutant female mice. In agreement with the observations in mice, HCN3 amplification and overexpression in human HCC specimens, ~28% of which had a history of chronic HBV infection, are more frequent in female patients than male patients and are correlated with a poorer prognosis in female patients. HCN3 amplification/overexpression appears mutually exclusive with the *CTNNB1* mutation. Several interpretations could explain this mutually exclusive event, one of which is that HCN3 overexpression possibly leads to the same outcome as *CTNNB1* mutations. *CTNNB1* mutations are known to occur preferentially in male HCC

patients[363], especially those infected with HBV[364]. We propose that female HCC patients might preferentially overexpress HCN3 in hepatocytes to drive liver oncogenesis, given the higher HCN3 levels in female HCCs and HCC adjacent liver tissues (Fig. 3.17A, 3.17C, and 3.17F). In support of this possibility, we show that HCN3 expression could be enhanced by the female sex hormone Pg and its receptors. Moreover, HCN3 increases HCC cell proliferation *in vitro* and cooperates with MYC to promote the initiation and progression of HCC in female mice *in vivo*. Genetic knockout of *Hcn3* preferentially hinders HCC development induced by MYC and MCL1 in female mice. Collectively, our data establish TIP30 and NCOA5 as crucial tumor suppressors in suppressing hepatocarcinogenesis in females and suggest that HCN3 is a female-biased cancer driver for liver oncogenesis. However, it remains to be determined how TIP30 and NCOA5 regulate HCN3 expression controlled by Pg-activated progesterone receptors as well as estrogen and androgen signaling pathways.

Cancer cells are known to overexpress ion channels to drive malignant behavior. Notably, HCN ion channel family members, including HCN3, serving as nonselective voltage-gated cation channels in the plasma membranes of cells, have been implicated in controlling cell-cycle progression. Consistently, HCN3 blockage inhibits the proliferation and cell-cycle progression of stem cells[358,365]. HCN3 has been reported to be overexpressed in breast, renal, and colorectal cancers and associated with poor survival outcomes in breast and renal cancer patients[366]. HCN3 inhibition has been shown to suppress breast cancer cell proliferation and tumor growth in patient-derived breast cancer xenograft models, suggesting HCN3 is a new molecular target that could be developed into targeted therapy for breast cancer patients[352]. Mechanistically, HCN3

might regulate the cell cycle, ER stress, and apoptosis through various mechanisms, including cell volume regulation, membrane potential modulation, generation of driving for Ca^{2+}, and protein-protein interaction[352,356,357,367]. Our findings are in line with previous studies and suggest that HCN3 overexpression in HCC cells promotes cell proliferation via a similar mechanism, making it a potential therapeutic target for personalized anti-HCC therapy.

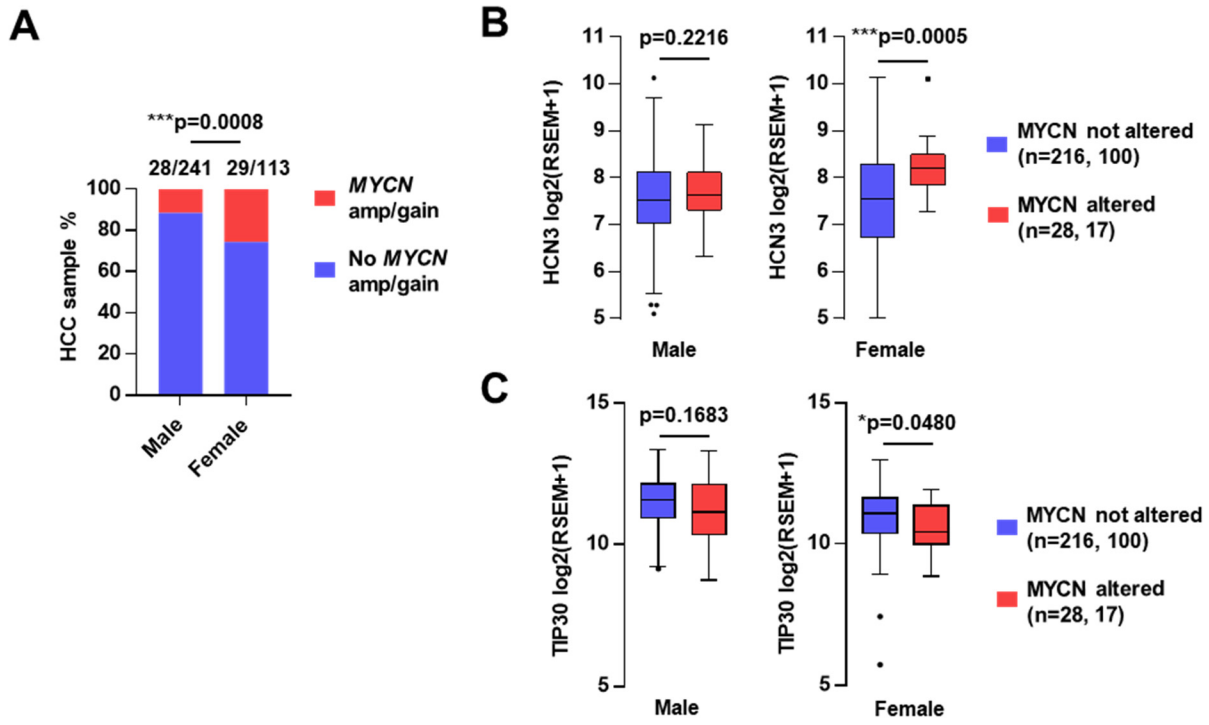

Figure 3.20 Incidence of increased *MYCN* copy number in HCC samples from male and female patients and the mRNA expression of *HCN3* and *TIP30* in HCCs from male and female patients of the TCGA cohort grouped by the *MYCN* alteration status of their HCCs. (A) Incidence of increased *MYCN* copy number in primary HCC samples from male and female patients in the TCGA cohort. The total sample numbers and samples with increased *MYCN* copy numbers were shown. Chi-squared test. (B) mRNA expression of *HCN3* in primary HCCs without or with *MYCN* alterations in male (left) or female (right) patients in the TCGA cohort. Samples with *MYCN* amplification and/or *MYCN* mRNA expression z score >0.5 or <-0.5 were recognized as *MYCN* altered. Two-tailed unpaired Welch's t-test. Box plot was drawn using the Tukey method. (C) mRNA expression of *TIP30* in primary HCCs without or with *MYCN* alterations in male (left) or female (right) patients in the TCGA cohort. Two-tailed unpaired Welch's t test. Box plots were drawn using the Tukey method. ***p<0.001, *p<0.05.

Table 2.3 Test of mutual exclusivity and co-occurrence of MYCN and HCN3 alteration events in male and female HCCs

Patient sex group	Total	Number of samples with MYCN or HCN3 alterations				Log2 Odds Ratio	p-Value
		Neither	Only MYCN	Only HCN3	Both		
Male	244	170 (69.7%)	20 (8.2%)	46 (18.9%)	8 (3.3%)	0.5639	0.4670
Female	117	76 (65.0%)	8 (6.8%)	24 (20.5%)	9 (7.7%)	1.8329	0.0205

In addition to HCN3, other genes dysregulated by NCOA5 and TIP30 deficiency in the female mouse livers might also contribute to the HCC development in *Ncoa5*$^{+/-}$ *Tip30*$^{+/-}$ female mice. One of these genes is *Mycn*, a member of the *myc* proto-oncogene family, which was overexpressed at the mRNA level in the livers of *Ncoa5*$^{+/-}$ *Tip30*$^{+/-}$ female mice. Analysis of the TCGA cohort of human HCC specimens revealed that *MYCN* amplification and gain occurred more frequently in female patients than male patients, with an incidence of 26% in females compared to 12% in males (Fig. 3.20A). Interestingly, *MYCN* amplification and overexpression co-occurred with *HCN3* amplification and overexpression in female patients but not male patients (Table 2.3). Moreover, the concurrence of *MYCN* alterations and *HCN3* overexpression was associated with a decreased *TIP30* mRNA in female patients but not in males (Fig. 3.20B and 3.20C). As *MYCN* is known to be an oncogene, its overexpression likely contributes significantly to female-biased HCC development. However, further experiments are necessary to determine the collaborative role of HCN3 and MYCN in promoting HCC development.

In conclusion, this study highlights that female hepatocarcinogenesis could be driven by a female-biased mechanism regulated by NCOA5 and TIP30 (Fig. 3.21). Our work also suggests the ion channel HCN3 as a female-biased HCC driver, providing a

possible personalized therapeutic target for treating female patients with HCC.

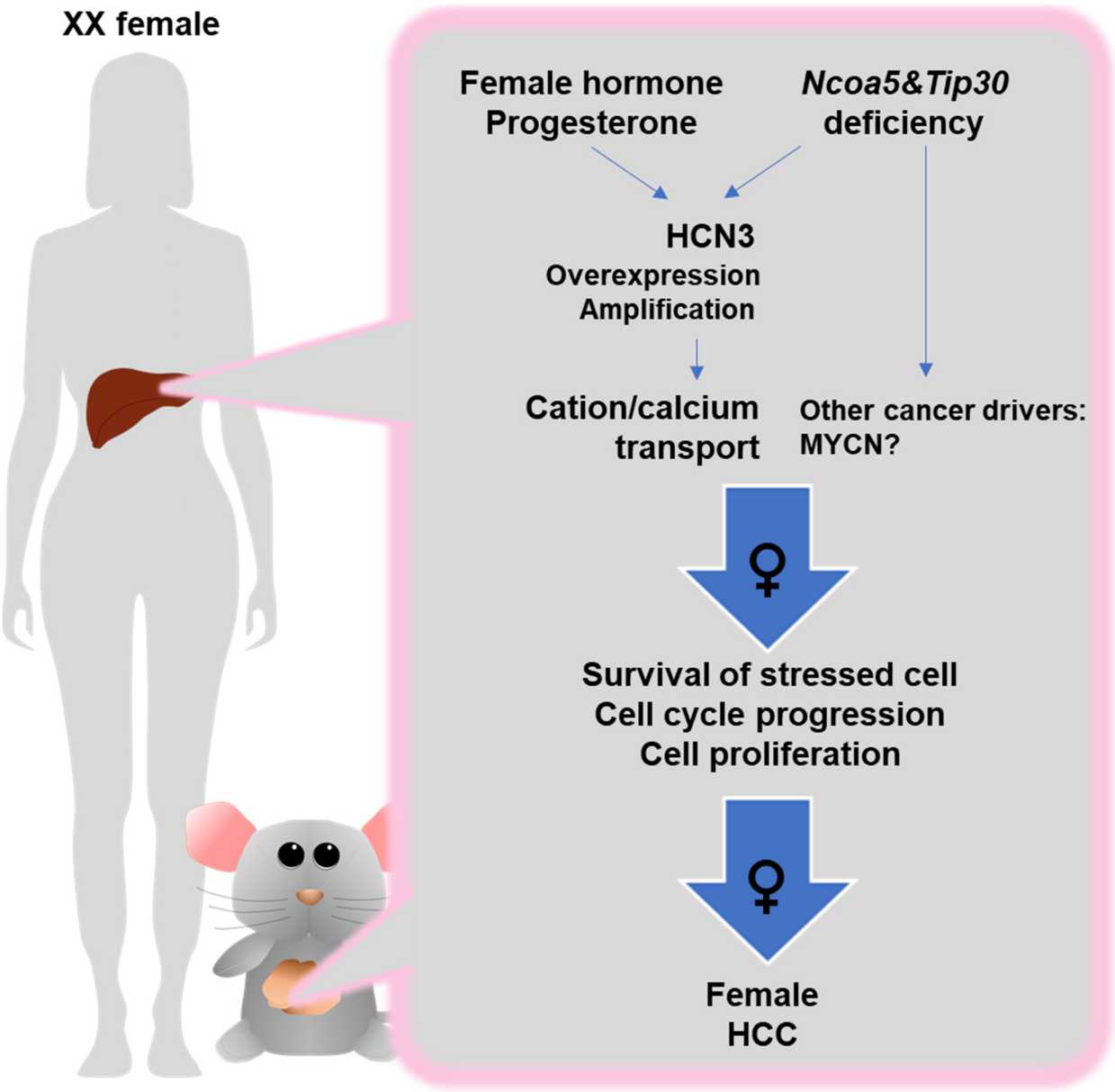

Figure 3.21 A graphical summary of the study.

4.6 Materials and methods

4.6.1 Mice

Generation of *Ncoa5* or *Tip30* deficient mice was described previously[187,208,227]. Double deficient BALB/c *Ncoa5*$^{+/-}$*Tip30*$^{+/-}$ mice and control *Ncoa5*$^{+/-}$, *Tip30*$^{+/-}$, and wild-

type mice were generated by crossing *Ncoa5*$^{+/-}$ female mice and *Tip30*$^{+/-}$ male mice because male *Ncoa5*$^{+/-}$ mice were infertile[187,189]. *Hcn3*$^{-/-}$ C57BL/6 mice provided by Dr. Martin Biel[361] were backcrossed for seven generations to the BALB/c genetic background. Wild-type BALB/c mice used in the hydrodynamic tail vein injection experiments were purchased from the Jackson Laboratory. BALB/c male and female mice were allocated to experimental groups randomly for hydrodynamic tail vein injection experiments or according to genotypes for spontaneous tumor development experiments. All mice were under a standard normal diet and 12 h light/12 h dark cycle at the Michigan State University animal facilities and housed in Optimice cages. All experimental procedures on mice were approved by the Michigan State University Institutional Animal Care and Use Committee and were performed in accordance with their regulatory standards.

4.6.2 Cell culture

Mouse fibroblast NIH/3T3 (derived from male), human kidney cell HEK293T (derived from female), and human liver cancer cell line PLC/PRF/5 (derived from male) and SNU-387 (derived from female) were purchased from ATCC. Cell lines were authenticated by STR profiling. SNU-387 cells were cultured using ATCC-formulated RPMI-1640 medium supplemented with 10% fetal bovine serum, 100 U/mL of penicillin, and 100 μg/mL of streptomycin at 37 °C in 5% CO_2. Other cell lines were cultured using DMEM high glucose medium (Thermo Fisher) supplemented with 10% FBS, 100 U/mL of penicillin, and 100 μg/mL of streptomycin. For hormone treatment experiments, cells were cultured and treated in phenol red-free DMEM (Thermo Fisher) supplemented with charcoal-stripped FBS (Biowest). Proteasome inhibition was induced by treatment of 10

μM of (R)-MG132 (Cayman Chemical) for 6 hours. Selective HCN blocker ZD7288 was purchased from Tocris. Thapsigargin was purchased from Millipore-Sigma. Cells were treated with ZD7288 in a complete medium for 3 days.

4.6.3 Transcriptomic analyses of human samples

Processed gene expression, copy number variation, mutation, and clinical data of the TCGA LIHC cohort were retrieved with UCSC Xena and cBioportal[331,362,368,369]. Differences in gene mRNA levels between TCGA patient subgroups were determined with the comparison functionality of cBioportal[331]. The protein-protein interaction network of gene products of interest was analyzed using STRING[370]. For pathway analyses, GSEA version 4.2.1 and ssGSEA v10 were used[285,299] and carried out on GenePattern.

4.6.4 Quantitative PCR and mouse transcriptome analyses

Total RNA was isolated using TRIzol (Thermo Fisher) according to the manufacturer's instructions. RNA for high throughput sequencing was isolated using a combined TRIzol and RNeasy Mini Kit (Qiagen) method according to the manufacturer's instructions. cDNA was generated using the SuperScript IV First-Strand Synthesis System (Thermo Fisher) according to the manufacturer's instructions. Quantitative real-time PCR was performed on a QuantStudio 3 Real-Time PCR machine using the PowerUp SYBR Green reagent (Thermo Fisher). PCR primer sequences are available in Table 2.4.

Isolated total RNA from mouse liver was first quality-controlled using a Nanodrop Spectrophotometer (Thermo Fisher) and the Bioanalyzer System (Agilent). Total RNA was then sent to Novogene, which carried out further RNA quality control, mRNA

selection, cDNA library preparation, sequencing with a NovaSeq 6000 (Illumina), raw data quality control, and raw data delivery. Raw data were then trimmed to remove low-quality adapter reads using Trimmomatic[371] and aligned to the Ensembl GRCm38 genome using STAR[330]. Count normalization and differential gene expression analysis were conducted using DESeq2[329]. Pathway analysis was analyzed using GAGE[283].

Table 2.4 Oligos used in the study

	Genes	Forward	Reverse
Mouse	Polr2a	GCGGTTGACCCCATGACGAGTGAT	GCCTGATGCGGGTGCTGAGTGAG
Mouse	Tip30	CTGGGACAGAACCTGTTTTCCA	AAAGTCCACCACTTCTTGATTC
Mouse	Tnf	GCCTATGTCTCAGCCTCTTCT	TTGAGATCCATGCCGTTGGCC
Mouse	Il6	TGATTGTATGAACAACGATGATGC	GGACTCTGGCTTTGTCTTTCTTGT
Mouse	Wnt5a	GTCCTTTGAGATGGGTGGTATC	ACCTCTGGGTTAGGGAGTGTCT
Mouse	Mycn	CCTCCGGAGAGGATACCTTG	TCTCTACGGTGACCACATCG
Mouse	Hcn3	GCAGCATTTGGTACAACACG	AGCGTCTAGCAGATCGAGC
Human	ACTB	TACGCCAACACAGTGCTGTCT	CTGATCCACATCTGCTGGAAG
Human	HCN3	GACACACGCCTCACCGATGG	GGGAACTCCTCAAGCACAGC

4.6.5 Histological and serological analyses

Neutrally buffered 10% formalin solution (Sigma-Aldrich) fixed mouse tissues were sent to the Investigative Histopathology Laboratory of Michigan State University and processed, embedded, sectioned, and H & E stained. Liver histological features were scored using the Modified Hepatic Activity Index system[350]. Mouse blood was freshly collected, and serum was separated by centrifugation. Serum α-fetoprotein levels were quantified using the mouse AFP Quantikine ELISA kit (R&D Systems) according to the manufacturer's instructions. Serum ALT activity was quantified using the Alanine Transaminase Colorimetric Activity Assay Kit (Cayman Chemical) according to the manufacturer's instructions. Liver tissue IL-6 levels were quantified using the

mouse IL-6 ELISA Kit (Proteintech). Absorbance was read by a FLUOstar OPTIMA microplate reader (BMG LABTECH).

4.6.6 Immunohistochemistry

Immunohistochemistry staining was performed using the VECTASTAIN ABC-HRP system (Vector Laboratories) according to the manufacturer's instructions. IHC staining intensity was scored using the IRS system[266]. The human HCC tissue array (LV1505a) was purchased from TissueArray.Com LLC, and the clinical information of patients included in the array is available on the supplier's website.

4.6.7 Lentiviral gene expression

The coding sequence of the human *HCN3* gene was amplified and HA-tagged from the plasmid HsCD00348243 (DF/HCC DNA Resource Core), which contains the consensus coding sequence of human *HCN3* (CCDS 1108.1). The sequence was then cloned into the pSin-EF2-Pur vector[372] (Addgene). Polyethyleneimine-mediated transfection of HCN3 or GFP expression plasmids with pCMV delta R8.2 packaging plasmid (Addgene) and pMD2.G envelope plasmid (Addgene) was performed on HEK293T cells, and lentivirus was collected after transfection. Cells stably overexpressing HCN3 or control protein were established by infecting cells with lentivirus and selected by puromycin.

4.6.8 Soft agar colony formation assay

Soft agar colony formation assay was performed as described[373]. Briefly, 6-well plates were plated with a bottom layer of 0.5% agar in DMEM medium and a top layer of 0.3% agar in DMEM medium containing 5000 cells/well. Cells were cultured for 21 days

while maintaining a layer of growth medium on top. Cells were finally stained with Nitrotetrazolium Blue chloride (Sigma-Aldrich), and photos were captured under a microscope. Colony number and size were analyzed using ImageJ.

4.6.9 CRISPR/Cas-mediated gene knockout

The CRISPR/Cas9 mediated HCN3 knockout was achieved using the pSpCas9(BB)-2A-Puro (PX459) V2.0 plasmid[325] obtained from Addgene, and the following guide sequences were used: target 1 (exon 6): CGGGACACACGCCTCACCGA; target 2 (exon 5): GAGCGAGCCGCTTCGCGAGG. The guide target sequences and PAMs were cloned into the PX459 vector according to a cloning protocol described on Addgene. Cells were transfected with vector control or targeting constructs using Lipofectamine 3000 (Thermo Fisher) according to the manufacturer's instructions and were then selected with 2 μg/mL puromycin. Selected cells were cultured in single clones, genomic DNA was extracted using QuickExtract (Lucigen), and gene knockout was validated by PCR, sanger sequencing, and western blotting.

4.6.10 Cell proliferation assay

1 or 1.5 x 10^3 cells were seeded in 96-well plates and cultured for 2 to 4 days in DMEM medium containing 10%, 2%, or 0.2% FBS. For HCN3 inhibition and thapsigargin treatment experiments, 1 or 2.5 x 10^3 cells in DMEM medium containing 10% FBS were seeded in 96-well plates and treated for 72 hours. CCK-8 (Dojindo) was used to determine the relative cell growth according to the manufacturer's instructions. Absorbance was read by a FLUOstar OPTIMA microplate reader (BMG LABTECH).

4.6.11 Western blotting

Protein was isolated from tissue and cell samples using RIPA buffer (Thermo Fisher) or Laemmli Sample Buffer (BIO-RAD). SDS-PAGE of processed protein samples was performed using BIORAD Mini-protein TGX gels. LICOR IRDye secondary antibodies were used for fluorescent detection, and photos were captured using the LICOR Odyssey Imaging system. Quantification was performed using LICOR Odyssey and Image Studio software.

4.6.12 Dual-luciferase reporter assay

Transcription factor binding site prediction was performed using PROMO[354,355]. The genomic DNA fraction from -742 to +752 bp relative to the HCN3 transcription start site containing the putative promoter region was amplified from MCF-7 genomic DNA. This fraction includes the SNP rs12749306, which has an ALFA allele frequency of 26.6%. The fraction was cloned into the pGL2-Basic vector (Promega) to get the pGL2-promoHCN3. Human TIP30 expression plasmid pcDNA3-TIP30 was previously described[224]. pcDNA3-hPRA and pcDNA3-hPRB expression plasmids were obtained from Addgene[374]. pRL (Promega) was used as the control reporter. Cells were transfected with pRL, pGL2-promoHCN3, and other expression plasmids using Lipofectamine 3000 (Thermo Fisher) according to the manufacturer's instructions. The treatment of cells started 24 hours after transfection, and cells were processed 48 hours after transfection and tested for luciferase activity using the Dual-Luciferase Reporter Assay System (Promega). The bioluminescence signal was read by a Veritas Microplate Luminometer (Turner Biosystems).

4.6.13 Hydrodynamic tail vein injection for stable gene expression in hepatocytes

pT3-EF1α-c-MYC, pT3-EF1α-MCL1, and pCMV/SB plasmids were kindly provided by Dr. Xin Chen[360]. The pT3-EF1α-c-MYC plasmid was manipulated to generate pT3-EF1α-HCN3 carrying the HA-tagged human HCN3 coding sequence and pT3-EF1α empty vector (EV). Different combinations of plasmids were injected into 7-week-old wild-type or *Hcn3*$^{-/-}$ male and female BALB/c mice according to the published method[360]. A total of 20 μg of pT3-EF1α-c-MYC, 20 μg of EV, and 1.6 μg of pCMV/SB (wild-type female BALB/c mice), or a total of 20 μg of pT3-EF1α-c-MYC, 20 μg of pT3-EF1α-HCN3, and 1.6 μg of pCMV/SB (wild-type female BALB/c mice), or a total of 10 μg of pT3-EF1α-c-MYC, 5 μg of pT3-EF1α-MCL1, and 0.6 μg of pCMV/SB (wild-type and *Hcn3*$^{-/-}$ male and female BALB/c) in 2 mL of 0.9% NaCl solution were injected to each mouse. Mice that received *MCL1* overexpression were monitored for liver tumor formation for 8 weeks, and mice that received other injections were monitored for 14 weeks or until morbid and then euthanized and necropsied.

4.6.14 Antibodies

Primary antibodies used in this study include anti: Mac-2 (Galectin-3, CL8942AP) by Cedarlane Labs; IL-6 (sc-1265), Na^+/K^+-ATPases (sc-48345), and β-Actin (sc-47778) by Santa Cruz Biotechnology; HCN3 (ab84818) by Abcam; HCN3 (APC-057) by Alomone Labs; HCN3 (MA3-902) by Thermo Fisher; HA-tag (#3724) and PR (#8757) by Cell Signaling Technology; AFP (14550-1-AP) and Albumin (16475-1-AP) by Proteintech; Ki-67 (AB9260) by Millipore-Sigma; NCOA5 (A300-790A) by Bethyl; TIP30 made by Xiao Lab which was described previously[208].

4.6.15 Quantification and statistical analyses

All data are shown as mean ± SEM if not specified otherwise. Statistical significance of differences was determined by one-way ANOVA Tukey's multiple comparisons test, two-way ANOVA Tukey's multiple comparisons test and Sidak's multiple comparisons test, two-tailed unpaired Student's t test, Welch's t test with the FDR methods, Pearson's correlation two-tailed significance test, Chi-squared test, Mann-Whitney U test, or log-rank test in GraphPad Prism 7 with details listed in the corresponding figure legends. ****p<0.0001, ***p<0.001, **p<0.01, *p<0.05, ns = not significant.

4.6.16 Deposited data

Raw and processed RNA-sequencing data were deposited in NCBI's Gene Expression Omnibus and are accessible through GEO Series accession number GSE228531.

BIBLIOGRAPHY

1. Ferlay, J., Colombet, M., Soerjomataram, I., Parkin, D.M., Pineros, M., Znaor, A., and Bray, F. (2021). Cancer statistics for the year 2020: An overview. Int J Cancer. 10.1002/ijc.33588.

2. Sung, H., Ferlay, J., Siegel, R.L., Laversanne, M., Soerjomataram, I., Jemal, A., and Bray, F. (2021). Global Cancer Statistics 2020: GLOBOCAN Estimates of Incidence and Mortality Worldwide for 36 Cancers in 185 Countries. CA Cancer J Clin *71*, 209-249. 10.3322/caac.21660.

3. Cronin, K.A., Scott, S., Firth, A.U., Sung, H., Henley, S.J., Sherman, R.L., Siegel, R.L., Anderson, R.N., Kohler, B.A., Benard, V.B., et al. (2022). Annual report to the nation on the status of cancer, part 1: National cancer statistics. Cancer *128*, 4251-4284. 10.1002/cncr.34479.

4. Llovet, J.M., Kelley, R.K., Villanueva, A., Singal, A.G., Pikarsky, E., Roayaie, S., Lencioni, R., Koike, K., Zucman-Rossi, J., and Finn, R.S. (2021). Hepatocellular carcinoma. Nat Rev Dis Primers *7*, 6. 10.1038/s41572-020-00240-3.

5. Llovet, J.M., Zucman-Rossi, J., Pikarsky, E., Sangro, B., Schwartz, M., Sherman, M., and Gores, G. (2016). Hepatocellular carcinoma. Nat Rev Dis Primers *2*, 16018. 10.1038/nrdp.2016.18.

6. Zucman-Rossi, J., Villanueva, A., Nault, J.C., and Llovet, J.M. (2015). Genetic Landscape and Biomarkers of Hepatocellular Carcinoma. Gastroenterology *149*, 1226-1239 e1224. 10.1053/j.gastro.2015.05.061.

7. Rebouissou, S., and Nault, J.C. (2020). Advances in molecular classification and precision oncology in hepatocellular carcinoma. J Hepatol *72*, 215-229. 10.1016/j.jhep.2019.08.017.

8. Singh, S., Allen, A.M., Wang, Z., Prokop, L.J., Murad, M.H., and Loomba, R. (2015). Fibrosis progression in nonalcoholic fatty liver vs nonalcoholic steatohepatitis: a systematic review and meta-analysis of paired-biopsy studies. Clin Gastroenterol Hepatol *13*, 643-654 e641-649; quiz e639-640. 10.1016/j.cgh.2014.04.014.

9. Younossi, Z.M., Koenig, A.B., Abdelatif, D., Fazel, Y., Henry, L., and Wymer, M. (2016). Global epidemiology of nonalcoholic fatty liver disease-Meta-analytic assessment of prevalence, incidence, and outcomes. Hepatology *64*, 73-84. 10.1002/hep.28431.

10. Campigotto, M., Giuffre, M., Colombo, A., Visintin, A., Aversano, A., Budel, M., Masutti, F., Abazia, C., and Croce, L.S. (2020). Comparison between hepatocellular carcinoma prognostic scores: A 10-year single-center experience and brief review of the current literature. World J Hepatol *12*, 1239-1257. 10.4254/wjh.v12.i12.1239.

11. Mittal, S., El-Serag, H.B., Sada, Y.H., Kanwal, F., Duan, Z., Temple, S., May, S.B., Kramer, J.R., Richardson, P.A., and Davila, J.A. (2016). Hepatocellular Carcinoma in the Absence of Cirrhosis in United States Veterans is Associated With Nonalcoholic Fatty Liver Disease. Clin Gastroenterol Hepatol *14*, 124-131 e121. 10.1016/j.cgh.2015.07.019.

12. Estes, C., Razavi, H., Loomba, R., Younossi, Z., and Sanyal, A.J. (2018). Modeling the epidemic of nonalcoholic fatty liver disease demonstrates an exponential increase in burden of disease. Hepatology *67*, 123-133. 10.1002/hep.29466.

13. Henley, S.J., Ward, E.M., Scott, S., Ma, J., Anderson, R.N., Firth, A.U., Thomas, C.C., Islami, F., Weir, H.K., Lewis, D.R., et al. (2020). Annual report to the nation on the status of cancer, part I: National cancer statistics. Cancer *126*, 2225-2249. 10.1002/cncr.32802.

14. Brar, G., Greten, T.F., Graubard, B.I., McNeel, T.S., Petrick, J.L., McGlynn, K.A., and Altekruse, S.F. (2020). Hepatocellular Carcinoma Survival by Etiology: A SEER-Medicare Database Analysis. Hepatol Commun *4*, 1541-1551. 10.1002/hep4.1564.

15. El-Serag, H.B. (2011). Hepatocellular carcinoma. N Engl J Med *365*, 1118-1127. 10.1056/NEJMra1001683.

16. Ma, W.L., Hsu, C.L., Wu, M.H., Wu, C.T., Wu, C.C., Lai, J.J., Jou, Y.S., Chen, C.W., Yeh, S., and Chang, C. (2008). Androgen receptor is a new potential therapeutic target for the treatment of hepatocellular carcinoma. Gastroenterology *135*, 947-955, 955 e941-945. 10.1053/j.gastro.2008.05.046.

17. Li, Y., Xu, A., Jia, S., and Huang, J. (2019). Recent advances in the molecular mechanism of sex disparity in hepatocellular carcinoma. Oncol Lett *17*, 4222-4228. 10.3892/ol.2019.10127.

18. Zhang, Y., Wang, H., and Xiao, H. (2021). Metformin Actions on the Liver: Protection Mechanisms Emerging in Hepatocytes and Immune Cells against NASH-Related HCC. Int J Mol Sci *22*. 10.3390/ijms22095016.

19. Buzzetti, E., Pinzani, M., and Tsochatzis, E.A. (2016). The multiple-hit pathogenesis of non-alcoholic fatty liver disease (NAFLD). Metabolism *65*, 1038-1048. 10.1016/j.metabol.2015.12.012.

20. Masarone, M., Rosato, V., Aglitti, A., Bucci, T., Caruso, R., Salvatore, T., Sasso, F.C., Tripodi, M.F., and Persico, M. (2017). Liver biopsy in type 2 diabetes mellitus: Steatohepatitis represents the sole feature of liver damage. PLoS One *12*, e0178473. 10.1371/journal.pone.0178473.

21. Feingold, K.R. (2018). Obesity and Dyslipidemia. In Endotext, K.R. Feingold, B. Anawalt, A. Boyce, G. Chrousos, W.W. de Herder, K. Dhatariya, K. Dungan, A. Grossman, J.M. Hershman, J. Hofland, et al., eds.

22. Samuel, V.T., and Shulman, G.I. (2018). Nonalcoholic Fatty Liver Disease as a Nexus of Metabolic and Hepatic Diseases. Cell Metab *27*, 22-41. 10.1016/j.cmet.2017.08.002.

23. Chaurasia, B., and Summers, S.A. (2015). Ceramides - Lipotoxic Inducers of Metabolic Disorders. Trends Endocrinol Metab *26*, 538-550. 10.1016/j.tem.2015.07.006.

24. Friedman, S.L., Neuschwander-Tetri, B.A., Rinella, M., and Sanyal, A.J. (2018). Mechanisms of NAFLD development and therapeutic strategies. Nat Med *24*, 908-922. 10.1038/s41591-018-0104-9.

25. Ferre, P., and Foufelle, F. (2010). Hepatic steatosis: a role for de novo lipogenesis and the transcription factor SREBP-1c. Diabetes Obes Metab *12 Suppl 2*, 83-92. 10.1111/j.1463-1326.2010.01275.x.

26. Mendez-Sanchez, N., Cruz-Ramon, V.C., Ramirez-Perez, O.L., Hwang, J.P., Barranco-Fragoso, B., and Cordova-Gallardo, J. (2018). New Aspects of Lipotoxicity in Nonalcoholic Steatohepatitis. Int J Mol Sci *19*. 10.3390/ijms19072034.

27. Mouzaki, M., Wang, A.Y., Bandsma, R., Comelli, E.M., Arendt, B.M., Zhang, L., Fung, S., Fischer, S.E., McGilvray, I.G., and Allard, J.P. (2016). Bile Acids and Dysbiosis in Non-Alcoholic Fatty Liver Disease. PLoS One *11*, e0151829. 10.1371/journal.pone.0151829.

28. Yerushalmi, B., Dahl, R., Devereaux, M.W., Gumpricht, E., and Sokol, R.J. (2001). Bile acid-induced rat hepatocyte apoptosis is inhibited by antioxidants and blockers of the mitochondrial permeability transition. Hepatology *33*, 616-626. 10.1053/jhep.2001.22702.

29. Liu, B., Zhang, Z., Hu, Y., Lu, Y., Li, D., Liu, J., Liao, S., Hu, M., Wang, Y., Zhang, D., et al. (2019). Sustained ER stress promotes hyperglycemia by increasing glucagon action through the deubiquitinating enzyme USP14. Proc Natl Acad Sci U S A *116*, 21732-21738. 10.1073/pnas.1907288116.

30. Morgantini, C., Jager, J., Li, X., Levi, L., Azzimato, V., Sulen, A., Barreby, E., Xu, C., Tencerova, M., Naslund, E., et al. (2019). Liver macrophages regulate systemic metabolism through non-inflammatory factors. Nat Metab *1*, 445-459. 10.1038/s42255-019-0044-9.

31. Azzimato, V., Jager, J., Chen, P., Morgantini, C., Levi, L., Barreby, E., Sulen, A., Oses, C., Willerbrords, J., Xu, C., et al. (2020). Liver macrophages inhibit the

endogenous antioxidant response in obesity-associated insulin resistance. Sci Transl Med *12*. 10.1126/scitranslmed.aaw9709.

32. Frasca, F., Pandini, G., Scalia, P., Sciacca, L., Mineo, R., Costantino, A., Goldfine, I.D., Belfiore, A., and Vigneri, R. (1999). Insulin receptor isoform A, a newly recognized, high-affinity insulin-like growth factor II receptor in fetal and cancer cells. Mol Cell Biol *19*, 3278-3288. 10.1128/mcb.19.5.3278.

33. Belfiore, A., Malaguarnera, R., Vella, V., Lawrence, M.C., Sciacca, L., Frasca, F., Morrione, A., and Vigneri, R. (2017). Insulin Receptor Isoforms in Physiology and Disease: An Updated View. Endocr Rev *38*, 379-431. 10.1210/er.2017-00073.

34. Leung, K.C., Doyle, N., Ballesteros, M., Waters, M.J., and Ho, K.K. (2000). Insulin regulation of human hepatic growth hormone receptors: divergent effects on biosynthesis and surface translocation. J Clin Endocrinol Metab *85*, 4712-4720. 10.1210/jcem.85.12.7017.

35. Calle, E.E., and Kaaks, R. (2004). Overweight, obesity and cancer: epidemiological evidence and proposed mechanisms. Nat Rev Cancer *4*, 579-591. 10.1038/nrc1408.

36. Li, X., Wang, X., and Gao, P. (2017). Diabetes Mellitus and Risk of Hepatocellular Carcinoma. Biomed Res Int *2017*, 5202684. 10.1155/2017/5202684.

37. White, D.L., Kanwal, F., and El-Serag, H.B. (2012). Association between nonalcoholic fatty liver disease and risk for hepatocellular cancer, based on systematic review. Clin Gastroenterol Hepatol *10*, 1342-1359 e1342. 10.1016/j.cgh.2012.10.001.

38. Saitta, C., Pollicino, T., and Raimondo, G. (2019). Obesity and liver cancer. Ann Hepatol *18*, 810-815. 10.1016/j.aohep.2019.07.004.

39. El-Serag, H.B., Hampel, H., and Javadi, F. (2006). The association between diabetes and hepatocellular carcinoma: a systematic review of epidemiologic evidence. Clin Gastroenterol Hepatol *4*, 369-380. 10.1016/j.cgh.2005.12.007.

40. Tanaka, S., Miyanishi, K., Kobune, M., Kawano, Y., Hoki, T., Kubo, T., Hayashi, T., Sato, T., Sato, Y., Takimoto, R., and Kato, J. (2013). Increased hepatic oxidative DNA damage in patients with nonalcoholic steatohepatitis who develop hepatocellular carcinoma. J Gastroenterol *48*, 1249-1258. 10.1007/s00535-012-0739-0.

41. Raghunath, A., Sundarraj, K., Arfuso, F., Sethi, G., and Perumal, E. (2018). Dysregulation of Nrf2 in Hepatocellular Carcinoma: Role in Cancer Progression and Chemoresistance. Cancers (Basel) *10*. 10.3390/cancers10120481.

42. Kouroumalis, E., Voumvouraki, A., Augoustaki, A., and Samonakis, D.N. (2021). Autophagy in liver diseases. World J Hepatol *13*, 6-65. 10.4254/wjh.v13.i1.6.

43. Schults, M.A., Nagle, P.W., Rensen, S.S., Godschalk, R.W., Munnia, A., Peluso, M., Claessen, S.M., Greve, J.W., Driessen, A., Verdam, F.J., et al. (2012). Decreased nucleotide excision repair in steatotic livers associates with myeloperoxidase-immunoreactivity. Mutat Res *736*, 75-81. 10.1016/j.mrfmmm.2011.11.001.

44. Cornell, L., Munck, J.M., Alsinet, C., Villanueva, A., Ogle, L., Willoughby, C.E., Televantou, D., Thomas, H.D., Jackson, J., Burt, A.D., et al. (2015). DNA-PK-A candidate driver of hepatocarcinogenesis and tissue biomarker that predicts response to treatment and survival. Clin Cancer Res *21*, 925-933. 10.1158/1078-0432.CCR-14-0842.

45. Wu, X., Dong, Z., Wang, C.J., Barlow, L.J., Fako, V., Serrano, M.A., Zou, Y., Liu, J.Y., and Zhang, J.T. (2016). FASN regulates cellular response to genotoxic treatments by increasing PARP-1 expression and DNA repair activity via NF-kappaB and SP1. Proc Natl Acad Sci U S A *113*, E6965-E6973. 10.1073/pnas.1609934113.

46. Remmerie, A., Martens, L., and Scott, C.L. (2020). Macrophage Subsets in Obesity, Aligning the Liver and Adipose Tissue. Front Endocrinol (Lausanne) *11*, 259. 10.3389/fendo.2020.00259.

47. McGettigan, B., McMahan, R., Orlicky, D., Burchill, M., Danhorn, T., Francis, P., Cheng, L.L., Golden-Mason, L., Jakubzick, C.V., and Rosen, H.R. (2019). Dietary Lipids Differentially Shape Nonalcoholic Steatohepatitis Progression and the Transcriptome of Kupffer Cells and Infiltrating Macrophages. Hepatology *70*, 67-83. 10.1002/hep.30401.

48. Cai, D., Yuan, M., Frantz, D.F., Melendez, P.A., Hansen, L., Lee, J., and Shoelson, S.E. (2005). Local and systemic insulin resistance resulting from hepatic activation of IKK-beta and NF-kappaB. Nat Med *11*, 183-190. 10.1038/nm1166.

49. Ambade, A., Satishchandran, A., Saha, B., Gyongyosi, B., Lowe, P., Kodys, K., Catalano, D., and Szabo, G. (2016). Hepatocellular carcinoma is accelerated by NASH involving M2 macrophage polarization mediated by hif-1alphainduced IL-10. Oncoimmunology *5*, e1221557. 10.1080/2162402X.2016.1221557.

50. Tsunashima, H., Tsuneyama, K., Moritoki, Y., Hara, M., and Kikuchi, K. (2015). Accumulated myeloid-derived suppressor cells demonstrate distinct phenotypes and functions in two non-alcoholic steatohepatitis mouse models. Hepatobiliary Surg Nutr *4*, 313-319. 10.3978/j.issn.2304-3881.2015.04.08.

51. Gabrilovich, D.I., and Nagaraj, S. (2009). Myeloid-derived suppressor cells as regulators of the immune system. Nat Rev Immunol *9*, 162-174. 10.1038/nri2506.

52. Lu, L.C., Chang, C.J., and Hsu, C.H. (2019). Targeting myeloid-derived suppressor cells in the treatment of hepatocellular carcinoma: current state and future perspectives. J Hepatocell Carcinoma *6*, 71-84. 10.2147/JHC.S159693.

53. Lacotte, S., Slits, F., Orci, L.A., Meyer, J., Oldani, G., Delaune, V., Gonelle-Gispert, C., Morel, P., and Toso, C. (2016). Impact of myeloid-derived suppressor cell on Kupffer cells from mouse livers with hepatocellular carcinoma. Oncoimmunology *5*, e1234565. 10.1080/2162402X.2016.1234565.

54. Zhou, J., Liu, M., Sun, H., Feng, Y., Xu, L., Chan, A.W.H., Tong, J.H., Wong, J., Chong, C.C.N., Lai, P.B.S., et al. (2018). Hepatoma-intrinsic CCRK inhibition diminishes myeloid-derived suppressor cell immunosuppression and enhances immune-checkpoint blockade efficacy. Gut *67*, 931-944. 10.1136/gutjnl-2017-314032.

55. Wolf, M.J., Adili, A., Piotrowitz, K., Abdullah, Z., Boege, Y., Stemmer, K., Ringelhan, M., Simonavicius, N., Egger, M., Wohlleber, D., et al. (2014). Metabolic activation of intrahepatic CD8+ T cells and NKT cells causes nonalcoholic steatohepatitis and liver cancer via cross-talk with hepatocytes. Cancer Cell *26*, 549-564. 10.1016/j.ccell.2014.09.003.

56. Van Herck, M.A., Weyler, J., Kwanten, W.J., Dirinck, E.L., De Winter, B.Y., Francque, S.M., and Vonghia, L. (2019). The Differential Roles of T Cells in Non-alcoholic Fatty Liver Disease and Obesity. Front Immunol *10*, 82. 10.3389/fimmu.2019.00082.

57. Ye, Y., Xie, X., Yu, J., Zhou, L., Xie, H., Jiang, G., Yu, X., Zhang, W., Wu, J., and Zheng, S. (2010). Involvement of Th17 and Th1 effector responses in patients with Hepatitis B. J Clin Immunol *30*, 546-555. 10.1007/s10875-010-9416-3.

58. Tang, Y., Bian, Z., Zhao, L., Liu, Y., Liang, S., Wang, Q., Han, X., Peng, Y., Chen, X., Shen, L., et al. (2011). Interleukin-17 exacerbates hepatic steatosis and inflammation in non-alcoholic fatty liver disease. Clin Exp Immunol *166*, 281-290. 10.1111/j.1365-2249.2011.04471.x.

59. Ma, C., Kesarwala, A.H., Eggert, T., Medina-Echeverz, J., Kleiner, D.E., Jin, P., Stroncek, D.F., Terabe, M., Kapoor, V., ElGindi, M., et al. (2016). NAFLD causes selective CD4(+) T lymphocyte loss and promotes hepatocarcinogenesis. Nature *531*, 253-257. 10.1038/nature16969.

60. Ma, X., Hua, J., Mohamood, A.R., Hamad, A.R., Ravi, R., and Li, Z. (2007). A high-fat diet and regulatory T cells influence susceptibility to endotoxin-induced liver injury. Hepatology *46*, 1519-1529. 10.1002/hep.21823.

61. Lan, Y.T., Fan, X.P., Fan, Y.C., Zhao, J., and Wang, K. (2017). Change in the Treg/Th17 cell imbalance in hepatocellular carcinoma patients and its clinical value. Medicine (Baltimore) *96*, e7704. 10.1097/MD.0000000000007704.

62. Yang, X.H., Yamagiwa, S., Ichida, T., Matsuda, Y., Sugahara, S., Watanabe, H., Sato, Y., Abo, T., Horwitz, D.A., and Aoyagi, Y. (2006). Increase of CD4+ CD25+ regulatory T-cells in the liver of patients with hepatocellular carcinoma. J Hepatol *45*, 254-262. 10.1016/j.jhep.2006.01.036.

63. Hwang, S., Yun, H., Moon, S., Cho, Y.E., and Gao, B. (2021). Role of Neutrophils in the Pathogenesis of Nonalcoholic Steatohepatitis. Front Endocrinol (Lausanne) *12*, 751802. 10.3389/fendo.2021.751802.

64. van der Windt, D.J., Sud, V., Zhang, H., Varley, P.R., Goswami, J., Yazdani, H.O., Tohme, S., Loughran, P., O'Doherty, R.M., Minervini, M.I., et al. (2018). Neutrophil extracellular traps promote inflammation and development of hepatocellular carcinoma in nonalcoholic steatohepatitis. Hepatology *68*, 1347-1360. 10.1002/hep.29914.

65. Wang, H., Zhang, H., Wang, Y., Brown, Z.J., Xia, Y., Huang, Z., Shen, C., Hu, Z., Beane, J., Ansa-Addo, E.A., et al. (2021). Regulatory T-cell and neutrophil extracellular trap interaction contributes to carcinogenesis in non-alcoholic steatohepatitis. J Hepatol *75*, 1271-1283. 10.1016/j.jhep.2021.07.032.

66. Mikulak, J., Bruni, E., Oriolo, F., Di Vito, C., and Mavilio, D. (2019). Hepatic Natural Killer Cells: Organ-Specific Sentinels of Liver Immune Homeostasis and Physiopathology. Front Immunol *10*, 946. 10.3389/fimmu.2019.00946.

67. Tosello-Trampont, A., Surette, F.A., Ewald, S.E., and Hahn, Y.S. (2017). Immunoregulatory Role of NK Cells in Tissue Inflammation and Regeneration. Front Immunol *8*, 301. 10.3389/fimmu.2017.00301.

68. Cepero-Donates, Y., Lacraz, G., Ghobadi, F., Rakotoarivelo, V., Orkhis, S., Mayhue, M., Chen, Y.G., Rola-Pleszczynski, M., Menendez, A., Ilangumaran, S., and Ramanathan, S. (2016). Interleukin-15-mediated inflammation promotes non-alcoholic fatty liver disease. Cytokine *82*, 102-111. 10.1016/j.cyto.2016.01.020.

69. Gomez-Santos, L., Luka, Z., Wagner, C., Fernandez-Alvarez, S., Lu, S.C., Mato, J.M., Martinez-Chantar, M.L., and Beraza, N. (2012). Inhibition of natural killer cells protects the liver against acute injury in the absence of glycine N-methyltransferase. Hepatology *56*, 747-759. 10.1002/hep.25694.

70. Tosello-Trampont, A.C., Krueger, P., Narayanan, S., Landes, S.G., Leitinger, N., and Hahn, Y.S. (2016). NKp46(+) natural killer cells attenuate metabolism-induced hepatic fibrosis by regulating macrophage activation in mice. Hepatology *63*, 799-812. 10.1002/hep.28389.

71. Stiglund, N., Strand, K., Cornillet, M., Stal, P., Thorell, A., Zimmer, C.L., Naslund, E., Karlgren, S., Nilsson, H., Mellgren, G., et al. (2019). Retained NK Cell Phenotype and Functionality in Non-alcoholic Fatty Liver Disease. Front Immunol *10*, 1255. 10.3389/fimmu.2019.01255.

72. Sun, C., Sun, H., Zhang, C., and Tian, Z. (2015). NK cell receptor imbalance and NK cell dysfunction in HBV infection and hepatocellular carcinoma. Cell Mol Immunol *12*, 292-302. 10.1038/cmi.2014.91.

73. Hoechst, B., Voigtlaender, T., Ormandy, L., Gamrekelashvili, J., Zhao, F., Wedemeyer, H., Lehner, F., Manns, M.P., Greten, T.F., and Korangy, F. (2009). Myeloid derived suppressor cells inhibit natural killer cells in patients with hepatocellular carcinoma via the NKp30 receptor. Hepatology *50*, 799-807. 10.1002/hep.23054.

74. Tan, S., Xu, Y., Wang, Z., Wang, T., Du, X., Song, X., Guo, X., Peng, J., Zhang, J., Liang, Y., et al. (2020). Tim-3 Hampers Tumor Surveillance of Liver-Resident and Conventional NK Cells by Disrupting PI3K Signaling. Cancer Res *80*, 1130-1142. 10.1158/0008-5472.CAN-19-2332.

75. Bi, J., and Tian, Z. (2017). NK Cell Exhaustion. Front Immunol *8*, 760. 10.3389/fimmu.2017.00760.

76. Nishina, S., Yamauchi, A., Kawaguchi, T., Kaku, K., Goto, M., Sasaki, K., Hara, Y., Tomiyama, Y., Kuribayashi, F., Torimura, T., and Hino, K. (2019). Dipeptidyl Peptidase 4 Inhibitors Reduce Hepatocellular Carcinoma by Activating Lymphocyte Chemotaxis in Mice. Cell Mol Gastroenterol Hepatol *7*, 115-134. 10.1016/j.jcmgh.2018.08.008.

77. Kurien, B.T., and Scofield, R.H. (2008). Autoimmunity and oxidatively modified autoantigens. Autoimmun Rev *7*, 567-573. 10.1016/j.autrev.2008.04.019.

78. DeFuria, J., Belkina, A.C., Jagannathan-Bogdan, M., Snyder-Cappione, J., Carr, J.D., Nersesova, Y.R., Markham, D., Strissel, K.J., Watkins, A.A., Zhu, M., et al. (2013). B cells promote inflammation in obesity and type 2 diabetes through regulation of T-cell function and an inflammatory cytokine profile. Proc Natl Acad Sci U S A *110*, 5133-5138. 10.1073/pnas.1215840110.

79. Davis, B.K., Wen, H., and Ting, J.P. (2011). The inflammasome NLRs in immunity, inflammation, and associated diseases. Annu Rev Immunol *29*, 707-735. 10.1146/annurev-immunol-031210-101405.

80. McPherson, S., Henderson, E., Burt, A.D., Day, C.P., and Anstee, Q.M. (2014). Serum immunoglobulin levels predict fibrosis in patients with non-alcoholic fatty liver disease. J Hepatol *60*, 1055-1062. 10.1016/j.jhep.2014.01.010.

81. Brunner, S.M., Itzel, T., Rubner, C., Kesselring, R., Griesshammer, E., Evert, M., Teufel, A., Schlitt, H.J., and Fichtner-Feigl, S. (2017). Tumor-infiltrating B cells producing antitumor active immunoglobulins in resected HCC prolong patient survival. Oncotarget *8*, 71002-71011. 10.18632/oncotarget.20238.

82. Zhang, Z., Ma, L., Goswami, S., Ma, J., Zheng, B., Duan, M., Liu, L., Zhang, L., Shi, J., Dong, L., et al. (2019). Landscape of infiltrating B cells and their clinical

significance in human hepatocellular carcinoma. Oncoimmunology *8*, e1571388. 10.1080/2162402X.2019.1571388.

83. Xiao, X., Lao, X.M., Chen, M.M., Liu, R.X., Wei, Y., Ouyang, F.Z., Chen, D.P., Zhao, X.Y., Zhao, Q., Li, X.F., et al. (2016). PD-1hi Identifies a Novel Regulatory B-cell Population in Human Hepatoma That Promotes Disease Progression. Cancer Discov *6*, 546-559. 10.1158/2159-8290.CD-15-1408.

84. Ouyang, F.Z., Wu, R.Q., Wei, Y., Liu, R.X., Yang, D., Xiao, X., Zheng, L., Li, B., Lao, X.M., and Kuang, D.M. (2016). Dendritic cell-elicited B-cell activation fosters immune privilege via IL-10 signals in hepatocellular carcinoma. Nat Commun *7*, 13453. 10.1038/ncomms13453.

85. Shalapour, S., Lin, X.J., Bastian, I.N., Brain, J., Burt, A.D., Aksenov, A.A., Vrbanac, A.F., Li, W., Perkins, A., Matsutani, T., et al. (2017). Inflammation-induced IgA+ cells dismantle anti-liver cancer immunity. Nature *551*, 340-345. 10.1038/nature24302.

86. Koo, S.Y., Park, E.J., and Lee, C.W. (2020). Immunological distinctions between nonalcoholic steatohepatitis and hepatocellular carcinoma. Exp Mol Med *52*, 1209-1219. 10.1038/s12276-020-0480-3.

87. Kanwal, F., Kramer, J.R., Mapakshi, S., Natarajan, Y., Chayanupatkul, M., Richardson, P.A., Li, L., Desiderio, R., Thrift, A.P., Asch, S.M., et al. (2018). Risk of Hepatocellular Cancer in Patients With Non-Alcoholic Fatty Liver Disease. Gastroenterology *155*, 1828-1837 e1822. 10.1053/j.gastro.2018.08.024.

88. El-Serag, H.B., and Rudolph, K.L. (2007). Hepatocellular carcinoma: epidemiology and molecular carcinogenesis. Gastroenterology *132*, 2557-2576. 10.1053/j.gastro.2007.04.061.

89. Pinyopornpanish, K., Khoudari, G., Saleh, M.A., Angkurawaranon, C., Pinyopornpanish, K., Mansoor, E., Dasarathy, S., and McCullough, A. (2021). Hepatocellular carcinoma in nonalcoholic fatty liver disease with or without cirrhosis: a population-based study. BMC Gastroenterol *21*, 394. 10.1186/s12876-021-01978-0.

90. Garrido, A., and Djouder, N. (2021). Cirrhosis: A Questioned Risk Factor for Hepatocellular Carcinoma. Trends Cancer *7*, 29-36. 10.1016/j.trecan.2020.08.005.

91. Ozdemir, B.C., Pentcheva-Hoang, T., Carstens, J.L., Zheng, X., Wu, C.C., Simpson, T.R., Laklai, H., Sugimoto, H., Kahlert, C., Novitskiy, S.V., et al. (2014). Depletion of carcinoma-associated fibroblasts and fibrosis induces immunosuppression and accelerates pancreas cancer with reduced survival. Cancer Cell *25*, 719-734. 10.1016/j.ccr.2014.04.005.

92. Rhim, A.D., Oberstein, P.E., Thomas, D.H., Mirek, E.T., Palermo, C.F., Sastra, S.A., Dekleva, E.N., Saunders, T., Becerra, C.P., Tattersall, I.W., et al. (2014). Stromal elements act to restrain, rather than support, pancreatic ductal adenocarcinoma. Cancer Cell *25*, 735-747. 10.1016/j.ccr.2014.04.021.

93. Natri, H.M., Wilson, M.A., and Buetow, K.H. (2019). Distinct molecular etiologies of male and female hepatocellular carcinoma. BMC Cancer *19*, 951. 10.1186/s12885-019-6167-2.

94. Li, C.H., Haider, S., Shiah, Y.J., Thai, K., and Boutros, P.C. (2018). Sex Differences in Cancer Driver Genes and Biomarkers. Cancer Res *78*, 5527-5537. 10.1158/0008-5472.CAN-18-0362.

95. Jackson, S.S., Marks, M.A., Katki, H.A., Cook, M.B., Hyun, N., Freedman, N.D., Kahle, L.L., Castle, P.E., Graubard, B.I., and Chaturvedi, A.K. (2022). Sex disparities in the incidence of 21 cancer types: Quantification of the contribution of risk factors. Cancer *128*, 3531-3540. 10.1002/cncr.34390.

96. Liu, P., Xie, S.H., Hu, S., Cheng, X., Gao, T., Zhang, C., and Song, Z. (2017). Age-specific sex difference in the incidence of hepatocellular carcinoma in the United States. Oncotarget *8*, 68131-68137. 10.18632/oncotarget.19245.

97. Osborne, C.K., and Schiff, R. (2005). Estrogen-receptor biology: continuing progress and therapeutic implications. J Clin Oncol *23*, 1616-1622. 10.1200/JCO.2005.10.036.

98. Naugler, W.E., Sakurai, T., Kim, S., Maeda, S., Kim, K., Elsharkawy, A.M., and Karin, M. (2007). Gender disparity in liver cancer due to sex differences in MyD88-dependent IL-6 production. Science *317*, 121-124. 10.1126/science.1140485.

99. Galien, R., and Garcia, T. (1997). Estrogen receptor impairs interleukin-6 expression by preventing protein binding on the NF-kappaB site. Nucleic Acids Res *25*, 2424-2429. 10.1093/nar/25.12.2424.

100. Ray, P., Ghosh, S.K., Zhang, D.H., and Ray, A. (1997). Repression of interleukin-6 gene expression by 17 beta-estradiol: inhibition of the DNA-binding activity of the transcription factors NF-IL6 and NF-kappa B by the estrogen receptor. FEBS Lett *409*, 79-85. 10.1016/s0014-5793(97)00487-0.

101. Liu, H., Liu, K., and Bodenner, D.L. (2005). Estrogen receptor inhibits interleukin-6 gene expression by disruption of nuclear factor kappaB transactivation. Cytokine *31*, 251-257. 10.1016/j.cyto.2004.12.008.

102. Cvoro, A., Tatomer, D., Tee, M.K., Zogovic, T., Harris, H.A., and Leitman, D.C. (2008). Selective estrogen receptor-beta agonists repress transcription of proinflammatory genes. J Immunol *180*, 630-636. 10.4049/jimmunol.180.1.630.

103. Hou, J., Xu, J., Jiang, R., Wang, Y., Chen, C., Deng, L., Huang, X., Wang, X., and Sun, B. (2013). Estrogen-sensitive PTPRO expression represses hepatocellular carcinoma progression by control of STAT3. Hepatology *57*, 678-688. 10.1002/hep.25980.

104. Zhu, L., Brown, W.C., Cai, Q., Krust, A., Chambon, P., McGuinness, O.P., and Stafford, J.M. (2013). Estrogen treatment after ovariectomy protects against fatty liver and may improve pathway-selective insulin resistance. Diabetes *62*, 424-434. 10.2337/db11-1718.

105. Palmisano, B.T., Zhu, L., and Stafford, J.M. (2017). Role of Estrogens in the Regulation of Liver Lipid Metabolism. Adv Exp Med Biol *1043*, 227-256. 10.1007/978-3-319-70178-3_12.

106. Bryzgalova, G., Gao, H., Ahren, B., Zierath, J.R., Galuska, D., Steiler, T.L., Dahlman-Wright, K., Nilsson, S., Gustafsson, J.A., Efendic, S., and Khan, A. (2006). Evidence that oestrogen receptor-alpha plays an important role in the regulation of glucose homeostasis in mice: insulin sensitivity in the liver. Diabetologia *49*, 588-597. 10.1007/s00125-005-0105-3.

107. Della Torre, S., Mitro, N., Fontana, R., Gomaraschi, M., Favari, E., Recordati, C., Lolli, F., Quagliarini, F., Meda, C., Ohlsson, C., et al. (2016). An Essential Role for Liver ERalpha in Coupling Hepatic Metabolism to the Reproductive Cycle. Cell Rep *15*, 360-371. 10.1016/j.celrep.2016.03.019.

108. Gao, H., Falt, S., Sandelin, A., Gustafsson, J.A., and Dahlman-Wright, K. (2008). Genome-wide identification of estrogen receptor alpha-binding sites in mouse liver. Mol Endocrinol *22*, 10-22. 10.1210/me.2007-0121.

109. Palmisano, B.T., Le, T.D., Zhu, L., Lee, Y.K., and Stafford, J.M. (2016). Cholesteryl ester transfer protein alters liver and plasma triglyceride metabolism through two liver networks in female mice. J Lipid Res *57*, 1541-1551. 10.1194/jlr.M069013.

110. Zhang, Z.C., Liu, Y., Xiao, L.L., Li, S.F., Jiang, J.H., Zhao, Y., Qian, S.W., Tang, Q.Q., and Li, X. (2015). Upregulation of miR-125b by estrogen protects against non-alcoholic fatty liver in female mice. J Hepatol *63*, 1466-1475. 10.1016/j.jhep.2015.07.037.

111. Wang, X., Lu, Y., Wang, E., Zhang, Z., Xiong, X., Zhang, H., Lu, J., Zheng, S., Yang, J., Xia, X., et al. (2015). Hepatic estrogen receptor alpha improves hepatosteatosis through upregulation of small heterodimer partner. J Hepatol *63*, 183-190. 10.1016/j.jhep.2015.02.029.

112. Pedram, A., Razandi, M., O'Mahony, F., Harvey, H., Harvey, B.J., and Levin, E.R. (2013). Estrogen reduces lipid content in the liver exclusively from membrane receptor signaling. Sci Signal *6*, ra36. 10.1126/scisignal.2004013.

113. Camporez, J.P., Jornayvaz, F.R., Lee, H.Y., Kanda, S., Guigni, B.A., Kahn, M., Samuel, V.T., Carvalho, C.R., Petersen, K.F., Jurczak, M.J., and Shulman, G.I. (2013). Cellular mechanism by which estradiol protects female ovariectomized mice from high-fat diet-induced hepatic and muscle insulin resistance. Endocrinology *154*, 1021-1028. 10.1210/en.2012-1989.

114. Ribas, V., Nguyen, M.T., Henstridge, D.C., Nguyen, A.K., Beaven, S.W., Watt, M.J., and Hevener, A.L. (2010). Impaired oxidative metabolism and inflammation are associated with insulin resistance in ERalpha-deficient mice. Am J Physiol Endocrinol Metab *298*, E304-319. 10.1152/ajpendo.00504.2009.

115. Wang, H.H., Afdhal, N.H., and Wang, D.Q. (2004). Estrogen receptor alpha, but not beta, plays a major role in 17beta-estradiol-induced murine cholesterol gallstones. Gastroenterology *127*, 239-249. 10.1053/j.gastro.2004.03.059.

116. Poynard, T., Lebray, P., Ingiliz, P., Varaut, A., Varsat, B., Ngo, Y., Norha, P., Munteanu, M., Drane, F., Messous, D., et al. (2010). Prevalence of liver fibrosis and risk factors in a general population using non-invasive biomarkers (FibroTest). BMC Gastroenterol *10*, 40. 10.1186/1471-230X-10-40.

117. Nah, E.H., Cho, S., Kim, S., Chu, J., Kwon, E., and Cho, H.I. (2021). Prevalence of liver fibrosis and associated risk factors in the Korean general population: a retrospective cross-sectional study. BMJ Open *11*, e046529. 10.1136/bmjopen-2020-046529.

118. Man, S., Deng, Y., Ma, Y., Fu, J., Bao, H., Yu, C., Lv, J., Liu, H., Wang, B., and Li, L. (2023). Prevalence of Liver Steatosis and Fibrosis in the General Population and Various High-Risk Populations: A Nationwide Study With 5.7 Million Adults in China. Gastroenterology *165*, 1025-1040. 10.1053/j.gastro.2023.05.053.

119. Shimizu, I., Mizobuchi, Y., Yasuda, M., Shiba, M., Ma, Y.R., Horie, T., Liu, F., and Ito, S. (1999). Inhibitory effect of oestradiol on activation of rat hepatic stellate cells in vivo and in vitro. Gut *44*, 127-136. 10.1136/gut.44.1.127.

120. Liu, Q.H., Li, D.G., Huang, X., Zong, C.H., Xu, Q.F., and Lu, H.M. (2004). Suppressive effects of 17beta-estradiol on hepatic fibrosis in CCl4-induced rat model. World J Gastroenterol *10*, 1315-1320. 10.3748/wjg.v10.i9.1315.

121. Zhang, B., Zhang, C.G., Ji, L.H., Zhao, G., and Wu, Z.Y. (2018). Estrogen receptor beta selective agonist ameliorates liver cirrhosis in rats by inhibiting the activation and proliferation of hepatic stellate cells. J Gastroenterol Hepatol *33*, 747-755. 10.1111/jgh.13976.

122. Que, R., Shen, Y., Ren, J., Tao, Z., Zhu, X., and Li, Y. (2018). Estrogen receptor-beta-dependent effects of saikosaponin-d on the suppression of oxidative stress-induced rat hepatic stellate cell activation. Int J Mol Med *41*, 1357-1364. 10.3892/ijmm.2017.3349.

123. Zhang, Y., Wu, L., Wang, Y., Zhang, M., Li, L., Zhu, D., Li, X., Gu, H., Zhang, C.Y., and Zen, K. (2012). Protective role of estrogen-induced miRNA-29 expression in carbon tetrachloride-induced mouse liver injury. J Biol Chem *287*, 14851-14862. 10.1074/jbc.M111.314922.

124. Ge, S., Xie, J., Liu, F., He, J., and He, J. (2015). MicroRNA-19b reduces hepatic stellate cell proliferation by targeting GRB2 in hepatic fibrosis models in vivo and in vitro as part of the inhibitory effect of estradiol. J Cell Biochem *116*, 2455-2464. 10.1002/jcb.25116.

125. Xu, H., Wei, Y., Zhang, Y., Xu, Y., Li, F., Liu, J., Zhang, W., Han, X., Tan, R., and Shen, P. (2012). Oestrogen attenuates tumour progression in hepatocellular carcinoma. J Pathol *228*, 216-229. 10.1002/path.4009.

126. Deng, L., Yang, H., Tang, J., Lin, Z., Yin, A., Gao, Y., Wang, X., Jiang, R., and Sun, B. (2015). Inhibition of MTA1 by ERalpha contributes to protection hepatocellular carcinoma from tumor proliferation and metastasis. J Exp Clin Cancer Res *34*, 128. 10.1186/s13046-015-0248-0.

127. Lin, Y.M., Velmurugan, B.K., Yeh, Y.L., Tu, C.C., Ho, T.J., Lai, T.Y., Tsai, C.H., Tsai, F.J., Tsai, C.H., and Huang, C.Y. (2013). Activation of estrogen receptors with E2 downregulates peroxisome proliferator-activated receptor gamma in hepatocellular carcinoma. Oncol Rep *30*, 3027-3031. 10.3892/or.2013.2793.

128. Teng, Y., Litchfield, L.M., Ivanova, M.M., Prough, R.A., Clark, B.J., and Klinge, C.M. (2014). Dehydroepiandrosterone-induces miR-21 transcription in HepG2 cells through estrogen receptor beta and androgen receptor. Mol Cell Endocrinol *392*, 23-36. 10.1016/j.mce.2014.05.007.

129. Tummala, K.S., Gomes, A.L., Yilmaz, M., Grana, O., Bakiri, L., Ruppen, I., Ximenez-Embun, P., Sheshappanavar, V., Rodriguez-Justo, M., Pisano, D.G., et al. (2014). Inhibition of de novo NAD(+) synthesis by oncogenic URI causes liver tumorigenesis through DNA damage. Cancer Cell *26*, 826-839. 10.1016/j.ccell.2014.10.002.

130. Kanda, T., Jiang, X., and Yokosuka, O. (2014). Androgen receptor signaling in hepatocellular carcinoma and pancreatic cancers. World J Gastroenterol *20*, 9229-9236. 10.3748/wjg.v20.i28.9229.

131. Ma, W.L., Lai, H.C., Yeh, S., Cai, X., and Chang, C. (2014). Androgen receptor roles in hepatocellular carcinoma, fatty liver, cirrhosis and hepatitis. Endocr Relat Cancer *21*, R165-182. 10.1530/ERC-13-0283.

132. Feng, H., Cheng, A.S., Tsang, D.P., Li, M.S., Go, M.Y., Cheung, Y.S., Zhao, G.J., Ng, S.S., Lin, M.C., Yu, J., et al. (2011). Cell cycle-related kinase is a direct androgen receptor-regulated gene that drives beta-catenin/T cell factor-dependent hepatocarcinogenesis. J Clin Invest *121*, 3159-3175. 10.1172/JCI45967.

133. Chen, P.J., Yeh, S.H., Liu, W.H., Lin, C.C., Huang, H.C., Chen, C.L., Chen, D.S., and Chen, P.J. (2012). Androgen pathway stimulates microRNA-216a transcription to suppress the tumor suppressor in lung cancer-1 gene in early hepatocarcinogenesis. Hepatology *56*, 632-643. 10.1002/hep.25695.

134. Hartwell, H.J., Petrosky, K.Y., Fox, J.G., Horseman, N.D., and Rogers, A.B. (2014). Prolactin prevents hepatocellular carcinoma by restricting innate immune activation of c-Myc in mice. Proc Natl Acad Sci U S A *111*, 11455-11460. 10.1073/pnas.1404267111.

135. Manieri, E., Herrera-Melle, L., Mora, A., Tomas-Loba, A., Leiva-Vega, L., Fernandez, D.I., Rodriguez, E., Moran, L., Hernandez-Cosido, L., Torres, J.L., et al. (2019). Adiponectin accounts for gender differences in hepatocellular carcinoma incidence. J Exp Med *216*, 1108-1119. 10.1084/jem.20181288.

136. Ji, J., Shi, J., Budhu, A., Yu, Z., Forgues, M., Roessler, S., Ambs, S., Chen, Y., Meltzer, P.S., Croce, C.M., et al. (2009). MicroRNA expression, survival, and response to interferon in liver cancer. N Engl J Med *361*, 1437-1447. 10.1056/NEJMoa0901282.

137. Kota, J., Chivukula, R.R., O'Donnell, K.A., Wentzel, E.A., Montgomery, C.L., Hwang, H.W., Chang, T.C., Vivekanandan, P., Torbenson, M., Clark, K.R., et al. (2009). Therapeutic microRNA delivery suppresses tumorigenesis in a murine liver cancer model. Cell *137*, 1005-1017. 10.1016/j.cell.2009.04.021.

138. Ji, F., Zhang, J., Liu, N., Gu, Y., Zhang, Y., Huang, P., Zhang, N., Lin, S., Pan, R., Meng, Z., et al. (2022). Blocking hepatocarcinogenesis by a cytochrome P450 family member with female-preferential expression. Gut *71*, 2313-2324. 10.1136/gutjnl-2021-326050.

139. Kido, T., Lo, R.C., Li, Y., Lee, J., Tabatabai, Z.L., Ng, I.O., and Lau, Y.F. (2014). The potential contributions of a Y-located protooncogene and its X homologue in sexual dimorphisms in hepatocellular carcinoma. Hum Pathol *45*, 1847-1858. 10.1016/j.humpath.2014.05.002.

140. Kido, T., and Lau, Y.C. (2019). The Y-linked proto-oncogene TSPY contributes to poor prognosis of the male hepatocellular carcinoma patients by promoting the pro-oncogenic and suppressing the anti-oncogenic gene expression. Cell Biosci *9*, 22. 10.1186/s13578-019-0287-x.

141. Murakami, S., Chishima, S., Uemoto, H., Sakamoto, E., Sato, T., Kurabe, N., Kawasaki, Y., Shibata, T., Akiyama, H., and Tashiro, F. (2014). The male-specific factor Sry harbors an oncogenic function. Oncogene *33*, 2978-2986. 10.1038/onc.2013.262.

142. Murakami, S., Ninomiya, W., Sakamoto, E., Shibata, T., Akiyama, H., and Tashiro, F. (2015). SRY and OCT4 Are Required for the Acquisition of Cancer

Stem Cell-Like Properties and Are Potential Differentiation Therapy Targets. Stem Cells *33*, 2652-2663. 10.1002/stem.2059.

143. Liu, C., Ren, Y.F., Dong, J., Ke, M.Y., Ma, F., Monga, S.P.S., Wu, R., Lv, Y., and Zhang, X.F. (2017). Activation of SRY accounts for male-specific hepatocarcinogenesis: Implication in gender disparity of hepatocellular carcinoma. Cancer Lett *410*, 20-31. 10.1016/j.canlet.2017.09.013.

144. Tsuei, D.J., Hsu, H.C., Lee, P.H., Jeng, Y.M., Pu, Y.S., Chen, C.N., Lee, Y.C., Chou, W.C., Chang, C.J., Ni, Y.H., and Chang, M.H. (2004). RBMY, a male germ cell-specific RNA-binding protein, activated in human liver cancers and transforms rodent fibroblasts. Oncogene *23*, 5815-5822. 10.1038/sj.onc.1207773.

145. Tsuei, D.J., Lee, P.H., Peng, H.Y., Lu, H.L., Su, D.S., Jeng, Y.M., Hsu, H.C., Hsu, S.H., Wu, J.F., Ni, Y.H., and Chang, M.H. (2011). Male germ cell-specific RNA binding protein RBMY: a new oncogene explaining male predominance in liver cancer. PLoS One *6*, e26948. 10.1371/journal.pone.0026948.

146. Chua, H.H., Tsuei, D.J., Lee, P.H., Jeng, Y.M., Lu, J., Wu, J.F., Su, D.S., Chen, Y.H., Chien, C.S., Kao, P.C., et al. (2015). RBMY, a novel inhibitor of glycogen synthase kinase 3beta, increases tumor stemness and predicts poor prognosis of hepatocellular carcinoma. Hepatology *62*, 1480-1496. 10.1002/hep.27996.

147. Baecker, A., Liu, X., La Vecchia, C., and Zhang, Z.F. (2018). Worldwide incidence of hepatocellular carcinoma cases attributable to major risk factors. Eur J Cancer Prev *27*, 205-212. 10.1097/CEJ.0000000000000428.

148. Huang, D.Q., Mathurin, P., Cortez-Pinto, H., and Loomba, R. (2023). Global epidemiology of alcohol-associated cirrhosis and HCC: trends, projections and risk factors. Nat Rev Gastroenterol Hepatol *20*, 37-49. 10.1038/s41575-022-00688-6.

149. Baraona, E., Abittan, C.S., Dohmen, K., Moretti, M., Pozzato, G., Chayes, Z.W., Schaefer, C., and Lieber, C.S. (2001). Gender differences in pharmacokinetics of alcohol. Alcohol Clin Exp Res *25*, 502-507.

150. Boutari, C., and Mantzoros, C.S. (2022). A 2022 update on the epidemiology of obesity and a call to action: as its twin COVID-19 pandemic appears to be receding, the obesity and dysmetabolism pandemic continues to rage on. Metabolism *133*, 155217. 10.1016/j.metabol.2022.155217.

151. Nevola, R., Tortorella, G., Rosato, V., Rinaldi, L., Imbriani, S., Perillo, P., Mastrocinque, D., La Montagna, M., Russo, A., Di Lorenzo, G., et al. (2023). Gender Differences in the Pathogenesis and Risk Factors of Hepatocellular Carcinoma. Biology (Basel) *12*. 10.3390/biology12070984.

152. Wang, S.H., Chen, P.J., and Yeh, S.H. (2015). Gender disparity in chronic hepatitis B: Mechanisms of sex hormones. J Gastroenterol Hepatol *30*, 1237-1245. 10.1111/jgh.12934.

153. Wang, S.H., Yeh, S.H., Lin, W.H., Wang, H.Y., Chen, D.S., and Chen, P.J. (2009). Identification of androgen response elements in the enhancer I of hepatitis B virus: a mechanism for sex disparity in chronic hepatitis B. Hepatology *50*, 1392-1402. 10.1002/hep.23163.

154. Yang, W.J., Chang, C.J., Yeh, S.H., Lin, W.H., Wang, S.H., Tsai, T.F., Chen, D.S., and Chen, P.J. (2009). Hepatitis B virus X protein enhances the transcriptional activity of the androgen receptor through c-Src and glycogen synthase kinase-3beta kinase pathways. Hepatology *49*, 1515-1524. 10.1002/hep.22833.

155. Wang, S.H., Yeh, S.H., Lin, W.H., Yeh, K.H., Yuan, Q., Xia, N.S., Chen, D.S., and Chen, P.J. (2012). Estrogen receptor alpha represses transcription of HBV genes via interaction with hepatocyte nuclear factor 4alpha. Gastroenterology *142*, 989-998 e984. 10.1053/j.gastro.2011.12.045.

156. Velthuijs, N., Meldal, B., Geessinck, Q., Porras, P., Medvedeva, Y., Zubritskiy, A., Orchard, S., and Logie, C. (2021). Integration of transcription coregulator complexes with sequence-specific DNA-binding factor interactomes. Biochim Biophys Acta Gene Regul Mech *1864*, 194749. 10.1016/j.bbagrm.2021.194749.

157. Stallcup, M.R., and Poulard, C. (2020). Gene-Specific Actions of Transcriptional Coregulators Facilitate Physiological Plasticity: Evidence for a Physiological Coregulator Code. Trends Biochem Sci *45*, 497-510. 10.1016/j.tibs.2020.02.006.

158. Knutti, D., and Kralli, A. (2001). PGC-1, a versatile coactivator. Trends Endocrinol Metab *12*, 360-365. 10.1016/s1043-2760(01)00457-x.

159. Yoon, J.C., Puigserver, P., Chen, G., Donovan, J., Wu, Z., Rhee, J., Adelmant, G., Stafford, J., Kahn, C.R., Granner, D.K., et al. (2001). Control of hepatic gluconeogenesis through the transcriptional coactivator PGC-1. Nature *413*, 131-138. 10.1038/35093050.

160. Villena, J.A., and Kralli, A. (2008). ERRalpha: a metabolic function for the oldest orphan. Trends Endocrinol Metab *19*, 269-276. 10.1016/j.tem.2008.07.005.

161. Huss, J.M., Kopp, R.P., and Kelly, D.P. (2002). Peroxisome proliferator-activated receptor coactivator-1alpha (PGC-1alpha) coactivates the cardiac-enriched nuclear receptors estrogen-related receptor-alpha and -gamma. Identification of novel leucine-rich interaction motif within PGC-1alpha. J Biol Chem *277*, 40265-40274. 10.1074/jbc.M206324200.

162. Monsalve, M., Wu, Z., Adelmant, G., Puigserver, P., Fan, M., and Spiegelman, B.M. (2000). Direct coupling of transcription and mRNA processing through the

thermogenic coactivator PGC-1. Mol Cell *6*, 307-316. 10.1016/s1097-2765(00)00031-9.

163. Onate, S.A., Tsai, S.Y., Tsai, M.J., and O'Malley, B.W. (1995). Sequence and characterization of a coactivator for the steroid hormone receptor superfamily. Science *270*, 1354-1357. 10.1126/science.270.5240.1354.

164. Heery, D.M., Kalkhoven, E., Hoare, S., and Parker, M.G. (1997). A signature motif in transcriptional co-activators mediates binding to nuclear receptors. Nature *387*, 733-736. 10.1038/42750.

165. Darimont, B.D., Wagner, R.L., Apriletti, J.W., Stallcup, M.R., Kushner, P.J., Baxter, J.D., Fletterick, R.J., and Yamamoto, K.R. (1998). Structure and specificity of nuclear receptor-coactivator interactions. Genes Dev *12*, 3343-3356. 10.1101/gad.12.21.3343.

166. Long, W., and O'Malley, B.W. (2014). Steroid Receptor Coactivators (SRCs) as Integrators of Multiple Signaling Pathways in Cancer Progression. In Nuclear Signaling Pathways and Targeting Transcription in Cancer, R. Kumar, ed. (Springer New York), pp. 3-32. 10.1007/978-1-4614-8039-6_1.

167. Leo, C., and Chen, J.D. (2000). The SRC family of nuclear receptor coactivators. Gene *245*, 1-11. 10.1016/s0378-1119(00)00024-x.

168. Dasgupta, S., and O'Malley, B.W. (2014). Transcriptional coregulators: emerging roles of SRC family of coactivators in disease pathology. J Mol Endocrinol *53*, R47-59. 10.1530/JME-14-0080.

169. Torres-Arzayus, M.I., Font de Mora, J., Yuan, J., Vazquez, F., Bronson, R., Rue, M., Sellers, W.R., and Brown, M. (2004). High tumor incidence and activation of the PI3K/AKT pathway in transgenic mice define AIB1 as an oncogene. Cancer Cell *6*, 263-274. 10.1016/j.ccr.2004.06.027.

170. Planas-Silva, M.D., Shang, Y., Donaher, J.L., Brown, M., and Weinberg, R.A. (2001). AIB1 enhances estrogen-dependent induction of cyclin D1 expression. Cancer Res *61*, 3858-3862.

171. Karmakar, S., Gao, T., Pace, M.C., Oesterreich, S., and Smith, C.L. (2010). Cooperative activation of cyclin D1 and progesterone receptor gene expression by the SRC-3 coactivator and SMRT corepressor. Mol Endocrinol *24*, 1187-1202. 10.1210/me.2009-0480.

172. Fereshteh, M.P., Tilli, M.T., Kim, S.E., Xu, J., O'Malley, B.W., Wellstein, A., Furth, P.A., and Riegel, A.T. (2008). The nuclear receptor coactivator amplified in breast cancer-1 is required for Neu (ErbB2/HER2) activation, signaling, and mammary tumorigenesis in mice. Cancer Res *68*, 3697-3706. 10.1158/0008-5472.CAN-07-6702.

173. Kuang, S.Q., Liao, L., Zhang, H., Lee, A.V., O'Malley, B.W., and Xu, J. (2004). AIB1/SRC-3 deficiency affects insulin-like growth factor I signaling pathway and suppresses v-Ha-ras-induced breast cancer initiation and progression in mice. Cancer Res *64*, 1875-1885. 10.1158/0008-5472.can-03-3745.

174. Maehama, T., and Dixon, J.E. (1998). The tumor suppressor, PTEN/MMAC1, dephosphorylates the lipid second messenger, phosphatidylinositol 3,4,5-trisphosphate. J Biol Chem *273*, 13375-13378. 10.1074/jbc.273.22.13375.

175. Trotman, L.C., Wang, X., Alimonti, A., Chen, Z., Teruya-Feldstein, J., Yang, H., Pavletich, N.P., Carver, B.S., Cordon-Cardo, C., Erdjument-Bromage, H., et al. (2007). Ubiquitination regulates PTEN nuclear import and tumor suppression. Cell *128*, 141-156. 10.1016/j.cell.2006.11.040.

176. Horie, Y., Suzuki, A., Kataoka, E., Sasaki, T., Hamada, K., Sasaki, J., Mizuno, K., Hasegawa, G., Kishimoto, H., Iizuka, M., et al. (2004). Hepatocyte-specific Pten deficiency results in steatohepatitis and hepatocellular carcinomas. J Clin Invest *113*, 1774-1783. 10.1172/JCI20513.

177. Lehman, J.A., Waning, D.L., Batuello, C.N., Cipriano, R., Kadakia, M.P., and Mayo, L.D. (2011). Induction of apoptotic genes by a p73-phosphatase and tensin homolog (p73-PTEN) protein complex in response to genotoxic stress. J Biol Chem *286*, 36631-36640. 10.1074/jbc.M110.217620.

178. Sauve, F., McBroom, L.D., Gallant, J., Moraitis, A.N., Labrie, F., and Giguere, V. (2001). CIA, a novel estrogen receptor coactivator with a bifunctional nuclear receptor interacting determinant. Mol Cell Biol *21*, 343-353. 10.1128/MCB.21.1.343-353.2001.

179. Gillespie, M.A., Gold, E.S., Ramsey, S.A., Podolsky, I., Aderem, A., and Ranish, J.A. (2015). An LXR-NCOA5 gene regulatory complex directs inflammatory crosstalk-dependent repression of macrophage cholesterol efflux. EMBO J *34*, 1244-1258. 10.15252/embj.201489819.

180. Jiang, C., Ito, M., Piening, V., Bruck, K., Roeder, R.G., and Xiao, H. (2004). TIP30 interacts with an estrogen receptor alpha-interacting coactivator CIA and regulates c-myc transcription. J Biol Chem *279*, 27781-27789. 10.1074/jbc.M401809200.

181. Liao, D.J., and Dickson, R.B. (2000). c-Myc in breast cancer. Endocr Relat Cancer *7*, 143-164. 10.1677/erc.0.0070143.

182. Sarachana, T., and Hu, V.W. (2013). Differential recruitment of coregulators to the RORA promoter adds another layer of complexity to gene (dys) regulation by sex hormones in autism. Mol Autism *4*, 39. 10.1186/2040-2392-4-39.

183. Sayad, A., Salmani, T., Hemmesi, M.K., Ganji, M., Ghafouri-Fard, S., Hatami, M., Soudyab, M., and Taheri, M. (2018). Down-regulation of RORA gene expression

in the blood of multiple sclerosis patients. Hum Antibodies *26*, 219-224. 10.3233/HAB-180341.

184. Iliev, D.B., Skjaeveland, I., and Jorgensen, J.B. (2013). CpG oligonucleotides bind TLR9 and RRM-containing proteins in Atlantic salmon (Salmo salar). BMC Immunol *14*, 12. 10.1186/1471-2172-14-12.

185. Zervou, M.I., Goulielmos, G.N., Castro-Giner, F., Boumpas, D.T., Tosca, A.D., and Krueger-Krasagakis, S. (2011). A CD40 and an NCOA5 gene polymorphism confer susceptibility to psoriasis in a Southern European population: a case-control study. Hum Immunol *72*, 761-765. 10.1016/j.humimm.2011.05.014.

186. Boser, A., Drexler, H.C., Reuter, H., Schmitz, H., Wu, G., Scholer, H.R., Gentile, L., and Bartscherer, K. (2013). SILAC proteomics of planarians identifies Ncoa5 as a conserved component of pluripotent stem cells. Cell Rep *5*, 1142-1155. 10.1016/j.celrep.2013.10.035.

187. Gao, S., Li, A., Liu, F., Chen, F., Williams, M., Zhang, C., Kelley, Z., Wu, C.L., Luo, R., and Xiao, H. (2013). NCOA5 haploinsufficiency results in glucose intolerance and subsequent hepatocellular carcinoma. Cancer Cell *24*, 725-737. 10.1016/j.ccr.2013.11.005.

188. Guerrini, V., and Gennaro, M.L. (2019). Foam Cells: One Size Doesn't Fit All. Trends Immunol *40*, 1163-1179. 10.1016/j.it.2019.10.002.

189. Gao, S., Zhang, Y., Yang, C., Perez, G.I., and Xiao, H. (2019). NCOA5 Haplo-insufficiency Results in Male Mouse Infertility through Increased IL-6 Expression in the Epididymis. Sci Rep *9*, 15525. 10.1038/s41598-019-52105-9.

190. Liu, X., Liu, F., Gao, S., Reske, J., Li, A., Wu, C.L., Yang, C., Chen, F., Luo, R., and Xiao, H. (2017). A single non-synonymous NCOA5 variation in type 2 diabetic patients with hepatocellular carcinoma impairs the function of NCOA5 in cell cycle regulation. Cancer Lett *391*, 152-161. 10.1016/j.canlet.2017.01.028.

191. Rivera-Reyes, R., Kleppa, M.J., and Kispert, A. (2018). Proteomic analysis identifies transcriptional cofactors and homeobox transcription factors as TBX18 binding proteins. PLoS One *13*, e0200964. 10.1371/journal.pone.0200964.

192. Chen, G.Q., Tian, H., Yue, W.M., Li, L., Li, S.H., Qi, L., Gao, C., Si, L.B., and Lu, M. (2014). NCOA5 low expression correlates with survival in esophageal squamous cell carcinoma. Med Oncol *31*, 376. 10.1007/s12032-014-0376-y.

193. Zheng, Z.C., Wang, Q.X., Zhang, W., Zhang, X.H., and Huang, D.P. (2018). A novel tumor suppressor gene NCOA5 is correlated with progression in papillary thyroid carcinoma. Onco Targets Ther *11*, 307-311. 10.2147/OTT.S154158.

194. Liang, Y., Zhang, T., Shi, M., Zhang, S., Guo, Y., Gao, J., and Yang, X. (2019). Low expression of NCOA5 predicts poor prognosis in human cervical cancer and

promotes proliferation, migration, and invasion of cervical cancer cell lines by regulating notch3 signaling pathway. J Cell Biochem *120*, 6237-6249. 10.1002/jcb.27911.

195. Ye, X.H., Huang, D.P., and Luo, R.C. (2017). NCOA5 is correlated with progression and prognosis in luminal breast cancer. Biochem Biophys Res Commun *482*, 253-256. 10.1016/j.bbrc.2016.11.051.

196. Xia, E., Hu, W., Bhandari, A., Sindan, N., and Huang, D. (2021). Nuclear Receptor Coactivator 5 is Correlated with Progression in Breast Carcinoma. Anticancer Agents Med Chem *21*, 2520-2524. 10.2174/1871520621666210126093630.

197. Sun, K., Wang, S., He, J., Xie, Y., He, Y., Wang, Z., and Qin, L. (2017). NCOA5 promotes proliferation, migration and invasion of colorectal cancer cells via activation of PI3K/AKT pathway. Oncotarget *8*, 107932-107946. 10.18632/oncotarget.22429.

198. Song, X., Qian, D., Dai, P., Li, Q., Xi, Q., and Sun, K. (2023). Expression and clinical significance of NCOA5 in epithelial ovarian cancer. Front Oncol *13*, 1117033. 10.3389/fonc.2023.1117033.

199. Yuan, X., Zhang, L., Cui, Y., Yu, Y., Gao, X., and Ao, J. (2020). NCOA5 is a master regulator of amino acid-induced mTOR activation and beta-casein synthesis in bovine mammary epithelial cells. Biochem Biophys Res Commun *529*, 569-574. 10.1016/j.bbrc.2020.05.193.

200. He, J., Zhang, W., Li, A., Chen, F., and Luo, R. (2018). Knockout of NCOA5 impairs proliferation and migration of hepatocellular carcinoma cells by suppressing epithelial-to-mesenchymal transition. Biochem Biophys Res Commun *500*, 177-183. 10.1016/j.bbrc.2018.04.017.

201. Deng, Y., Zhu, W., and Zhou, X. (2018). Immune Regulatory Genes Are Major Genetic Factors to Behcet Disease: Systematic Review. Open Rheumatol J *12*, 70-85. 10.2174/1874312901812010070.

202. Rustemoglu, A., Erkol Inal, E., Inanir, A., Ekinci, D., Gul, U., Yigit, S., Ates, O., and Karakus, N. (2017). Clinical significance of NCOA5 gene rs2903908 polymorphism in Behcet's disease. EXCLI J *16*, 609-617. 10.17179/excli2017-189.

203. Koptan, D.M.T., Rasheed Bahgat, D.M., Abdelrasool, A.A., Allam, R., Elgengehy, F.T., Abdel Baki, N.M., and Medhat, B.M. (2022). Analysis of Nuclear Receptor Coactivator 5 (NCOA5) Messenger RNA Expression and rs2903908 Single Nucleotide Polymorphism of NCOA5 in an Egyptian Cohort with Behcet's Disease: A Single-Center Case-control Study. Ocul Immunol Inflamm *30*, 1436-1446. 10.1080/09273948.2021.1889610.

204. Rustemoglu, H., Arslan, E., Atasever, S., Cevik, B., Taspinar, F., Turhan, A.B., and Rustemoglu, A. (2023). Could NCOA5 a novel candidate gene for multiple sclerosis susceptibility? Mol Biol Rep. 10.1007/s11033-023-08830-6.

205. Shtivelman, E. (1997). A link between metastasis and resistance to apoptosis of variant small cell lung carcinoma. Oncogene *14*, 2167-2173. 10.1038/sj.onc.1201059.

206. Xiao, H., Tao, Y., Greenblatt, J., and Roeder, R.G. (1998). A cofactor, TIP30, specifically enhances HIV-1 Tat-activated transcription. Proc Natl Acad Sci U S A *95*, 2146-2151. 10.1073/pnas.95.5.2146.

207. Baker, M.E. (1999). TIP30, a cofactor for HIV-1 Tat-activated transcription, is homologous to short-chain dehydrogenases/reductases. Curr Biol *9*, R471. 10.1016/s0960-9822(99)80297-8.

208. Ito, M., Jiang, C., Krumm, K., Zhang, X., Pecha, J., Zhao, J., Guo, Y., Roeder, R.G., and Xiao, H. (2003). TIP30 deficiency increases susceptibility to tumorigenesis. Cancer Res *63*, 8763-8767.

209. Xiao, H., Palhan, V., Yang, Y., and Roeder, R.G. (2000). TIP30 has an intrinsic kinase activity required for up-regulation of a subset of apoptotic genes. EMBO J *19*, 956-963. 10.1093/emboj/19.5.956.

210. Zhao, J., Lu, B., Xu, H., Tong, X., Wu, G., Zhang, X., Liang, A., Cong, W., Dai, J., Wang, H., et al. (2008). Thirty-kilodalton Tat-interacting protein suppresses tumor metastasis by inhibition of osteopontin transcription in human hepatocellular carcinoma. Hepatology *48*, 265-275. 10.1002/hep.22280.

211. Shuai, S., Yan, X., Zhang, J., Kang, S., Chen, F., Luo, R., and Li, A. (2014). TIP30 nuclear translocation negatively regulates EGF-dependent cyclin D1 transcription in human lung adenocarcinoma. Cancer Lett *354*, 200-209. 10.1016/j.canlet.2014.08.008.

212. Alves de Souza Rios, L., Mapekula, L., Mdletshe, N., Chetty, D., and Mowla, S. (2021). HIV-1 Transactivator of Transcription (Tat) Co-operates With AP-1 Factors to Enhance c-MYC Transcription. Front Cell Dev Biol *9*, 693706. 10.3389/fcell.2021.693706.

213. Baker, M.E., Yan, L., and Pear, M.R. (2000). Three-dimensional model of human TIP30, a coactivator for HIV-1 Tat-activated transcription, and CC3, a protein associated with metastasis suppression. Cell Mol Life Sci *57*, 851-858. 10.1007/s000180050047.

214. El Omari, K., Bird, L.E., Nichols, C.E., Ren, J., and Stammers, D.K. (2005). Crystal structure of CC3 (TIP30): implications for its role as a tumor suppressor. J Biol Chem *280*, 18229-18236. 10.1074/jbc.M501113200.

215. Filling, C., Berndt, K.D., Benach, J., Knapp, S., Prozorovski, T., Nordling, E., Ladenstein, R., Jornvall, H., and Oppermann, U. (2002). Critical residues for structure and catalysis in short-chain dehydrogenases/reductases. J Biol Chem *277*, 25677-25684. 10.1074/jbc.M202160200.

216. Salim, M., Brown-Kipphut, B.A., and Maines, M.D. (2001). Human biliverdin reductase is autophosphorylated, and phosphorylation is required for bilirubin formation. J Biol Chem *276*, 10929-10934. 10.1074/jbc.M010753200.

217. King, F.W., and Shtivelman, E. (2004). Inhibition of nuclear import by the proapoptotic protein CC3. Mol Cell Biol *24*, 7091-7101. 10.1128/MCB.24.16.7091-7101.2004.

218. Zhao, J., Chen, J., Lu, B., Dong, L., Wang, H., Bi, C., Wu, G., Guo, H., Wu, M., and Guo, Y. (2008). TIP30 induces apoptosis under oxidative stress through stabilization of p53 messenger RNA in human hepatocellular carcinoma. Cancer Res *68*, 4133-4141. 10.1158/0008-5472.CAN-08-0432.

219. Zhu, M., Yin, F., Fan, X., Jing, W., Chen, R., Liu, L., Zhang, L., Liu, Y., Liang, Y., Bu, F., et al. (2015). Decreased TIP30 promotes Snail-mediated epithelial-mesenchymal transition and tumor-initiating properties in hepatocellular carcinoma. Oncogene *34*, 1420-1431. 10.1038/onc.2014.73.

220. Liu, Y.P., Chen, C.H., Yen, C.H., Tung, C.W., Chen, C.J., Chen, Y.A., and Huang, M.S. (2018). Human immunodeficiency virus Tat-TIP30 interaction promotes metastasis by enhancing the nuclear translocation of Snail in lung cancer cell lines. Cancer Sci *109*, 3105-3114. 10.1111/cas.13768.

221. Nguyen, T.T., Rajakannu, P., Pham, M.D.T., Weman, L., Jucht, A., Buri, M.C., Van Dommelen, K., and Hegi, M.E. (2023). Epigenetic silencing of HTATIP2 in glioblastoma contributes to treatment resistance by enhancing nuclear translocation of the DNA repair protein MPG. Mol Oncol *17*, 1744-1762. 10.1002/1878-0261.13494.

222. Nakahara, J., Kanekura, K., Nawa, M., Aiso, S., and Suzuki, N. (2009). Abnormal expression of TIP30 and arrested nucleocytoplasmic transport within oligodendrocyte precursor cells in multiple sclerosis. J Clin Invest *119*, 169-181. 10.1172/JCI35440.

223. Zhang, C., Li, A., Gao, S., Zhang, X., and Xiao, H. (2011). The TIP30 protein complex, arachidonic acid and coenzyme A are required for vesicle membrane fusion. PLoS One *6*, e21233. 10.1371/journal.pone.0021233.

224. Zhang, C., Li, A., Zhang, X., and Xiao, H. (2011). A novel TIP30 protein complex regulates EGF receptor signaling and endocytic degradation. J Biol Chem *286*, 9373-9381. 10.1074/jbc.M110.207720.

225. Tomas, A., Futter, C.E., and Eden, E.R. (2014). EGF receptor trafficking: consequences for signaling and cancer. Trends Cell Biol *24*, 26-34. 10.1016/j.tcb.2013.11.002.

226. Zhang, C., Mori, M., Gao, S., Li, A., Hoshino, I., Aupperlee, M.D., Haslam, S.Z., and Xiao, H. (2010). Tip30 deletion in MMTV-Neu mice leads to enhanced EGFR signaling and development of estrogen receptor-positive and progesterone receptor-negative mammary tumors. Cancer Res *70*, 10224-10233. 10.1158/0008-5472.CAN-10-3057.

227. Li, A., Zhang, C., Gao, S., Chen, F., Yang, C., Luo, R., and Xiao, H. (2013). TIP30 loss enhances cytoplasmic and nuclear EGFR signaling and promotes lung adenocarcinogenesis in mice. Oncogene *32*, 2273-2281, 2281e 2271-2212. 10.1038/onc.2012.253.

228. Yin, F., Sharen, G., Yuan, F., Peng, Y., Chen, R., Zhou, X., Wei, H., Li, B., Jing, W., and Zhao, J. (2017). TIP30 regulates lipid metabolism in hepatocellular carcinoma by regulating SREBP1 through the Akt/mTOR signaling pathway. Oncogenesis *6*, e347. 10.1038/oncsis.2017.49.

229. Grund, A., Szaroszyk, M., Korf-Klingebiel, M., Malek Mohammadi, M., Trogisch, F.A., Schrameck, U., Gigina, A., Tiedje, C., Gaestel, M., Kraft, T., et al. (2019). TIP30 counteracts cardiac hypertrophy and failure by inhibiting translational elongation. EMBO Mol Med *11*, e10018. 10.15252/emmm.201810018.

230. Cardinale, C.J., Chang, X., Wei, Z., Qu, H.Q., Bradfield, J.P., Polychronakos, C., and Hakonarson, H. (2023). Genome-wide association study of the age of onset of type 1 diabetes reveals HTATIP2 as a novel T cell regulator. Front Immunol *14*, 1101488. 10.3389/fimmu.2023.1101488.

231. Patel, A.S., Ludwinski, F.E., Mondragon, A., Nuthall, K., Saha, P., Lyons, O., Squadrito, M.L., Siow, R.C., De Palma, M., Smith, A., and Modarai, B. (2023). HTATIP2 regulates arteriogenic activity in monocytes from patients with limb ischemia. JCI Insight. 10.1172/jci.insight.131419.

232. Zhang, H., Zhang, Y., Duan, H.O., Kirley, S.D., Lin, S.X., McDougal, W.S., Xiao, H., and Wu, C.L. (2008). TIP30 is associated with progression and metastasis of prostate cancer. Int J Cancer *123*, 810-816. 10.1002/ijc.23638.

233. Li, X., Zhang, Y., Cao, S., Chen, X., Lu, Y., Jin, H., Sun, S., Chen, B., Liu, J., Ding, J., et al. (2009). Reduction of TIP30 correlates with poor prognosis of gastric cancer patients and its restoration drastically inhibits tumor growth and metastasis. Int J Cancer *124*, 713-721. 10.1002/ijc.23967.

234. Lu, B., Ma, Y., Wu, G., Tong, X., Guo, H., Liang, A., Cong, W., Liu, C., Wang, H., Wu, M., et al. (2008). Methylation of Tip30 promoter is associated with poor prognosis in human hepatocellular carcinoma. Clin Cancer Res *14*, 7405-7412. 10.1158/1078-0432.CCR-08-0409.

235. Zhang, X., Lv, L., Ouyang, X., Zhang, S., Fang, J., Cai, L., and Li, D. (2016). Association of TIP30 expression and prognosis of hepatocellular carcinoma in patients with HBV infection. Cancer Med *5*, 2180-2189. 10.1002/cam4.728.

236. Fan, S.S., Liao, C.S., Cao, Y.D., Xiao, P.L., Deng, T., Luo, R.C., and Duan, H.X. (2017). A low serum Tat-interacting protein 30 level is a diagnostic and prognostic biomarker for hepatocellular carcinoma. Oncol Lett *13*, 4208-4214. 10.3892/ol.2017.6024.

237. Tong, X., Li, K., Luo, Z., Lu, B., Liu, X., Wang, T., Pang, M., Liang, B., Tan, M., Wu, M., et al. (2009). Decreased TIP30 expression promotes tumor metastasis in lung cancer. Am J Pathol *174*, 1931-1939. 10.2353/ajpath.2009.080846.

238. Chen, C.J., Chou, P.A., Huang, M.S., and Liu, Y.P. (2019). Low TIP30 Protein Expression is Associated with a High Risk of Metastasis and Poor Prognosis for Non-Small-Cell Lung Cancer. J Clin Med *8*. 10.3390/jcm8010083.

239. Chen, X., Cao, X., Dong, W., Luo, S., Suo, Z., and Jin, Y. (2010). Expression of TIP30 tumor suppressor gene is down-regulated in human colorectal carcinoma. Dig Dis Sci *55*, 2219-2226. 10.1007/s10620-009-0992-0.

240. Guo, S., Jing, W., Hu, X., Zhou, X., Liu, L., Zhu, M., Yin, F., Chen, R., Zhao, J., and Guo, Y. (2014). Decreased TIP30 expression predicts poor prognosis in pancreatic cancer patients. Int J Cancer *134*, 1369-1378. 10.1002/ijc.28471.

241. Dong, W., Shen, R., and Cheng, S. (2014). Reduction of TIP30 in esophageal squamous cell carcinoma cells involves promoter methylation and microRNA-10b. Biochem Biophys Res Commun *453*, 772-777. 10.1016/j.bbrc.2014.10.016.

242. Zhu, M., Yin, F., Yang, L., Chen, S., Chen, R., Zhou, X., Jing, W., Fan, X., Jia, R., Wang, H., et al. (2014). Contribution of TIP30 to chemoresistance in laryngeal carcinoma. Cell Death Dis *5*, e1468. 10.1038/cddis.2014.424.

243. Chen, J., Zhu, C., Zhu, M., Geng, M., Tian, Y., Li, G., and Zheng, H. (2015). Clinicopathologic significance and survival of TIP30 expression in laryngeal squamous cell carcinoma. Int J Clin Exp Med *8*, 6024-6031.

244. Dong, X., Deng, Q., Nie, X., Zhang, M., Jia, W., Chen, C., Xu, C., and Xu, R. (2015). Downregulation of HTATIP2 expression is associated with promoter methylation and poor prognosis in glioma. Exp Mol Pathol *98*, 192-199. 10.1016/j.yexmp.2015.01.013.

245. Liu, Z., Yang, Z., Jiang, S., Zou, Q., Yuan, Y., Li, J., Li, D., Liang, L., Chen, M., and Chen, S. (2016). MCM2 and TIP30 are prognostic markers in squamous cell/adenosquamous carcinoma and adenocarcinoma of the gallbladder. Mol Med Rep *14*, 4581-4592. 10.3892/mmr.2016.5851.

246. Gerbes, A., Zoulim, F., Tilg, H., Dufour, J.F., Bruix, J., Paradis, V., Salem, R., Peck-Radosavljevic, M., Galle, P.R., Greten, T.F., et al. (2018). Gut roundtable meeting paper: selected recent advances in hepatocellular carcinoma. Gut *67*, 380-388. 10.1136/gutjnl-2017-315068.

247. Sia, D., Jiao, Y., Martinez-Quetglas, I., Kuchuk, O., Villacorta-Martin, C., Castro de Moura, M., Putra, J., Camprecios, G., Bassaganyas, L., Akers, N., et al. (2017). Identification of an Immune-specific Class of Hepatocellular Carcinoma, Based on Molecular Features. Gastroenterology *153*, 812-826. 10.1053/j.gastro.2017.06.007.

248. Nakagawa, H., and Maeda, S. (2012). Inflammation- and stress-related signaling pathways in hepatocarcinogenesis. World journal of gastroenterology : WJG *18*, 4071-4081. 10.3748/wjg.v18.i31.4071.

249. Park, E.J., Lee, J.H., Yu, G.Y., He, G., Ali, S.R., Holzer, R.G., Osterreicher, C.H., Takahashi, H., and Karin, M. (2010). Dietary and genetic obesity promote liver inflammation and tumorigenesis by enhancing IL-6 and TNF expression. Cell *140*, 197-208. 10.1016/j.cell.2009.12.052.

250. Dhar, D., Seki, E., and Karin, M. (2014). NCOA5, IL-6, type 2 diabetes, and HCC: The deadly quartet. Cell metabolism *19*, 6-7. 10.1016/j.cmet.2013.12.010.

251. Martin-Caballero, J., Flores, J.M., Garcia-Palencia, P., and Serrano, M. (2001). Tumor susceptibility of p21(Waf1/Cip1)-deficient mice. Cancer Res *61*, 6234-6238.

252. Nicolae, C.M., O'Connor, M.J., Constantin, D., and Moldovan, G.L. (2018). NFkappaB regulates p21 expression and controls DNA damage-induced leukemic differentiation. Oncogene *37*, 3647-3656. 10.1038/s41388-018-0219-y.

253. Sturmlechner, I., Zhang, C., Sine, C.C., van Deursen, E.J., Jeganathan, K.B., Hamada, N., Grasic, J., Friedman, D., Stutchman, J.T., Can, I., et al. (2021). p21 produces a bioactive secretome that places stressed cells under immunosurveillance. Science *374*, eabb3420. 10.1126/science.abb3420.

254. Levi, N., Papismadov, N., Majewska, J., Roitman, L., Wigoda, N., Eilam, R., Tsoory, M., Rotkopf, R., Ovadya, Y., Akiva, H., et al. (2023). p21 facilitates chronic lung inflammation via epithelial and endothelial cells. Aging (Albany NY) *15*, 2395-2417. 10.18632/aging.204622.

255. Warfel, N.A., and El-Deiry, W.S. (2013). p21WAF1 and tumourigenesis: 20 years after. Curr Opin Oncol *25*, 52-58. 10.1097/CCO.0b013e32835b639e.

256. Gartel, A.L., and Tyner, A.L. (1999). Transcriptional regulation of the p21((WAF1/CIP1)) gene. Exp Cell Res *246*, 280-289. 10.1006/excr.1998.4319.

257. Abbas, T., and Dutta, A. (2009). p21 in cancer: intricate networks and multiple activities. Nat Rev Cancer *9*, 400-414. 10.1038/nrc2657.

258. Cmielova, J., and Rezacova, M. (2011). p21Cip1/Waf1 protein and its function based on a subcellular localization [corrected]. J Cell Biochem *112*, 3502-3506. 10.1002/jcb.23296.

259. Nguyen, P., Valanejad, L., Cast, A., Wright, M., Garcia, J.M., El-Serag, H.B., Karns, R., and Timchenko, N.A. (2018). Elimination of Age-Associated Hepatic Steatosis and Correction of Aging Phenotype by Inhibition of cdk4-C/EBPalpha-p300 Axis. Cell reports *24*, 1597-1609. 10.1016/j.celrep.2018.07.014.

260. Tomita, K., Teratani, T., Suzuki, T., Oshikawa, T., Yokoyama, H., Shimamura, K., Nishiyama, K., Mataki, N., Irie, R., Minamino, T., et al. (2012). p53/p66Shc-mediated signaling contributes to the progression of non-alcoholic steatohepatitis in humans and mice. Journal of hepatology *57*, 837-843. 10.1016/j.jhep.2012.05.013.

261. Wu, H., Wade, M., Krall, L., Grisham, J., Xiong, Y., and Van Dyke, T. (1996). Targeted in vivo expression of the cyclin-dependent kinase inhibitor p21 halts hepatocyte cell-cycle progression, postnatal liver development and regeneration. Genes Dev *10*, 245-260.

262. Yano, M., Ohkoshi, S., Aoki, Y.H., Takahashi, H., Kurita, S., Yamazaki, K., Suzuki, K., Yamagiwa, S., Sanpei, A., Fujimaki, S., et al. (2013). Hepatitis B virus X induces cell proliferation in the hepatocarcinogenesis via up-regulation of cytoplasmic p21 expression. Liver international : official journal of the International Association for the Study of the Liver *33*, 1218-1229. 10.1111/liv.12176.

263. Marhenke, S., Buitrago-Molina, L.E., Endig, J., Orlik, J., Schweitzer, N., Klett, S., Longerich, T., Geffers, R., Sanchez Munoz, A., Dorrell, C., et al. (2014). p21 promotes sustained liver regeneration and hepatocarcinogenesis in chronic cholestatic liver injury. Gut *63*, 1501-1512. 10.1136/gutjnl-2013-304829.

264. Ehedego, H., Boekschoten, M.V., Hu, W., Doler, C., Haybaeck, J., Gabetaler, N., Muller, M., Liedtke, C., and Trautwein, C. (2015). p21 ablation in liver enhances DNA damage, cholestasis, and carcinogenesis. Cancer Res *75*, 1144-1155. 10.1158/0008-5472.CAN-14-1356.

265. Zhang, Y., Luo, Y., Liu, X., Kiupel, M., Li, A., Wang, H., Mi, Q.S., and Xiao, H. (2024). NCOA5 Haploinsufficiency in Myeloid-Lineage Cells Sufficiently Causes Nonalcoholic Steatohepatitis and Hepatocellular Carcinoma. Cell Mol Gastroenterol Hepatol *17*, 1-27. 10.1016/j.jcmgh.2023.09.007.

266. Remmele, W., and Stegner, H.E. (1987). [Recommendation for uniform definition of an immunoreactive score (IRS) for immunohistochemical estrogen receptor detection (ER-ICA) in breast cancer tissue]. Pathologe *8*, 138-140.

267. Cotter, T.G., and Rinella, M. (2020). Nonalcoholic Fatty Liver Disease 2020: The State of the Disease. Gastroenterology *158*, 1851-1864. 10.1053/j.gastro.2020.01.052.

268. Anstee, Q.M., and Day, C.P. (2015). The Genetics of Nonalcoholic Fatty Liver Disease: Spotlight on PNPLA3 and TM6SF2. Semin Liver Dis *35*, 270-290. 10.1055/s-0035-1562947.

269. Kazankov, K., Jorgensen, S.M.D., Thomsen, K.L., Moller, H.J., Vilstrup, H., George, J., Schuppan, D., and Gronbaek, H. (2019). The role of macrophages in nonalcoholic fatty liver disease and nonalcoholic steatohepatitis. Nat Rev Gastroenterol Hepatol *16*, 145-159. 10.1038/s41575-018-0082-x.

270. Lewis, J.P., Palmer, N.D., Ellington, J.B., Divers, J., Ng, M.C., Lu, L., Langefeld, C.D., Freedman, B.I., and Bowden, D.W. (2010). Analysis of candidate genes on chromosome 20q12-13.1 reveals evidence for BMI mediated association of PREX1 with type 2 diabetes in European Americans. Genomics *96*, 211-219. 10.1016/j.ygeno.2010.07.006.

271. Williams, M., Liu, X., Zhang, Y., Reske, J., Bahal, D., Gohl, T.G., Hollern, D., Ensink, E., Kiupel, M., Luo, R., et al. (2020). NCOA5 deficiency promotes a unique liver protumorigenic microenvironment through p21(WAF1/CIP1) overexpression, which is reversed by metformin. Oncogene *39*, 3821-3836. 10.1038/s41388-020-1256-x.

272. Abram, C.L., Roberge, G.L., Hu, Y., and Lowell, C.A. (2014). Comparative analysis of the efficiency and specificity of myeloid-Cre deleting strains using ROSA-EYFP reporter mice. J Immunol Methods *408*, 89-100. 10.1016/j.jim.2014.05.009.

273. Itoh, M., Kato, H., Suganami, T., Konuma, K., Marumoto, Y., Terai, S., Sakugawa, H., Kanai, S., Hamaguchi, M., Fukaishi, T., et al. (2013). Hepatic crown-like structure: a unique histological feature in non-alcoholic steatohepatitis in mice and humans. PLoS One *8*, e82163. 10.1371/journal.pone.0082163.

274. Benhamed, F., Denechaud, P.D., Lemoine, M., Robichon, C., Moldes, M., Bertrand-Michel, J., Ratziu, V., Serfaty, L., Housset, C., Capeau, J., et al. (2012). The lipogenic transcription factor ChREBP dissociates hepatic steatosis from insulin resistance in mice and humans. J Clin Invest *122*, 2176-2194. 10.1172/JCI41636.

275. Foretz, M., Guichard, C., Ferre, P., and Foufelle, F. (1999). Sterol regulatory element binding protein-1c is a major mediator of insulin action on the hepatic expression of glucokinase and lipogenesis-related genes. Proc Natl Acad Sci U S A *96*, 12737-12742. 10.1073/pnas.96.22.12737.

276. Knebel, B., Haas, J., Hartwig, S., Jacob, S., Kollmer, C., Nitzgen, U., Muller-Wieland, D., and Kotzka, J. (2012). Liver-specific expression of transcriptionally

active SREBP-1c is associated with fatty liver and increased visceral fat mass. PLoS One *7*, e31812. 10.1371/journal.pone.0031812.

277. Lee, Y.K., Park, J.E., Lee, M., and Hardwick, J.P. (2018). Hepatic lipid homeostasis by peroxisome proliferator-activated receptor gamma 2. Liver Res *2*, 209-215. 10.1016/j.livres.2018.12.001.

278. Schmidt-Arras, D., and Rose-John, S. (2016). IL-6 pathway in the liver: From physiopathology to therapy. J Hepatol *64*, 1403-1415. 10.1016/j.jhep.2016.02.004.

279. Zhang, X., Han, J., Man, K., Li, X., Du, J., Chu, E.S., Go, M.Y., Sung, J.J., and Yu, J. (2016). CXC chemokine receptor 3 promotes steatohepatitis in mice through mediating inflammatory cytokines, macrophages and autophagy. J Hepatol *64*, 160-170. 10.1016/j.jhep.2015.09.005.

280. Remmerie, A., Martens, L., Thone, T., Castoldi, A., Seurinck, R., Pavie, B., Roels, J., Vanneste, B., De Prijck, S., Vanhockerhout, M., et al. (2020). Osteopontin Expression Identifies a Subset of Recruited Macrophages Distinct from Kupffer Cells in the Fatty Liver. Immunity *53*, 641-657 e614. 10.1016/j.immuni.2020.08.004.

281. Xiong, X., Kuang, H., Ansari, S., Liu, T., Gong, J., Wang, S., Zhao, X.Y., Ji, Y., Li, C., Guo, L., et al. (2019). Landscape of Intercellular Crosstalk in Healthy and NASH Liver Revealed by Single-Cell Secretome Gene Analysis. Mol Cell *75*, 644-660 e645. 10.1016/j.molcel.2019.07.028.

282. Barreby, E., Sulen, A., and Aouadi, M. (2019). Glucan-Encapsulated siRNA Particles (GeRPs) for Specific Gene Silencing in Adipose Tissue Macrophages. Methods Mol Biol *1951*, 49-57. 10.1007/978-1-4939-9130-3_4.

283. Luo, W., Friedman, M.S., Shedden, K., Hankenson, K.D., and Woolf, P.J. (2009). GAGE: generally applicable gene set enrichment for pathway analysis. BMC Bioinformatics *10*, 161. 10.1186/1471-2105-10-161.

284. Arendt, B.M., Comelli, E.M., Ma, D.W., Lou, W., Teterina, A., Kim, T., Fung, S.K., Wong, D.K., McGilvray, I., Fischer, S.E., and Allard, J.P. (2015). Altered hepatic gene expression in nonalcoholic fatty liver disease is associated with lower hepatic n-3 and n-6 polyunsaturated fatty acids. Hepatology *61*, 1565-1578. 10.1002/hep.27695.

285. Barbie, D.A., Tamayo, P., Boehm, J.S., Kim, S.Y., Moody, S.E., Dunn, I.F., Schinzel, A.C., Sandy, P., Meylan, E., Scholl, C., et al. (2009). Systematic RNA interference reveals that oncogenic KRAS-driven cancers require TBK1. Nature *462*, 108-112. 10.1038/nature08460.

286. Rigamonti, E., Chinetti-Gbaguidi, G., and Staels, B. (2008). Regulation of macrophage functions by PPAR-alpha, PPAR-gamma, and LXRs in mice and

men. Arterioscler Thromb Vasc Biol *28*, 1050-1059. 10.1161/ATVBAHA.107.158998.

287. Scheuerer, B., Ernst, M., Durrbaum-Landmann, I., Fleischer, J., Grage-Griebenow, E., Brandt, E., Flad, H.D., and Petersen, F. (2000). The CXC-chemokine platelet factor 4 promotes monocyte survival and induces monocyte differentiation into macrophages. Blood *95*, 1158-1166.

288. Drescher, H.K., Brandt, E.F., Fischer, P., Dreschers, S., Schwendener, R.A., Kowalska, M.A., Canbay, A., Wasmuth, H.E., Weiskirchen, R., Trautwein, C., et al. (2019). Platelet Factor 4 Attenuates Experimental Acute Liver Injury in Mice. Front Physiol *10*, 326. 10.3389/fphys.2019.00326.

289. Gleissner, C.A. (2012). Macrophage Phenotype Modulation by CXCL4 in Atherosclerosis. Front Physiol *3*, 1. 10.3389/fphys.2012.00001.

290. Pan, Y., Yu, Y., Wang, X., and Zhang, T. (2020). Tumor-Associated Macrophages in Tumor Immunity. Front Immunol *11*, 583084. 10.3389/fimmu.2020.583084.

291. Lin, Y., Xu, J., and Lan, H. (2019). Tumor-associated macrophages in tumor metastasis: biological roles and clinical therapeutic applications. J Hematol Oncol *12*, 76. 10.1186/s13045-019-0760-3.

292. Fleischer, J., Grage-Griebenow, E., Kasper, B., Heine, H., Ernst, M., Brandt, E., Flad, H.D., and Petersen, F. (2002). Platelet factor 4 inhibits proliferation and cytokine release of activated human T cells. J Immunol *169*, 770-777. 10.4049/jimmunol.169.2.770.

293. Liu, C.Y., Battaglia, M., Lee, S.H., Sun, Q.H., Aster, R.H., and Visentin, G.P. (2005). Platelet factor 4 differentially modulates CD4+CD25+ (regulatory) versus CD4+CD25- (nonregulatory) T cells. J Immunol *174*, 2680-2686. 10.4049/jimmunol.174.5.2680.

294. Joseph, R., Soundararajan, R., Vasaikar, S., Yang, F., Allton, K.L., Tian, L., den Hollander, P., Isgandarova, S., Haemmerle, M., Mino, B., et al. (2021). CD8(+) T cells inhibit metastasis and CXCL4 regulates its function. Br J Cancer *125*, 176-189. 10.1038/s41416-021-01338-5.

295. Newman, A.M., Steen, C.B., Liu, C.L., Gentles, A.J., Chaudhuri, A.A., Scherer, F., Khodadoust, M.S., Esfahani, M.S., Luca, B.A., Steiner, D., et al. (2019). Determining cell type abundance and expression from bulk tissues with digital cytometry. Nat Biotechnol *37*, 773-782. 10.1038/s41587-019-0114-2.

296. Aran, D., Hu, Z., and Butte, A.J. (2017). xCell: digitally portraying the tissue cellular heterogeneity landscape. Genome Biol *18*, 220. 10.1186/s13059-017-1349-1.

297. Alshetaiwi, H., Pervolarakis, N., McIntyre, L.L., Ma, D., Nguyen, Q., Rath, J.A., Nee, K., Hernandez, G., Evans, K., Torosian, L., et al. (2020). Defining the emergence of myeloid-derived suppressor cells in breast cancer using single-cell transcriptomics. Sci Immunol *5*. 10.1126/sciimmunol.aay6017.

298. Zheng, C., Zheng, L., Yoo, J.K., Guo, H., Zhang, Y., Guo, X., Kang, B., Hu, R., Huang, J.Y., Zhang, Q., et al. (2017). Landscape of Infiltrating T Cells in Liver Cancer Revealed by Single-Cell Sequencing. Cell *169*, 1342-1356 e1316. 10.1016/j.cell.2017.05.035.

299. Subramanian, A., Tamayo, P., Mootha, V.K., Mukherjee, S., Ebert, B.L., Gillette, M.A., Paulovich, A., Pomeroy, S.L., Golub, T.R., Lander, E.S., and Mesirov, J.P. (2005). Gene set enrichment analysis: a knowledge-based approach for interpreting genome-wide expression profiles. Proc Natl Acad Sci U S A *102*, 15545-15550. 10.1073/pnas.0506580102.

300. Roessler, S., Jia, H.L., Budhu, A., Forgues, M., Ye, Q.H., Lee, J.S., Thorgeirsson, S.S., Sun, Z., Tang, Z.Y., Qin, L.X., and Wang, X.W. (2010). A unique metastasis gene signature enables prediction of tumor relapse in early-stage hepatocellular carcinoma patients. Cancer Res *70*, 10202-10212. 10.1158/0008-5472.CAN-10-2607.

301. Gao, Q., Zhu, H., Dong, L., Shi, W., Chen, R., Song, Z., Huang, C., Li, J., Dong, X., Zhou, Y., et al. (2019). Integrated Proteogenomic Characterization of HBV-Related Hepatocellular Carcinoma. Cell *179*, 561-577 e522. 10.1016/j.cell.2019.08.052.

302. Hansen, H.H., Feigh, M., Veidal, S.S., Rigbolt, K.T., Vrang, N., and Fosgerau, K. (2017). Mouse models of nonalcoholic steatohepatitis in preclinical drug development. Drug Discov Today *22*, 1707-1718. 10.1016/j.drudis.2017.06.007.

303. Farrell, G., Schattenberg, J.M., Leclercq, I., Yeh, M.M., Goldin, R., Teoh, N., and Schuppan, D. (2019). Mouse Models of Nonalcoholic Steatohepatitis: Toward Optimization of Their Relevance to Human Nonalcoholic Steatohepatitis. Hepatology *69*, 2241-2257. 10.1002/hep.30333.

304. Zhong, F., Zhou, X., Xu, J., and Gao, L. (2020). Rodent Models of Nonalcoholic Fatty Liver Disease. Digestion *101*, 522-535. 10.1159/000501851.

305. Carter-Kent, C., Zein, N.N., and Feldstein, A.E. (2008). Cytokines in the pathogenesis of fatty liver and disease progression to steatohepatitis: implications for treatment. Am J Gastroenterol *103*, 1036-1042. 10.1111/j.1572-0241.2007.01709.x.

306. Fuentes, L., Roszer, T., and Ricote, M. (2010). Inflammatory mediators and insulin resistance in obesity: role of nuclear receptor signaling in macrophages. Mediators Inflamm *2010*, 219583. 10.1155/2010/219583.

307. Roberts, M.D., Mobley, C.B., Toedebush, R.G., Heese, A.J., Zhu, C., Krieger, A.E., Cruthirds, C.L., Lockwood, C.M., Hofheins, J.C., Wiedmeyer, C.E., et al. (2015). Western diet-induced hepatic steatosis and alterations in the liver transcriptome in adult Brown-Norway rats. BMC Gastroenterol *15*, 151. 10.1186/s12876-015-0382-3.

308. Dominguez, M., Miquel, R., Colmenero, J., Moreno, M., Garcia-Pagan, J.C., Bosch, J., Arroyo, V., Gines, P., Caballeria, J., and Bataller, R. (2009). Hepatic expression of CXC chemokines predicts portal hypertension and survival in patients with alcoholic hepatitis. Gastroenterology *136*, 1639-1650. 10.1053/j.gastro.2009.01.056.

309. Zaldivar, M.M., Pauels, K., von Hundelshausen, P., Berres, M.L., Schmitz, P., Bornemann, J., Kowalska, M.A., Gassler, N., Streetz, K.L., Weiskirchen, R., et al. (2010). CXC chemokine ligand 4 (Cxcl4) is a platelet-derived mediator of experimental liver fibrosis. Hepatology *51*, 1345-1353. 10.1002/hep.23435.

310. Pertuy, F., Aguilar, A., Strassel, C., Eckly, A., Freund, J.N., Duluc, I., Gachet, C., Lanza, F., and Leon, C. (2015). Broader expression of the mouse platelet factor 4-cre transgene beyond the megakaryocyte lineage. J Thromb Haemost *13*, 115-125. 10.1111/jth.12784.

311. Gray, A.L., Karlsson, R., Roberts, A.R.E., Ridley, A.J.L., Pun, N., Khan, B., Lawless, C., Luis, R., Szpakowska, M., Chevigne, A., et al. (2023). Chemokine CXCL4 interactions with extracellular matrix proteoglycans mediate widespread immune cell recruitment independent of chemokine receptors. Cell Rep *42*, 111930. 10.1016/j.celrep.2022.111930.

312. Deiuliis, J.A., Oghumu, S., Duggineni, D., Zhong, J., Rutsky, J., Banerjee, A., Needleman, B., Mikami, D., Narula, V., Hazey, J., et al. (2014). CXCR3 modulates obesity-induced visceral adipose inflammation and systemic insulin resistance. Obesity (Silver Spring) *22*, 1264-1274. 10.1002/oby.20642.

313. Lasagni, L., Francalanci, M., Annunziato, F., Lazzeri, E., Giannini, S., Cosmi, L., Sagrinati, C., Mazzinghi, B., Orlando, C., Maggi, E., et al. (2003). An alternatively spliced variant of CXCR3 mediates the inhibition of endothelial cell growth induced by IP-10, Mig, and I-TAC, and acts as functional receptor for platelet factor 4. J Exp Med *197*, 1537-1549. 10.1084/jem.20021897.

314. Tan, S., Li, S., Min, Y., Gistera, A., Moruzzi, N., Zhang, J., Sun, Y., Andersson, J., Malmstrom, R.E., Wang, M., et al. (2020). Platelet factor 4 enhances CD4(+) T effector memory cell responses via Akt-PGC1alpha-TFAM signaling-mediated mitochondrial biogenesis. J Thromb Haemost *18*, 2685-2700. 10.1111/jth.15005.

315. Willox, I., Mirkina, I., Westwick, J., and Ward, S.G. (2010). Evidence for PI3K-dependent CXCR3 agonist-induced degranulation of human cord blood-derived mast cells. Mol Immunol *47*, 2367-2377. 10.1016/j.molimm.2010.05.005.

316. Xu, T., Xu, L., Meng, P., Ma, X., Yang, X., Zhou, Y., and Feng, M. (2020). Angptl7 promotes insulin resistance and type 2 diabetes mellitus by multiple mechanisms including SOCS3-mediated IRS1 degradation. FASEB J *34*, 13548-13560. 10.1096/fj.202000246RR.

317. Banini, B.A., and Sanyal, A.J. (2021). NAFLD-related HCC. Adv Cancer Res *149*, 143-169. 10.1016/bs.acr.2020.11.001.

318. Peiseler, M., and Tacke, F. (2021). Inflammatory Mechanisms Underlying Nonalcoholic Steatohepatitis and the Transition to Hepatocellular Carcinoma. Cancers (Basel) *13*. 10.3390/cancers13040730.

319. Karin, M. (2018). New insights into the pathogenesis and treatment of non-viral hepatocellular carcinoma: a balancing act between immunosuppression and immunosurveillance. Precis Clin Med *1*, 21-28. 10.1093/pcmedi/pby005.

320. Gleissner, C.A., Shaked, I., Little, K.M., and Ley, K. (2010). CXC chemokine ligand 4 induces a unique transcriptome in monocyte-derived macrophages. J Immunol *184*, 4810-4818. 10.4049/jimmunol.0901368.

321. Ruytinx, P., Proost, P., Van Damme, J., and Struyf, S. (2018). Chemokine-Induced Macrophage Polarization in Inflammatory Conditions. Front Immunol *9*, 1930. 10.3389/fimmu.2018.01930.

322. Ruytinx, P., Proost, P., and Struyf, S. (2018). CXCL4 and CXCL4L1 in cancer. Cytokine *109*, 65-71. 10.1016/j.cyto.2018.02.022.

323. Mehlem, A., Hagberg, C.E., Muhl, L., Eriksson, U., and Falkevall, A. (2013). Imaging of neutral lipids by oil red O for analyzing the metabolic status in health and disease. Nat Protoc *8*, 1149-1154. 10.1038/nprot.2013.055.

324. Junqueira, L.C., Bignolas, G., and Brentani, R.R. (1979). Picrosirius staining plus polarization microscopy, a specific method for collagen detection in tissue sections. Histochem J *11*, 447-455. 10.1007/BF01002772.

325. Ran, F.A., Hsu, P.D., Wright, J., Agarwala, V., Scott, D.A., and Zhang, F. (2013). Genome engineering using the CRISPR-Cas9 system. Nat Protoc *8*, 2281-2308. 10.1038/nprot.2013.143.

326. Charni-Natan, M., and Goldstein, I. (2020). Protocol for Primary Mouse Hepatocyte Isolation. STAR Protoc *1*, 100086. 10.1016/j.xpro.2020.100086.

327. Chen, S., Zhou, Y., Chen, Y., and Gu, J. (2018). fastp: an ultra-fast all-in-one FASTQ preprocessor. Bioinformatics *34*, i884-i890. 10.1093/bioinformatics/bty560.

328. Patro, R., Duggal, G., Love, M.I., Irizarry, R.A., and Kingsford, C. (2017). Salmon provides fast and bias-aware quantification of transcript expression. Nat Methods *14*, 417-419. 10.1038/nmeth.4197.

329. Love, M.I., Huber, W., and Anders, S. (2014). Moderated estimation of fold change and dispersion for RNA-seq data with DESeq2. Genome Biol *15*, 550. 10.1186/s13059-014-0550-8.

330. Dobin, A., Davis, C.A., Schlesinger, F., Drenkow, J., Zaleski, C., Jha, S., Batut, P., Chaisson, M., and Gingeras, T.R. (2013). STAR: ultrafast universal RNA-seq aligner. Bioinformatics *29*, 15-21. 10.1093/bioinformatics/bts635.

331. Gao, J., Aksoy, B.A., Dogrusoz, U., Dresdner, G., Gross, B., Sumer, S.O., Sun, Y., Jacobsen, A., Sinha, R., Larsson, E., et al. (2013). Integrative analysis of complex cancer genomics and clinical profiles using the cBioPortal. Sci Signal *6*, pl1. 10.1126/scisignal.2004088.

332. Ritchie, M.E., Phipson, B., Wu, D., Hu, Y., Law, C.W., Shi, W., and Smyth, G.K. (2015). limma powers differential expression analyses for RNA-sequencing and microarray studies. Nucleic Acids Res *43*, e47. 10.1093/nar/gkv007.

333. Steen, C.B., Liu, C.L., Alizadeh, A.A., and Newman, A.M. (2020). Profiling Cell Type Abundance and Expression in Bulk Tissues with CIBERSORTx. Methods Mol Biol *2117*, 135-157. 10.1007/978-1-0716-0301-7_7.

334. Chen, Z., Huang, A., Sun, J., Jiang, T., Qin, F.X., and Wu, A. (2017). Inference of immune cell composition on the expression profiles of mouse tissue. Sci Rep *7*, 40508. 10.1038/srep40508.

335. Jemal, A., Ward, E.M., Johnson, C.J., Cronin, K.A., Ma, J., Ryerson, B., Mariotto, A., Lake, A.J., Wilson, R., Sherman, R.L., et al. (2017). Annual Report to the Nation on the Status of Cancer, 1975-2014, Featuring Survival. J Natl Cancer Inst *109*. 10.1093/jnci/djx030.

336. Siegel, R.L., Miller, K.D., and Jemal, A. (2019). Cancer statistics, 2019. CA Cancer J Clin *69*, 7-34. 10.3322/caac.21551.

337. Nakatani, T., Roy, G., Fujimoto, N., Asahara, T., and Ito, A. (2001). Sex hormone dependency of diethylnitrosamine-induced liver tumors in mice and chemoprevention by leuprorelin. Jpn J Cancer Res *92*, 249-256. 10.1111/j.1349-7006.2001.tb01089.x.

338. Kemp, C.J., and Drinkwater, N.R. (1989). Genetic variation in liver tumor susceptibility, plasma testosterone levels, and androgen receptor binding in six inbred strains of mice. Cancer Res *49*, 5044-5047.

339. Haupt, S., Caramia, F., Klein, S.L., Rubin, J.B., and Haupt, Y. (2021). Sex disparities matter in cancer development and therapy. Nat Rev Cancer *21*, 393-407. 10.1038/s41568-021-00348-y.

340. Sykiotis, G.P., Pitteloud, N., Seminara, S.B., Kaiser, U.B., and Crowley, W.F., Jr. (2010). Deciphering genetic disease in the genomic era: the model of GnRH deficiency. Sci Transl Med *2*, 32rv32. 10.1126/scitranslmed.3000288.

341. Nault, J.C., Martin, Y., Caruso, S., Hirsch, T.Z., Bayard, Q., Calderaro, J., Charpy, C., Copie-Bergman, C., Ziol, M., Bioulac-Sage, P., et al. (2020). Clinical Impact of Genomic Diversity From Early to Advanced Hepatocellular Carcinoma. Hepatology *71*, 164-182. 10.1002/hep.30811.

342. Yuan, Y., Liu, L., Chen, H., Wang, Y., Xu, Y., Mao, H., Li, J., Mills, G.B., Shu, Y., Li, L., and Liang, H. (2016). Comprehensive Characterization of Molecular Differences in Cancer between Male and Female Patients. Cancer Cell *29*, 711-722. 10.1016/j.ccell.2016.04.001.

343. Ye, W., Siwko, S., and Tsai, R.Y.L. (2021). Sex and Race-Related DNA Methylation Changes in Hepatocellular Carcinoma. Int J Mol Sci *22*. 10.3390/ijms22083820.

344. Chen, C.L., Kuo, M.J., Yen, A.M., Yang, W.S., Kao, J.H., Chen, P.J., and Chen, H.H. (2020). Gender Difference in the Association Between Metabolic Factors and Hepatocellular Carcinoma. JNCI Cancer Spectr *4*, pkaa036. 10.1093/jncics/pkaa036.

345. Li, Z., Tuteja, G., Schug, J., and Kaestner, K.H. (2012). Foxa1 and Foxa2 are essential for sexual dimorphism in liver cancer. Cell *148*, 72-83. 10.1016/j.cell.2011.11.026.

346. Xu, C., Cheng, S., Chen, K., Song, Q., Liu, C., Fan, C., Zhang, R., Zhu, Q., Wu, Z., Wang, Y., et al. (2023). Sex Differences in Genomic Features of Hepatitis B-Associated Hepatocellular Carcinoma With Distinct Antitumor Immunity. Cell Mol Gastroenterol Hepatol *15*, 327-354. 10.1016/j.jcmgh.2022.10.009.

347. Yu, X., Li, Z., and Wu, W.K. (2014). TIP30: A Novel Tumor-Suppressor Gene. Oncol Res *22*, 339-348. 10.3727/096504015X14424348426116.

348. Facciorusso, A., and Barone, M. (2014). Glucose intolerance and hepatocellular carcinoma: recent findings for old diseases. Hepatobiliary Surg Nutr *3*, 91-92. 10.3978/j.issn.2304-3881.2014.02.15.

349. Bosman, F.T., Carneiro, F., Hruban, R.H., and Theise, N.D. (2010). WHO classification of tumours of the digestive system (World Health Organization).

350. Ishak, K., Baptista, A., Bianchi, L., Callea, F., De Groote, J., Gudat, F., Denk, H., Desmet, V., Korb, G., MacSween, R.N., and et al. (1995). Histological grading

and staging of chronic hepatitis. J Hepatol *22*, 696-699. 10.1016/0168-8278(95)80226-6.

351. Stieber, J., Stockl, G., Herrmann, S., Hassfurth, B., and Hofmann, F. (2005). Functional expression of the human HCN3 channel. J Biol Chem *280*, 34635-34643. 10.1074/jbc.M502508200.

352. Mok, K.C., Tsoi, H., Man, E.P., Leung, M.H., Chau, K.M., Wong, L.S., Chan, W.L., Chan, S.Y., Luk, M.Y., Chan, J.Y.W., et al. (2021). Repurposing hyperpolarization-activated cyclic nucleotide-gated channels as a novel therapy for breast cancer. Clin Transl Med *11*, e578. 10.1002/ctm2.578.

353. Fedchenko, N., and Reifenrath, J. (2014). Different approaches for interpretation and reporting of immunohistochemistry analysis results in the bone tissue - a review. Diagn Pathol *9*, 221. 10.1186/s13000-014-0221-9.

354. Messeguer, X., Escudero, R., Farre, D., Nunez, O., Martinez, J., and Alba, M.M. (2002). PROMO: detection of known transcription regulatory elements using species-tailored searches. Bioinformatics *18*, 333-334. 10.1093/bioinformatics/18.2.333.

355. Farre, D., Roset, R., Huerta, M., Adsuara, J.E., Rosello, L., Alba, M.M., and Messeguer, X. (2003). Identification of patterns in biological sequences at the ALGGEN server: PROMO and MALGEN. Nucleic Acids Res *31*, 3651-3653. 10.1093/nar/gkg605.

356. Urrego, D., Tomczak, A.P., Zahed, F., Stuhmer, W., and Pardo, L.A. (2014). Potassium channels in cell cycle and cell proliferation. Philos Trans R Soc Lond B Biol Sci *369*, 20130094. 10.1098/rstb.2013.0094.

357. Koch, K.S., and Leffert, H.L. (1979). Increased sodium ion influx is necessary to initiate rat hepatocyte proliferation. Cell *18*, 153-163. 10.1016/0092-8674(79)90364-7.

358. Lau, Y.T., Wong, C.K., Luo, J., Leung, L.H., Tsang, P.F., Bian, Z.X., and Tsang, S.Y. (2011). Effects of hyperpolarization-activated cyclic nucleotide-gated (HCN) channel blockers on the proliferation and cell cycle progression of embryonic stem cells. Pflugers Arch *461*, 191-202. 10.1007/s00424-010-0899-9.

359. Chen, X., and Calvisi, D.F. (2014). Hydrodynamic transfection for generation of novel mouse models for liver cancer research. Am J Pathol *184*, 912-923. 10.1016/j.ajpath.2013.12.002.

360. Mendez-Lucas, A., Li, X., Hu, J., Che, L., Song, X., Jia, J., Wang, J., Xie, C., Driscoll, P.C., Tschaharganeh, D.F., et al. (2017). Glucose Catabolism in Liver Tumors Induced by c-MYC Can Be Sustained by Various PKM1/PKM2 Ratios and Pyruvate Kinase Activities. Cancer Res *77*, 4355-4364. 10.1158/0008-5472.CAN-17-0498.

361. Fenske, S., Mader, R., Scharr, A., Paparizos, C., Cao-Ehlker, X., Michalakis, S., Shaltiel, L., Weidinger, M., Stieber, J., Feil, S., et al. (2011). HCN3 contributes to the ventricular action potential waveform in the murine heart. Circ Res *109*, 1015-1023. 10.1161/CIRCRESAHA.111.246173.

362. Liu, J., Lichtenberg, T., Hoadley, K.A., Poisson, L.M., Lazar, A.J., Cherniack, A.D., Kovatich, A.J., Benz, C.C., Levine, D.A., Lee, A.V., et al. (2018). An Integrated TCGA Pan-Cancer Clinical Data Resource to Drive High-Quality Survival Outcome Analytics. Cell *173*, 400-416 e411. 10.1016/j.cell.2018.02.052.

363. Dow, M., Pyke, R.M., Tsui, B.Y., Alexandrov, L.B., Nakagawa, H., Taniguchi, K., Seki, E., Harismendy, O., Shalapour, S., Karin, M., et al. (2018). Integrative genomic analysis of mouse and human hepatocellular carcinoma. Proc Natl Acad Sci U S A *115*, E9879-E9888. 10.1073/pnas.1811029115.

364. Martinez-Jimenez, F., Muinos, F., Sentis, I., Deu-Pons, J., Reyes-Salazar, I., Arnedo-Pac, C., Mularoni, L., Pich, O., Bonet, J., Kranas, H., et al. (2020). A compendium of mutational cancer driver genes. Nat Rev Cancer *20*, 555-572. 10.1038/s41568-020-0290-x.

365. Omelyanenko, A., Sekyrova, P., and Andang, M. (2016). ZD7288, a blocker of the HCN channel family, increases doubling time of mouse embryonic stem cells and modulates differentiation outcomes in a context-dependent manner. Springerplus *5*, 41. 10.1186/s40064-016-1678-7.

366. Phan, N.N., Huynh, T.T., and Lin, Y.C. (2017). Hyperpolarization-activated cyclic nucleotide-gated gene signatures and poor clinical outcome of cancer patient. Transl Cancer Res *6*, 698-+. 10.21037/tcr.2017.07.22.

367. Johard, H., Omelyanenko, A., Fei, G., Zilberter, M., Dave, Z., Abu-Youssef, R., Schmidt, L., Harisankar, A., Vincent, C.T., Walfridsson, J., et al. (2020). HCN Channel Activity Balances Quiescence and Proliferation in Neural Stem Cells and Is a Selective Target for Neuroprotection During Cancer Treatment. Mol Cancer Res *18*, 1522-1533. 10.1158/1541-7786.MCR-20-0292.

368. Goldman, M.J., Craft, B., Hastie, M., Repecka, K., McDade, F., Kamath, A., Banerjee, A., Luo, Y., Rogers, D., Brooks, A.N., et al. (2020). Visualizing and interpreting cancer genomics data via the Xena platform. Nat Biotechnol *38*, 675-678. 10.1038/s41587-020-0546-8.

369. Cerami, E., Gao, J., Dogrusoz, U., Gross, B.E., Sumer, S.O., Aksoy, B.A., Jacobsen, A., Byrne, C.J., Heuer, M.L., Larsson, E., et al. (2012). The cBio cancer genomics portal: an open platform for exploring multidimensional cancer genomics data. Cancer Discov *2*, 401-404. 10.1158/2159-8290.CD-12-0095.

370. Szklarczyk, D., Gable, A.L., Lyon, D., Junge, A., Wyder, S., Huerta-Cepas, J., Simonovic, M., Doncheva, N.T., Morris, J.H., Bork, P., et al. (2019). STRING v11: protein-protein association networks with increased coverage, supporting

functional discovery in genome-wide experimental datasets. Nucleic Acids Res *47*, D607-D613. 10.1093/nar/gky1131.

371. Bolger, A.M., Lohse, M., and Usadel, B. (2014). Trimmomatic: a flexible trimmer for Illumina sequence data. Bioinformatics *30*, 2114-2120. 10.1093/bioinformatics/btu170.

372. Yu, J., Vodyanik, M.A., Smuga-Otto, K., Antosiewicz-Bourget, J., Frane, J.L., Tian, S., Nie, J., Jonsdottir, G.A., Ruotti, V., Stewart, R., et al. (2007). Induced pluripotent stem cell lines derived from human somatic cells. Science *318*, 1917-1920. 10.1126/science.1151526.

373. Borowicz, S., Van Scoyk, M., Avasarala, S., Karuppusamy Rathinam, M.K., Tauler, J., Bikkavilli, R.K., and Winn, R.A. (2014). The soft agar colony formation assay. J Vis Exp, e51998. 10.3791/51998.

374. Su, S., Blackwelder, A.J., Grossman, G., Minges, J.T., Yuan, L., Young, S.L., and Wilson, E.M. (2012). Primate-specific melanoma antigen-A11 regulates isoform-specific human progesterone receptor-B transactivation. J Biol Chem *287*, 34809-34824. 10.1074/jbc.M112.372797.